UNIVERSITY OF CALIFORNIA
RIVERSIDE

Biochemical Characterization of the Replication of Damaged DNA Mediated by Eukaryotic DNA Polymerases

A Dissertation submitted in partial satisfaction
of the requirements for the degree of

Doctor of Philosophy

in

Environmental Toxicology

by

Ashley Lorraine Swanson

June 2014

Dissertation Committee:
Dr. Yinsheng Wang, Chairperson
Dr. David Eastmond
Dr. Constance Nugent

The Dissertation of Ashley Lorraine Swanson is approved:

_____

_____

_____

Committee Chairperson

University of California, Riverside

COPYRIGHT ACKNOWLEDGEMENTS

The text and figures in Chapter 2 and Appendix A, in part or in full, are a reprint of the material as it appears in ***Biochemistry 2011***, 50 (35), p. 7666-7673 and the supporting information therein. The co-author (Dr. Jianshuang Wang) listed in this publication synthesized the carboxymethylated phosphoramidites and constructed the lesion-containing templates used for the replication experiments. The co-author (Dr. Yinsheng Wang) listed in this publication directed and supervised the research dictated in this chapter.

The text and figures in Chapter 3 and Appendix B, in part or in full, are a reprint of the material as it appears in ***Chemical Research in Toxicology 2012***, 25 (8), p. 1682-1691 and the supporting information therein. The co-author (Dr. Yinsheng Wang) listed in this publication directed and supervised the research which forms the basis for this chapter. The co-author (Dr. Jianshuang Wang) listed in this publication synthesized the cyclopurine phosphoramidites and constructed the damage-containing templates for the replication studies.

The text and figures in Chapter 4 and Appendix C, in part or in full, are a reprint of the material as it appears in ***Journal of Biological Chemistry 2013***, 288 (40), p. 28548-28556 and the supporting information therein. The co-authors (Dr. Changjun You) performed the cellular replication experiments, (Dr. Xiaoxia Dai) and (Dr. Bifeng Yuan) assisted with the construction of the lesion-containing vectors, and (Dr. Jianshuang

Wang) synthesized the damage-containing templates for the replication studies. The co-author (Dr. Yinsheng Wang) directed and supervised the research that comprises this chapter.

PROFESSIONAL ACKNOWLEDGEMENTS

This dissertation was supported by an NRSA Institutional Training grant (T32 ES018827), as well as a Dissertation Year Program fellowship awarded by the University of California, Riverside. I would also like to thank Drs. Roger Woodgate, Wei Yang, William C. Copeland, James E. Cleaver, and Timothy R. O'Connor for providing polymerases, cells, and reagents for the replication experiments detailed herein.

I would like to thank Dr. Phil Hanawalt, the founder of DNA excision repair, who was instrumental in helping me attend my first Gordon Research Conference in 2012. He has become a mentor to me these last few years, and I am so grateful to him. What an opportunity it has been for me to have such an esteemed colleague and friend that I can go to for career advice and bounce scientific ideas off of. This Gordon conference also allowed me to interact with the top scientists in my field, and through it, I met Dr. Roger Woodgate, my future postdoc advisor. I would like to specially thank Roger, who has become a fabulous mentor to me over the years, for taking the time to introduce me to people at these conferences, allowing me to interact closely with professors and researchers from all over the world on bike rides and restaurant trips, and helping to put my name out there. I very much look forward to working with you.

DEDICATION AND ACKNOWLEDGEMENTS

This dissertation is dedicated to the memories of my loving grandfather, Edward Kwik, who first inspired me to pursue a career in cancer research, Dr. Laura Abbott, who motivated me to always put others first and give people the benefit of the doubt, and Timothy James "TJ" Waite, who is a reminder every day to enjoy life and cherish others.

I would first like to thank my advisor, Dr. Yinsheng Wang, who has supported me the past 5 years. He has given me the freedom to grow as a researcher and a person, was always available to give advice and engage in insightful conversations, has pushed me to be my best, and shown me compassion when I have made mistakes along the way. He has put me on a path for great future success. I would also like to thank my committee members, Dr. David Eastmond and Dr. Connie Nugent, who were always available for career advice, writing myriads of recommendation letters, and made many helpful suggestions during my graduate career. I would like to thank Dean Leah Haimo, who I had the pleasure of TAing for, and has been extremely supportive of me during my time here at UCR. I look up to and admire her for her dedication to her students, exceptional teaching style, and most importantly, her care for others. I am also forever indebted to Assitant Dean Geoffrey Thompson at UW-Madison, who took me under his wing when I was at my lowest, and restored my faith in myself. It is because of this experience that I try to be accomodating and understanding towards others, especially my students. You never know what people are dealing with behind closed doors. As a result, I have met some amazing people in my classrooms that I am honored to now call my friends. I'm so proud of of them and look forward to seeing what their futures hold.

I have made some amazing friends during my time at UCR who have made these last 5 years some of the best of my life. A special shoutout to Juliane, who I first bonded with over our mutual love of Atmosphere, and consider my sister. No matter the miles, or amount of time between when we last talked, we always pick up right where we left off. Thank you for always being there, from the good to the bad. To Preston, Nicole, and Consuelo, I'll miss our kickbacks and puppy play dates with Colby, which kept me sane. To my mentees, Allison, Graciel, Justin, and Nicole, I was so fortunate to get to know you and wish you all the best in grad school and beyond. To Chloe, who was so supportive during the difficult times, as well as Brian, Laurel, Don, Lauren, JP, Lindsey, and Neil; I had so much fun with all of you and I'm going to miss you way more than you know.

Last but certainly not least, I would like to thank my family, including my Grandma, aunts, and uncles, for their unending support and helping to shape me into the person I am today. To my parents, who gave me the best start in life, sacrificed and worked so hard to make sure I grew up in a comfortable and loving home. I love you so much, and thank you for instilling in me a great work ethic, compassion, sense of humor, love for science, and providing me a top notch education. I can never repay you for everything you've done, but I hope to make you proud. To my brothers, Erik and Ryan, you two mean the world to me. We've been through a lot together, and I wouldn't be the person I am today without you both being there and supporting me, and calling me out when I need it. I have so much fun with you two, and I'm so grateful that we're as close as we are. I love you both more than life itself.

ABSTRACT OF THE DISSERTATION

Biochemical Characterization of the Replication of Damaged DNA Mediated by Eukaryotic DNA Polymerases

by

Ashley Lorraine Swanson

Doctor of Philosophy, Graduate Program in Environmental Toxicology
University of California, Riverside, June 2014
Dr. Yinsheng Wang, Chairperson

DNA lesions can be generated at an estimated rate of up to one million molecular lesions per cell per day, and are induced by a wide range of endogenous and exogenous damaging agents. These can include reactive oxygen species, alkylating agents, and genotoxic chemicals, all of which can yield lesion formation upon reaction with all four nucleobases of DNA. The mutagenic potential of a lesion rests on its intrinsic chemical structure, as well as the polymerase involved in its bypass. Many lesions distort DNA double helix, and are known blocks to replication. Stalled or blocked replication forks can trigger cell death and lead to genomic instability, so the cell has evolved numerous pathways to either repair or tolerate the damage in the event that it is unable to be excised and repaired. Given the wide range of damaging agents and resultant damaged bases, understanding their effects on replication can be complex, and requires the individual analysis of each lesion to determine its mutagenic potential.

During lesion bypass, the polymerase encounters two kinetic barriers, which coincides with the insertion opposite the lesion, as well as the subsequent extension. This dissertation monitors the kinetics of nucleotide insertion opposite and past four different types of lesions mediated by polymerases known to be important in lesion bypass, which include the Pols η, ι, κ, ζ, and γ. The carboxymethylated lesions, cyclopurine lesions, ethylated thymidine lesions, and ribonucleotides embedded in DNA compromised the accuracy and efficiency of DNA replication to varying degrees. Most strikingly was the mutation profile generated from these replication studies closely matched the known mutation signature for several human diseases, including gastrointestinal cancers in the case of the carboxymethylated lesions. As a result, the studied lesions are attractive candidates for further research on their potential roles in the etiology of human diseases, and use as biomarkers for various ailments.

Table of Contents

List of Figures

List of Tables

Chapter 1: Introduction

General Introduction

1.1 DNA Damage

There are innumerable exogenous and endogenous agents that continuously attack the human genome, generating an estimated one million molecular lesions per cell per day (1). Exogenous sources of those agents include ionizing radiation, ultraviolet light, chemotherapeutics, and other genotoxic chemicals, whereas sources of endogenous damage encompass cellular metabolites and reactive oxygen species (ROS), resulting from consequences of normal aerobic respiration and lipid peroxidation (2-4).

Endogenous DNA damage is a driving force for mutagenesis and carcinogenesis and a major focus of this dissertation. Oxidatively induced nucleobase damage is an inevitable byproduct of aerobic metabolism resulting from ROS production (5,6). Superoxide anion ($O_2^{\bullet-}$) can be generated by O_2 reacting with electrons leaking from the electron transport chain and it can be converted to O_2 and hydrogen peroxide (H_2O_2) via superoxide dismutase (SOD) (4,7). H_2O_2 can react further with transition metal ions, Fe^{2+} or Cu^{+}, to yield the extremely reactive hydroxyl radical ($^{\bullet}OH$) via the Fenton-type reactions (8,9). ROS can also result from the chronic induction of the inflammatory response, as neutrophils release H_2O_2 and $O_2^{\bullet-}$, which can lead to $^{\bullet}OH$ (10,11). These reactive species can interact with nucleobases of DNA both in the nucleus and mitochondria to generate a number of oxidatively generated base damage products,

including the abundant 8-oxo-7,8-dihydroguanine (8-oxoG), 5,6-dihydroxy-5,6-dihydrothymine (thymine glycol, Tg), 5-hydroxycytosine, 5-formyluracil, 5-hydroxymethyluracil, and 2-hydroxyadenine (12,13). Bulky DNA lesions are also induced in calf thymus DNA from exposure to γ-rays, and include 8,5′-cyclo-2′-deoxyadenosine (cdA), 8,5′-cyclo-2′-deoxyguanosine (cdG), as well as intrastrand cross-link lesions (14,15). Upon excessive accumulation of ROS, the cell experiences oxidative stress, which can lead to cell death, and has been linked to cardiovascular disease, cancer, and accelerated aging (16). In addition to oxidatively generated base damage, endogenous alkylation of DNA can also occur in cells. A significant source of endogenous alkylation stems from DNA methylation by *S*-adenosyl-L-methionine (SAM), a methyl group donor resultant from the conjugation of adenosine triphosphate with methionine that is catalyzed by methionine adenosyltransferase (17,18). While regulatory methylation of the C5 position of cytosine at CpG sites mediated by DNA cytosine 5-methyltransferases and SAM is crucial to a large number of biological processes, including gene expression regulation, transcription, and regulation of the biological clock, inadvertent methylation is also a large source of mutagenic base damage, including 7-methylguanine, 3-methyladenine, and O^6-methylguanine (O^6-meG), a base lesion responsible for a significant number of G→A transition mutations in cells (18-20). Endogenous *N*-nitroso compounds (NOCs) are also a significant source of alkylation damage, including O^4-methylthymine and N^7-carboxymethylguanine, and are discussed in further detail in section 1.1 (21). DNA hydrolysis is also a significant contributor to endogenous damage in the cell, primarily through the generation of abasic

sites and deamination of cytosine to uracil (1,22). The *N*-glycosidic bond between the 2'-deoxyribose and nucleobase can be cleaved due to heat or alkylation of the base, resulting in an abasic site at an estimated load of up to 10,000 sites per human cell per day (1). Abasic sites have been detected in DNA isolated from mammalian tissues, including the brain, colon, and liver, and they direct significant misincorporations of adenine during DNA replication (23-25).

Exogenous damage also presents a major challenge for the cell, with both avoidable and unavoidable sources of base damage. A major contributor to adduct formation is exposure to ultraviolet (UV) light from the sun (26). UV light emissions primarily generate the highly mutagenic *cis-syn* thymine-thymine cyclobutane pyrimidine dimer (TT-CPD) and the pyrimidine [6-4] pyrimidone photoproduct ([6-4]-PP), the former of which significantly contributes to the etiology of skin cancers and abnormalities (27-29). Ionizing radiation (IR) is another common source of exogenous DNA damage, where humans are exposed to IR in the form of γ-rays, x-rays, naturally occurring radioactive isotopes, as well as cosmic radiation (30,31). IR can induce a number of quantifiable lesions in cells and tissues both directly and indirectly, through generation of reactive radicals, including Tg, formamide, and 8-oxoG, as well as the bulky cdA and cdG, and intrastrand cross-links (32-35). Other major exogenous damaging agents are polycylic aromatic hydrocarbons (PAHs), a class of ~twenty chemicals that can exist in over 100 different combinations, and can be generated during the burning process of grilling or charring meats, as well as found in tobacco smoke (36). PAHs can be metabolically activated by the cytochrome P450 class of enzymes to yield a

reactive diol epoxide intermediate that can react with all four nucleobases of DNA to generate a number of mutagenic and carcinogenic adducts, including N^2-(benzo[*a*]pyrene-7,8-diol-9,10-epoxide)-2′-deoxyguanosine (BPDE- N^2-dG) (37-39). In addition to PAHs, there are an extensive number of other genotoxic chemicals that can damage DNA, one of which is urethane, a carcinogen found in alcoholic beverages that generates etheno adducts including 3,N^2-ethenoguanine (εG), 1,N^6-ethenoadenine (εA), and 3,N^4-ethenocytosine (εC) (40).

The research herein focuses on four types of lesions that are induced exogenously and endogenously: the carboxymethylated lesions N^6-carboxymethyl-2′-deoxyadenosine (N^6-CMdA), N^4-carboxymethyl-2′-deoxycytidine (N^4-CMdC), *N*3-carboxymethylthymidine (*N*3-CMdT), O^4-carboxymethylthymidine (O^4-CMdT), the cyclopurine lesions (i.e. cdA and cdG), ribonucleotides (rNs) inadvertently incorporated in DNA, and the regioisomeric ethylated thymidine lesions O^2-ethylthymidine (O^2-EtdT), *N*3-ethylthymidine (*N*3-EtdT), and O^4-ethylthymidine (O^4-EtdT) (Figure 1.1).

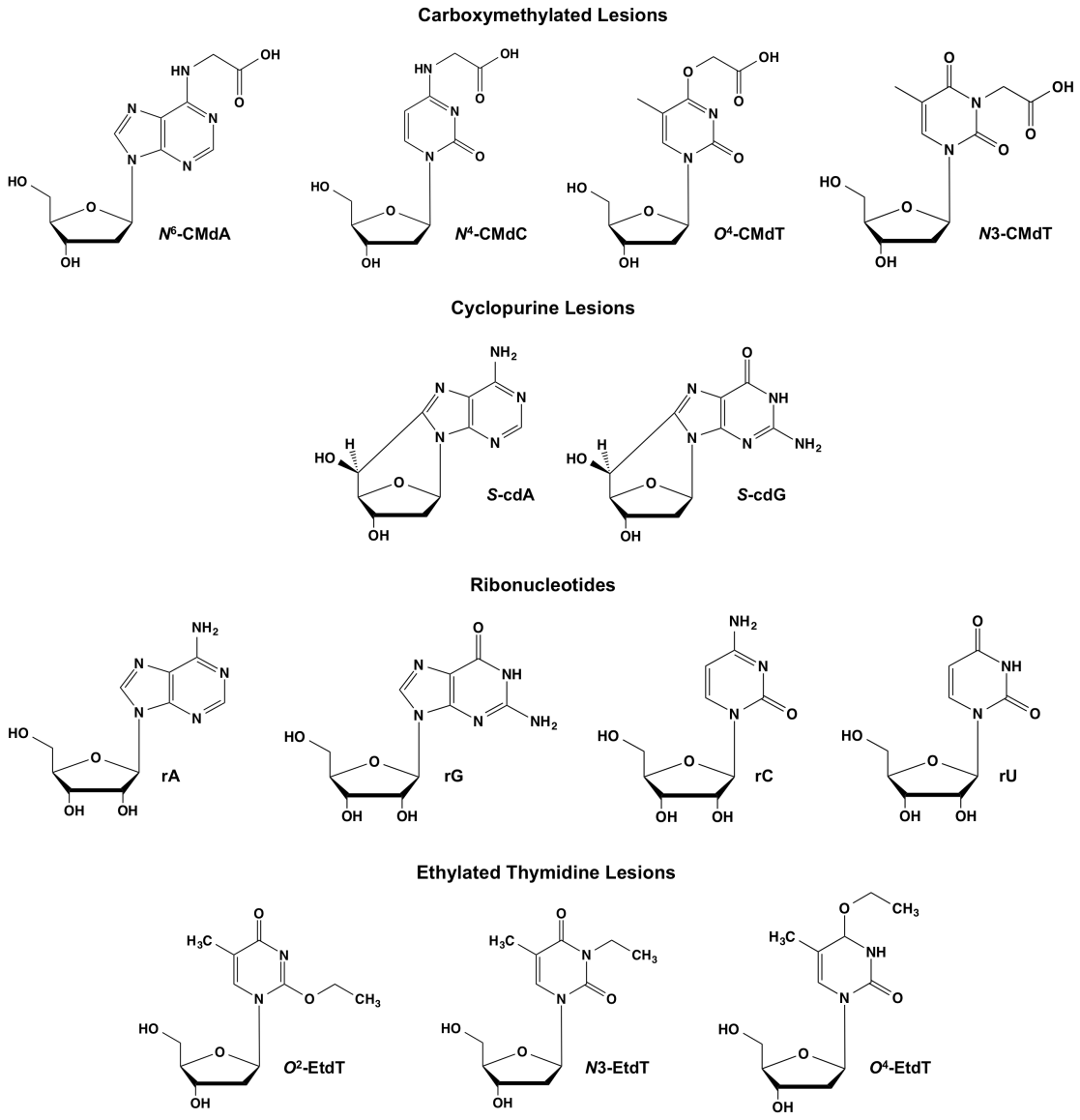

Figure 1.1. Structures of the DNA lesions investigated

1.1.1. Carboxymethylated Lesions

Carboxymethylated lesions can be induced by *N*-nitroso compounds (NOCs), which are known mutagens and carcinogens (41). Humans are exposed to NOCs both endogenously and exogenously, with exogenous sources comprising tobacco smoke, drugs, industrial exposure, and diet (41). Dietary sources of NOCs include *N*-nitrosodimethylamine (NDMA) and *N*-nitrosopyrrolidine (NPYR), both of which can be quantified at high levels in smoked, processed, cured, and fried meats, such as bacon, with small amounts being detected in cheese, beer, and other malt beverages (42,43). However, endogenous sources account for 45-75% of total human NOC exposure (44). A European Prospective Investigation into Cancer (EPIC) study monitoring over 500,000 individuals demonstrated that exposure to endogenously-produced NOCs was associated with an increased risk of developing non-cardia gastric cancer (44). A common endogenous source of NOCs results from the nitrosation of glycocholic acid, a conjugate of bile acid, in the gut, which can be stimulated under normal gastric conditions to generate *N*-nitrosoglycocholic acid (NOGC) (45). A previous study monitored the treatment of Fisher rats with NOGC and reported high levels of hepatocarcinoma in 50-70% of treated animals, and ~13% of rats developed gastric tumors (45). When calf thymus DNA was treated with NOGC, it generated the stable formation of O^6-CMdG, and to a lesser extent, methylation on the O^6 position of guanine- O^6-methyl-2′-deoxyguanosine (O^6-MdG) (46). It had been demonstrated that both *N*-nitrosoglycine (NG) and azaserine, a common pancreatic carcinogen, could also induce carboxymethylation and methylation of guanine bases in DNA (47,48). Search for a

common reactive intermediate led to the prospect that diazoacetate may promote the carboxymethylation of DNA, substantiated by a series of research articles by Shuker et al (48,49). Work in our laboratory has also shown that diazoacetate can induce carboxymethylation of all four nucleobases of DNA, generating N^6-CMdA, N^4-CMdC, *N*3-CMdT, O^4-CMdT, and O^6-CMdG (50,51). A study by Gottschalg and coworkers (52) monitored the mutation spectra of potassium diazoacetate-treated *p53* gene-containing plasmid in yeast cells, and found a relatively even distribution of transition and transversion mutations. This was in stark contrast to mutations induced by *N*-methyl-*N*-nitrosourea (MNU), a known methylating agent, which was dominated by GC→AT transition mutations (52). Given that diazoacetate predominantly generates carboxymethylation as opposed to methylation of DNA, it has been suggested that carboxymethylation, rather than methylation, significantly contributes to mutations in *p53* gene of gastrointestinal tumors (52). Given the potential biological consequences, it is important to understand the mechanisms by which these lesions may induce mutations and contribute to incidence and progression of gastrointestinal tumors.

1.1.2. Cyclopurine Lesions

The cyclopurine lesions, including cdA and cdG, are a class of oxidatively-generated lesions that can exist as the *R* or *S* diastereomer (5'*R*-cdA, 5'*R*-cdG, 5'*S*-cdA, 5'*S*-cdG) (53). These bulky adducts are largely induced through a two-step mechanism in which an •OH radical, formed by exposure to ionizing radiation or from endogenous processes, reacts with the 2'-deoxyribose and abstracts a hydrogen atom from the 5'C, generating a C5' radical, after which an intramolecular cyclization occurs where the C5'

radical attacks the C8 of the purine base, resulting in an 8,5' C-C bond (53). Due to the bulky nature of these adducts, the cyclopurine lesions are not substrates for base excision repair (BER), and are repaired ineffectively by nucleotide excision repair (NER) (54,55). Along these lines, there is recent interest in whether cyclopurine lesions may play a role in XP neurological disease, which results from defective NER (53). The *R* and *S* forms of each lesion have been quantified using a variety of methods both in cells and tissues, including liquid chromatography tandem mass spectrometry (LC-MS/MS) with a stable isotope-dilution method (56-58). Interestingly, the *R* isomer appears to be readily repaired in cells, and is present at significantly lower levels than the corresponding *S* isomers, though both isomers accumulate in tissues in an age-dependent manner (56). A previous biochemical study also demonstrated that the *R* isomer of cdA is not significantly blocking to replicative DNA polymerases, whereas *S*-cdA disrupts the replication machinery (54). Both cdA and cdG have also been shown to block transcription both *in vitro* and in cells, as well as induce mutations (59,60). This suggests that these lesions may contribute to XP neurological disease via this mechanism, though further research is needed to mechanistically understand how this may occur (60).

1.1.3. Ribonucleotides Incorporated into DNA

A number of research articles published within the last three years have demonstrated that ribonucleotides can be incorporated into DNA with much greater frequency than previously thought. The replicative polymerases (Pols) α, ε, and δ all incorporate ribonucleotides into DNA during normal synthesis to varying degrees, with Pol ε, responsible for leading strand synthesis, incorporating about one ribonucleoside

monophosphate (rNMP) per every 1250 nucleotides (61,62). In this respect, ribonucleotides are now considered the most common lesions in cells. Additionally, it is now understood that the rNTP pool exists in much larger molar quantities than the corresponding dNTP pool (61,63). Mutagenicity studies have shown that ribonucleotides incorporated by Pol ε during DNA replication generate a significant amount of mutations, and their proper removal from genomic DNA is dependent on the activity of ribonuclease H2 (RNase H2), which cleaves the RNA from the RNA:DNA hetero duplex (64,65). However, this process is not perfect and a number of rNMPs incorporated into the nascent DNA strand are left unrepaired, as they are inefficiently removed by the 3'→5' proofreading activity of replicative polymerases (65,66). This further confounds the discussion of why the cell has evolved to incorporate ribonucleotides into DNA, given that the presence of a single ribonucleotide in the DNA strand severely compromises the integrity of the duplex, leaving the strand susceptible to spontaneous hydrolysis and breakage (64). One idea out of Kunkel's laboratory is that ribonucleotides may serve as a signal for the initiation of mismatch repair (MMR) by flagging a replication error in the nascent continuous leading strand (67,68). While this finding is remarkable, it is clear that a significant portion of rNMPs remains embedded in the genome and poses a constant threat to genomic stability.

1.1.4. Ethylated Thymidine Lesions

Ethylated thymidine lesions are induced by tobacco smoke likely through the action of tobacco-specific nitrosamines and acetaldehyde, which can result in alkylation

of DNA (69,70). The tobacco-specific nitrosamines 4-(methylnitrosamino)-1-(3-pyridyl)-1-butanone (NNK) and *N*'-nitrosonornicotine (NNN) can be formed endogenously when nicotine is metabolized by cytochrome P450 enzymes and comes into contact with nitrosating agents in the gut (69). NNK is capable of producing a number of alkylation products, including the methylated adducts O^2-methylthymidine (O^2-MdT), O^4-methylthymidine (O^4-MdT), O^6-MdG, and *N*7-methyl-2'-deoxyguanosine (*N7*-MdG), as well as the bulkier pyridyloxobutyl (POB) and pyridylhydroxybutyl (PHB) DNA lesions (71,72). NNN also generates alkylated adducts, though preferentially at the N^2 position of guanine, including N^2-propano-2'-deoxyguanosine (N^2-PdG) (72). NNN can also be metabolized to give POB DNA adducts (73). Moreover, exposure of DNA to cigarette smoke induced a dose-dependent increase in *N*7-ethylguanine, indicating the presence of a direct ethylating agent in cigarette smoke (74). The ethylated thymidine adducts O^2-EtdT, O^4-EtdT, and *N*3-EtdT, have been quantified in the leukocyte DNA of smokers, levels of which are significantly elevated compared to non-smokers (75). Interestingly, the ethylated thymidine lesions are poorly repaired, unlike O^6-ethyl-2'-deoxyguanosine (O^6-EtdG), and persist in DNA (76,77). In order to characterize the mutagenic potential of these lesions, one study exposed Chinese Hamster Ovary (CHO) cells to *N*-ethyl-*N*-nitrosourea (ENU), which led to a rise in GC→AT, AT→TA, and AT→GC mutations in the *Hprt* gene, and O^4-EtdT was implicated in directing AT→GC mutations during replication (78). These studies highlight the potential biological consequences of these lesions, and implicate their possible role in contributing to the etiology of lung cancer.

1.2. DNA Damage Response

The accumulation of DNA lesions in the genome can affect DNA replication and transcription, and lead to a number of cellular consequences, including mutations and cell death. Due to the high prevalence of lesion formation and integration into the genome, our cells are outfitted with a number of protective DNA damage response mechanisms, including various signaling cascades that activate DNA repair pathways and cell cycle checkpoints to prevent proliferation of mutations and allow time for lesion repair (79-81). The DNA damage response (DDR) pathway is a sophisticated network of over 700 proteins, which are regulated by post-translational modifications in order to amplify the damage signal and initiate a global genome response (81). The proteins of the PIKK (phosphatidylinositol 3-kinase related protein kinase) family, including ATM (ataxia telangiectesia mutated) and ATR (ATM and Rad3 related), are central to the DDR and are responsible for phosphorylating a number of proteins within the network (82,83). The presence of nucleobase lesions in DNA activates ATR, likely through replication fork stalling, which exposes segments of single-stranded DNA (ssDNA) (84). Upon activation, ATR phosphorylates proteins in the signaling cascade, including Chk1, which consequently stabilizes the blocked replication fork and prevents cell-cycle progression (85). On the other hand, double-strand breaks are sensed by the MRN complex (Mre11-Rad50-Nbs1), which recruits ATM to the break site (84). ATM can then phosphorylate a wide range of proteins at or downstream from the damage site, which, similar to the ATR-dependent pathway, activates cell-cycle checkpoints, DNA repair pathways, and apoptotic pathways (86).

1.3. DNA Damage Repair

Given the wide range of damaging agents and infinite adduct structure possibilities, our cells are equipped with a number of evolutionarily conserved repair pathways, including three excision pathways- base excision repair (BER), nucleotide excision repair (NER), and mismatch repair (MMR), to correct various forms of DNA damage and preserve genome integrity (Figure 1.2.) (87).

1.3.1. Base Excision repair

BER is employed in the nucleus, as well as the mitochondrion to remedy a number of single-base lesions, including those arising from alkylation, deamination, and oxidative damage (88,89). The core BER pathway utilizes four proteins, including a lesion-specific DNA glycosylase, an apurinic/apyrimidinic (AP) endonuclease, a DNA polymerase, and a DNA ligase to recognize and excise a damaged base and replace it with the correct one, with a variety of proteins available to mount a lesion-specific repair response (Figure 1.2) (88,90,91). Some common lesions repaired by BER include 8-oxoG, Tg, 3-methyladenine (3-meA), εA, abasic sites, and 2'-deoxyuridine (dU) (91). In the presence of an oxidative base lesion, such as 8-oxoG, the DNA glycosylase Ogg1 recognizes the damaged substrate and cleaves the *N*-glycosidic bond, removing the damaged base (92). An AP endonuclease, such as APE1, recognizes the AP site generated by the DNA glycosylase and nicks the DNA 5' to the AP site (93). The AP site is further processed by an AP lyase to yield a 3'-hydroxyl and 5'-phosphate, generating a single nucleotide gap that can then be filled in by a DNA polymerase, such as Pol β, and

sealed by a DNA ligase (Lig III), thereby completing repair (93). Though BER can process a variety of nucleobase lesions, it is limited to those that are targeted specifically by an available DNA glycosylase and are non-distorting to the DNA secondary structure.

1.3.2 Nucleotide Excision Repair

Many DNA lesions, including the above-described cyclopurine lesions, UV light-induced thymine-thymine dimers, inter- and intra-strand crosslinks, and cisplatin adducts, cause significant distortion to the DNA double-helix, block replicative polymerases, and are inaccessible to the BER machinery (94). In these instances, NER machinery can recognize the bulky DNA adduct, excise a stretch of nucleotides that span the lesion site, then fill the gap with a traditional replicative DNA polymerase, such as Pol δ or ε, and seal the nick with a DNA ligase to restore integrity to the DNA strand (94,95). Since NER recognizes general distortions in the double helix, as opposed to a single base, it can be used to excise a countless number of damage-containing substrates, though with varying degrees of efficiency (95).

NER proceeds through two distinct pathways: global genome NER (GG-NER) and transcription-coupled NER (TC-NER) (96). GG-NER repairs damage throughout the genome, whereas TC-NER only repairs damage in transcribed strands (96). In the core excision model for GG-NER (Figure 1.2), a protein complex that includes xeroderma pigmentosum A (XPA), replication protein A (RPA), and XPC recognizes a helix-distorting lesion (97). Transcription factor II H (TFIIH) assists in opening of the DNA around the damage site in an ATP-dependent reaction to allow access for the NER

machinery (97). An XPG nuclease makes an incision 3' to the damage site, while ERCC1-XPF complex cleaves 5' to the damaged base, which liberates a short damage-containing oligonucleotide ~25-30 bases long (97). The oligonucleotide gap can then be filled in by Pols δ or ε, mediated by proliferating cell nuclear antigen (PCNA) clamp and RFC, and the nicks are sealed by a DNA ligase, such as LIG1 (97). TC-NER is significantly less established than GG-NER, but current theories show several distinct differences in recognition and recruitment of NER factors compared to GG-NER, though the core excision model is thought to be the same (98). Briefly, TC-NER is initiated following blockage of an actively elongating RNA polymerase II (RNAPII), at which point CSB and possibly XPG are recruited to the damage site (98). CSB and CSA are then thought to recruit the core excision repair machinery to excise the damaged DNA from the transcribed strand of the active gene (98). Given that NER is capable of excising a large number of base lesions without structure specificity, it is often the preferred mechanism for lesion removal in nuclear DNA (96). However, NER has not been demonstrated to occur in mitochondrial DNA, rendering bulky adducts significantly more problematic in the mitochondrial genome (99).

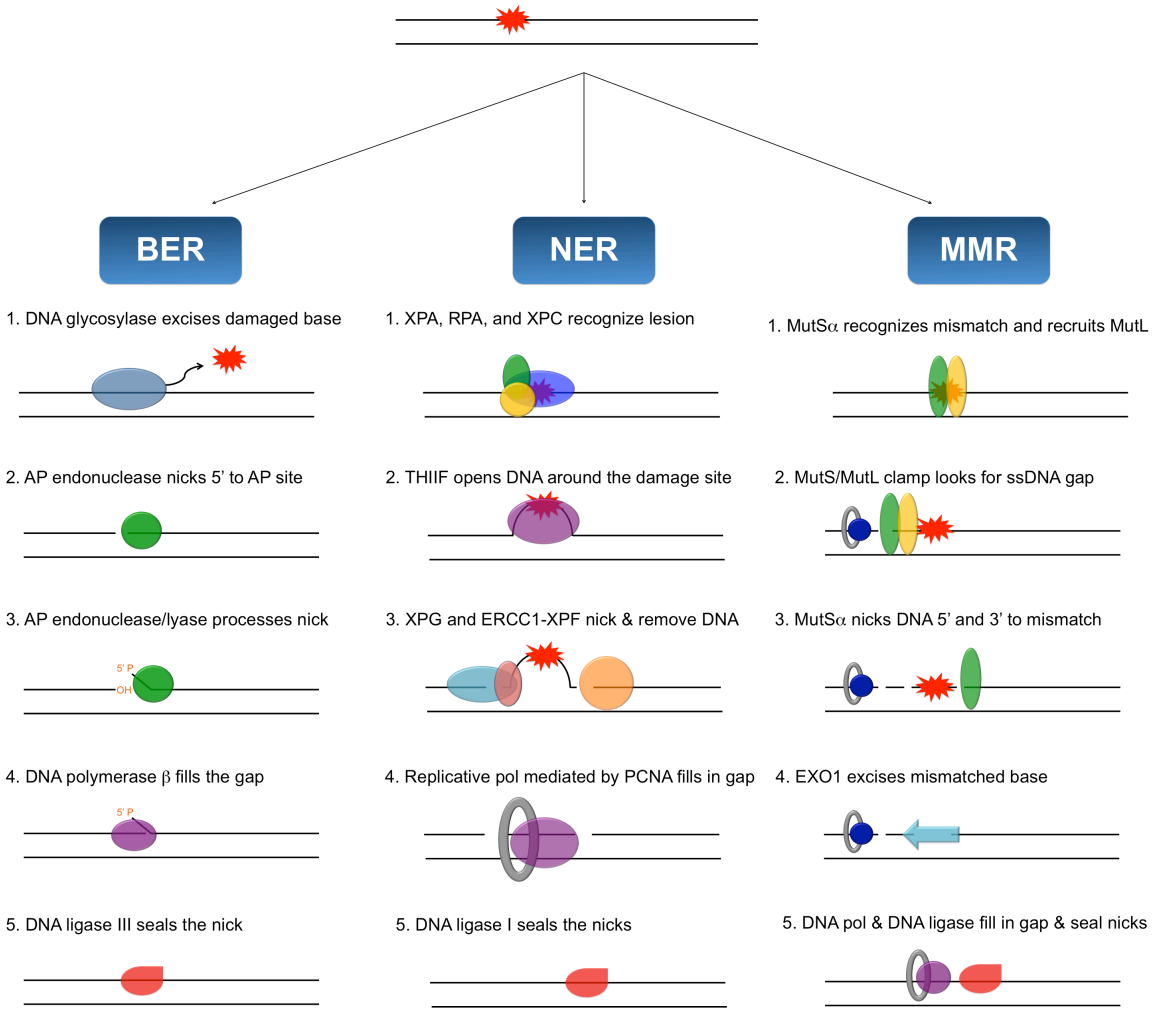

Figure 1.2. Core models for base excision repair (BER), nucleotide excision repair (NER), and mismatch repair (MMR).

1.3.3. Mismatch Repair

As opposed to BER and NER which repair adducts and cross-links in DNA, MMR is employed primarily to correct nucleotide incorporation errors that may arise during DNA replication and evade the polymerase proofreading capabilities (100). However, more recent studies have demonstrated that MMR may also play a key role in removing/repairing oxidatively induced DNA damage (101,102). In a simple MMR model in mammalian cells (Figure 1.2), MutSα recognizes the mismatch and binds to the DNA (103). It then recruits and complexes with MutL, generating a sliding clamp that scans up and down the DNA strand in an ATP-dependent mechanism until it encounters a "strand determination signal," which is an ssDNA gap tagged by PCNA and RFC (100). Mismatch excision is then initiated when MutLα nicks the DNA 3' and then 5' to the base, allowing EXO1 to catalyze the excision (100). The replicative DNA Pol δ fills in the gap, mediated by the PCNA clamp, and a DNA ligase seals the nicks (100). It has been shown in *Escherichia coli* that MMR can directly excise an 8-oxoG, as well as a misincorporated adenine opposite the lesion, indicating that MMR may assist BER and NER in protecting cells during periods of oxidative stress (104). It has been well established that MMR plays a role in the mitochondrion as well, albeit limited in function compared to its role in the nucleus (105). This new insight into mismatch repair of oxidative damage in nuclear DNA may hold true for oxidative damage in mitochondrial DNA as well, where a high amount of oxidative stress and ROS form due to electron leaking from the electron transport chain. This warrants further exploration, as MMR

may complement BER to combat oxidatively generated damage, given the lack of NER in the mitochondrion.

1.4. DNA Damage Tolerance

Even with the extensive array of repair systems throughout the cell, the speed of lesion formation and assimilation into genomic DNA is extremely rapid, allowing a number of lesions to escape these traditional pathways, and remain embedded in the genome and block DNA replication (106). During normal DNA replication, the B-family Pols δ or ε highly efficiently and accurately replicate DNA, but in the presence of a lesion they can become stalled due to the helical distortions and bulky nature of most adducts (107,108). Their active sites are evolutionarily conserved to snugly fit a correct A:T or C:G base pair, leaving little additional space to accommodate most damaged sites (107). Multiple stalled replication forks trigger programmed cell death, so translesion synthesis (TLS) serves as a protective measure to prevent collapsed replication forks in the presence of damaged bases, allowing them to be excised later (109,110).

1.4.1. Translesion Synthesis Pathways

Although TLS has been extensively studied in recent years, its molecular mechanism is still not fully understood. There are two proposed pathways for TLS in cells: a postreplicative gap-filling model and polymerase switching model (Figure 1.3) (111). In the postreplicative gap-filling model, it is thought that the replication complex skips a lesion and reassociates with the template DNA downstream to continue replication, whereafter a TLS polymerase is recruited to the gapped damage site and

carries out synthesis opposite the lesion and subsequent skipped bases (112). In the polymerase switching model, when a replicative polymerase stalls at a lesion, a TLS polymerase is recruited to the primer-template complex to synthesize past the lesion before a replicase switches back in to continue high-fidelity DNA replication (109,113). It is generally believed that the polymerase-switching model can occur with one TLS polymerase, or two TLS polymerases working in concert to bypass a lesion (114,115). In a single polymerase model, the PCNA clamp becomes monoubiquitinated by the Rad18/Rad6 complex post-stalling by the replicase, which recruits a TLS polymerase to the damage site (114). Subsequently, the replicative polymerase loses affinity for the primer-template complex. In the initial insertion step the TLS polymerase inserts a nucleotide opposite the lesion, followed by the adjacent base, referred to as the extension step (114). In a dual-polymerase model, one TLS polymerase performs insertion, and another TLS polymerase conducts the extension. After successful lesion bypass, the PCNA clamp becomes de-ubiquitinated and the TLS polymerase disengages from the template, allowing the replicative polymerase to bind the primer-template complex and continue with high-efficiency DNA replication (111). This form of damage tolerance is crucial for cell survival, yet has the propensity to introduce mutations into the genome (116).

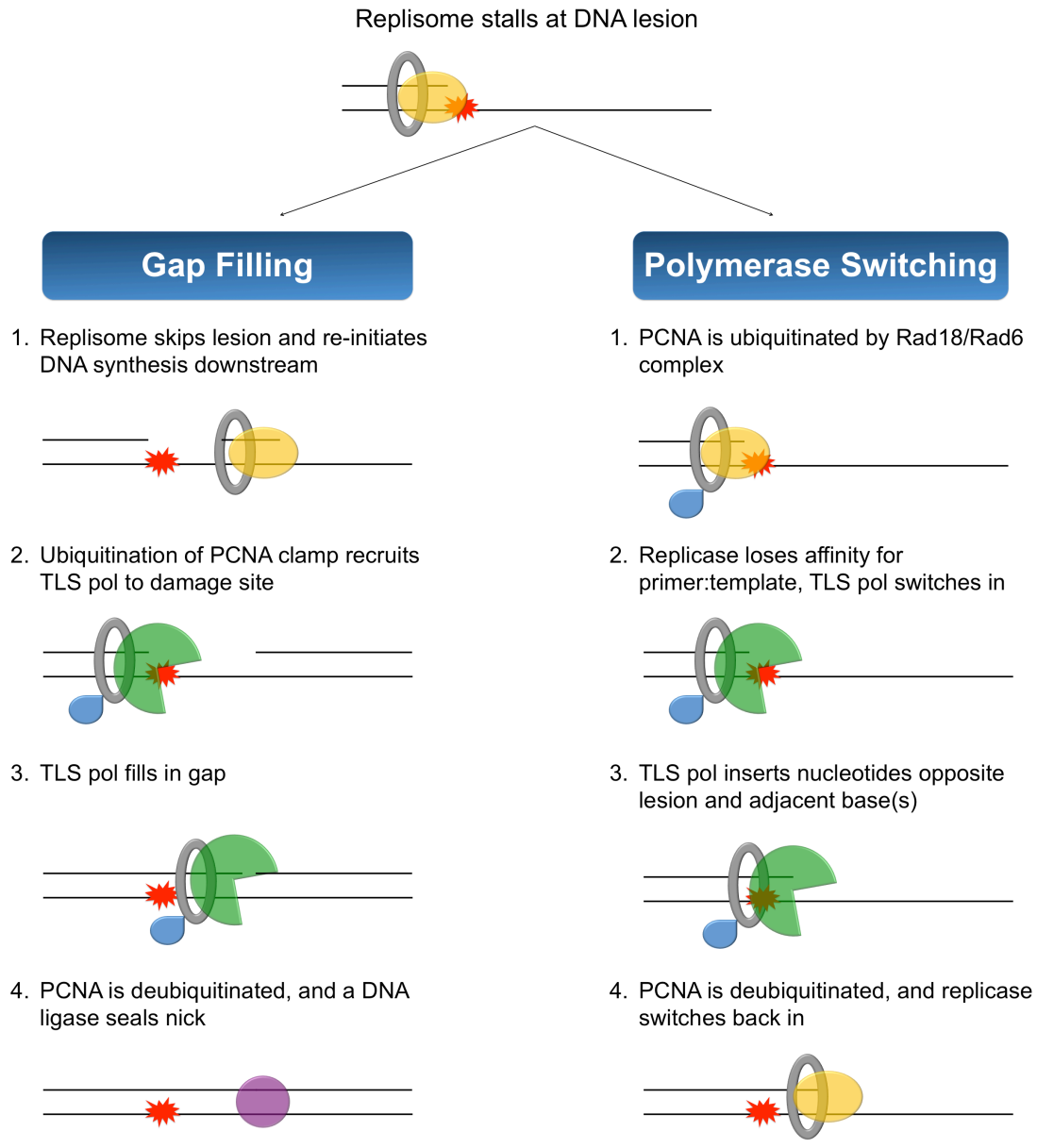

Figure 1.3. Representation of the gap-filling and polymerase switching models of translesion synthesis

1.4.2. Post-translational Modifications of PCNA at the Replication Fork

Modifications on the PCNA clamp are responsible for coordinating the response to stalled replication forks. PCNA can be mono- and polyubiquitinated, mono- and poly-, as well as SUMOylated to recruit other proteins to the stalled replisome, including those involved in TLS and homologous recombination (HR) (117). TLS is primarily regulated by the monoubiquitination of lysine 164 (K164) residue on PCNA during the S-phase, though it has been shown to extend into G_2/M as well (118,119). Ubiquitin (Ub) conjugation to PCNA occurs via an ATP-dependent, 3-step mechanism, in which it is first activated by an ubiquitin activating enzyme (Uba), then transferred to the ubiquitin conjugating enzyme, Rad6, which complexes with a ubiquitin ligase, Rad18, to catalyze the Ub protein transfer to K164. Rad18 possesses a Rad6-binding domain (R6BD) at residues 340-395, as well as a RING domain at the N-terminus, which facilitate tight binding with Rad6 (120-124). The monoubiquitination of PCNA has been detected following cellular exposure to a range of damaging agents, including BPDE, methyl methanesulfonate (MMS), hydroxyurea, and UV-radiation (125-127). Ubiquitinated PCNA (Ub-PCNA) can then interact with TLS polymerases, including Pols η, ι, κ, and ζ, which perform lesion bypass, the mechanism of which is discussed in 4.2. The importance of the monoubiquitination on PCNA for lesion bypass is evolutionarily conserved from yeast to humans, and was demonstrated in budding yeast and chicken DT40 B cell line through mutation of the ubiquitin binding site (K164R), which resulted in elevated sensitivity to DNA damaging agents, including MMS, cisplatin, UV-light, and γ-radiation (128,129). Once the lesion has been replicated by the TLS polymerase(s),

PCNA can be de-ubiquitinated through the action of ubiquitin-specific peptidase 1 (USP1), which cleaves the Ub moiety from PCNA (130). PCNA can also be polyubiquitinated, in which Ub on K164 of PCNA is extended by the addition of subsequent Ub moieties linked together by each K63 residue, which is thought to play roles in template switching and replication fork restart, though its exact biological functions are still unknown (131,132).

1.4.3. Protein-Protein Interactions

PCNA-TLS Polymerases

The switching between the replicative and TLS polymerases at the damaged primer termini heavily relies on interactions between TLS Pols and the PCNA sliding clamp. One such site of binding is a conserved PCNA interacting protein (PIP) domain, which has been demonstrated at the C-termini of Pol η, Pol ι, and Pol κ, as well as in the accessory subunit Pol32 of the four-subunit Pol ζ (133-137). This PIP box motif interacts specifically with the interdomain connector loop of unmodified PCNA and is thought to facilitate TLS Pol recruitment to the replication complex, though this domain does not aid in processivity or replication of a damaged site (133-137). The Rev1 protein does not possess this PIP box motif, yet it has a BRCA1 C-terminal (BRCT) domain that can interact with PCNA and enhance the recruitment of Rev1 to the stalled replication complex (138,139). While the PIP and BRCT domains allow direct binding to PCNA, TLS Pols also possess ubiquitin-binding domains (UBDs) at the C-terminus (140). UBDs, which include ubiquitin-binding motifs (UBMs) and ubiquitin-binding zinc finger

(UBZ) domains, allow TLS polymerases to tightly bind the ubiquitin moiety on PCNA and confer enhanced processivity and bypass of damaged bases (140,141). Both Pol ι and Rev1 contain UBMs, whereas TLS Pols η and κ possess UBZs which differ from UBMs in the presence of a zinc finger in the binding site (140). These domains permit interaction specifically with Ub-PCNA, and are crucial for regulating lesion bypass activity.

Rev1-TLS Polymerases

While it is maintained that Rev1 possesses some catalytic activity, including replication of abasic sites, it also interacts with other TLS polymerases and plays a crucial role as a scaffold for polymerase binding to the primer-template complex (142-144). A comprehensive study by Friedberg and colleagues (143) indicated that the mouse Rev1 protein could interact with Pols η, ι, and κ, as well as Rev7, a subunit of Pol ζ. This interaction relies on the contact between a 100 amino acid stretch of residues at the C-terminus of Rev1, and Rev1-interacting region (RIR) motifs on Pols η, ι, and κ, or the Rev1-C-terminal (Rev1-CT) binding site on Rev7 (143,145,146). It has also recently been shown that Rev1 can bind Pol η and Rev7 simultaneously (142). This is particularly exciting as it implies that Rev1 can serve as a binding platform and load both Pol η, which inserts opposite the lesion, and Pol ζ, which could seamlessly extend past the damaged base (142). This is possible because Pol ζ, a common extender in TLS, does not occupy the RIR binding site on Rev1 like the traditional inserter Pols η, ι, and κ

(142). In this regard, Rev1 is an important TLS expediter at damaged sites and may coordinate the polymerase response.

PCNA-Spartan (C1orf124)

A novel protein termed Spartan has also been identified as a player in the orchestration of TLS by interactions with Ub-PCNA (147,148). Similar to the aforementioned TLS Pols, Spartan possesses a PIP box motif and UBZ binding motif, which allows the recognition of, and binding to, ubiquitinated PCNA, yet it also contains an SprT domain, which can bind POLD3, an accessory subunit of Pol δ (147,149). When Spartan recognizes Ub-PCNA, it co-localizes with Rad18 and promotes more efficient ubiquitination of the PCNA clamp, helping to enhance the damage response and promote more efficient ubiquitination of PCNA (147). Spartan can also recruit Pol η to damaged foci following UV irradiation (147,150). In this respect, it is proposed that Spartan may help regulate the polymerase switch at damage sites. This is supported by observations that Spartan can preferentially bind Pol δ prior to damage induction, then subsequently binds Pol η after UV-irradiation (150). A recent study has also implicated Spartan as a regulator of error-prone TLS, specifically in extension past UV-induced mutagenesis (149). Single or double knockdown of Spartan and POLD3 revealed that UV-induced mutagenesis was conferred by Pol δ in the absence of Spartan (149). Interestingly, knockdown of Rev1 and Rev7 (subunit of Pol ζ) in Spartan-depleted cells lessened the mutagenic potential, and Pol δ also more frequently associated with Rev7 (149). In this regard, it is an intriguing possibility that Spartan may also play a role in regulating error-prone TLS with Pols δ and ζ. While the exact mechanisms and extent of Spartan-

mediated TLS are unknown, it is certainly an exciting new player in the regulation of TLS at the replication fork.

1.5. Non-traditional Polymerases Involved in Lesion Bypass

There are a number of polymerases that have been implicated in possessing lesion bypass activity, most notably the Y-family DNA polymerases η, ι, κ, and Rev1, the B-family Pol ζ, the A-family Pol γ, and the newly discovered PrimPol of the AEP (archaeo-eukaryotic primase) family. Unlike the replicative polymerases, traditional TLS polymerases, including Pols η, ι, κ, ζ, and Rev1, typically are significantly less processive and accurate when replicating DNA, with the potential to induce mutations into the genome through error-prone lesion bypass (111,116,151,152). Most TLS polymerases are members of the Y-family, except for Pol ζ, a B-family polymerase generally thought to play a role as an extender in the dual polymerase model (151). The Y-family polymerases all possess PCNA interacting peptide (PIP) motifs and ubiquitin-binding domains known as ubiquitin-binding zinc fingers (UBZs) or ubiquitin-binding motifs (UBMs), which allow for direct interaction with the PCNA clamp and facilitate recruitment to the damage site (111). The polymerase association with ubiquitinated PCNA is essential for bypass function, and regulates the TLS process. All TLS polymerases also take advantage of a more spacious active site, due to the presence of an additional little finger domain (polymerase associated domain, PAD), to accommodate bulky lesions, but lack a 3'→5' proofreading exonuclease domain which prevents them from recognizing and excising misinsertions (111). However, there are notable

exceptions where TLS Pols play a crucial role in error-free bypass of common DNA lesions.

1.5.1. Polymerase η

Pol η is one of the most thoroughly studied polymerases of the Y-family. It is evolutionarily conserved from bacteria to humans, with close homology to Pol V, crucial for TLS in *Escherichia coli* (153,154). Pol V was first identified as UmuD'$_2$C, an error-prone polymerase operating in *E. coli* as part of the SOS response (153). It was later discovered that Pol V was a homologue for *RAD30* gene in *Saccharomyces cerevisiae*, which encodes Pol η, and is also found in humans (154,155). It is well documented that Pol η is the polymerase responsible for accurately and efficiently bypassing UV-light induced thymine-thymine cyclobutane pyrimidine dimers (TT-CPDs), since humans with defects in *POLH* (encoding Pol η) exhibit the xeroderma pigmentosum variant phenotype (XPV), which is characterized by sunlight sensitivity and the early onset of skin cancers (156-158). Subsequent X-ray crystal structures revealed that Pol η has the largest active site of the TLS polymerases, allowing the incorporation and stabilization of both linked thymines into the active site at once (159). Once incorporated into the active site, Pol η has a β-strand in the little finger domain that serves as a "molecular splint" and ensures that the primer:template complex remains contorted into the preferential B-form during lesion bypass, facilitating accurate replication (159). This β-strand also creates a consistent, positively charged surface, which increases contact with the DNA duplex and aids in the accuracy of replication by maintaining the reading frame (159). These unique

structural features render Pol η an attractive candidate for biochemical studies monitoring its accuracy and efficiency of nucleotide insertion opposite and past a variety of lesions.

In addition to the UV light-induced TT-CPDs, studies have shown that Pol η bypasses 8-oxoG, a common lesion generated under oxidative stress conditions, as well as the 1,2-intrastrand d(GpG)-cisplatin cross-link adduct induced during treatment with platinum-based chemotherapeutics, with similar accuracy and efficiency as a template guanine (111). Pol η also promotes mutagenic bypass of a number of lesions, including BPDE-induced adducts and alkylated lesions, such as O^4-methylthymidine (160,161). It has been shown that Pol η can be recruited to damaged replication foci through the protein Spartan, detailed in section 4.3.3, and there is also some evidence that phosphorylation of the Pol η protein upon UV irradiation may aid in localization to UV damaged sites, though the mechanisms for this are unclear (162). In addition to lesion bypass, it is alleged that Pol η may also play non-traditional roles in the cell, such as somatic hypermutation (163).

1.5.2. Polymerase ι

While multiple laboratories have tried to identify the major biological function of Pol ι, its cellular role remains enigmatic, largely because mice lacking Pol ι have no discernable phenotype (164). However, given its conservation throughout higher eukaryotes, it is clear that Pol ι must be advantageous to these organisms (151). Pol ι was first discovered as a homologue of *RAD30* gene in mouse and humans, termed *RAD30B* (165). One of the first reported major roles for Pol ι was 5'-deoxyribose

phosphate (dRP) lyase activity, which can excise dRP from an AP site and then fill the gap, implying a role in BER (166). Steady-state kinetic analyses showed that when filling the short gaps, Pol ι preferred to incorporate a G opposite template T (166). Interestingly, later the crystal structure of Pol ι bound to a DNA template with an incoming nucleotide was solved and it showed that Pol ι uses Hoogsteen base-pairing during replication, as opposed to traditional Watson-Crick base-pairing like most DNA polymerases (167). As a result, Pol ι preferentially inserts nucleotides opposite template purines, as opposed to pyrimidines (111). This is exemplified by efficient Pol ι-mediated replication of 8-oxoG and N^2-adducted-2'-deoxyguanosines, including the cyclic adduct γ-hydroxy-1,N^2-propano-2'-deoxyguanosine (γ-HOPdG) (168,169). Of the Y-family TLS Pols, Pol ι is largely considered the most error-prone, given the mutagenic replication of undamaged bases, particularly an incorrect G opposite a template T, which is remarkably more efficient than insertion of the correct A (170).

Genetic studies of inbred mice deficient in Pol ι have also pinpointed susceptibilities to lung tumor formation upon treatment with urethane, a potent carcinogen that induces the DNA lesions εG, εA, and εC (171-173). *In vitro* lesion bypass studies have determined the accuracy and efficiency of nucleotide incorporation by Pol ι opposite an array of DNA lesions including the above etheno-adducts, and found that Polι inserts the correct T opposite εA with relatively high efficiency, but promotes mutagenic bypass of εG (174,175). It is possible that Pol ι provides protection against lung tumorigenesis by promoting error-free replication of the major adducts generated by

pulmonary carcinogens. However, the mutagenic bypass of εG implies that Pol ι may curb tumorigenesis through some other mechanisms, perhaps unrelated to lesion bypass activity. While it appears that Pol ι may play a critical role in protecting against lung tumorigenesis, future studies are needed to substantiate this claim (171).

1.5.3. Polymerase κ

Pol κ is the only known TLS polymerase to be conserved through all domains of life, identified in archaea, bacteria, yeast, and humans (176,177). The Pol κ homologue in archaea is Dpo4 and in bacteria is Pol IV, also known as DinB (178). Similar to Pol ι, the biological role for Pol κ is not fully understood, though it has been demonstrated to play roles as both an efficient inserter and extender past exogenously- and endogenously-generated lesions, albeit with varying degrees of fidelity (111). Most notably, Pol κ has demonstrated proficiency in replicating the minor groove N^2-(1-carboxyethyl)-2'-deoxyguanosine (N^2-CEdG) adduct, along with a template BPDE-N^2-dG (179,180). Along these lines, mice deficient in Pol κ exhibit sensitivity to the carcinogenic BPDE, pointing to a possible role in protecting against polycyclic aromatic hydrocarbons (PAHs) found in tobacco smoke and other environmental sources (181). Pol κ is also capable of promoting extension past mismatched primer:templates, as well as interstrand cross-links, such as an adducted N^2-N^2-guanine interstrand crosslink (182,183). X-ray crystallography has provided structural insights into how Pol κ can function as such an efficient extender, and revealed a unique N-clasp, which allows Pol κ to form a ring

around the DNA substrate, fully enveloping and stabilizing the duplex during replication (180). This aids in bypass of helix-distorting lesions, such as minor-groove lesions, that normally disrupt binding toward replicative polymerases, with its importance particularly pronounced in structural studies depicting bypass of BPDE-N^2-dG adducts (181).

In addition to lesion bypass, it has been suggested that Pol κ may also play roles in cellular repair, including NER and strand break repair (184,185). *Polk*-deficient chicken DT40 cells and mouse embryonic fibroblasts (MEFs) displayed heightened sensitivity to UV irradiation, as well as dysfunctional NER activity (184,186). While it is traditionally believed that the replicative Pols δ or ε synthesize DNA across the gap generated in NER, this finding entertains the possibility that Pol κ may also function as a gap-filling polymerase in the NER pathway (184). *Polk*-deficient MEFs are also highly sensitive to H_2O_2 (185). Under these oxidative stress conditions, the *Polk*-deficient MEFs were also defective in both single-strand and double-strand break repair, implying a possible role of Pol κ in BER as well (185).

1.5.4. Polymerase ζ

The B-family Pol ζ is mainly considered an extender, with very little demonstrated ability to insert nucleotides opposite a range of damaged bases (152). This polymerase is found in both yeast and humans, as a 2-subunit, and 4-subunit complex, respectively (187-189). In humans, Pol ζ is composed of the catalytic Rev3 subunit, and accessory subunits Rev7, Pol31, and Pol32 (189). The Rev3/Rev7 complex is the minimum requirement for polymerase function, and until recently, the yeast Rev3/Rev7

homologue was the only available substrate for biochemical studies (189). With the recent purification of the human four-subunit complex (189), Pol ζ's lesion bypass activity can now be characterized using the human polymerase as opposed to the previous yeast homologues. Though Pol ζ is in the same family as the replicative Pols δ and ε, it lacks the 3'→5' proofreading activity, and exhibits the same low processivity as the other Y-family TLS polymerases (152). Pol ζ is highly capable of extending past mismatched primer:template termini and bulky DNA lesions, especially those that significantly distort the helical structure. These include Tg, TT-CPDs, 8-oxoG, O^6-methylguanine, and abasic sites (111). Pol ζ can also complement Pol η in bypass of cisplatin adducts, serving as an efficient extender past the intrastrand crosslinks, which ultimately poses a threat to the efficacy of cisplatin chemotherapy (108).

There have been several studies monitoring the importance of Pol ζ in cellular and murine models. It was recently detailed that *Rev3L*-inactivated MEFs, with Rev3L being the mammalian homologue of the catalytic subunit of Pol ζ in *S. cerevisiae* (187), were prone to senescence and apoptosis, as well as the accumulation of chromosomal abnormalities and double-strand breaks (190). This effect on cellular proliferation is unique to Pol ζ and has not yet been demonstrated with other TLS Pols (190). Several papers have confirmed that in mice, knockout of *Rev3L* is embryonic lethal, further highlighting the importance of Pol ζ in higher organisms (191-193).

1.5.5. Rev1

Rev1 is unique among the aforementioned TLS polymerases in that its main role does not appear to be a catalytic lesion bypass polymerase, but rather as a platform for the loading of TLS Pols onto the replication complex. Rev1 is conserved from yeast to humans, and even though it is a member of the Y-family, exhibits minimal synthetic ability (151,194,195). As the scaffold activity has been described above in section 1.4.3, this section will focus on the basis of Rev1's catalytic activity. Kinetic studies of Rev1-mediated nucleotide incorporation opposite the four nucleobases of DNA revealed that Rev1 solely incorporates a dCTP during replication, regardless of the template base (194-196). Consequently, Rev1 is relatively limited to dCTP insertion opposite guanine base lesions, though this can be accurate and efficient. This has been demonstrated in replicating the γ-HOPdG, 8-oxoG, and BPDE-N^2-dG adducts (197,198). Rev1 has also been shown to accurately and efficiently replicate an abasic site through dCTP insertion, with the implication that abasic sites are cognate lesions of Rev1 (144,199). Crystal structure analysis of the yeast Rev1 protein bound to a template G and complexed with an incoming dCTP revealed unique G-loop and N-digit features that provide a structural basis for Rev1 catalytic function (200). The N-digit, found at the N-terminus, is an α-loop addendum to an α-helix on the traditional little finger domain found in all Y-family TLS Pols (200). This N-digit then connects with the G-loop, a longer loop present in the little finger domain that can interact with the template G. For dCTP insertion opposite the G, Rev1 first flips out the template base through interactions with Leu^{325} in the N-digit, similar to the glycosylase base-flipping mechanism in BER (200). The incoming

dCTP, bound to Arg^{324} on the N-digit of Rev1, is then hydrogen bonded to the template G through this conserved residue (200).

1.5.6. Polymerase γ

Though not traditionally considered a TLS polymerase, Pol γ is the main polymerase known to function in mitochondrial DNA, and largely carries the burden for replicating past and repairing lesions that become embedded in the mitochondrial genome (201). Pol γ was first identified in HeLa cells, and later found to localize and function in the mitochondria (202,203). Unlike the Y-family TLS polymerases and B-family Pol ζ, Pol γ retains a 3'→5' exonuclease domain, allowing for proofreading of misincorporated bases (201,204). Similar to Pol ι, Pol γ also possesses dRP lyase activity, which allows it to function in gap-filling during BER of mitochondrial DNA (205,206). It is also remarkably more processive than other replicative and TLS polymerases, due in large part to a channel of positively charged residues, termed the K-tract (207). This K-tract assists in maintaining contacts with the negatively charged phosphodiester backbone of the DNA substrate, which improves replication accuracy and processivity (207). It has been demonstrated that Pol γ is essential for development, and *POLG* knockout mice are embryonic lethal (208). In this respect, several laboratories have recently begun to examine Pol γ's ability to perform TLS of DNA lesions, especially those that accumulate in the mitochondria during oxidative stress, or are produced endogenously during lipid peroxidation and normal aerobic metabolism (209). For example, acrolein is generated endogenously during lipid peroxidation, and generates the exocyclic DNA adducts γ-

HOPdG and γ-hydroxy-1,N^6-propano-2'-deoxyadenosine (γ-HOPdA). Pol γ was shown to direct highly mutagenic and inefficient bypass of these acrolein-derived lesions indicating these lesions are likely to be highly disruptive in mitochondrial DNA (209). On the other hand, Pol γ appears highly capable of performing efficient replication past TT-CPDs, though it has the potential to induce point mutations into the mitochondrial genome (210). Pol γ-mediated lesion bypass is still considered a relatively new research area, with many lesions pertinent to mitochondrial function remaining to be explored.

1.5.7. PrimPol

A recent report has identified a new translesion synthesis polymerase of the archaeo-eukaryotic primase (AEP) superfamily operating in the nucleus and mitochondria of human cells, dubbed PrimPol due to its dual primase and polymerase functions (211). Until recently, Pol α was thought to be the main primase in cells, which initiates DNA synthesis through the incorporation of ribonucleoside 5'- triphosphates (NTPs) that are subsequently removed from the newly synthesized DNA strand (212,213). PrimPol is unique in that it is able to prime DNA synthesis using both NTPs and dNTPs (211). It is also able to efficiently extend the primed template strand up to 7kb, an exclusive function to PrimPol (211). This new primase/polymerase appears to aid Pol γ in TLS of damaged bases, specifically the oxidatively generated 8-oxoG and abasic sites (211). It is well established that BER and oxidative damage of mitochondrial DNA (and nuclear DNA) results in the generation of abasic sites. It was previously believed that Pol γ was solely responsible for replicating these damaged sites; however,

PrimPol can efficiently insert the correct dCTP opposite 8-oxoG, though it may also generate point mutations in mtDNA through the misincorporation of dATP (211). Along these lines, PrimPol also inserts nucleotides opposite and past an abasic site with much greater efficiency than Pol γ (211). In this regard, PrimPol may function as a TLS polymerase operating in the polymerase-switching model to replicate lesions in both nuclear and mitochondrial DNA. PrimPol has also been implicated as a regulator of the replication fork (214). This is with observation that *PrimPol*-deficient chicken DT40 cells are highly sensitive to UV-irradiation and accumulate stalled replication forks, indicating PrimPol's importance for replication fork progression (214). This may occur via the replication of the DNA photoadducts, including [6-4]-PPs and TT-CPDs, though this has not been established and may occur through another mechanism.

Another enticing role for PrimPol in cells may be in the postreplication repair pathway of TLS. In the postreplication repair pathway, the replicase skips the lesion site and reassociates with the primer-template downstream, after which a TLS Pol is recruited to the stalled replication foci to bypass the lesion (111). It has recently been shown that PrimPol is also capable of priming DNA at stalled replication forks induced by UV damage, and promoting TLS of the replication blocking CPDs (215). Though it is still unclear how extensive a role PrimPol plays in bypass of mitochondrial and nuclear DNA adducts, especially given that *PrimPol*-deficient mice are viable and have no discernable phenotype (211), it is clearly an exciting new target for biochemical studies that could have major implications in human health.

1.6. TLS Polymerases and Cancer

The mutagenic bypass of damaged bases by non-traditional polymerases, such as the TLS Pols η, ι, κ, ζ, and mitochondrial Pol γ, has the potential to induce mutations into the genome and contribute to the etiology of a host of human diseases, including cancer, neurodegeneration, accelerated aging, and mitochondrial disorders (152). In this respect, it is critical to understand the mutagenic potential of lesions when bypassed by various TLS polymerases. However, even error-free bypass of DNA lesions can be problematic, such as that of damaged sites generated by chemotherapeutic agents (216,217). Platinum-based chemotherapy drugs, e.g. cisplatin, are commonly used to treat a number of carcinomas, including lung and ovarian cancers, as well as lymphomas and germ cell tumors (218). After administration, the platinum atom can bind to DNA, preferentially the guanine base, and generate DNA inter- and intrastrand cross-linking in cancer cells, which activates apoptotic pathways following ineffective repair (218). However, cisplatin-adducts, including the most commonly induced 1,2-intrastrand d(GpG) adduct, are cognate lesions for Pol η, which facilitates accurate and efficient bypass, compromising the therapeutic benefits in cancer patients (217,219,220). Recent interest has turned to developing an inhibitor for Pol η that could be administered in conjunction with platinum-based chemotherapies, substantially improving the efficacy of treatment (221). Along these lines, another potential drug targets includes the TLS Pol ζ, which can efficiently extend from interstrand cross-link adducts, including those generated by cisplatin, de-sensitizing the cells to treatment (183,216). A recent study inhibited *REV3*

expression in a mouse xenograft model, the catalytic subunit of Pol ζ, and reported increased sensitivity to cisplatin therapies in chemoresistant adenocarcinomas (222).

TLS polymerases may prove to be valuable drug targets in their own right as well, as seen in recent research on Pol ι. Genetic mapping of inbred mice treated with urethane, a potent pulmonary carcinogen that generates etheno adducts, revealed that the resistance to lung tumorigenesis lies on the distal chromosome 18 and can be attributed to a locus designated as pulmonary adenoma susceptibility 2 (*Par2*) (172,173). Of the genes encoded in the *Par2* locus, the most convincing is *Poli*, and recent studies have shown that mice lacking Pol ι are susceptible to lung tumors, thereby pointing to a protective role for Pol ι against lung tumorigenesis (171). It remains unseen whether Pol ι curbs lung tumor progression through error-free bypass of DNA lesions, or possibly by preventing other error-prone polymerases from bypassing urethane-induced adducts. The mechanism by which Pol ι confers resistance to lung tumor formation could give rise to more effective lung cancer treatment strategies that specifically target Pol ι.

Pol κ is also an intriguing drug target, specifically in the treatment of gliomas. Pol κ bypass of interstrand crosslinks (ICLs) may also interfere with efficacy of therapeutics, specifically mitomycin C, a common chemotherapy drug that generates ICLs (223). It was shown that Pol κ knockdown resulted in decreased cell survival and chromosomal stability following mitomycin C treatment, pointing to Pol κ as the main polymerase responsible for tolerating N^2-N^2-guanine ICLs (223). Along these lines, gliomas, a type of aggressive brain cancer, are resistant to numerous chemotherapeutics,

but is often treated with temozolomide, which functions to methylate DNA at the *N*3 position of adenine, and *N*7 or O^6 positions of guanine to initiate futile-cycle MMR (224). Elevated levels of Pol κ have been detected in glioma patients, and are correlated with decreased prognosis (225). Resultingly, Pol κ is an attractive candidate for an inhibitor that could be delivered in conjunction with glioma therapy that may render treatment more effective. A study by Lloyd and coworkers (226) recently outlined a strategy for developing Pol κ inhibitors, which could be crucial in the ultimate development of more effective treatments for gliomas and other chemotherapy-resistant cancers. There are no current targeted therapies for TLS polymerases commercially available, yet the framework is in place for development, and they remain attractive candidates for use alone or in conjunction with existing chemotherapeutics.

1.7. Scope of Dissertation

Chapter 2 focuses on the bypass of diazoacetate-induced carboxymethylated lesions by the *Saccharomyces cerevisiae* Pol η. It had previously been shown that XPV cells exhibited hypersensitivity to azaserine, which induces carboxymethylation of DNA (227). As a result we were highly interested in whether Pol η may play a role in bypass of carboxymethylated adducts, including N^6-CMdA, N^4-CMdC, *N*3-CMdT, and O^4-CMdT. I monitored the kinetics of Pol η-mediated nucleotide insertion opposite the lesions and their adjacent base, as well as the ability to extend the primer terminus past the damaged bases. I found that Pol η promotes error-free bypass of N^6-CMdA, while generating misinsertions opposite N^4-CMdC, *N*3-CMdT, and O^4-CMdT (228). The high

misincorporation of dGMP opposite both *N*3-CMdT and O^4-CMdT are consistent with diazoacetate-induced T→C mutations in human *p53* gene observed in gastrointestinal tumors (52,228). These studies suggest that Pol η may play a role in the etiology of gastrointestinal cancers through error-prone lesion bypass.

The focus of Chapter 3 is to monitor the accuracy and efficiency of nucleotide insertion opposite and past the oxidatively-induced cyclopurine lesions by the TLS Pol η. These lesions are known blocks to DNA replication, and are implicated in the development of human diseases such as neurodegeneration, cancer, and aging (60). I characterized the kinetics of nucleotide insertion opposite the 5'*S* diastereomers of cdA and cdG, as well as the adjacent base (229,230). I used primer extension and steady-state kinetic assays to examine the efficiency and fidelity for Pol η to insert nucleotides opposite, and extend primer past, these cyclopurine lesions. I found that *Saccharomyces cerevisiae* (yeast) and human Pol η inserted 2'-deoxynucleotides opposite *S*-cdA, *S*-cdG, and their adjacent 5' nucleosides at fidelities and efficiencies that were similar as their respective undamaged nucleosides. Moreover, the yeast enzyme exhibited similar processivity in DNA synthesis on templates housing an *S*-cdA or *S*-cdG as those carrying an unmodified dA or dG; the human polymerase, however, dissociated from the primer-template complex after inserting one or two additional nucleotides after the lesion. Pol η's accurate and efficient bypass of *S*-cdA and *S*-cdG indicate that this polymerase may be responsible for error-free bypass of these lesions, whereas other TLS polymerases may introduce mutations into the genome. Together, my results suggested that Pol η may

have an additional function in cells, i.e., to alleviate the cellular burden of endogenously induced DNA lesions, including *S*-cdA and *S*-cdG.

Chapter 4 builds upon my work monitoring the Pol η-mediated bypass of the *S*-cdA and *S*-cdG lesions. My *in vitro* biochemical assays discussed in Chapter 3 suggested a role for human Pol η in the insertion step of translesion synthesis (TLS) across the (5'*S*) diastereomers of cdA and cdG (229). In order to determine if any other TLS Pols played a role in bypassing *S*-cdA and *S*-cdG, I monitored kinetics of nucleotide insertion opposite the cyclopurine lesions, as well as the adjacent two bases downstream using the TLS Pols ι, κ, and ζ. Using *in vitro* steady-state kinetic assay, I found that human Pol ι and a two-subunit yeast Pol ζ complex (REV3/REV7) could function efficiently in the insertion and extension steps, respectively, of TLS across *S*-cdA and *S*-cdG; human Pol κ and Pol η could also extend past these lesions, albeit much less efficiently (230). Results from a quantitative TLS assay showed that, in human cells, *S*-cdA and *S*-cdG inhibited strongly DNA replication and induced substantial frequencies of mutations at the lesion sites (230). Additionally, Pol η, Pol ι, and Pol ζ, but not Pol κ, had important roles in promoting replication through *S*-cdA and *S*-cdG in human cells. Based on these results, we propose a model for TLS across *S*-cdA and *S*-cdG in human cells, where Pol η and/or Pol ι carries out nucleotide insertion opposite the lesion, whereas Pol ζ executes the extension step.

Chapter 5 discusses the erroneous bypass of ribonucleotides embedded in DNA by TLS Pols η, ι, κ, and ζ. It has been shown that ribonucleotides are frequently misincorporated into the genome by replicative polymerases, posing a severe threat to

genomic stability. Translesion synthesis was shown to play a possible protective role in tolerating ribonucleotides in yeast; however, the mechanism for this is unknown. I performed steady-state kinetic assays to monitor kinetics of nucleotide insertion opposite a single ribonucleotide embedded in a DNA template, and demonstrated that Pol ζ can perform accurate and efficient insertion, whereas ribonucleotides direct significant misincorporations in Pols η- and κ-mediated replication. Interestingly, rC directed the most significant misincorporations by each TLS polymerase and was also the most blocking. This work sheds light on the mutagenic potential of ribonucleotides when erroneously incorporated into DNA.

Chapter 6 addresses how Pol γ replicates ethylated thymidine lesions that can be stably generated in mitochondrial DNA following exposure to a wide range of genotoxic chemicals, including those found in tobacco smoke, and are known to be both mutagenic and carcinogenic (161,231,232). Mitochondrial DNA is more susceptible to alkylation than nuclear DNA, and it has previously been shown that O^4-EtdT is poorly repaired in the mitochondrion, exacerbating the need to understand how Pol γ may replicate this, and other ethylated thymidine lesions, including O^2-EtdT and *N*3-EtdT (233,234). I performed steady-state kinetic assays monitoring the accuracy and efficiency of nucleotide insertion opposite O^2-EtdT, O^4-EtdT, and *N*3-EtdT, as well as excision assays to characterize whether the lesions may be substrates for Pol γ's proofreading activity. I found that O^2- and *N*3-EtdT, but not O^4-EtdT, were strongly blocking to Polγ, with all three lesions directing substantial frequencies of nucleotide misincorporation. Excision assays also showed that the proofreading activity of Polγ was incapable of effectively

removing the misincorporated nucleotides. This work suggests that the EtdT lesions may contribute significantly to genome instability in mitochondria.

Chapter 2: *In vitro* Replication Studies of Carboxymethylated DNA Lesions with *Saccharomyces cerevisiae* Polymerase η

Introduction

Normal metabolic activities and environmental factors can cause DNA damage, which can result in up to one million molecular lesions per cell per day (235). These lesions, such as nucleobase modifications, strand breaks, and cross-link lesions, can induce single-base substitutions, frameshifts, and deletions into the genome, affecting the cell's ability to replicate its DNA, transcribe genes, stimulate apoptosis, and regulate cell division (236,237). To counteract the deleterious effects of DNA lesions, cells are equipped with various DNA damage response pathways, including a battery of DNA repair pathways and translesion synthesis (TLS) (238,239). TLS is a type of damage tolerance that provides a way to replicate past potentially harmful DNA lesions as opposed to repairing them (236,239,240). This prevents long-term blockage of replication fork and ensures continuing DNA replication (236,239,240). This pathway is critical for maintaining replication fork progression and increasing cell survival.

TLS DNA polymerases, many of which belong to the Y-family, are a group of specialized DNA polymerases which can bypass DNA damage by facilitating nucleotide insertion opposite damaged bases and enabling extension past the damage site (239,241). The insertion and extension steps often involve different polymerases, though the same polymerase may be responsible for both steps (242). These polymerases typically have larger active sites than traditional replicative polymerases which allow them to

accommodate erroneous base pairs and bulky DNA lesions (243). Consequently, TLS polymerases often lack the efficiency and fidelity of replicative polymerases (239), though in some instances the nucleotide incorporation mediated by these polymerases opposite DNA lesions can be both accurate and efficient (155,244,245). Among the Y-family polymerases, polymerase η (Pol η) is capable of bypassing a variety of DNA lesions (243). The predominant established cellular role of Pol η involves bypassing, with high efficiency and accuracy, thymine-thymine cyclobutane pyrimidine dimers (CPDs) that accumulate following exposure to UV light (156,246). The importance in bypassing these dimers is pronounced in those with XPV syndrome, as these patients lack a functional Pol η and exhibit a dramatic increase in susceptibility to developing skin tumors (156,246,247). In addition to replicating across CPDs with high efficiency and accuracy, Pol η is also capable of bypassing a broad spectrum of other DNA lesions with varying degrees of efficiency and fidelity (243).

N-nitroso compounds (NOCs) cause damage to DNA and are both mutagenic and carcinogenic (248,249). Humans are exposed to NOCs both endogenously and exogenously through diet, tobacco smoke, and other environmental sources (250). Endogenous sources account for 45-75% of total NOC exposure, and an European Prospective Investigation into Cancer and Nutrition (EPIC) study revealed that NOC exposure is associated with elevated risk of developing non-cardia gastric cancer (44). Some endogenously formed NOCs could be converted metabolically to diazoacetate (46). A study by Gottschalg and coworkers (52) demonstrated that the replication of potassium diazoacetate (KDA)-treated, human *p53* gene-carrying plasmid in yeast cells could lead

to substantial single-base substitutions at both GC and AT base pairs. More importantly, the patterns of mutations induced by KDA at non-CpG sites resemble closely those found in *p53* gene of human stomach and colorectal cancers (52), indicating that diazoacetate may be an important etiological factor for the development of human gastrointestinal cancers (52). Diazoacetate could induce carboxymethylation and, to a lesser extent, methylation of DNA (46); nevertheless, the mutation spectrum induced by KDA differs markedly from that induced by a methylating agent, suggesting that carboxymethylation is the major source for KDA-induced mutations (52). The known carboxymethylated DNA lesions include N7-carboxymethylguanine (N7-CMGua), O^6-carboxymethyl-2'-deoxyguanosine (O^6-CMdG), N^6-carboxymethyl-2'-deoxyadenosine (N^6-CMdA), N^4-carboxymethyl-2'-deoxycytidine (N^4-CMdC), *N*3-carboxymethylthymidine (*N*3-CMdT), and O^4-carboxymethylthymidine (O^4-CMdT) (46,47,50,51,251,252).

In the present study, we examined how four site-specifically inserted, carboxymethylated DNA lesions previously synthesized by our laboratory, which include N^6-CMdA, N^4-CMdC, *N*3-CMdT, and O^4-CMdT (Structures depicted in Figure 2.1) (50,51), perturb DNA replication by hindering yeast Pol η and inducing mutations. We chose Pol η for the present study based on a previous observation that the growth of human lymphoblastoid cells deficient in XPV gene, which encodes human Pol η (156), was inhibited substantially upon treatment with 10-20 μM azaserine, a DNA carboxymethylating agent (251). We assessed, by using steady-state kinetic assay, the efficiency and fidelity of yeast Pol η to incorporate nucleotides opposite the four carboxymethylated DNA lesions and to extend past these lesions.

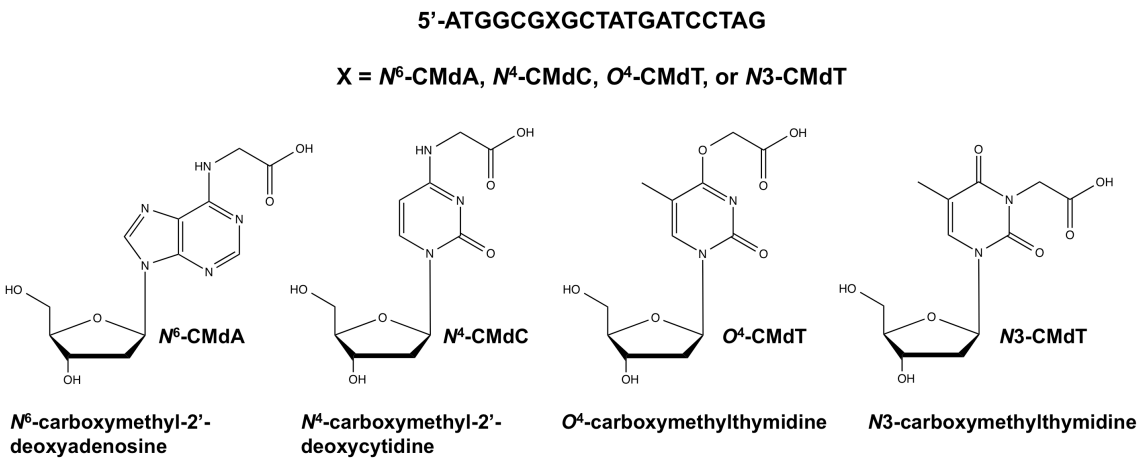

Figure 2.1. Structures of the four carboxymethylated nucleosides, N^6-CMdA, N^4-CMdC, *N*3-CMdT, and O^4-CMdT, as well as the 20mer sequence of the lesion-containing substrates used for the *in vitro* replication studies.

Materials and Methods

Materials

All unmodified oligodeoxyribonucleotides (ODNs) were purchased from Integrated DNA Technologies (Coralville, IA), and [γ-^{32}P]ATP was acquired from Perkin-Elmer (Boston, MA). *Saccharomyces cerevisiae* DNA polymerase η (Pol η) was expressed and purified following previously published procedures (253,254). The Bio-Rad Protein Assay kit (Bio-Rad, Hercules, CA) was used to quantify the concentration of Pol η, and enzyme purity was confirmed to be ~95% based on SDS-PAGE analysis. All other enzymes used in this study were purchased from New England BioLabs (Ipswich, MA).

Preparation of Lesion-containing Substrates

ODNs carrying carboxymethylated 2'-deoxyribonucleoside derivatives were previously synthesized (50,51). The 12mer lesion-bearing substrates, d(ATGGCGXGCTAT) [X represents an N^6-CMdA, N^4-CMdC, or O^4-CMdT] were ligated with the 5'-phosphorylated d(GATCCTAG) in the presence of a template ODN, d(CCGCTCCCTAGGATCATAGCYCGCCAT) (Y is a dT, dG, or dA), using previously described procedures (255). The resultant lesion-bearing 20mer substrates were purified using 20% denaturing polyacrylamide gel electrophoresis (PAGE). Purity and identities of the substrates were further confirmed by PAGE and LC-MS/MS analysis. The corresponding 20mer *N*3-CMdT-containing substrate was synthesized in our previous study (51).

Primer Extension Assay

The 20mer lesion-containing ODNs or the corresponding unmodified ODNs (0.05 μM) were annealed with a 5'-^{32}P-labeled 13mer primer (0.05 μM), by heating to 95°C and cooling slowly to room temperature. A mixture of all four dNTPs (250 μM each) and yeast Pol η (concentrations indicated in Figure 2.2 and Appendix Figure C.1) were added to the duplex mixture. The reaction was carried out under standing-start conditions in the presence of a buffer containing 10 mM Tris-HCl (pH 7.5), 5 mM $MgCl_2$, and 7.5 mM dithiothreitol (DTT) at 37°C for 1 hr. The reaction was terminated with an equal volume of formamide gel-loading buffer (80% formamide, 10 mM EDTA, pH 8.0, 1 mg/mL xylene cyanol, and 1 mg/mL bromophenol blue). The products were resolved on 20% denaturing polyacrylamide gels with 8 M urea, and gel-band intensities were quantified using a Typhoon 9410 Variable Mode Imager (Amersham Biosciences Co.).

Steady-state Kinetic Measurements

Steady-state kinetic assays were performed following previously published procedures (256). The ^{32}P-labeled primer-template complex (0.05 μM, produced using procedures described in primer extension assay) was incubated with yeast Pol η (1.2 nM) at 37°C for 10 min in the presence of individual dNTPs at various concentrations indicated in Figures 2.3-2.4 and Appendix Figures A.2-A.4. The reaction was terminated with an equal volume of formamide gel-loading buffer used in the primer extension assay. Extension products were separated on 20% denaturing polyacrylamide gels containing 8 M urea. Gel-band intensities of the primer and its extension products were quantified using a Typhoon 9410 Variable Mode Imager and ImageQuant 5.2 Software

(Amersham Biosciences Co.). The concentration of dNTP was optimized to allow for less than 20% nucleotide incorporation. The kinetic parameters, V_{max} and K_m, for the incorporation of incorrect and correct nucleotides were determined by plotting the observed rate of nucleotide incorporation (V_{obs}) as a function of dNTP concentration using non-linear curve regression with Origin 6.0 (OriginLab, Northampton, MA). The data was then fit with the Michaelis-Menten equation:

$$V_{obs} = \frac{V_{max} \times [dNTP]}{K_m + [dNTP]}$$

The k_{cat} values were calculated by dividing the V_{max} with the concentration of Pol η used. The efficiency of nucleotide incorporation was calculated by the ratio of k_{cat}/K_m and frequency of nucleotide misincorporation (f_{inc}) and frequency of extension (f_{ext}) were determined based on the following equations:

$$f_{inc} = \frac{(k_{cat} / K_m)_{incorrect}}{(k_{cat} / K_m)_{correct}}, \text{ for insertion step; and } f_{ext} = \frac{(k_{cat} / K_m)_{incorrect}}{(k_{cat} / K_m)_{correct}}, \text{ for extension step.}$$

Results

To understand how the carboxymethylated lesions N^6-CMdA, N^4-CMdC, *N*3-CMdT, and O^4-CMdT are recognized by yeast Pol η, we prepared 20mer ODN substrates containing these lesions at defined sites as previously described (50,51), and examined the effect of these lesions on the fidelity and efficiency of DNA replication by using primer extension and steady-state kinetic assays.

Primer Extension across N^6-CMdA, N^4-CMdC, N3-CMdT, and O^4-CMdT with Yeast Pol η

We first performed primer extension assays to assess the ability of yeast Pol η to extend a 13mer primer in the presence of 20mer DNA templates containing a site-specifically inserted N^6-CMdA, N^4-CMdC, *N*3-CMdT, O^4-CMdT and the corresponding unmodified nucleosides. The primer extension results indicate that, in the presence of all four dNTPs, yeast Pol η can bypass successfully N^6-CMdA and N^4-CMdC, as well as generate full-length products (Figure 2.2a,b). However, N^4-CMdC was much more difficult for yeast Pol η to bypass than N^6-CMdA, which is manifested by the presence of significant amount of unextended primer (Figure 2.2b). On the other hand, yeast Pol η is extremely hindered by *N*3-CMdT and O^4-CMdT, only generating extension products up to three nucleotides past the lesion (Figure C.1); no full-length extension product(s) could be detected.

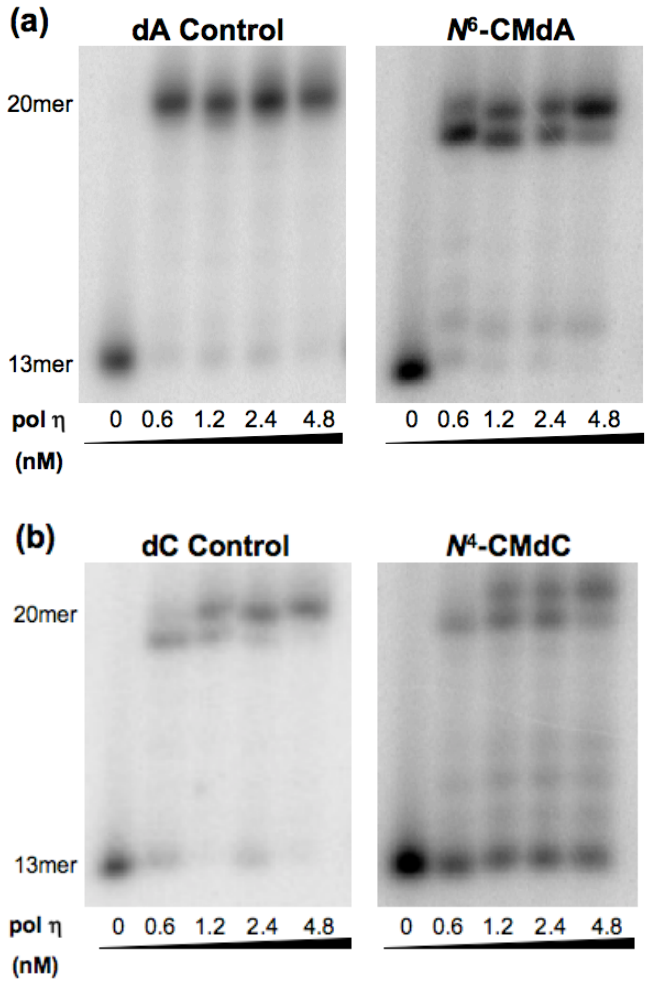

Figure 2.2. Primer extension assays opposite the (a) N^6-CMdA and (b) N^4-CMdC lesions and corresponding controls with yeast polymerase η in the presence of all four dNTPs [250 μM each]. The products were resolved with 20% denaturing polyacrylamide gels.

Steady-state Kinetic Analyses of Yeast Pol η-mediated Nucleotide Insertion opposite N^6-CMdA, N^4-CMdC, N3-CMdT, and O^4-CMdT

We next employed steady-state kinetic assays to measure the kinetic parameters for nucleotide incorporation by yeast Pol η opposite the four carboxymethylated DNA lesions, and unmodified dA, dC, and dT (see Experimental Procedures, and representative gel images are shown in Figure 2.3 and A.2).

Significant differences were found in the accuracy and efficiency of nucleotide insertion opposite the four carboxymethylated DNA lesions. Yeast Pol η preferentially incorporated the correct nucleotide, dTMP, opposite N^6-CMdA, at an efficiency that is ~87% of that for dTMP incorporation opposing unmodified dA (Table 2.1). Misinsertion of dAMP, dCMP, and dGMP opposite N^6-CMdA occurred at very low frequencies (0.075%, 0.44%, and 0.84%, respectively). By contrast, yeast Pol η substantially misincorporated dCMP (132%, relative to the correct dGMP insertion) and dAMP (31%) opposite N^4-CMdC (Table 2.1). Efficiency for the correct dGMP incorporation opposite N^4-CMdC is also ~7 fold lower than that for the corresponding insertion opposite undamaged dC. Additionally, nucleotide insertion across *N*3-CMdT and O^4-CMdT occurred with compromised efficiency, which was accompanied with substantial misincorporation of dGMP (Table 2.1). Yeast Pol η incorporates dGMP ~80 times more efficiently than dAMP opposite O^4-CMdT, and a 1.3-fold higher efficiency in dGMP than dAMP insertion opposite *N*3-CMdT was observed. Yeast Pol η also incorporates dTMP and dCMP opposite O^4-CMdT and *N*3-CMdT, though at efficiencies lower than that for the corresponding insertion of the correct dAMP (Table 2.1).

Table 2.1. Steady-state kinetic parameters for *S. cerevisiae* Pol η-mediated nucleotide incorporation opposite N^4-CMdC, N^6-CMdA, *N*3-CMdT, and O^4-CMdT, as well as opposite unmodified dA, dC, and dT[a]

dNTP	k_{cat} (min^{-1})	K_m (μM)	k_{cat}/K_m ($\mu M^{-1}min^{-1}$)	f_{inc}
		N^4-CMdC-containing substrate		
dTTP	12 ± 1	93 ± 7	0.13 ± 0.05	6.4×10^{-2}
dGTP	14 ± 1	7 ± 1	2.0 ± 0.2	1
dCTP	14 ± 1	5.1 ± 0.5	2.6 ± 0.2	1.3
dATP	15 ± 1	25 ± 2	0.62 ± 0.08	0.31
		dC-containing substrate		
dTTP	20 ± 1	470 ± 40	0.045 ± 0.005	1.9×10^{-3}
dGTP	24 ± 0.2	1.0 ± 0.06	24 ± 0.9	1
dCTP	10 ± 1	120 ± 10	0.082 ± 0.001	3.5×10^{-3}
dATP	N/A	N/A	N/A	N/A
		N^6-CMdA-containing substrate		
dTTP	16 ± 1	0.50 ± 0.07	32 ± 4	1
dGTP	8.7 ± 0.7	33 ± 2	0.27 ± 0.04	8.4×10^{-3}
dCTP	19 ± 2	130 ± 20	0.14 ± 0.01	4.4×10^{-3}
dATP	13 ± 1	540 ± 40	0.024 ± 0.002	7.5×10^{-4}
		dA-containing substrate		
dTTP	15 ± 1	0.41 ± 0.01	37 ± 4	1
dGTP	8.2 ± 0.5	210 ± 20	0.039 ± 0.001	1.1×10^{-3}
dCTP	40 ± 3	400 ± 30	0.089 ± 0.002	2.5×10^{-3}
dATP	10 ± 1	310 ± 13	0.033 ± 0.001	8.7×10^{-4}
		***N*3-CMdT-containing substrate**		
dTTP	13 ± 1	87 ± 6	0.15 ± 0.01	0.4
dGTP	11 ± 1	23 ± 2	0.48 ± 0.03	1.3
dCTP	5.2 ± 1	63 ± 5	0.083 ± 0.008	0.2
dATP	13 ± 1	35 ± 3	0.38 ± 0.02	1
		O^4-CMdT-containing substrate		
dTTP	11 ± 1	260 ± 30	0.043 ± 0.003	0.57
dGTP	11 ± 1	1.8 ± 0.2	6.1 ± 0.8	84
dCTP	7.1 ± 1	280 ± 20	0.025 ± 0.002	0.35
dATP	14 ± 1	200 ± 15	0.072 ± 0.003	1
		dT-containing substrate		
dTTP	N/A	N/A	N/A	N/A
dGTP	28 ± 2	20 ± 2	1.4 ± 0.01	2.5×10^{-3}
dCTP	43 ± 2	35 ± 3	1.3 ± 0.02	2.3×10^{-3}
dATP	78 ± 4	0.16 ± 0.01	490 ± 20	1

[a] k_{cat} and K_m values based on three independent measurements
'N/A' indicates data not available, where no nucleotide incorporation was detected even when high concentrations of dNTP was used (2 mM).

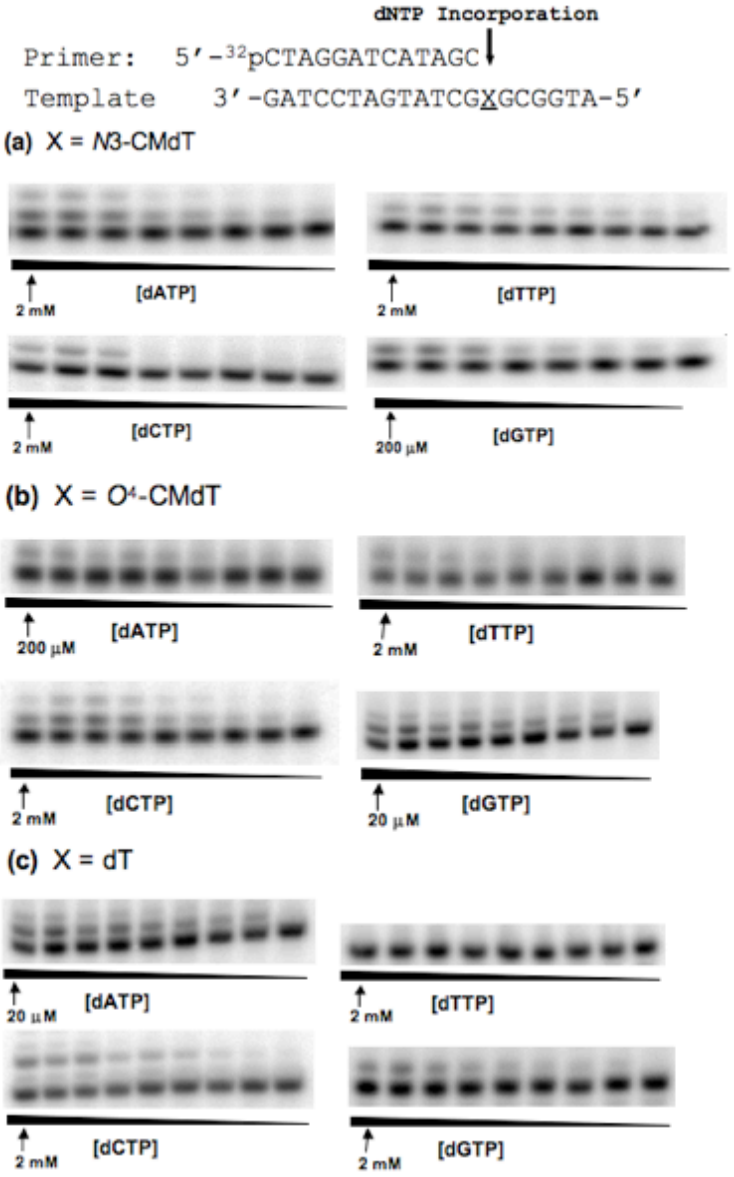

Figure 2.3. Representative gel images for steady-state kinetic assays measuring nucleotide incorporation opposite the *N*3-CMdT and O^4-CMdT lesions and unmodified dT using 1.2 nM yeast polymerase η. Reactions were carried out in the presence of individual dNTPs with the highest concentrations indicated in the figures. The concentration ratios between neighboring lanes were 0.50.

Relative to nucleotide incorporation opposite unmodified dT, efficiencies for correct nucleotide insertion opposite *N*3-CMdT and O^4-CMdT dropped substantially to ~0.08% and ~0.015%, respectively. The reduced efficiency and fidelity underscore the mutagenic potential of *N*3-CMdT and O^4-CMdT, and significant difficulty experienced by yeast Pol η in bypassing the two lesions.

Steady-state Kinetic Analyses of Yeast Pol η-mediated Extension past N^6-CMdA, N^4-CMdC, N3-CMdT, and O^4-CMdT

We next employed steady-state kinetic assays to determine the efficiency and fidelity of yeast Pol η-mediated extension past the carboxymethylated lesions and their respective controls (representative gel images shown in Figures 2.4, S3 & S4). Based on the kinetic parameters for the insertion step opposite N^4-CMdC, *N*3-CMdT, and O^4-CMdT, we utilized multiple primers for the extension past these lesions. In addition to measuring the kinetics for extension when the correct dNTP is inserted opposite these lesions, we also included a mismatched base pair based on the nucleotide preferentially incorporated during the insertion step (Figure 2.4 and Figure S3) to more accurately account for the polymerase's role in insertion and extension.

Significant differences were found in the extension past the four carboxymethylated lesions depending on the nature of the unmodified nucleoside placed opposite the lesion. For the extension past the N^6-CMdA**:**dT pair, yeast Pol η incorporated preferentially the correct dCMP opposite dG, the next nucleoside in the template sequence after the lesion site (Figure S3 and Table 2.2). Misincorporation of dAMP, dTMP, and dGMP occurred at low frequencies (0.48%, 0.60%, and 0.88%,

respectively, Table 2.2). The k_{cat}/K_m for dCMP insertion was calculated to be 25 μM^{-1} min^{-1}, slightly lower than the 50 μM^{-1} min^{-1} observed in the insertion of dCMP opposite dG while extending the lesion-free dA**:**dT pair (Table 2.2), indicating that Pol η can both bypass and extend past N^6-CMdA with high efficiency and fidelity. Extension past N^4-CMdC occurred with varying degrees of fidelity, which is dependant on the nucleotide inserted opposite the lesion. In the presence of the N^4-CMdC**:**dC mispair (dCMP was the most preferentially inserted opposite N^4-CMdC, *vide supra*), extension occurred at low efficiency and fidelity; dGMP was incorrectly inserted opposite the template dG ~52% of the time, which was accompanied with a ~2% misincorporation of dTMP (Table 2.2). In contrast, with the correct N^4-CMdC**:**dG base pair, the correct dCMP was predominantly incorporated opposite the dG in the template, with misinsertion of dAMP, dTMP, and dGMP occurring at frequencies of 0.22%, 0.67%, and 1.4% respectively (Table 2.2).

A similar trend was observed for extension past the *N*3- and O^4-CMdT lesions. Along this line, when the preferentially inserted nucleotide (i.e., dGMP) is placed opposite the two dT lesions, extension occurred at low fidelity, with dGMP being incorporated opposite the dG on the 5' side of *N*3-CMdT and O^4-CMdT at frequencies of 18% and 6.8%, respectively (Table 2.2). However, when the correct dA was placed opposite *N*3-CMdT and O^4-CMdT, there is only 0.96% and 1.1% misinsertion of dGMP (Table 2.2). Taken together, the extension past all four carboxymethylated lesions has better efficiency and accuracy when the correct nucleotide was incorporated opposite the lesions.

Table 2.1. Steady-state kinetic parameters for *S. cerevisiae* Pol η-mediated extension past N^4-CMdC, N^6-CMdA, *N*3-CMdT, and O^4-CMdT, as well as unmodified dA, dC, and dT (designated by 'X'). 'N' represents the nucleoside placed opposite the 'X' (See Figure 4)[a]

dNTP	k_{cat} (min^{-1})	K_m (μM)	k_{cat}/K_m ($\mu M^{-1}min^{-1}$)	f_{ext}
		X = N^6-CMdA, N = dT		
dTTP	3 ± 0.2	20 ± 1	0.15 ± 0.01	6.0×10^{-3}
dGTP	10 ± 1	45 ± 4	0.22 ± 0.02	8.8×10^{-3}
dCTP	28 ± 2	1.1 ± 0.01	25 ± 2	1
dATP	14 ± 1	110 ± 10	0.12 ± 0.01	4.8×10^{-3}
		X = N^4-CMdC, N = dC		
dTTP	14 ± 1	92 ± 6	0.15 ± 0.01	0.016
dGTP	12 ± 1	2.5 ± 0.21	4.9 ± 0.3	0.52
dCTP	16 ± 1	1.7 ± 0.1	9.4 ± 0.9	1
dATP	12 ± 1	500 ± 50	0.024 ± 0.001	2.6×10^{-3}
		X = N^4-CMdC, N = dG		
dTTP	13 ± 1	110 ± 9	0.12 ± 0.01	6.7×10^{-3}
dGTP	21 ± 1	82 ± 7	0.26 ± 0.02	0.014
dCTP	25 ± 2	1.4 ± 0.13	18 ± 2	1
dATP	15 ± 1	380 ± 20	0.039 ± 0.003	2.2×10^{-3}
		X = *N*3-CMdT, N = dG		
dTTP	17 ± 1	82 ± 8	0.21 ± 0.01	7.5×10^{-3}
dGTP	15 ± 1	3 ± 0.3	5 ± 0.4	0.18
dCTP	12 ± 1	0.44 ± 0.03	28 ± 2	1
dATP	15 ± 1	64 ± 5	0.24 ± 0.02	8.6×10^{-3}
		X = O^4-CMdT, N = dG		
dTTP	20 ± 2	140 ± 12	0.14 ± 0.01	7.4×10^{-3}
dGTP	13 ± 1	10 ± 1	1.3 ± 0.13	0.068
dCTP	15 ± 1	0.79 ± 0.06	19 ± 3	1
dATP	12 ± 1	140 ± 10	0.085 ± 0.007	4.5×10^{-3}

dNTP	k_{cat} (min^{-1})	K_m (μM)	k_{cat}/K_m ($\mu M^{-1}min^{-1}$)	f_{ext}
		X = N3-CMdT, N = dA		
dTTP	N/A	N/A	N/A	N/A
dGTP	22 ± 2	95 ± 8	0.23 ± 0.1	9.6×10^{-3}
dCTP	27 ± 2	1.1 ± 0.1	24 ± 2	1
dATP	21 ± 2	700 ± 60	0.031 ± 0.002	1.3×10^{-3}
		X = O^4-CMdT, N = dA		
dTTP	20 ± 2	330 ± 20	0.061 ± 0.003	3.1×10^{-3}
dGTP	21 ± 2	94 ± 8	0.22 ± 0.02	0.011
dCTP	28 ± 2	1.4 ± 0.1	20 ± 1	1
dATP	23 ± 2	550 ± 50	0.042 ± 0.002	2.0×10^{-3}
		X = dC, N = dG		
dTTP	N/A	N/A	N/A	N/A
dGTP	16 ± 1	260 ± 20	0.062 ± 0.005	1.9×10^{-3}
dCTP	28 ± 2	0.87 ± 0.08	32 ± 2	1
dATP	10 ± 1	450 ± 30	0.022 ± 0.002	6.9×10^{-4}
		X = dA, N = dT		
dTTP	19 ± 1	770 ± 10	0.024 ± 0.001	4.9×10^{-4}
dGTP	13 ± 1	220 ± 10	0.059 ± 0.005	1.2×10^{-3}
dCTP	30 ± 2	0.61 ± 0.03	50 ± 3	1
dATP	N/A	N/A	N/A	N/A
		X = dT, N = dA		
dTTP	25 ± 2	300 ± 20	0.083 ± 0.006	1.8×10^{-3}
dGTP	13 ± 1	110 ± 10	0.12 ± 0.01	2.7×10^{-3}
dCTP	17 ± 1	0.38 ± 0.03	45 ± 3	1
dATP	N/A	N/A	N/A	N/A

[a] k_{cat} and K_m values based on three independent measurements

'N/A' indicates data not available, where no nucleotide incorporation was detected even when high concentrations of dNTP was used (2 mM).

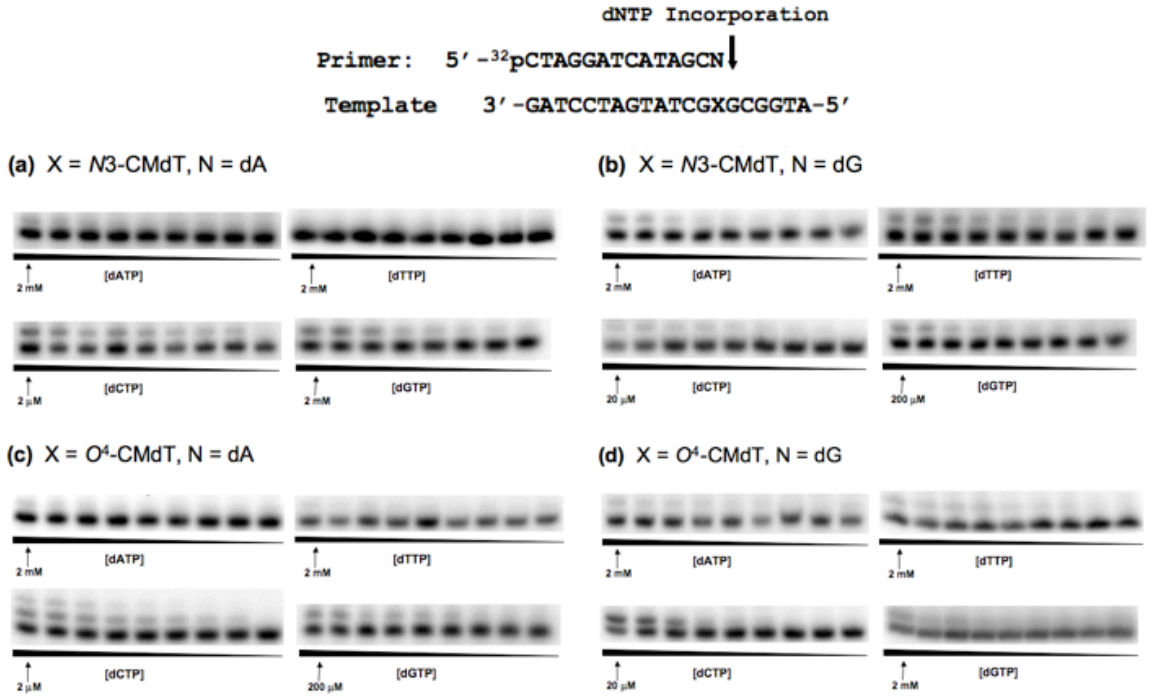

Figure 2.4. Representative gel images for steady-state kinetic assays measuring extension past *N*3-CMdT and O^4-CMdT lesions with base opposite the lesions indicated in the figure as 'N'. Reactions were carried out using 1.2 nM yeast polymerase η and in the presence of individual dNTPs with the highest concentrations indicated in the figures. The concentration ratios between neighboring lanes were 0.50.

Discussion

We previously reported the formation of the four carboxymethylated DNA lesions in calf thymus DNA following treatment with diazoacetate (50,51). In this paper, we performed *in vitro* replication studies on these lesion-containing DNA substrates using purified yeast Pol η. Results from primer extension and steady-state kinetic assays for nucleotide insertion demonstrate that, depending on the structures of the carboxymethylated DNA lesions, bypass by yeast Pol η can be error-prone or error-free. Replication across N^6-CMdA was both accurate and efficient, whereas yeast Pol η exhibited reduced ability to extend the primer across N^4-CMdC in the template strand and the polymerase preferentially inserted the incorrect dCMP opposite the lesion. In contrast, *N*3-CMdT and O^4-CMdT hindered yeast Pol η from generating full-length replication products and the polymerase displayed high frequencies of nucleotide misincorporation opposite the two lesions.

We also demonstrated that Pol η is capable of extending past the carboxymethylated lesions with high efficiency and fidelity when the correct nucleotide was inserted opposite the lesions; however, the Pol η-mediated extension beyond the damage site is neither efficient nor accurate when a wrong nucleotide was incorporated opposite the lesion. In this context, the placement of the preferentially inserted, incorrect nucleotide (dCMP) opposite the N^4-CMdC results in a misincorporation frequency of over 50% at the extension step. Likewise, the placement of the preferentially inserted dGMP opposite the *N*3-CMdT and O^4-CMdT led to lower fidelity in extension than when

the correct dAMP is incorporated opposite the lesions. Efficiency of extension is also considerably higher than that of insertion for N^4-CMdC, *N*3-CMdT, and O^4-CMdT, regardless of whether the correct or the preferentially inserted incorrect nucleotide was placed opposite the lesion.

It is important to discuss the results obtained from the steady-state kinetic measurements in the context of previous studies about this type of DNA lesions. Along this line, a recent study on the mutagenic potential of these carboxymethylated lesions in *E. coli* cells revealed that N^6-CMdA did not block DNA replication or induce mutations (257), which is in keeping with what we observed from the *in vitro* replication experiments using purified *S. cerevisiae* Pol η. N^4-CMdC only slightly blocked DNA replication in *E. coli* cells and it was not mutagenic (257), a finding distinct from steady-state kinetic measurement results showing that this lesion directs significant frequency of dCMP misincorporation. In line with what we found from primer extension and steady-state kinetic measurements, *N*3-CMdT and O^4-CMdT are strong blockades to DNA replication in *E. coli* cells (257). From the replication study in *E. coli* cells, the major mutation observed for *N*3-CMdT was T→A transversion at ~65% frequency, along with T→C transition at a frequency of ~5%, whereas O^4-CMdT induced predominantly T→C transition at ~85% frequency (257). Consistent with these findings, results from our steady-state kinetic measurements revealed substantial misincorporation of dGMP opposite O^4-CMdT. On the other hand, steady-state kinetic analysis revealed the preferential insertion of dGMP opposite *N*3-CMdT, whereas this lesion was found to direct considerable misincorporation of dTMP in *E. coli* cells (*vide supra*).

Together, aside from the similarities in results obtained from replication studies in *E. coli* cells and those from the *in vitro* replication studies using yeast Pol η, there are some notable differences revealed by these two assays, particularly for nucleotide misincorporation opposite *N*3-CMdT and N^4-CMdC. This is not unexpected viewing that the steady-state kinetic measurements were carried out with purified *S. cerevisiae* Pol η in the presence of one type of nucleotide at a time, whereas the *in vivo* replication experiment involved the participation of the entire replication machinery of *E. coli* cells. Along this line, it is worth noting that *E. coli* has two Y-family polymerases, Pol IV (encoded by the *dinB* gene) and Pol V ($UmuD'_2C$, encoded by the *umuDC* genes) (258). In addition, *E. coli* Pol V and eukaryotic Pol η exhibit a very similar pattern of dNTP insertion opposite a variety of lesions (259).

It is also of interest to compare our results with previous steady-state kinetic measurements on other structurely related DNA lesions, particularly the corresponding methylated DNA lesions. In this context, while there were no previous steady-state kinetic measurements on nucleotide incorporation opposite N^6-methyladenine or N^4-methylcytosine, such assays on O^4-methylthymine showed that this lesion could direct significant misincorporation of dGMP by Klenow fragment of *E. coli* DNA polymerase I or *Drosophila melanogaster* polymerase α-primase complex (260). In addition, *N*3-methylthymine was found to be a very strong block to Klenow fragment, and the lesion could direct the misinsertion of dAMP or dTMP (261). We found that the addition of a carboxymethyl group onto the O^4 and *N*3 positions of thymine hinders severely yeast Pol η, in addition to directing the polymerase to misincorporate dGMP.

The mutation spectra induced by diazoacetate in the yeast functional *p53* mutation assay displayed high frequencies of mutations observed at both AT and GC base pairs, including AT→TA, AT→GC, AT→CG as well as GC→AT, GC→TA, and GC→CG mutations (52). Additionally, the types and frequencies of these mutations at non-CpG sites are remarkably similar to those observed for *p53* gene in human gastrointestinal tract tumors, and are distinct from the mutation spectra induced by the methylating agent *N*-methyl-*N*-nitrosourea (MNU) (52). Our steady-state kinetic measurement results suggest that N^4-CMdC, *N*3-CMdT and O^4-CMdT may contribute to the diazoacetate-induced mutations in human p53 gene and those mutations observed in human gastrointestinal tract tumors.

A previous study demonstrated that deficiency in Pol η confers an elevated sensitivity of human lymphoblastoid cells toward azaserine exposure, suggesting the importance of this polymerase in bypassing the carboxymethylated DNA lesions induced by azaserine (251). Our results revealed the efficient bypass of N^6-CMdA and, to a lower degree, N^4-CMdC by *S. cerevisiae* Pol η. It can be envisaged that the failure in bypassing these and other carboxymethylated DNA lesions induced by azaserine may result in replication fork stalling, which may ultimately lead to increased cell death in Pol η-deficient cells. Along this line, future studies about the formation and replication of these DNA lesions in mammalian cells will reveal the role of Pol η and other TLS polymerases in bypassing the carboxymethylated DNA lesions in mammalian cells (262), and further illuminate the biological consequences of these carboxymethylated DNA lesions.

Chapter 3: Accurate and Efficient Bypass of 8,5'-Cyclopurine-2'-Deoxynucleosides by Human and Yeast DNA Polymerase η

Introduction

Living cells are constantly exposed to a variety of endogenous and exogenous agents that can lead to DNA damage (235). One example is reactive oxygen species (ROS), which can be produced during normal aerobic metabolism. Aside from single-nucleobase lesions, ROS can give rise to the formation of tandem DNA lesions, including 8,5'-cyclo-2'-deoxyadenosine (cdA) and 8,5'-cyclo-2'-deoxyguanosine (cdG) (263). The cdA and cdG lesions can be detected at appreciable levels in DNA isolated from tissues of healthy animals without exposure to exogenous genotoxic agents (264-266). The cyclopurine lesions have a unique structure in that the C8 of the purine base is bonded with the C5' of 2-deoxyribose within the same nucleoside (Figure 3.1), which causes a distortion to DNA double helix and stabilization of *N*-glycosidic bond (58,267,268). A recent NMR structural study showed that, in duplex DNA, the 2-deoxyribose of *S*-cdG exhibits an O4'-exo conformation; although the modified nucleoside maintains Watson-Crick hydrogen-bonding interaction with the complementary cytosine base, the lesion introduces significant helical and base stacking perturbations to the DNA duplex (269). Owing to these structural features, cdA and cdG block replicative DNA polymerases and mammalian RNA polymerase II, prevent their removal by base excision repair (BER), and subject them to nucleotide excision repair (NER) (266,270-272).

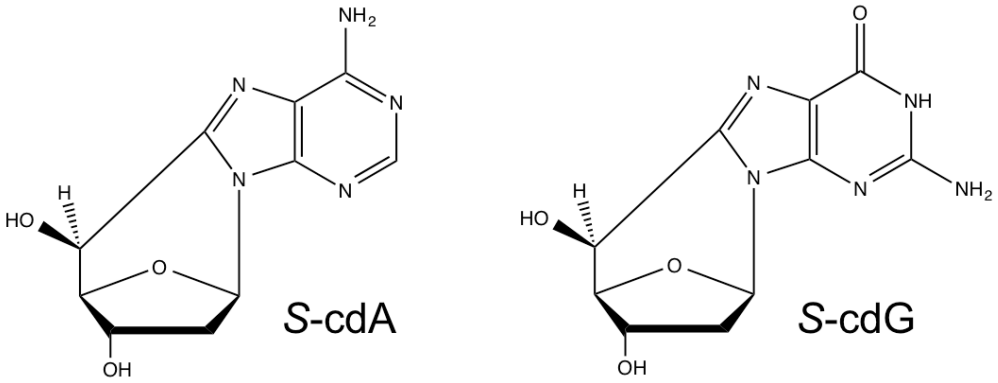

Primer Sequence: 5'-ATGGCGXGCTATGATCCTAG-3'

X = *S*-cdA or *S*-cdG

Figure 3.1. Structures of the two cyclopurine lesions, *S*-cdA and *S*-cdG, as well as the 20mer sequences used for the *in vitro* replication studies.

The endogenous accumulation of the cdA and cdG lesions may contribute to the development of cancer, neurodegeneration, and accelerated aging (53,265,270,273,274).

Translesion synthesis (TLS) is a damage tolerance pathway that facilitates replicative bypass of DNA lesions instead of repairing them (238,239). This process utilizes specialized DNA polymerases, many of which belong to the Y-family, to insert nucleotides opposite and past the damage site (114,275). These TLS polymerases often lack the efficiency and fidelity of traditional replicative polymerases because they have more spacious active sites, allowing them to accommodate bulky DNA lesions and erroneous base pairs (239). However, there are instances where TLS polymerases exhibit the ability to accurately and efficiently bypass certain DNA lesions (155,244,246,276). A striking example of this is Pol η's capability in bypassing UV light-induced thymine-thymine cyclobutane pyrimidine dimer (TT-CPD) with comparable efficiency and fidelity as that of an undamaged substrate (155,277,278). This is the main established role for Pol η in cells, and the importance of which is manifested in those patients with XPV syndrome, as they lack a functional Pol η and in turn display elevated mutagenesis and susceptibility in developing skin tumors (156,246). However, this may not be Pol η's sole role in cells, as this polymerase is capable of bypassing a wide array of DNA lesions with varying degrees of fidelity and efficiency (155,278-280).

All Y-family polymerases have a little finger domain that is absent in replicative DNA polymerases, and when combined with the palm, thumb, and finger domains, can open the active site to allow for binding of modified nucleobases (239,280,281). However, Pol η distinguishes itself from other Y-family polymerases in that the

polymerase core is rotated away from the little finger, thereby creating an even larger binding pocket for accommodating two nucleotides into the active site (282,283). Additionally, Pol η has a distinct molecular splint that rigidly maintains the B-conformation of replicating DNA in the active site, minimizing the introduction of errors into the genome (280,282,283). The unique structure feature of Pol η suggests that, apart from bypassing accurately CPD lesions, this polymerase may also be capable of handling other DNA lesions.

In the present study, we examined, by employing primer extension and steady-state kinetic assays, how site-specifically inserted *S*-cdA and *S*-cdG affect DNA replication mediated by *Saccharomyces cerevisiae* and human DNA Pol η *in vitro*. We also assessed the processivity of these polymerases in bypassing the two purine cyclonucleosides. Our results suggest a new role for polymerase η in cells.

Materials and Methods

Materials

All unmodified oligodeoxyribonucleotides (ODNs) were purchased from Integrated DNA Technologies (Coralville, IA), and [γ-^{32}P]ATP was obtained from Perkin-Elmer (Boston, MA). *Saccharomyces cerevisiae* DNA polymerase η was expressed and purified following previously published procedures (284). Human DNA polymerase η was purchased from Enzymax (Lexington, KY). All other enzymes used in this study were from New England BioLabs (Ipswich, MA), and all chemicals were obtained from Sigma-Aldrich (St. Louis, MO).

Preparation of Lesion-bearing ODN Substrates

ODNs containing a *S*-cdA or *S*-cdG were previously synthesized (285). The identities of the 12mer lesion-bearing substrates were confirmed by electrospray ionization-mass spectrometry (ESI-MS) and tandem mass spectrometry (MS/MS) analyses (276). The 12mer lesion-bearing substrates d(ATGGCGXGCTAT) [X = *S*-cdA or *S*-cdG] were ligated with a 5'-phosphorylated 8mer, d(GATCCTAG), in the presence of a 30mer template ODN, d(CCGCTCCCTAGGATCATAGCYCGCCATGCT) (Y = dT or dC), using previously published procedures (284). The resulting lesion-bearing 20mer substrates were purified using 20% denaturing polyacrylamide gel electrophoresis (PAGE). PAGE and LC-MS/MS were employed to confirm the purity and identity of the lesion-bearing substrates (LC-MS and MS/MS results are displayed in Figures B.1&B.2)

Primer Extension Assay

The 20mer lesion-bearing ODNs or their corresponding unmodified ODNs (0.05 μM) were annealed with a 5'-^{32}P-labeled 13mer primer (0.05 μM) to give substrates for primer extension and steady-state kinetic experiments. The primer extension reaction was carried out under standing-start conditions with the addition of a mixture of all four dNTPs (250 μM each), yeast or human Pol η (concentrations indicated in Figures B.3&B.4), and a buffer containing 10 mM Tris-HCl (pH 7.5), 5 mM $MgCl_2$, and 7.5 mM dithiothreitol (DTT) at 37°C for 1 hr. The reaction was terminated with an equal volume of formamide gel-loading buffer (80% formamide, 10 mM EDTA, pH 8.0, 1 mg/mL xylene cyanol, and 1 mg/mL bromophenol blue). The products were resolved on 20% denaturing polyacrylamide gels with 8 M urea, and gel-band intensities were quantified

using a Typhoon 9410 Variable Mode Imager (Amersham Biosciences Co.) and ImageQuant 5.2 Software (Amersham Biosciences Co.).

Processivity Assay

To determine the processivity of Pol η, the ^{32}P-labeled primer-template complex (10 nM) was preincubated with yeast or human Pol η (20 nM) at 25°C for 15 min in a buffer containing 25 mM Na_3PO_4 (pH 7.0), 5 mM DTT, 100 μg/mL bovine serum albumin, and 10% glycerol. The reaction was subsequently initiated with addition of excess amount of sonicated herring sperm DNA (1 mg/mL, Promega, Madison, WI) to serve as a trap, a mixture of all four dNTPs (250 μM each), and 5 mM $MgCl_2$. To demonstrate the effectiveness of the trap, yeast or human Pol η was also preincubated with the herring sperm DNA together with primer-template complex prior to dNTP and $MgCl_2$ addition; the lack of DNA synthesis under such conditions indicated that the excess herring sperm DNA was able to trap all polymerase molecules (Figure B.5). Reactions were terminated at 30, 60, and 120 sec by adding an equal volume of formamide gel-loading buffer, and analyzed on 20% denaturing polyacrylamide gels. Gel-band intensities were quantified with phosphorimager analysis as described above. The following equation was used to calculate the percentage of active polymerase molecules incorporating N^{th} nucleotides, with the intensity of the band at position 1 indicated by I_1, and intensity of the band at position N indicated by I_N (286):

$$\% \text{ active polymerases at } N = \frac{(I_N + I_{N+1} + ...) \times 100\%}{(I_1 + I_2 + ...)}$$

The processivity for each deoxynucleotide incorporation (N) is then obtained by the following equation (286):

$$P_N = \frac{\%\text{ active polymerases at } N+1}{\%\text{ active polymerases at } N}$$

Steady-state Kinetic Measurements

Steady-state kinetic assays were carried out using previously described procedures (256). The aforementioned ^{32}P-labeled primer-template complex (50 nM) was incubated with yeast or human Pol η (1.2 nM) at 37°C for 10 min in the presence of individual dNTPs at various concentrations (indicated in Figures 4-6 & S6-S8) and a buffer containing 10 mM Tris-HCl (pH 7.5), 5 mM $MgCl_2$, and 7.5 mM DTT. The reaction was terminated with an equal volume of formamide gel-loading buffer as described above. Extension products were separated using denaturing PAGE and gel band intensities of the primer and extension products were again quantified using a phosphorimager, as described above. The concentration of individual dNTP was optimized to allow for less than 20% nucleotide incorporation. The kinetic parameters for the incorporation of incorrect and correct nucleotides, V_{max} and K_m, were determined by plotting the observed rate of nucleotide incorporation (V_{obs}) as a function of dNTP concentration using Origin 6.0 Software (OriginLab) and fitting the data with a non-linear curve regression following the Michaelis-Menten equation (256).

The k_{cat} values were calculated by dividing the calculated V_{max} with the concentration of Pol η used. The efficiency of nucleotide incorporation was calculated by the ratio of k_{cat}/K_m, and the frequencies of incorrect nucleotide insertion (f_{inc}) and

extension (f_{ext}) were determined based on the ratio of k_{cat}/K_m value obtained for the insertion of incorrect nucleotide over that for the correct nucleotide incorporation at the insertion and extension steps, respectively.

Results

To understand how the cyclopurine lesions are bypassed by Pol η *in vitro*, we prepared 20mer ODN substrates harboring a site-specifically inserted *S*-cdA and *S*-cdG, and verified the integrities of the lesion-containing ODNs with mass spectrometric analyses (Appendix Figures B.1&B.2). We then performed primer extension, processivity, and steady-state kinetic assays to determine the effects of these lesions on the accuracy and efficiency of DNA replication mediated by yeast and human Pol η.

Primer Extension across S-cdA and S-cdG with Yeast and Human Pol η

We first performed primer extension assays to evaluate the ability of yeast and human Pol η to extend a 13mer primer in the presence of a 20mer template containing a *S*-cdA, *S*-cdG and their respective unmodified nucleosides at a defined site (Figures B.3&B.4). We found that, in the presence of all four dNTPs, yeast Pol η can bypass successfully *S*-cdA and *S*-cdG, and generate full-length extension products (Figure B.3). However, human Pol η is more hindered by these lesions, which is reflected by the significant amount of unextended primer and stalled extension one nucleotide away from the 3' end of the initial primer (Figure B.4). Additionally, the amount of full-length

replication products is very low (~ 1%), indicating that these lesions confer a significant blocking effect on the human polymerase (Figure B.4).

Processivity of Yeast and Human Pol η of S-cdA and S-cdG, and the Corresponding Undamaged Substrates

We utilized a previously reported assay to assess the processivity of yeast and human Pol η on nucleotide incorporation using the lesion-containing and undamaged templates (287). The assay allows for the measurement of the number of 2'-deoxynucleotides that the polymerase incorporates in a single DNA-binding event, where the presence of excess herring sperm DNA serves to trap all polymerase molecules dissociating from the DNA template. We calculated the percentage of Pol η molecules that incorporate *N* nucleotides, where the percentage of active polymerase molecules incorporating at least one nucleotide was set at 100% (see Materials & Methods, Figures 3.2&3.3 and Appendix Figure B.5). For the control dA- and dG-containing substrates, 88% and 84% of human Pol η molecules incorporated at least two nucleotides in the template, respectively, with the percentage of polymerase molecules dropping to 24% and 18% with seven nucleotide additions in the template (Figure 3.3). The decrease in the percentage of active polymerase molecules with each subsequent nucleotide addition is attributed to their dissociation from the template. The *S*-cdA- and *S*-cdG-containing templates had 81% and 75% of active enzyme molecules incorporating a minimum of two nucleotides, and 28% and 15% incorporating at least three nucleotides, respectively (Figure 3.3); no subsequent nucleotide additions were observed for *S*-cdA or *S*-cdG past the third nucleotide. By contrast, yeast Pol η synthesized DNA with remarkably similar

processivity past the *S*-cdA- and *S*-cdG-containing templates as their corresponding undamaged dA and dG. The percentages of active yeast Pol η molecules at each nucleotide addition on the *S*-cdA- and *S*-cdG-containing templates resemble closely those for their respective control substrates (Figure 3.3).

We also calculated the processivity, P_N, for yeast and human Pol η to insert each nucleotide past the damaged and the corresponding non-damaged sites. With human Pol η, the average P_N values were 0.81±0.19, 0.78±0.20, 0.58±0.33, and 0.47±0.40 for substrates containing dA, dG, *S*-cdA, and *S*-cdG, respectively (Figure 3.3). Thus, human Pol η-mediated DNA synthesis occurs at low processivity, and the processivity is further decreased significantly by the presence of the two lesions. With yeast Pol η, the average P_N values for dA-, dG-, *S*-cdA-, and *S*-cdG-containing substrates were 0.83±0.19, 0.80±0.22, 0.80±0.21, and 0.76±0.23, respectively, indicating that DNA synthesis with yeast Pol η also occurs with low processivity (Figure 3.3); nevertheless, the processivities for DNA synthesis with *S*-cdA- and *S*-cdG-containing substrates are very similar to those for the corresponding dA- and dG-containing substrates.

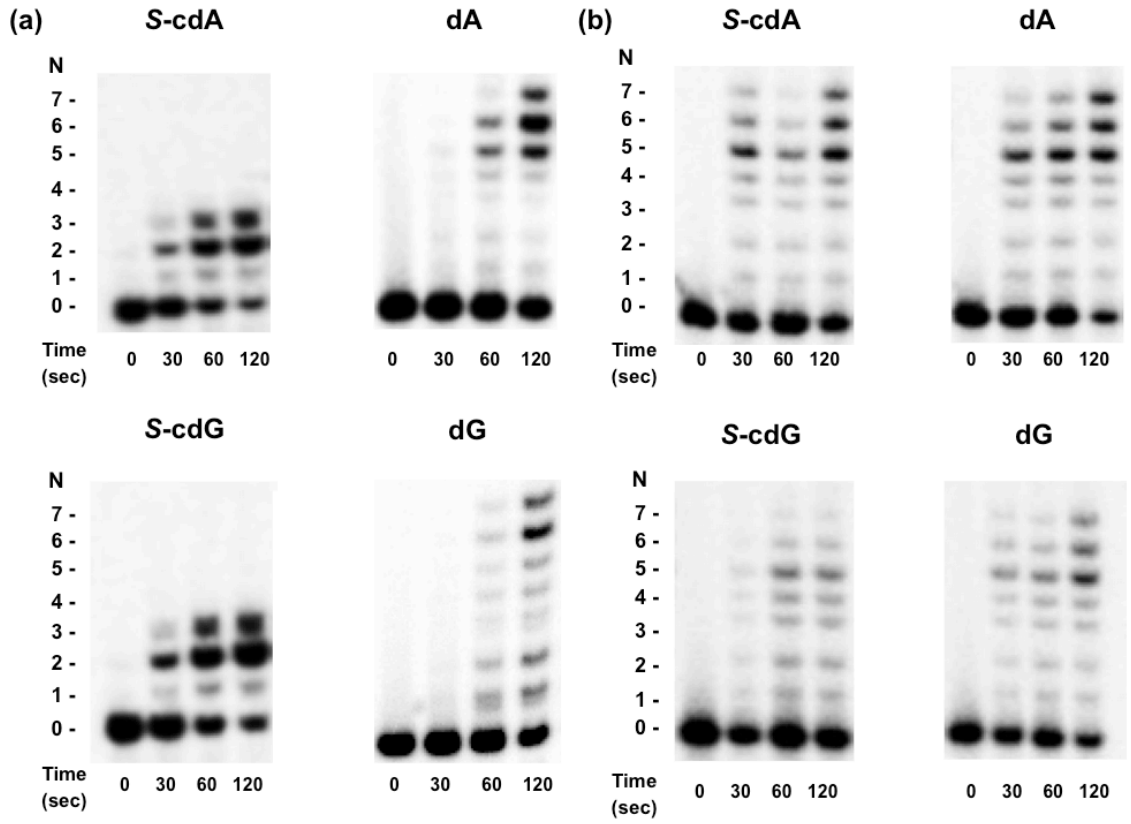

Figure 3.2. Processivity assays for substrates containing *S*-cdA, *S*-cdG, dA, and dG, with human (a) and yeast Pol η (b). The radiolabeled primer-template complex was preincubated with human Pol η for 15 min. The reaction was then initiated with excess herring sperm DNA as a trap, all four dNTPs, and $MgCl_2$. Reactions were stopped at various time points indicated in the figures. The 120 sec time-point was used to calculate the percentage of active polymerase molecules and processivity values. Products were resolved on 20% denaturing polyacrylamide gels.

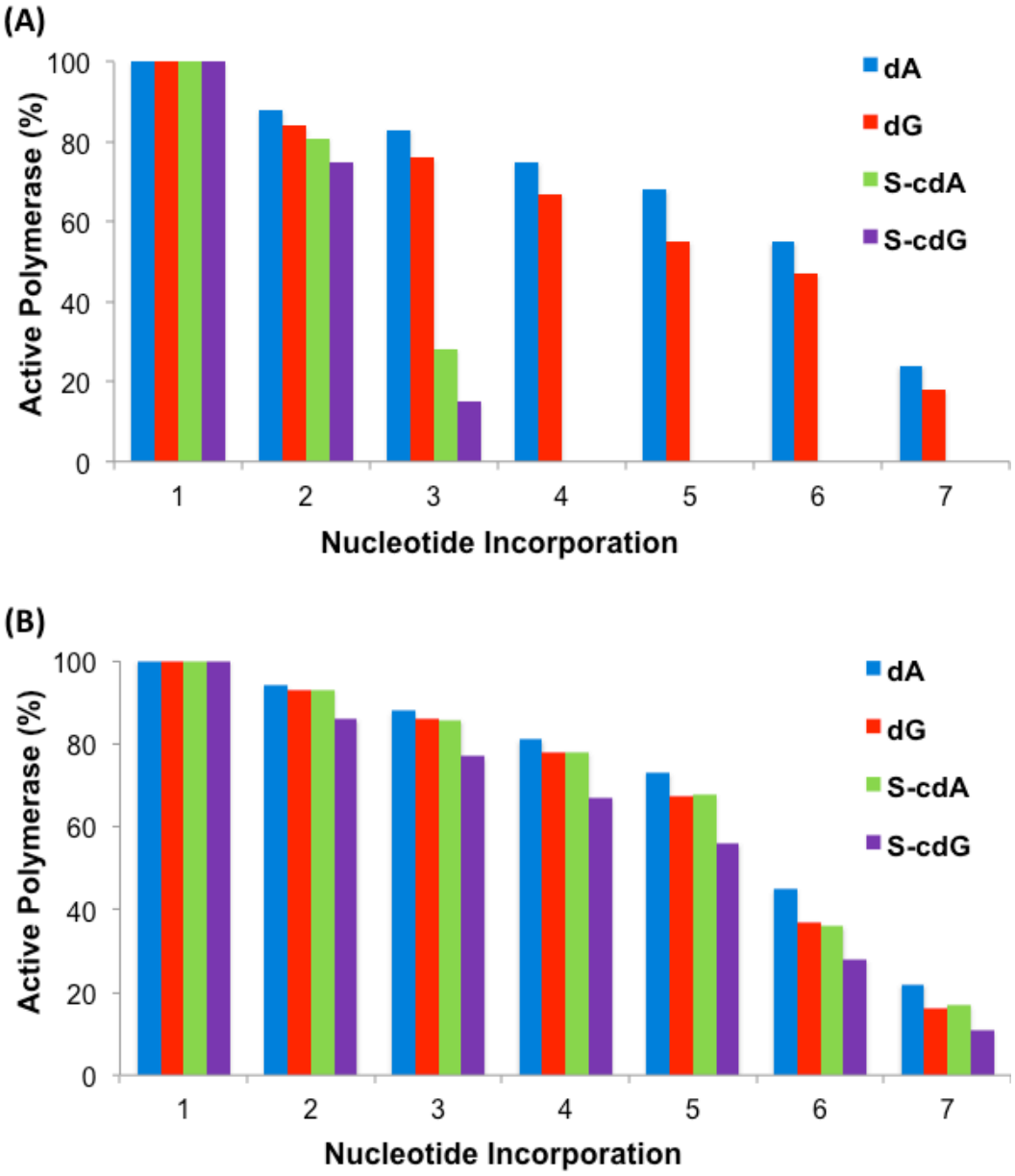

Figure 3.3. Graphs depicting the percentage of active human polymerase η (a) or yeast polymerase η (b) molecules at each position along the template strand containing a site-specifically inserted *S*-cdA, *S*-cdG, dA, or dG (indicated in the legend).

Steady-state Kinetic Analyses of Human Pol η-mediated Nucleotide Insertion opposite S-cdA, and S-cdG

We next employed steady-state kinetic assays to measure the kinetic parameters for nucleotide insertion opposite the lesions, as well as their respective unmodified nucleosides (Figure 3.4). Human Pol η predominantly incorporated the correct dTMP opposite *S*-cdA with high accuracy and efficiency. Misincorporation of dAMP, dCMP, and dGMP occurred at very low frequencies (1.0%, 0.38%, and 0.47%, respectively. Table 3.1). Importantly, the efficiency of dTMP insertion opposite *S*-cdA was similar as that of the control dA substrate, with the observed k_{cat}/K_m values being 85 and 140 $\mu M^{-1}min^{-1}$, respectively. Likewise, human Pol η mainly incorporated the correct dCMP opposite cyclo-dG, with little misincorporation of dAMP (0.17%), dTMP (1.2%) and dGMP (0.0015%, Table 3.1). Human Pol η also inserted the correct dCMP opposite *S*-cdG with comparable efficiency as that of the control substrate; the observed k_{cat}/K_m values for dCMP insertion opposite *S*-cdG and dG were 54 and 100 $\mu M^{-1}min^{-1}$, respectively.

Table 3.1. Steady-state Kinetic Parameters for Human Pol η-mediated Nucleotide Insertion opposite *S*-cdA and *S*-cdG, and opposite Unmodified dA and dG [a]

dNTP	k_{cat} (min^{-1})	K_m (μM)	k_{cat}/K_m ($\mu M^{-1}min^{-1}$)	f_{inc}
		***S*-cdA-containing substrate**		
dTTP	11 ± 1	0.13 ± 0.01	85 ± 8	1
dGTP	6.4 ± 0.6	16 ± 1	0.41 ± 0.04	4.7×10^{-3}
dCTP	3.9 ± 0.2	12 ± 1	0.32 ± 0.03	3.8×10^{-3}
dATP	22 ± 2	26 ± 2	0.85 ± 0.09	1.0×10^{-2}
		dA Control		
dTTP	18 ± 1	0.12 ± 0.01	140 ± 10	1
dGTP	11 ± 1	45 ± 4	0.25 ± 0.02	1.8×10^{-3}
dCTP	6.5 ± 0.6	13 ± 1	0.52 ± 0.05	3.7×10^{-3}
dATP	26 ± 2	24 ± 2	1.1 ± 0.01	7.8×10^{-3}
		***S*-cdG-containing substrate**		
dTTP	17 ± 1	28 ± 1	0.61 ± 0.06	1.2×10^{-2}
dGTP	0.71 ± 0.08	900 ± 100	0.00079 ± 0.00009	1.5×10^{-5}
dCTP	18 ± 1	0.36 ± 0.03	54 ± 6	1
dATP	16 ± 1	170 ± 15	0.094 ± 0.008	1.7×10^{-3}
		dG Control		
dTTP	9.1 ± 0.9	48 ± 5	0.19 ± 0.01	1.9×10^{-3}
dGTP	1.0 ± 0.2	720 ± 90	0.0014 ± 0.0003	1.4×10^{-5}
dCTP	15 ± 1	0.13 ± 0.01	100 ± 10	1
dATP	31 ± 3	460 ± 50	0.067 ± 0.006	6.7×10^{-4}

[a] k_{cat} and K_m values were based on three independent gel experiments

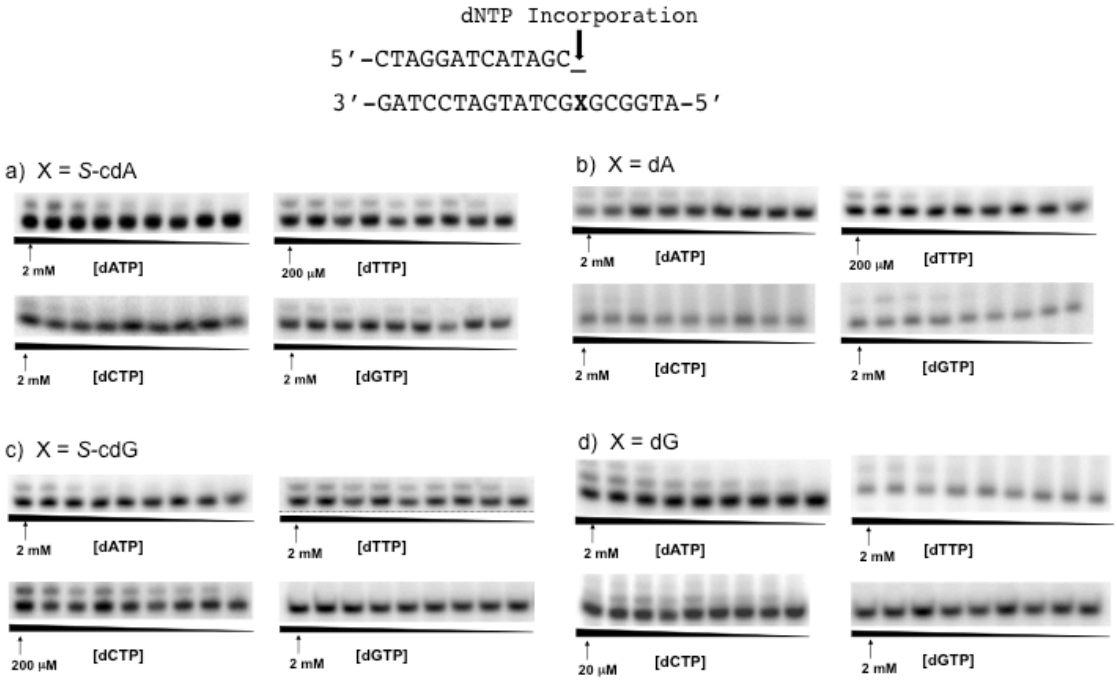

Figure 3.4. Representative gel images for steady-state kinetic assays measuring nucleotide incorporation opposite *S*-cdA and *S*-cdG, and unmodified dA and dG. Reactions were carried out using 1.2 nM human Pol η in the presence of individual dNTPs with the highest concentrations indicated in the figures. Concentration ratios between neighboring lanes were 0.50.

Steady-state Kinetic Analyses of Human Pol η-mediated Extension past S-cdA and S-cdG

We next evaluated the ability of human Pol η to extend past *S*-cdA and *S*-cdG and their respective undamaged substrates, again using steady-state kinetic assays to determine the efficiency and fidelity of nucleotide insertion opposite the downstream 5' nucleoside (Figures 3.5&B.6). Based on the kinetic parameters for the insertion step, we used a 14mer primer with the correct dNTP being inserted opposite the lesions and their controls, as well as the most preferentially misincorporated dNTP opposite *S*-cdA, and *S*-cdG (dAMP and dTMP, respectively). When the correct dT is paired with *S*-cdA, extension past the lesion is highly accurate, which was accompanied with very low frequencies of misincorporation of dAMP (1.5%), dGMP (0.67%), and dTMP (0.0067%) opposite dG (Table 3.2). The extension is also moderately efficient, where the insertion of the correct dCMP occurred at an efficiency that is ~35% relative to the corresponding extension past the control dA**:**dT pair (Table 3.2). However, extension past the *S*-cdA**:**dA base pair is highly error-prone, with significant misincorporation of dTMP opposite the adjacent base (f_{ext} = 83%, Table 3.2). The efficiencies for extension past the mismatch and correct base pairs are also markedly different, with dCMP insertion past the *S*-cdA**:**dA mismatch occurring at a frequency that is ~0.5% of that for the insertion past the correct *S*-cdA**:**dT base pair (i.e., 0.11 vs. 21 μM^{-1} min^{-1}, Table 3.2).

Similar findings were made for *S*-cdG. When the correct dC was placed opposite *S*-cdG at the primer end, human Pol η was able to extend the primer by inserting preferentially the correct dCMP opposite dG, the next nucleoside in the template, with misincorporations of dAMP, dTMP and dCMP occurring at frequencies of 1.5%, 0.88%

and 0.68%, respectively. The efficiency for dCMP insertion was, however, lower (~28%) than that observed for corresponding dCMP insertion past the dG:dC pair (Table 3.2). When the *S*-cdG**:**dT mismatch is placed at the primer/template junction, human Pol η, however, severely misincorporated dAMP (8500%), dGMP (130%), and dTMP (98%) opposite the next nucleoside (dG) though this occurred with extremely low efficiencies (Table 3.2). These results demonstrate that the presence of a misincorporated nucleotide opposite the lesion introduces errors and hinders human Pol η in the extension step. Collectively, the above results revealed that human Pol η-mediated nucleotide incorporation opposite the two purine cyclonucleosides and their adjacent 5' unmodified nucleoside were accurate, though the cumulative efficiencies for these two insertion steps were decreased by ~ 5 and 6 folds by the presence of *S*-cdA and *S*-cdG, respectively.

Table 3.2. Steady-state kinetic parameters for Human Pol η-mediated extension past *S*-cdA and *S*-cdG, and unmodified dA and dG (designated with an X, and N is the nucleoside placed opposite X)[a]

dNTP	k_{cat} (min^{-1})	K_m (μM)	k_{cat}/K_m ($\mu M^{-1}min^{-1}$)	f_{ext}
		X = *S*-cdA, N = dT		
dTTP	0.93 ± 0.1	660 ± 80	0.0014 ± 0.0003	6.7×10^{-5}
dGTP	3.3 ± 0.3	28 ± 2	0.12 ± 0.01	5.7×10^{-3}
dCTP	6.3 ± 0.6	0.35 ± 0.03	21 ± 1	1
dATP	4.2 ± 0.4	15 ± 1	0.28 ± 0.01	1.3×10^{-2}
		X = *S*-cdA, N = dA		
dTTP	3.8 ± 0.3	42 ± 4	0.091 ± 0.009	8.3×10^{-1}
dGTP	0.88 ± 0.1	710 ± 90	0.0012 ± 0.0002	1.1×10^{-2}
dCTP	3.9 ± 0.3	35 ± 3	0.11 ± 1	1
dATP	0.62 ± 0.09	850 ± 100	0.00073 ± 0.00009	6.6×10^{-3}
		X = dA, N = dT		
dTTP	6.6 ± 0.6	19 ± 1	0.35 ± 0.03	5.9×10^{-3}
dGTP	0.77 ± 0.09	830 ± 90	0.00093 ± 0.0001	1.6×10^{-5}
dCTP	14 ± 1	0.24 ± 0.02	59 ± 5	1
dATP	6.4 ± 0.6	15 ± 1	0.43 ± 0.04	7.3×10^{-3}
		X = *S*-cdG, N = dC		
dTTP	4.7 ± 0.4	34 ± 3	0.14 ± 0.01	8.8×10^{-3}
dGTP	3.9 ± 0.4	38 ± 3	0.11 ± 0.01	6.8×10^{-3}
dCTP	7.4 ± 0.7	0.46 ± 0.04	16 ± 1	1
dATP	5.4 ± 0.5	23 ± 2	0.24 ± 0.02	1.5×10^{-2}
		X = *S*-cdG, N = dT		
dTTP	0.82 ± 0.1	840 ± 100	0.00098 ± 0.0002	9.8×10^{-1}
dGTP	0.93 ± 0.2	690 ± 80	0.0013 ± 0.0003	1.3
dCTP	0.89 ± 0.1	880 ± 100	0.0010 ± 0.0002	1
dATP	3.3 ± 0.3	39 ± 3	0.085 ± 0.008	85
		X = dG, N = dC		
dTTP	9.6 ± 0.9	36 ± 3	0.27 ± 0.02	4.8×10^{-3}
dGTP	11 ± 1	24 ± 3	0.46 ± 0.04	8.2×10^{-3}
dCTP	12 ± 1	0.21 ± 0.02	56 ± 5	1
dATP	4.1 ± 0.4	19 ± 1	0.22 ± 0.02	3.9×10^{-3}

[a] k_{cat} and K_m values are based on three independent gel experiments

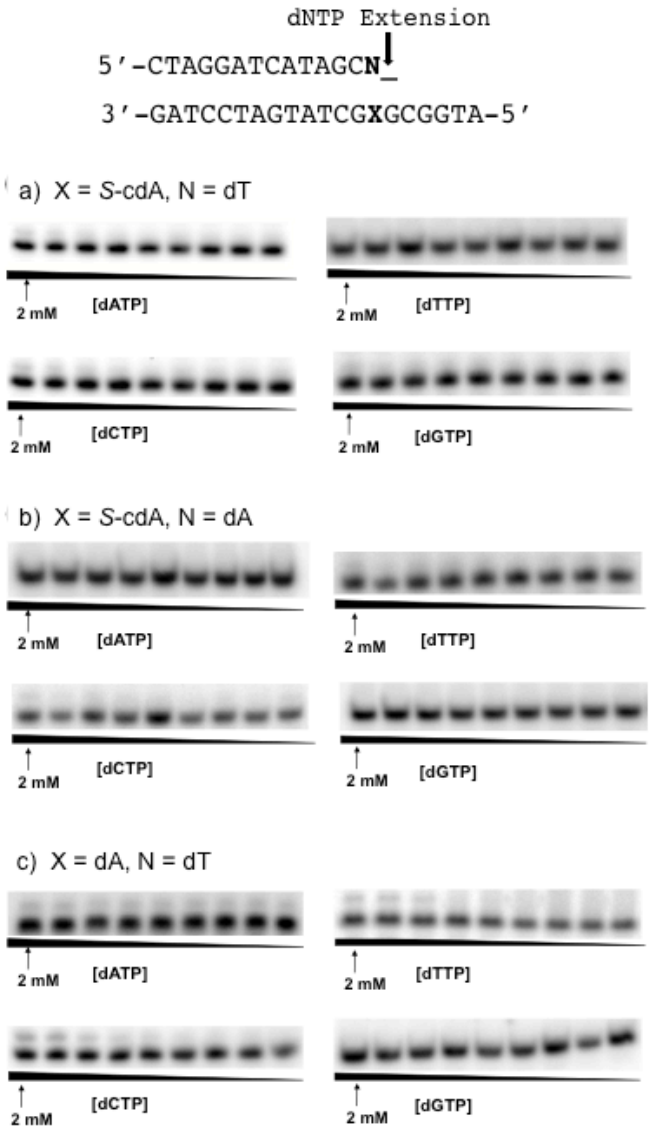

Figure 3.5. Representative gel images for steady-state kinetic assays measuring extension past *S*-cdA and dA, with the base opposite the lesions indicated as 'N'. Reactions were carried out using 1.2 nM human Pol η in the presence of individual dNTPs with the highest concentrations indicated in the figures. Concentration ratios between neighboring lanes were 0.50.

Steady-state Kinetic Analyses of Yeast Pol η-mediated Nucleotide Insertion opposite S-cdA and S-cdG

Similar as what we observed for human Pol η, yeast Pol η again preferentially incorporated the correct dTMP opposite *S*-cdA, with relatively low frequencies of misincorporation of dAMP (2.3%), dGMP (0.053%), and dCMP (0.042%, Table 3.3, Figure B.7). Similarly, yeast Pol η inserted preferentially the correct dCMP opposite *S*-cdG, with ~7.2% misincorporation of dTMP and very low frequencies of misinsertion of dGMP (0.14%) or dAMP (0.99%, Table 3.3, Figure B.8). Remarkably, insertion of the correct dTMP opposite *S*-cdA was about twice as efficient as dTMP incorporation opposite the unmodified dA (Table 3.3). Likewise, yeast Pol η exhibited an enhanced ability to insert the correct dCMP opposite *S*-cdG relative to an unmodified dG; the observed k_{cat}/K_m values for dCMP insertion opposite *S*-cdG and dG were 84 and 53 $\mu M^{-1}min^{-1}$, respectively (Table 3.3).

Steady-state Kinetic Analyses of Yeast Pol η-mediated Extension past S-cdA and S-cdG

Next we assessed the ability of yeast Pol η to extend past the above-described lesions and their respective controls, and our results showed that the extension step followed a similar pattern as that seen with human Pol η (Figure 3.6). For extension past *S*-cdA**:**dT base pair, the polymerase incorporated the correct dCMP opposite the template dG, with similar efficiency as that observed for dCMP insertion opposite the dG past dA**:**dT base pair. Misincorporation of dTMP, dAMP, and dGMP occurred at low frequencies (0.092%, 0.14%, and 1.3%, respectively, see Table 3.2). The observed

k_{cat}/K_m for the *S*-cdA**:**dT pair was 39 $\mu M^{-1}min^{-1}$, which is only slightly lower than the 50 $\mu M^{-1}\,min^{-1}$ observed for the control dA**:**dT base pair. On the other hand, the presence of a misincorporated dA nucleoside at the primer end led to significant frequencies of misincorporation of dAMP (23%), dGMP (1.3%), and dTMP (0.25%, Table 3.4) opposite the downstream dG in the template. Nevertheless, the efficiency for incorporating the correct dCMP remained similar to the control, with the observed k_{cat}/K_m value being 33 $\mu M^{-1}\,min^{-1}$.

Table 3.3. Steady-state Kinetic Parameters for *S. cerevisiae* Pol η-mediated Nucleotide Insertion opposite *S*-cdA and *S*-cdG, and opposite Unmodified dA and dG [a]

dNTP	k_{cat} (min^{-1})	K_m (μM)	k_{cat}/K_m ($\mu M^{-1}min^{-1}$)	f_{inc}
		***S*-cdA-containing substrate**		
dTTP	22 ± 1	0.14 ± 0.01	110 ± 10	1
dGTP	6.8 ± 0.3	130 ± 10	0.058 ± 0.005	5.3×10^{-4}
dCTP	5.4 ± 0.2	120 ± 10	0.046 ± 0.003	4.2×10^{-4}
dATP	16 ± 1	6.5 ± 0.4	2.5 ± 0.2	2.3×10^{-2}
		dA Control		
dTTP	15 ± 1	0.31 ± 0.02	48 ± 4	1
dGTP	11 ± 0.5	210 ± 20	0.052 ± 0.003	1.1×10^{-3}
dCTP	40 ± 3	400 ± 30	0.089 ± 0.002	1.8×10^{-3}
dATP	10 ± 1	310 ± 13	0.033 ± 0.001	6.9×10^{-4}
		***S*-cdG-containing substrate**		
dTTP	17 ± 1	2.8 ± 0.2	6.1 ± 0.6	7.2×10^{-2}
dGTP	12 ± 1	95 ± 8	0.12 ± 0.01	1.4×10^{-3}
dCTP	21 ± 2	0.25 ± 0.01	84 ± 7	1
dATP	14 ± 1	17 ± 1	0.82 ± 0.07	9.9×10^{-3}
		dG Control		
dTTP	18 ± 1	74 ± 6	0.24 ± 0.02	4.5×10^{-3}
dGTP	15 ± 1	520 ± 30	0.029 ± 0.001	5.5×10^{-4}
dCTP	27 ± 2	0.51 ± 0.04	53 ± 3	1
dATP	21 ± 2	110 ± 10	0.19 ± 0.01	3.6×10^{-3}

[a] k_{cat} and K_m values were based on three independent measurements

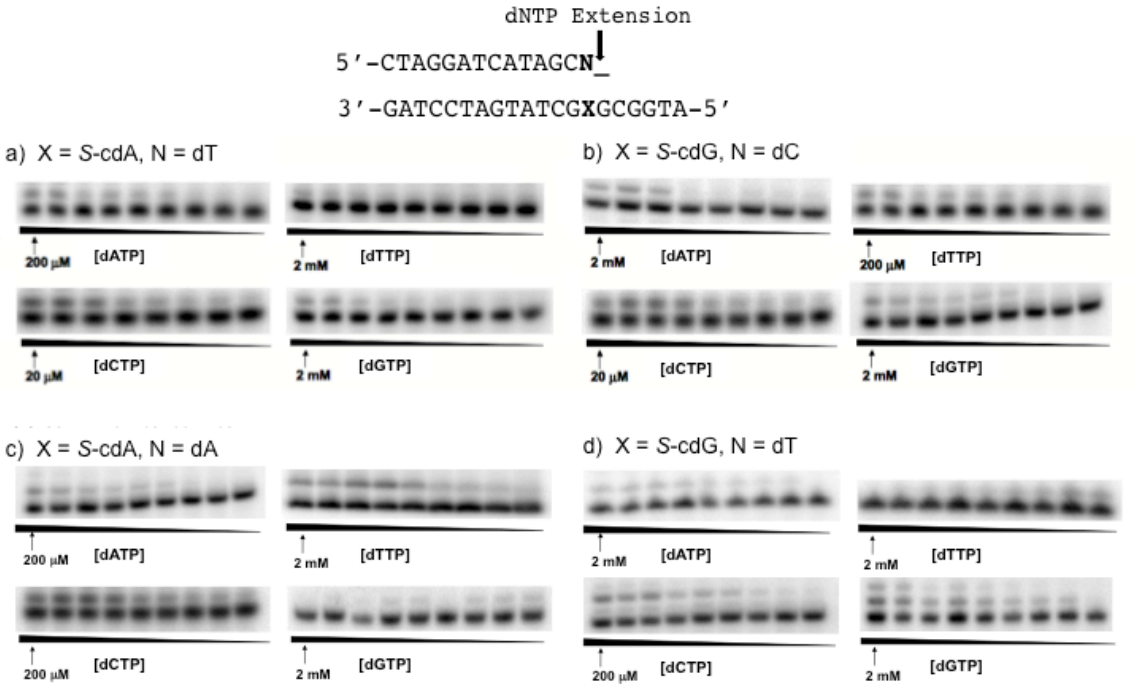

Figure 3.6. Representative gel images for steady-state kinetic assays measuring extension past *S*-cdA (a,c) and *S*-cdG (b,d). Reactions were carried out using 1.2 nM yeast Pol η in the presence of individual dNTPs with the highest concentrations indicated in the figures. Concentration ratios between neighboring lanes were 0.50.

For the *S*-cdG**:**dC base pair, yeast Pol η again incorporated preferentially the correct dCMP opposite the dG in the template, with misincorporations of dTMP, dGMP and dAMP occuring at frequencies of 4.2%, 0.12% and 0.14%, respectively (Table 3.4). Yeast Pol η also inserted dCMP at the extension step with similar efficiency as dCMP incorporation opposite dG for the control dG**:**dC base pair (45 vs. 52 $\mu M^{-1}min^{-1}$, Table 3.4). On the other hand, with a *S*-cdG:dT base pair at the primer/template junction, extension past the lesion was hindered and inaccurate, with substantial misincorporations of dAMP (2.8%), dGMP (49%), and dTMP (0.47%, Table 3.4). The k_{cat}/K_m for dCMP insertion past the *S*-cdG**:**dT base pair was 16 $\mu M^{-1}\,min^{-1}$, significantly lower than the 52 $\mu M^{-1}\,min^{-1}$ found for the control dG**:**dC base pair (Table 3.4). Together, the above results demonstrated that, similar to its human counterpart, yeast Pol η is capable of inserting nucleotides opposite *S*-cdA, *S*-cdG, and their neighboring 5' nucleoside with high accuracy. Moreover, the cumulative efficiencies for these two insertion steps were 1.8- and 1.4-fold higher for substrates containing *S*-cdA and *S*-cdG than their corresponding unmodified substrates, respectively.

Table 3.4. Steady-state Kinetic Parameters for *S. cerevisiae* Pol η-mediated Extension past *S*-cdA and *S*-cdG, and Unmodified dA and dG (designated with an X, and N is the nucleoside placed opposite X)[a]

dNTP	k_{cat} (min^{-1})	K_m (μM)	k_{cat}/K_m ($\mu M^{-1}min^{-1}$)	f_{ext}
		X = *S*-cdA, N = dT		
dTTP	12 ± 1	330 ± 20	0.036 ± 0.002	9.2×10^{-4}
dGTP	14 ± 1	250 ± 20	0.056 ± 0.003	1.4×10^{-3}
dCTP	18 ± 1	0.46 ± 0.02	39 ± 3	1
dATP	17 ± 1	35 ± 5	0.49 ± 0.4	1.3×10^{-2}
		X = *S*-cdA, N = dA		
dTTP	13 ± 1	160 ± 10	0.081 ± 0.007	2.5×10^{-3}
dGTP	12 ± 1	28 ± 2	0.43 ± 0.03	1.3×10^{-2}
dCTP	14 ± 1	0.42 ± 0.04	33 ± 1	1
dATP	13 ± 1	1.7 ± 0.1	7.6 ± 0.7	2.3×10^{-1}
		X = dA, N = dT		
dTTP	19 ± 1	170 ± 10	0.011 ± 0.0009	2.2×10^{-4}
dGTP	13 ± 1	220 ± 10	0.057 ± 0.0052	1.1×10^{-3}
dCTP	30 ± 2	0.61 ± 0.03	50 ± 3	1
dATP	0.96 ± 0.2	660 ± 80	0.0014 ± 0.0002	2.8×10^{-5}
		X = *S*-cdG, N = dC		
dTTP	19 ± 1	9.8 ± 0.7	1.9 ± 0.1	4.2×10^{-2}
dGTP	14 ± 1	250 ± 20	0.056 ± 0.004	1.2×10^{-3}
dCTP	22 ± 2	0.49 ± 0.04	45 ± 4	1
dATP	16 ± 1	250 ± 20	0.064 ± 0.005	1.4×10^{-3}
		X = *S*-cdG, N = dT		
dTTP	12 ± 1	160 ± 10	0.075 ± 0.007	4.7×10^{-3}
dGTP	15 ± 1	1.9 ± 0.1	7.9 ± 0.6	4.9×10^{-1}
dCTP	15 ± 1	0.95 ± 0.04	16 ± 1	1
dATP	14 ± 1	31 ± 3	0.45 ± 0.04	2.8×10^{-2}
		X = dG, N = dC		
dTTP	15 ± 1	270 ± 20	0.056 ± 0.005	1.1×10^{-3}
dGTP	11 ± 1	410 ± 35	0.027 ± 0.002	5.2×10^{-4}
dCTP	25 ± 2	0.48 ± 0.03	52 ± 4	1
dATP	14 ± 1	310 ± 15	0.045 ± 0.004	8.7×10^{-4}

[a] *k_{cat} and K_m* values based on three independent experiments

Discussion

The most striking finding made from the present study is that Pol η is able to insert nucleotides opposite *S*-cdA, *S*-cdG, and their adjacent 5' unmodified nucleoside, with comparable efficiency and fidelity as their respective undamaged substrates. Remarkably, *Saccharomyces cerevisiae* Pol η was able to insert the correct nucleotides opposite the lesions with greater efficiency than the corresponding insertions opposite the unmodified nucleosides (by ~2.3 and ~1.6 folds for *S*-cdA and *S*-cdG, respectively), though the yeast enzyme was slightly more error-prone than its human counterpart (Figure 3.7). Additionally, processivity of yeast Pol η-mediated DNA synthesis on the damaged and the corresponding undamaged substrates was strikingly similar. The enzyme, however, exhibits relatively low processivity toward the undamaged substrates (Figure 3.3), which is consistent with previous findings (286,288).

Insertion opposite the two lesions and their neighboring 5' undamaged nucleoside with human Pol η was highly accurate, with misincorporation frequencies being under 1.5% in both steps. The efficiencies for nucleotide insertion opposite the two lesions, however, were lower than those for the corresponding undamaged substrates (Figure 3.7). Different from its yeast counterpart, human Pol η is less processive in DNA synthesis past the two lesions than their respective control substrates (Figures 3.2&3.3). Although the steady-state kinetic results for human Pol η-mediated nucleotide insertion opposite *S*-cdA, *S*-cdG, and their neighboring 5' nucleosides suggest relatively high efficiency in lesion bypass, processivity data indicate that the polymerase can only insert one or two

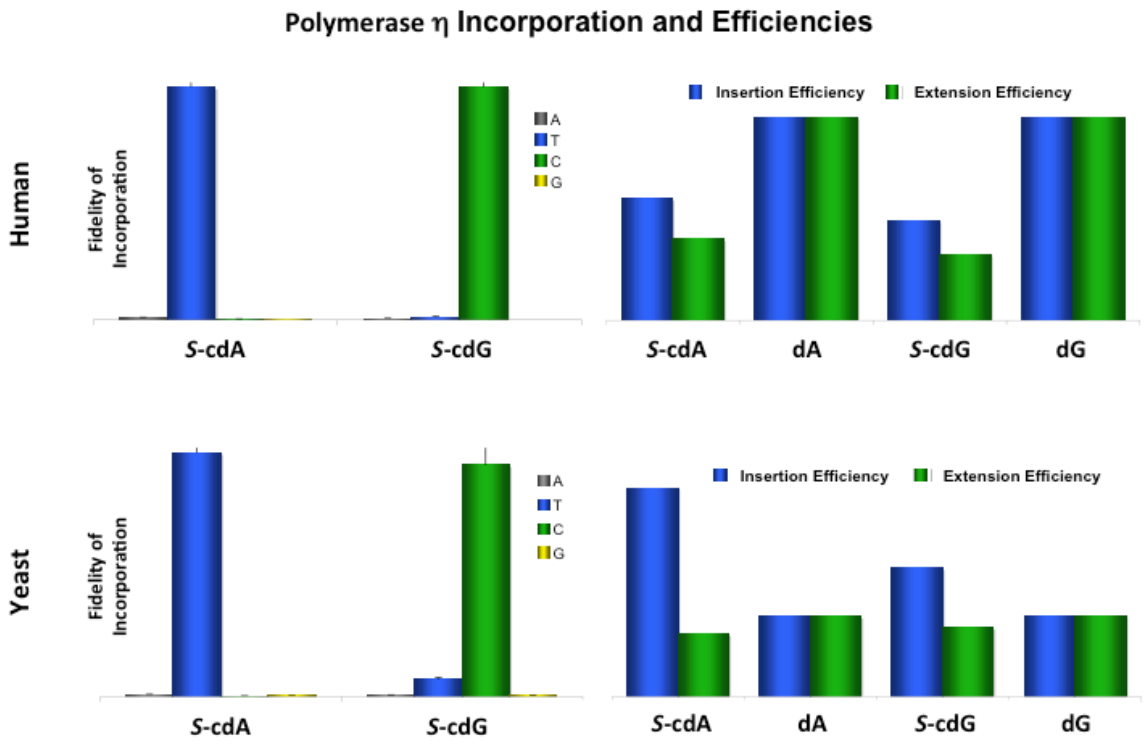

Figure 3.7. Comparison of the fidelity of incorporation, incorporation efficiencies, and extension efficiencies mediated by human Pol η and yeast Pol η opposite and past *S*-cdA and *S*-cdG, and the undamaged nucleosides dA and dG.

additional nucleotides past the two lesions before dissociating from the primer-template complex. Thus, human Pol η can efficiently insert nucleotides opposite *S*-cdA, *S*-cdG, and their immediate 5' neighboring nucleoside before another polymerase takes over to continue with DNA synthesis (239).

The steady-state kinetic results resemble closely those found for Pol η-mediated insertion and extension past the CPD lesion (155,278). The high efficiency and accuracy of nucleotide insertion opposite the two purine cyclonucleosides and their neighboring 5' nucleosides may be attributed to the structural features of Pol η. Among the Y-family polymerases, Pol η is unique in that the polymerase core has a large binding pocket capable of accommodating two nucleotides into its active site (282,283). In addition, Pol η has a distinct molecular splint that rigidly maintains the B-conformation of replicating DNA in the active site, which minimizes erroneous nucleotide incorporation (280,282,283). Future structural studies on complexes formed between Pol η and duplex DNA substrates housing a *S*-cdA and *S*-cdG will provide further insights about how these lesions are recognized by the polymerase.

Previous studies revealed that *S*-cdA and *S*-cdG are both cytotoxic and mutagenic in *E. coli* cells (289,290). A recent replication study showed that *S*-cdA and *S*-cdG strongly blocked DNA replication in AB1157 *E. coli* cells and produced mutations during replication, with *S*-cdA and *S*-cdG yielding A→T and G→A mutations at frequencies of 11% and 20%, respectively (289). This is in line with our observations that these lesions directed yeast and human Pol η to misincorporate mainly dAMP opposite *S*-cdA and dTMP opposite *S*-cdG at low frequencies of ~2.3% and 1.0% (for *S*-cdA), and ~7.0% and

1.2% (for *S*-cdG), respectively. *E. coli* Pol V and eukaryotic Pol η are considered orthologs because they exhibit similar patterns of dNTP insertion opposite many DNA lesions (281). Depletion of Pol V was found to result in compromised bypass of *S*-cdA and *S*-cdG in *E. coli* cells (289,290). Taken together, our results imply that Pol η is likely responsible for the error-free bypass of *S*-cdA and *S*-cdG, whereas other TLS polymerases possibly contribute to the mutagenic bypass seen in *E. coli* cells. Future replication studies will be needed for revealing how these cyclopurine lesions compromise DNA replication and how Pol η affects the bypass of these lesions in mammalian cells.

S-cdA and *S*-cdG are present at relatively abundant levels in genomic DNA of mammalian cells and tissues (53,264-266); thus, the failure to bypass these replication-blocking lesions may contribute to the pathogenesis of human diseases. The results from the present study provided direct biochemical evidence to support that both yeast and human Pol η are capable of bypassing accurately and efficiently the oxidatively induced *S*-cdA and *S*-cdG lesions. In this vein, aerobic metabolism and the resulting generation of ROS are also conserved across evolution. Therefore, aside from its well-established function in tolerating UV light-induced CPD lesions, Pol η perhaps also assumes an evolutionarily conserved role in cells' tolerance of purine cyclonucleosides that are induced endogenously from byproducts of aerobic metabolism. In this vein, it is also important to examine how *S*-cdA and *S*-cdG are bypassed by other TLS polymerases in the future.

Chapter 4: Translesion Synthesis of 8,5'-Cyclopurine-2'-deoxynucleosides by DNA Polymerases η, ι, and ζ

Introduction

Living cells are constantly challenged by endogenous and exogenous genotoxins (1). The resultant DNA damage can lead to mutations and altered gene function, cell senescence or apoptosis (291). To maintain normal cellular function, multiple DNA damage surveillance and repair systems have evolved (292). Among them, translesion synthesis (TLS) is a damage tolerance pathway by which mammalian cells overcome replication blockages imposed by various types of DNA damage (293,294). The most abundant class of TLS polymerases belong to the Y-family, including DNA polymerase η (Pol η), Pol κ, Pol ι, and REV1 (294). In this regard, Pol η, Pol κ, and Pol ι usually play major roles in the insertion step of TLS with occasional involvement in the subsequent extension step (295). In addition, REV1 is widely thought to serve as a scaffold protein to facilitate the recruitment of other TLS polymerases, including Pol η, Pol κ, Pol ι, and, a B-family polymerase, Pol ζ (146,296-298). Recently, it was suggested that yeast (and presumably mammalian) Pol ζ comprised of four subunits, including REV3, REV7, Pol31 and Pol32 (299,300).

Reactive oxygen species (ROS), formed as byproducts of normal aerobic metabolism as well as from exposure to ionizing radiation, can induce a battery of DNA damage products including the (5'*R*) and (5'*S*) diastereomers of 8,5'-cyclo-2'-deoxyadenosine (cdA) and 8,5'-cyclo-2'-deoxyguanosine (cdG) (Figure 4.1) (301,302).

8,5'-cyclopurine-2'-deoxynucleosides (cPus) are stable lesions and are found to be reliable markers for oxidative DNA damage (301,303,304). These cPu lesions have been readily detected *in vitro* and *in vivo* under various conditions (301,305-307). Moreover, it was recently shown that cPu lesions can accumulate in mammalian tissues in an age-dependent and tissue-specific manner, which may accelerate the natural processes of aging and contribute to the development of cancer, neurodegeneration and other human diseases (56,301,304,306,308).

Unlike most other ROS-induced DNA lesions that are removed by base excision repair (BER), cPu lesions are unique due to the presence of a C8-C5' bond between the purine base and 2-deoxyribose of the same nucleoside (Figure 4.1). This additional covalent bond induces helical distortion to DNA and substantially stabilizes the glycosidic bond against acid-induced hydrolysis, which may prevent initiation of BER by a DNA glycosylase and render the cPu lesions attractive substrates for nucleotide excision repair (NER) (301,308). Indeed, multiple lines of evidence supports that the cPu lesions are repaired by NER, but not by BER or direct enzymatic reversal (290,309-312).

Unrepaired cPu lesions may lead to detrimental biological consequences. In this regard, *S*-cdA and *S*-cdG located in the template DNA inhibit strongly DNA transcription and induce the generation of mutant transcripts in mammalian cells (309,310,312). In addition, a single cPu lesion may alter gene expression by preventing the binding of transcription factors and regulatory proteins to their recognition sequences (313,314). *S*-cdA and *S*-cdG can also act as strong inhibitors to DNA replication and induce nucleobase substitutions at the lesion site in *Escherichia coli* cells *(290,315)*. However, it

is still unclear how these cPu lesions compromise DNA replication in mammalian cells. In addition, although previous biochemical studies have suggested a role for Pol η in the TLS across the cPu lesions *in vitro* (316,317), it remains unknown whether Pol η is involved in the replicative bypass of cPu lesions in mammalian cells, and much less is known about whether other TLS polymerases, including Pol κ, Pol ι, and Pol ζ, participate in the TLS across cPu lesions *in vitro* and in mammalian cells.

To address these questions, herein we performed *in vitro* steady-state kinetic assays to understand the roles of Pol κ, Pol ι, and Pol ζ in the replicative bypass of cPu lesions. We also developed a strand-specific PCR-based competitive replication and adduct bypass (SSPCR-CRAB) assay and quantitatively examined how *S*-cdA and *S*-cdG lesions compromise the efficiency and accuracy of DNA replication in human cells. Moreover, we investigated the relative roles of TLS polymerases, including Pol η, Pol κ, Pol ι, and Pol ζ, in the bypass of *S*-cdA and *S*-cdG using human cells that are completely or partially deficient in one or more of these TLS Pols.

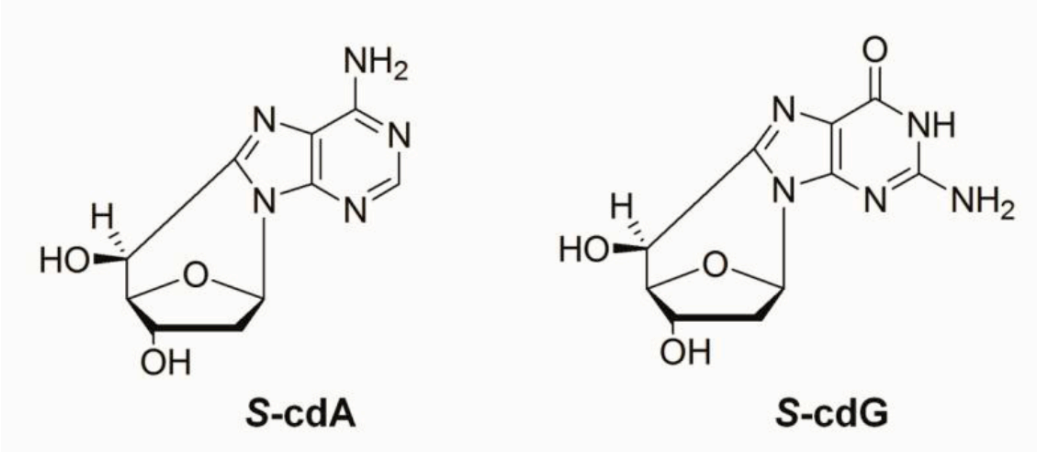

Figure 4.1. Chemical structures of *S*-cdA and *S*-cdG.

Materials and Methods

Materials and cell culture conditions

Unmodified oligodeoxyribonucleotides (ODNs), shrimp alkaline phosphatase, chemicals and [γ-^{32}P]ATP were purchased from Integrated DNA Technologies, USB Corporation, Sigma-Aldrich, and Perkin Elmer, respectively. The 12-mer lesion-bearing ODNs 5′-ATGGCGXGCTAT-3′ ('X' represents *S*-cdA or *S*-cdG) were previously synthesized following published procedures (315,318). Human DNA Pol η, Pol κ, and a two-subunit *Saccharomyces cerevisiae* DNA Pol ζ complex (Rev3/Rev7) were purchased from Enzymax, and human DNA Pol ι was provided by Professor Roger Woodgate. All other enzymes unless otherwise specified were purchased from New England BioLabs (NEB). The 293T human embryonic kidney epithelial cells were purchased from ATCC. The SV40-transformed Pol η-deficient XP30RO fibroblasts and the corrected cells (XP30RO + Pol η) were provided by Professor James E. Cleaver (319,320). Cells were cultured in Dulbecco's Modified Eagle's medium supplemented with 10% fetal bovine serum (Invitrogen), 100 U/mL penicillin, and 100 μg/mL streptomycin (ATCC), and incubated at 37°C in 5% CO_2 atmosphere.

Steady-state kinetic measurements

Steady-state kinetic assays were carried out following previously published procedures (321). The primer-template complex consisted of a 20mer *S*-cdA- or *S*-cdG-bearing template and a 5'-^{32}P-labeled 13mer, 14mer (with the correct nucleosides being placed opposite the lesions), or 15mer (carrying the correct nucleosides opposite the lesions and their adjacent 5' nucleoside, Figure 4.2 and Figure 4.3) primer (0.05 μM).

Template preparation for in vivo replication studies

We first constructed a parent vector for *S*-cdA by modifying the sequence of the original pTGFP-Hha10 plasmid, which contains an SV40 origin and is able to replicate in the SV40-transformed mammalian cells (322,323). To this end, a 50-mer oligodeoxyribonucleotide (ODN) with the sequence of 5'-AATTCGCAGCGAGTCATCCATGGCGAGGTATTGTGGAGTCGATGCATCCG-3' was annealed with its complementary strand and ligated to an NheI-EcoRI restriction fragment from the pTGFP-Hha10 plasmid. We next constructed the *S*-cdA-bearing double-stranded shuttle vector by using a previously described method (Figure 4.4*A*) (322,323). Briefly, we nicked the parent vector for *S*-cdA with Nt.BstNBI to produce a gapped vector by removing a 25-mer single-stranded ODN, followed by filling the gap with a 12-mer *S*-cdA-bearing ODN (5'-ATGGCGXGCTAT-3', X=*S*-cdA) and a 13-mer unmodified ODN (5'-TGTGGAGTCGATG-3'). The ligation mixture was incubated with ethidium bromide, and the resulting supercoiled lesion-bearing plasmid was purified by using agarose gel electrophoresis. Using the same method, we prepared the lesion-free control and competitor vectors for *S*-cdA, where the 12-mer *S*-cdA-containing ODN was replaced with a 12-mer ODN (5'-ATGGCGAGCTAT-3') and a 15-mer ODN (5'-ATGGCGAGCAGCTAT-3'), respectively. The *S*-cdG-bearing vector as well as its corresponding undamaged control and competitor vectors were constructed in a similar fashion.

In vivo transfection and plasmid isolation

The lesion-bearing or the corresponding non-lesion control plasmids were premixed with the competitor genome for *in vivo* transfection, with the molar ratios of competitor vector to control and lesion-bearing genome being 1:1 and 1:19, respectively. The 293T human embryonic kidney epithelial cells, XP30RO, and XP30RO + Pol η cells (1×10^5) were seeded in 24-well plates and cultured overnight, after which they were transfected with 300 ng mixed genome by using Lipofectamine 2000 (Invitrogen) following the manufacturer's instructions. The cells were harvested 24 h after transfection, and the progenies of the plasmid were isolated using the Qiagen Spin Kit (Qiagen), with minor changes (324). The residual unreplicated plasmid was further removed by DpnI digestion, followed by digesting the resulting linear DNA with exonuclease III as described elsewhere (325-327).

Highly efficient depletion of specific TLS DNA polymerases was achieved using siRNAs that were previously validated (328,329). All siRNAs were purchased from Dharmacon: *POLK SMART*pool (L-021038), *POLI SMART*pool (L-019650). *POLH SMART*pool (M-006454), *REV3L SMART*pool (L-006302) and siControl Non-Targeting pool (D-001210). The 293T cells were seeded in 24-well plates at 40-60% confluence level and transfected with approximately 25 pmol siRNAs for each gene using Lipofectamine 2000 (Invitrogen). After a 48-h incubation, 300 ng mixed genome was co-transfected into the cells together with another aliquot of siRNA by using Lipofectamine 2000. The progenies of the plasmid were isolated from the cells 24 h after transfection as described above.

Real-time quantitative RT-PCR

Total RNA was extracted from the cells 48 h after transfection with siRNA using the Total RNA Kit I (Omega), and subjected to DNase I treatment with the DNA-free kit (Ambion) to eliminate the DNA contamination. cDNA was generated by using M-MLV reverse transcriptase (Promega) and an oligo$(dT)_{16}$ primer. Real-time quantitative RT-PCR for evaluating the siRNA knockdown efficiency was performed by using the iQ SYBR Green Supermix kit (Bio-Rad) and gene-specific primers for *POLK*, *POLI*, *POLH*, *REV3L* or the control gene GAPDH as described elsewhere (309), and the primers for real-time RT-PCR are shown in Appendix Table C.1.

Western blot analysis

Western analysis was preformed with a total of 40 μg of whole cell lysate. Antibodies that specifically recognize human Pol η, Pol κ, Pol ι, or REV3L were purchased from Santa Cruz Biotechnology and they were all used at a 1:10,000 dilution. Human β-actin antibody (Abcam) was used at a 1:5000 dilution. Horseradish peroxidase-conjugated secondary goat anti-mouse antibody (Santa Cruz Biotechnology), donkey anti-goat antibody (Santa Cruz Biotechnology), and goat anti-rabbit antibody (Abcam) were used at a 1:10,000 dilution.

PCR, PAGE and LC-MS/MS analyses

The progeny genomes arising from *in vivo* replication were amplified in a PCR reaction (GoTaq green master mix, Promega) containing a pair of primers whose products cover the initial lesion site and span 8 DpnI recognition sites. The primers were 5'-GCTAGCGGATGCATCGACTCCACAA-CAG-3' and 5'-

GGCTCCCTTTAGGGTTC-CGATTTAGT-G-3', and the PCR amplification started at 95°C for 2 min; then, 35 cycles at 95°C for 30 s, 65°C for 30 s, and 72°C for 1.5 min, and a final 5-min extension at 72°C. The PCR products were purified by QIAquick PCR Purification Kit (Qiagen) and stored at -20°C until use.

For PAGE analysis, a portion of the PCR fragments was treated with 5 U NcoI and 1 U shrimp alkaline phosphatase at 37°C in 10 μL NEB buffer 3 for 1 h, followed by heating at 80°C for 20 min to deactivate the shrimp alkaline phosphatase. The above mixture was then treated in a 15 μL NEB buffer 3 with 5 mM DTT, ATP (50 pmol cold, premixed with 1.66 pmol [γ-^{32}P]ATP) and 5 U T4 polynucleotide kinase. The reaction was continued at 37°C for 1 h, followed by heating at 65°C for 20 min to deactivate the T4 polynucleotide kinase. To the reaction mixture was subsequently added 5 U SfaNI, and the solution was incubated at 37°C for 1 h, followed by quenching with 15 μL formamide gel loading buffer. The mixture was loaded onto a 30% polyacrylamide gel (acrylamide:bis-acrylamide=19:1) and products quantified by phosphorimager analysis. Similar to a previously described method for assessing the impact of DNA lesions on transcription (309,330), we determined the effects of DNA lesions on replication efficiency and fidelity by the 'relative bypass efficiency' (RBE) and 'relative mutation frequency' (RMF) values, respectively. Briefly, the RMF value was determined from the relative amounts of different products arising from the replication of the lesion-containing genome. The RBE value was calculated using the following formula, %RBE = (lesion signal/competitor signal)/(non-lesion control signal/competitor signal) (331,332).

LC-MS/MS was used to further identify the replication products arising from *S*-cdA- or *S*-cdG-bearing substrates similar to those described elsewhere (309,315,323,330). Briefly, PCR products were treated with 50 U NcoI and 20 U shrimp alkaline phosphatase in 250 μL NEB buffer 3 at 37°C for 4 h, followed by heating at 80°C for 20 min. To the resulting solution was added 50 U of SfaNI, and the reaction mixture was incubated at 37°C for 4 h followed by extraction with phenol/chloroform/isoamyl alcohol (25:24:1, v/v). The aqueous portion was dried with Speed-vac, desalted with HPLC and dissolved in 12 μL water. The ODN mixture was subjected to LC-MS/MS analysis, as described elsewhere (18, 25, 31, 38). An LTQ linear ion trap mass spectrometer (Thermo Electron) was set up for monitoring the fragmentation of the $[M-3H]^{3-}$ ions of the 13mer ODNs [d(CATGGCGMGCTGT), where "M" designates A, T, C, or G].

Results

Roles of TLS Pols in the bypass of S-cdA and S-cdG in vitro

We first performed steady-state kinetic assays to determine the ability of human Pol ι and Pol κ, as well as yeast Pol ζ to insert nucleotides opposite the *S*-cdA and *S*-cdG, and their respective undamaged substrates (Figure 4.2*A*). In this regard, due to the lack of availability of recombinant mammalian Pol ζ (295,333), herein we used a two-subunit *S. cerevisiae* Pol ζ complex (REV3/REV7) instead. In this regard, a heterodimeric complex, including the REV3 and REV7 subunits, was previously identified as the minimal assembly required for catalytic activity of Pol ζ *in vitro* (293,299). Our results showed that, like Pol η (26), Pol ι was highly error-free and efficient in inserting nucleotides

opposite the two cPu lesions; relative to the corresponding insertion for the unmodified substrates, incorporation of the correct nucleotides opposite *S*-cdA and *S*-cdG occurred at frequencies of ~59% and ~61%, respectively (Fig. 4.2 *B* and *C* and Figure 4.3 and Table 4.1). On the other hand, Pol κ and Pol ζ (REV3/REV7) incorporated nucleotides opposite the cPu lesions with extremely low efficiency (Figure 4.2 *B* and *C* and Tables C.2 and C.3).

We next assessed the accuracy and efficiency of nucleotide incorporation opposite the adjacent 5' nucleoside of the cPu lesions, where we employed a 14mer primer with the correct dNTP being placed opposite the cPu lesions and their respective controls (Figure C.1). It turned out that the efficiency for nucleotide incorporation opposite the 5' neighboring nucleoside (at +1 position) was very poor with Pol ι or Pol κ (Figure 4.2 *B* and *C* and Tables C.4 and C.5). However, Pol ζ (REV3/REV7) was modestly efficient, albeit error-prone, in extending past the *S*-cdA:dT and *S*-cdG:dC pairs (Figure 4.2 *B* and *C* and Table C.6). In this regard, when the correct *S*-cdA**:**dT pair was placed at the primer-template junction, yeast Pol ζ (REV3/REV7) preferentially incorporates the correct dCMP opposite dG at the +1 position, with misincorporation of dAMP, dTMP, and dGMP occurring at frequencies of 0.65%, 1.6%, and 35%, respectively (supplemental Table C.6). Similarly, Pol ζ (REV3/REV7) was highly error-prone in extending past the *S*-cdG**:**dC pair, with misincorporation of dAMP, dTMP, and dGMP opposite the +1 nucleoside (dG) occurring at frequencies of 10%, 21%, and 46%, respectively (Appendix Table C.6).

Table 4.1. Steady-state Kinetic Parameters for Human Pol ι-mediated Nucleotide Insertion opposite *S*-cdA and *S*-cdG, and Unmodified dA and dG[a]

dNTP	k_{cat} (min^{-1})	K_m (μM)	k_{cat}/K_m ($\mu M^{-1}min^{-1}$)	f_{inc}
		***S*-cdA lesion-containing substrate**		
dTTP	32 ± 4	0.19 ± 0.02	170 ± 20	1
dGTP	28 ± 0.3	2.5 ± 0.3	11 ± 2	6.5×10^{-2}
dCTP	16 ± 0.2	63 ± 7	0.25 ± 0.03	1.5×10^{-3}
dATP	21 ± 2	4.9 ± 0.5	4.3 ± 0.5	2.5×10^{-2}
		dA Control		
dTTP	32 ± 4	0.11 ± 0.01	290 ± 30	1
dGTP	11 ± 0.5	210 ± 20	0.052 ± 0.003	1.1×10^{-3}
dCTP	40 ± 3	400 ± 30	0.089 ± 0.002	1.8×10^{-3}
dATP	10 ± 1	310 ± 13	0.033 ± 0.001	6.9×10^{-4}
		***S*-cdG lesion-containing substrate**		
dTTP	20 ± 2	140 ± 20	0.14 ± 0.02	7.4×10^{-4}
dGTP	28 ± 3	95 ± 8	3.4 ± 0.4	1.8×10^{-2}
dCTP	39 ± 4	0.21 ± 0.02	190 ± 20	1
dATP	27 ± 3	2.8 ± 0.3	9.8 ± 1	5.2×10^{-2}
		dG Control		
dTTP	21 ± 2	88 ± 9	0.24 ± 0.03	7.7×10^{-4}
dGTP	25 ± 3	93 ± 10	0.27 ± 0.03	8.7×10^{-4}
dCTP	28 ± 3	0.09 ± 0.01	310 ± 30	1
dATP	23 ± 2	58 ± 6	0.39 ± 0.04	1.3×10^{-3}

[a]k_{cat} and K_m values were based on three independent experiments

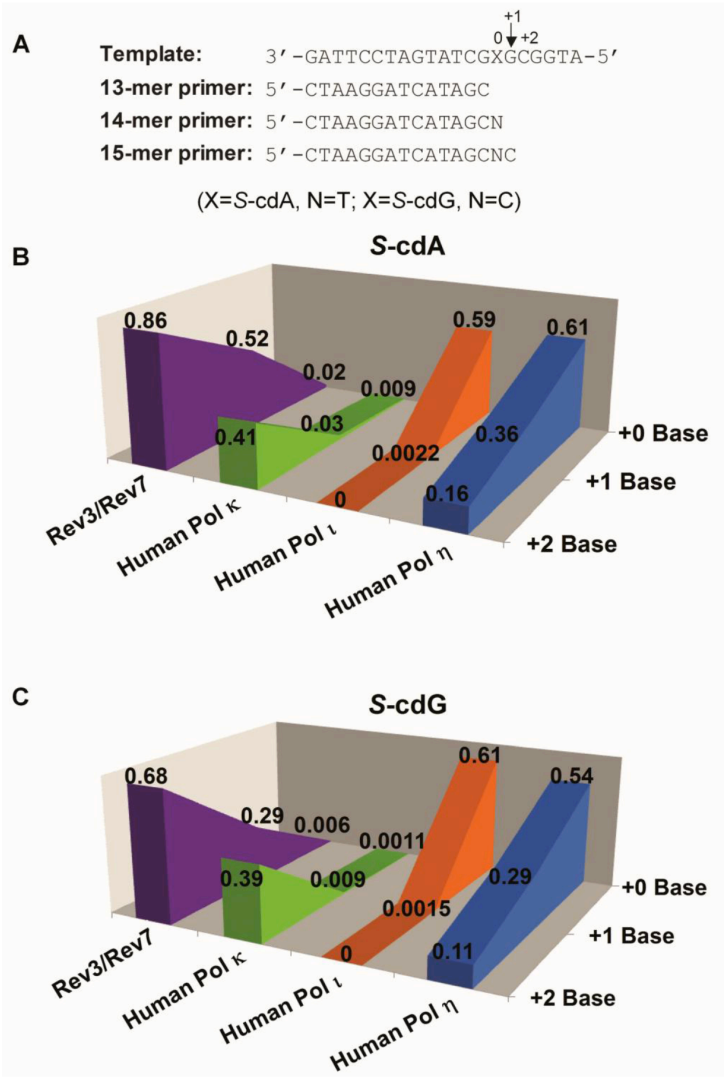

Figure 4.2. Translesion synthesis of cPu lesions *in vitro*. (*A*) The 20mer template and primer sequences used for the *in vitro* replication studies. (*B*-*C*) Relative efficiencies (with respect to the corresponding damage-free substrates) of nucleotide incorporation across and past *S*-cdA (*B*) and *S*-cdG (*C*) by human Pol κ, ι and η, and a two-subunit yeast Pol ζ complex (REV3/REV7). The efficiencies of Pol η-mediated nucleotide insertion opposite the lesion site or the neighboring 5' nucleotide of *S*-cdA or *S*-cdG were published previously (317).

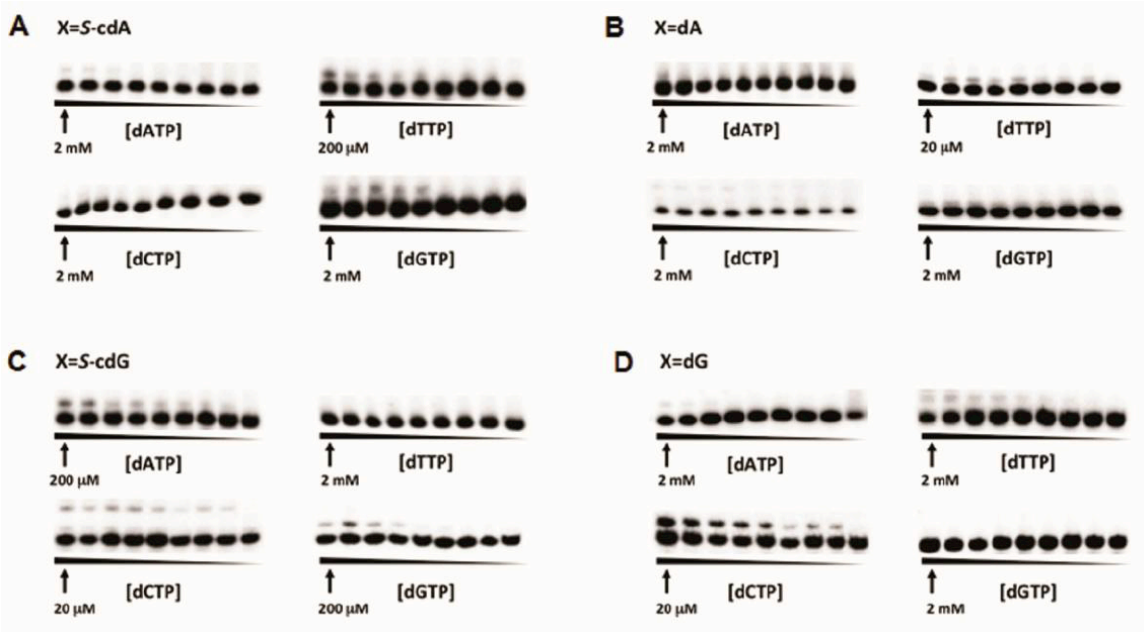

Figure 4.3. Representative gel images for steady-state kinetic assays measuring nucleotide insertion opposite *S*-cdA, *S*-cdG, or corresponding unmodified dA or dG by human Pol ι. The highest concentrations of dNTPs are indicated below the leftmost lane in each gel image, and no dNTP was added for the rightmost lane.

We further obtained the steady-state kinetic parameters for yeast Pol ζ (REV3/REV7)-, as well as human Pol κ- and Pol η-mediated nucleotide insertion at the +2 position with respect to the two cPu lesions. The results showed that yeast Pol ζ (REV3/REV7) extended past the *S*-cdA- and *S*-cdG-bearing substrates with high accuracy and efficiencies; relative to the corresponding insertion for the unmodified substrates, insertion of the correct nucleotides opposite the +2 base in the *S*-cdA- and *S*-cdG-bearing templates occurred at frequencies of ~86% and ~68%, respectively (Figure 4.2 *B* and *C* and Table C.7). In addition, Pol κ-mediated extension past the lesion-containing substrates was moderately efficient, as insertion of the correct dGMP occurred at efficiencies of ~40% relative to the corresponding extension past the dA- and dG-containing substrates (Figure 4.2 *B* and *C* and Appendix Figure C.2 and Table C.8). On the other hand, human Pol η was also able to extend past *S*-cdA and *S*-cdG when the correct nucleosides are placed opposite the lesions and their adjacent 5' nucleosides, albeit much less efficiently (by ~6-10 fold) than the corresponding extension for the unmodified substrates (Table C.8).

Effects of S-cdA and S-cdG on replication in human cells

To investigate how *S*-cdA and *S*-cdG compromise the efficiency and fidelity of DNA replication in human cells, we developed a new SSPCR-CRAB assay. This method evolved from the principle of the traditional competitive replication and adduct bypass assay, which has been widely used for assessing the cytotoxic and mutagenic properties of DNA lesions placed in a single-stranded M13 genome in *E. coli* cells (331,332).

We constructed doubled-stranded shuttle vectors containing a single site-specific lesion (*S*-cdA or *S*-cdG), as well as the corresponding non-lesion control vectors housing an unmodified nucleotide (A or G) at the lesion site. Given that the lesion-bearing strand may be replicated at a reduced efficiency from its opposing undamaged strand in mammalian cells (334,335), we employed a similar strategy as described previously (323,334,335) and incorporated a C/C mismatch two nucleotides away from the lesion site to distinguish the replication products fromed from the two strands (Figure 4.4*A*). The lesion-bearing or undamaged control vectors were mixed individually with an undamaged competitor vector at given molar ratios and co-transfected into human cells (Figure 4.4*B*). In this regard, the competitor vector contains three more nucleotides than the control vector situated between the two restriction sites used for SSPCR-CRAB assay. The progenies of the plasmids were isolated from human cells 24 h after transfection, and residual unreplicated plasmids were removed by a combined treatment with DpnI and exonuclease III as described previously (325-327). The progeny genomes were subsequently amplified using a pair of PCR primers spanning the lesion site. Notably, one of the primers (P1) carries a G as the terminal 3'-nucleotide corresponding to the C/C mismatch site (Figure 4.4*B*), which is used to amplify selectively the progeny genomes arising from the replication of the bottom, but not the top strand of the plasmids under appropriate conditions (336). In addition, P1 was designed deliberately to carry a C/A mismatch three bases from its 3'-end (Figure 4.4*B*) in order to increase the specificity of strand-specific PCR, as described previously (336). The resulting PCR

products were digested with appropriate restriction enzymes, i.e., NcoI and SfaNI, and subjected to LC-MS/MS and PAGE analyses.

We first asked whether Pol η is involved in TLS across cPu lesions in human cells. To this end, we performed the SSPCR-CRAB assay using the Pol η-deficient XP30RO fibroblasts and the corrected cells (XP30RO + Pol η) as hosts for *in vivo* replication. PAGE analysis of restriction fragments of PCR products showed that the RBE values for *S*-cdA and *S*-cdG in Pol η-deficient XP30RO cells were ~ 3% and ~ 2%, respectively, and the RBE values for the two lesions were substantially higher in Pol η-rescued human cells at 24 h after transfection (Figure 5 *A* and *B*). PAGE analysis also showed that *S*-cdA was mutagenic during replication, with A→T mutation occurring at frequencies of ~ 5% and ~ 9% in Pol η-deficient and Pol η-complemented cells, respectively (Figure 5 *A* and *C*). In addition, replicative bypass of *S*-cdG in Pol η-deficient and Pol η-rescued cells can give rise to G→A transition at frequencies of ~ 3% and ~ 11%, respectively, and G→T transversion at frequencies of ~27 % and ~ 32%, respectively (Figure 5*A* and *C*). We also determined the identities of these mutated products by LC-MS/MS analysis (Appendix Figure C.3).

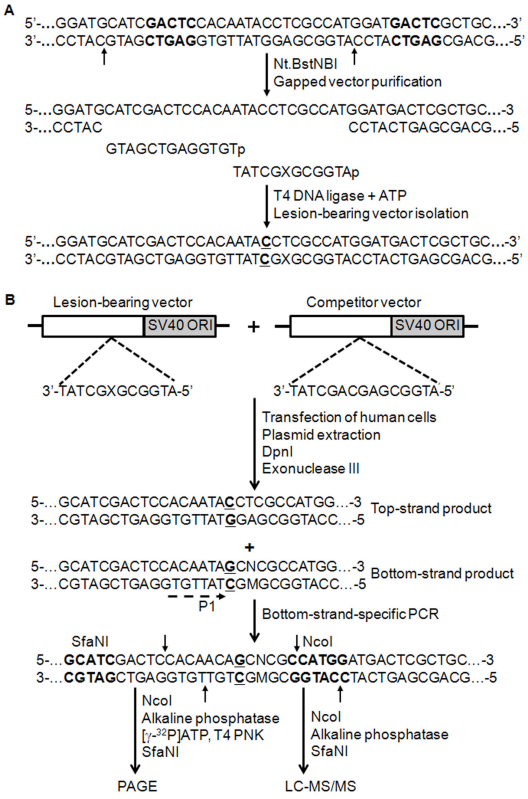

Figure 4.4. Schematic diagrams showing the procedures for the preparation of the lesion-bearing plasmid (*A*) and the SSPCR-CRAB assay (*B*) (See '*experimental procedures*' for details). Only the construction of *S*-cdA-bearing vector is shown. "SV40 ORI" and "X" indicate SV40 replication origin and *S*-cdA, respectively. C/C mismatch site is underlined. The cleavage sites of Nt.BstNBI, NcoI and SfaNI are designated with arrows. P1 represents one of the primers for PCR, i.e., d(GCTAGCGGATGCATCGACTCCACAACAG). P1 contains a G as the terminal 3'-nucleotide corresponding to the C/C mismatch site of lesion-bearing genome, and it also contains a C/A mismatch three bases away from its 3'-end for improving the specificity of PCR. "M" represents the nucleobase formed at the lesion site after replication, and "N" designates the paired nucleobase of "M" in the complementary strand.

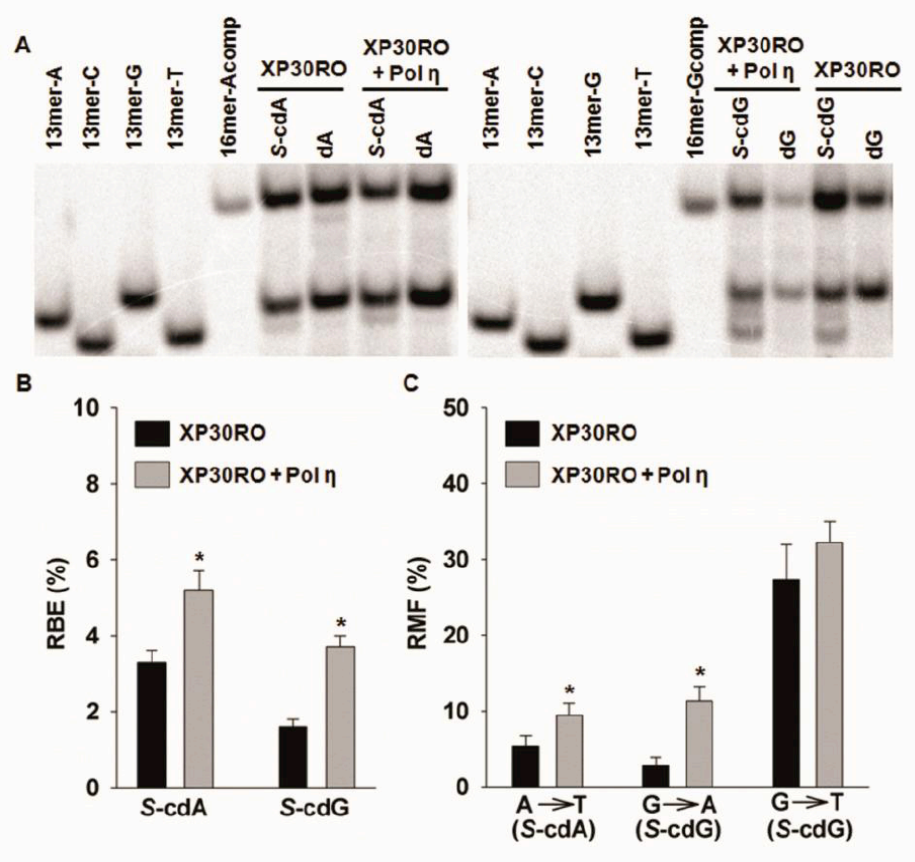

Figure 4.5. *In vivo* replication studies of *S*-cdA and *S*-cdG using Pol η-deficient XP30RO fibroblasts and the corrected cells (XP30RO + Pol η). (*A*) Representative gel images. The restriction fragments arising from the competitor vectors for *S*-cdA and *S*-cdG, i.e., d(CATGGCGAGCAGCTGT) and d(CATGGCGGGCAGCTGT), are designated with '16mer-Acomp' and '16mer-Gcomp', respectively; '13mer-A', '13mer-C', '13mer-G', and '13mer-T' represent standard ODNs d(CATGGCGMGCTGT), where M is A, C, G, and T, respectively. (*B*-*C*) The RBE (*B*) and RMF values (*C*) of *S*-cdA and *S*-cdG in Pol η-deficient XP30RO cells and the XP30RO + Pol η cells. The data represent the mean and standard error of results from three independent experiments. '*', $P < 0.05$. The *P* values were calculated by using unpaired, two-tailed Student's *t*-test.

We further confirmed the involvement of Pol η in TLS across *S*-cdA and *S*-cdG by using 293T cells in which the expression of Pol η was knocked down by siRNA. Consistent with previous report (329), our real-time PCR and Western blot results showed that siRNA knockdown was highly efficient for the *POLH* gene (Figure 4.6 *A* and *B*). As expected, the RBE values for *S*-cdA and *S*-cdG were markedly lower in Pol η knockdown cells than in control siRNA-treated cells (Figure 4.7 *A* and *C* and Appendix Figure C.4 *A* and *B*). In addition, we found that knocking down the expression of Pol η caused a considerable decrease in A→T mutation induced by *S*-cdA in 293T cells (Figure 4.7*B* and Figure C.4*A*). On the other hand, partial depletion of Pol η with siRNA did not confer a significant reduction in G→A or G→T mutation induced by *S*-cdG in human cells (Figure 4.7 *D*-*E* and Figure C.4*B*).

We next used siRNAs to inhibit the expression of other TLS polymerases, including Pol κ, Pol ι, and Rev3L (Figure 6 *A* and *B*), and determined their possible roles in TLS across cPu lesions in human cells. Relative to 293T cells treated with control siRNA, the RBE values for *S*-cdA and *S*-cdG were considerably lower in the cells treated with Pol ι or REV3L siRNAs (Figure 4.7 *A* and *C* and Figure C.4 *A* and *B*). On the other hand, we did not find any change in RMF values for *S*-cdA or *S*-cdG caused by siRNA knockdown of Pol ι or REV3L, except that knockdown of Pol ι led to a decrease in G→A mutation for *S*-cdG (Figure 4.7 *B* and *D* and *E* and Figure C.4 *A* and *B*). In addition, the siRNA depletion of Pol κ had no effect on the RBE or RMF values for *S*-cdA and *S*-cdG in human cells (Figure 4.7 *A*-*E* and Figure C.4 *A* and *B*).

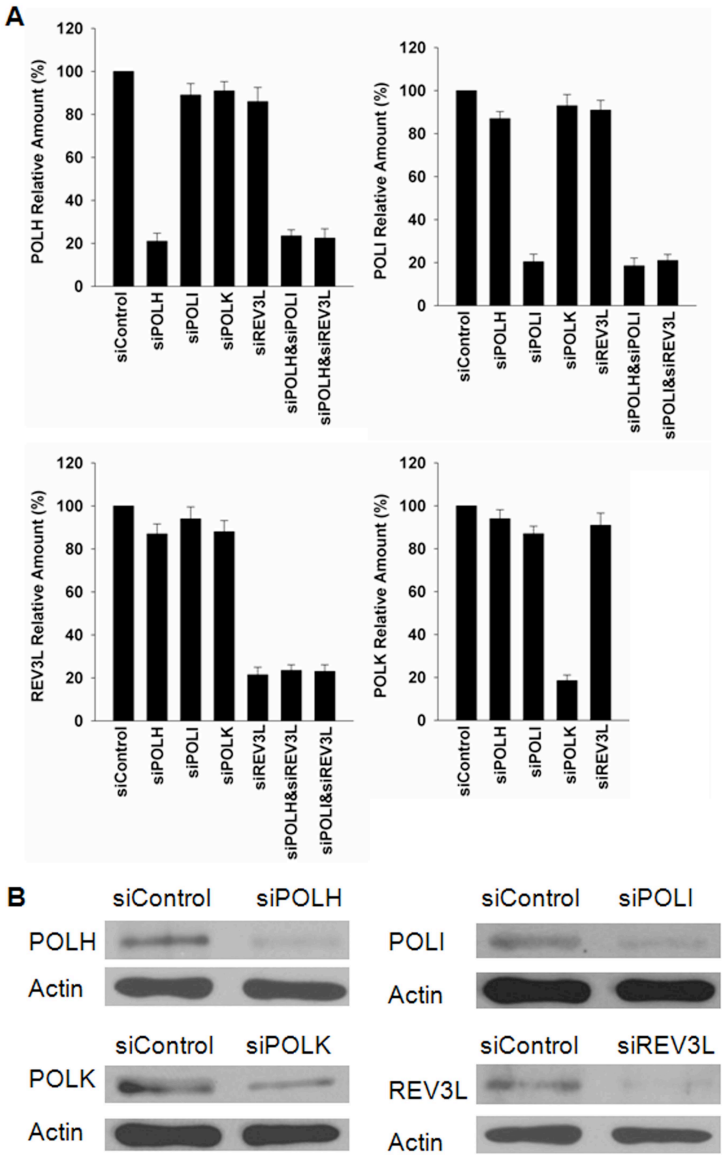

Figure 4.6. Real-time qRT-PCR (A) and Western blot (B) analysis for monitoring the siRNA-induced knockdown of TLS polymerases in 293T cells. The examined TLS polymerases include Pol η (POLH), Pol κ (POLK), Pol ι (POLI) and Pol ζ (Rev3L). GAPDH was used as control for real-time qRT-PCR analysis, and β-actin was used as the loading control for Western analysis. The data shown in (A) represent the mean and standard error of results from three separate experiments.

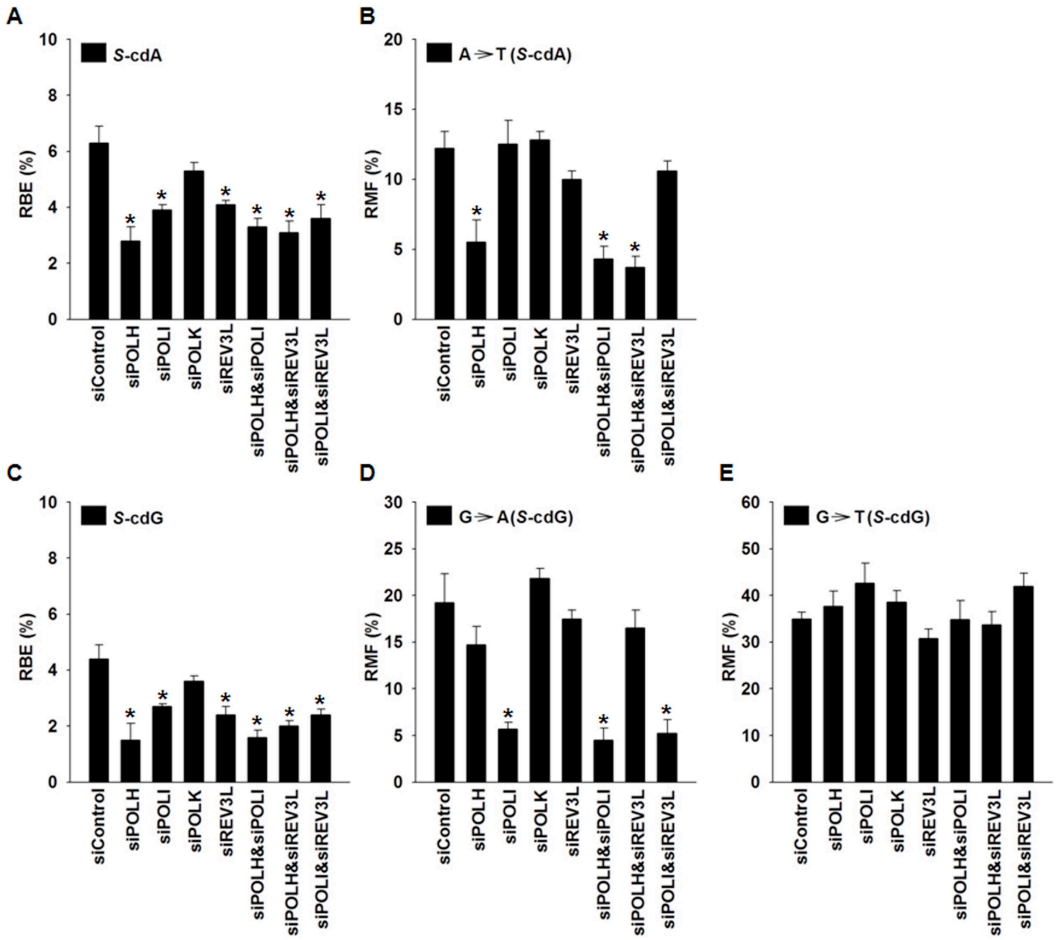

Figure 4.7. Effects of siRNA knockdowns of TLS Pols on the replicative bypass of *S*-cdA and *S*-cdG in human cells. Shown in (*A*) and (*C*) are the RBE values of *S*-cdA and *S*-cdG, respectively. Shown in (*B*), (*D*) and (*E*) are the RMF values of A→T induced by *S*-cdA, G→T and G→A mutations induced by *S*-cdG, respectively. The examined TLS polymerases include Pol η (POLH), Pol κ (POLK), Pol ι (POLI) and Pol ζ (Rev3L).The data represent the mean and standard error of results from three independent experiments. RBE or RMF values that were significantly different from that of the corresponding control siRNA (siControl) are indicated with an asterisk ($P < 0.05$). The *P* values were calculated by using unpaired, two-tailed *t*-test.

The above results suggested that Pol η, Pol ι, and Pol ζ had important roles in promoting replication through cPu lesions in human cells. To further ascertain whether these three polymerases function in the same or different pathways for replicative bypass of cPu lesions, we assessed the effects of simultaneous knockdowns of two out of the three TLS Pols (Figure 4.6 *A* and *B*). Our results showed that knockdown of both Pol η and REV3L had an effect similar to that of Pol η alone (Figure 4.7 *A*-*E* and Figure C.4 *C* and *D*). Similarly, we found that the dual knockdown of Pol η and Pol ι, or of Pol ι and REV3L, did not cause further change in TLS frequencies relative to that observed upon the knockdown of one of these polymerases alone (Figure 4.7 *A*-*D* and Figure C.4 *C* and *D*). Therefore, Pol η, Pol ι, and Pol ζ may cooperate with each other to carry out TLS across *S*-cdA and *S*-cdG in human cells.

Discussion

It has been previously shown that *S*-cdA is a strong blockage to mammalian DNA polymerase δ and T7 DNA polymerase *in vitro* (310), and the bypass efficiencies of *S*-cdA and *S*-cdG during replication are very low (less than ~5%) in wild-type *E. coli* cells (290,315). In agreement with these findings, our results demonstrated that both *S*-cdA and *S*-cdG constituted strong blockage to DNA replication machinery in human cells. We also found that replicative bypass of *S*-cdA and *S*-cdG generated mutations in human cells. Similar to the observation in *E. coli* cells (290,315), *S*-cdA was weakly mutagenic

and induced A→T transversion at a frequency of ~10% in 293T cells. On the other hand, the major type of mutation induced by *S*-cdG is G→A transition occurring at a frequency of ~20%, though a low frequency (less than ~5%) of G→T transversion was also observed in *E. coli* cells (290,315). Compared with *E. coli* cells, replicative bypass of *S*-cdG was more mutagenic in human 293T cells (~50%), where we observed a higher frequency of G→T than G→A mutation. The strong blocking and mutagenic effects of the cPu lesions on DNA replication in human cells, together with the abundant presence of these lesions in mammalian tissues (56,301,304,306,308), suggest that these lesions may constitute significant endogenous DNA lesions that may play important roles in the development of human diseases.

We further demonstrated a role for Pol η in promoting replication through the cPu lesions *in vivo*, by using human cells that are completely or partially deficient in Pol η. Consistent with our results, depletion of its ortholog, i.e., Pol V, also caused decreased bypass efficiencies of *S*-cdA and *S*-cdG in *E. coli* cells (290,315). In addition, depletion of Pol η in human cells conferred a considerable reduction in mutation frequency of *S*-cdA, suggesting that Pol η may be involved in error-prone replicative bypass of this lesion in mammalian system. This result is somewhat surprising, as our previous biochemical studies have suggested a role for Pol η in the error-free nucleotide insertion opposite cPu lesions (317). The difference in the fidelity of lesion bypass by Pol η between *in vitro* and *in vivo* studies may be attributed to two factors. Firstly, it has been proposed that the TLS machinery requires the functional interaction between TLS Pols and other accessory proteins, which may modulate the fidelity and/or efficiency of TLS

Pols in lesion bypass in cells (295,329,337,338). Secondly, the *in vitro* steady-state kinetic experiments were conducted in the presence of one nucleotide at a time, whereas the replication in cells occurs in the mutual presence of all four canonical nucleotides. Thus, the absence or presence of competition in nucleotide incorporation under the two replication conditions may also result in different efficiencies and fidelities of TLS (339).

We also demonstrated, for the first time, that Pol ι and Pol ζ have important roles in translesion synthesis of cPu lesions. Our biochemical results demonstrated that human Pol ι and yeast Pol ζ (REV3/REV7) could function efficiently in the insertion and extension steps, respectively, of TLS across *S*-cdA and *S*-cdG *in vitro*. Along this line, siRNA knockdown of Pol ι and REV3L led to a substantial decrease in RBE values for *S*-cdA and *S*-cdG in human cells. Like in the case of Pol η, although *in vitro* biochemical results showed that Pol ι predominantly incorporated the correct nucleotides opposite the cPu lesions, our *in vivo* replication studies showed that, siRNA knockdown of Pol ι could cause a reduction in *S*-cdG-induced G→A mutation. This result suggested that Pol ι may play a role in error-prone insertion opposite this lesion during replication in human cells.

Moreover, we found that the simultaneous depletion of any two of Pol η, Pol ι and Pol ζ had no additive effects on the replicative bypass of cPu lesions, indicating that these three polymerases might function in the same or partly overlapping genetic pathways for bypassing cPu lesions in human cells. On the other hand, although human Pol κ exhibited its ability to extend past these cPu lesions *in vitro*, knocking-down the expression of Pol κ had no effect on TLS across *S*-cdA and *S*-cdG in human cells. This is

in keeping with previous data indicating that Pol IV, an ortholog of Pol κ, may not be able to bypass these cPu lesions in *E. coli* cells (290,315).

It should be noted that, we observed lower frequencies of G→A mutation induced by *S*-cdG in Pol η-deficient human fibroblast cells than the isogenic cells rescued with wild-type human Pol η; however, siRNA knockdown of Pol η had no significant effect on the mutation frequencies of *S*-cdG in 293T cells. This result may reflect a role for the residual Pol η in TLS across *S*-cdG in cells. In this vein, it was suggested that residual TLS Pols might be sufficient for keeping the miscoding properties of some DNA lesions unchanged, even though sometimes lesion bypass efficiencies could be reduced by the siRNA knockdown of some specific TLS Pols (323,328,329).

Based on our findings, we proposed a model for the TLS across cPu lesions in human cells. In this model, a replicative polymerase stalled by cPu lesions on the template DNA is displaced by Pol η and/or Pol ι, which inserts a nucleotide opposite the lesion. A second polymerase-switch can then be made, where another TLS polymerase (i.e. Pol ζ) accurately extends the primer terminus past the damage site. In keeping with our study, two-polymerase mechanisms, in which insertion by one (or more) specific TLS Pol(s) is followed by extension with another polymerase, has been suggested to play important roles in the replicative bypass of several other DNA lesions in mammalian cells. These included thymidine glycol, *cis,syn*-cyclobutane pyrimidine dimer, and pyrimidine(6-4)pyrimidone photoproducts in mammalian cells (295,328,329,337,338). It would be interesting to unveal how different inserter and extender Pols as proposed here

and in other studies (295,328,329,337,338) coordinate their actions during TLS across DNA damage in human cells.

Chapter 5: Translesion Synthesis of Ribonucleotides by Purified DNA Polymerases *In Vitro*

Introduction

The integrity of the human genome depends partly on the ability of replicative DNA polymerases to exclude ribonucleotides from being incorporated into DNA (62,340). The presence of a reactive hydroxyl (OH) group at the 2' position of the ribose alters the global conformation of DNA and leaves the DNA backbone highly susceptible to spontaneous hydrolysis and subsequent breakage (341,342). To counteract this deleterious effect, DNA polymerases have evolved specific amino acids within their active sites that serve as a 'steric gate' to hinder the misinsertion of ribonucleoside monophosphate (rNMP) into DNA (343). However, recent studies have suggested that all three replicative DNA polymerases, α, δ, and ε, misinsert rNMPs much more frequently into the genome than previously anticipated, partly due to much higher concentrations of ribonucleoside triphosphates (rNTPs) than 2'-deoxyribonucleoside triphosphates (dNTPs) in the nucleotide pool (61,62). Additionally, the replicases have a compromised ability to bypass and proofread the misinserted ribonucleotides, especially for pol ε, which misinserts one rNMP per every 1250 dNMPs into the genome and bypasses rG and rU with efficiencies at ~32% and 39% compared to corresponding 2'-deoxynucleosides (344,345). As a result, ribonucleotides may constitute the most common endogenously produced DNA lesions in replicating cells (Figure 5.1) (64).

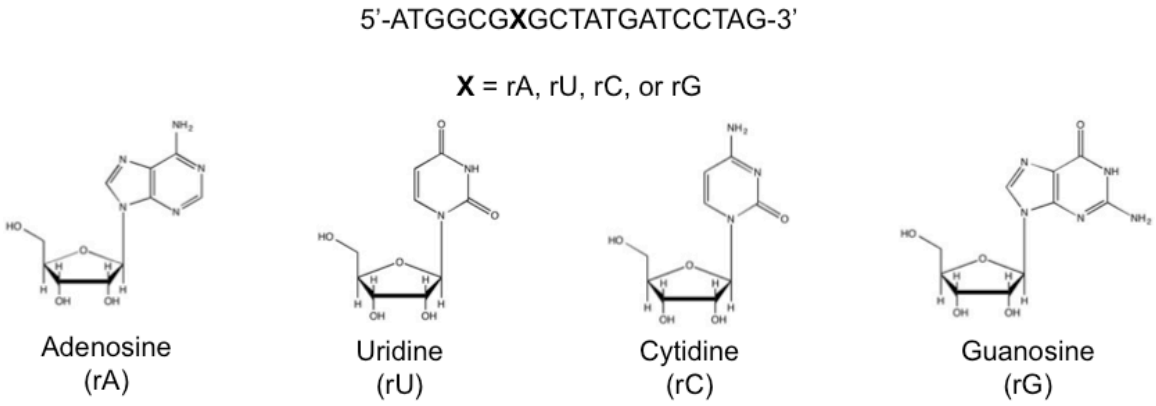

Figure 1. Structures of the four ribonucleotides, and the template used for the *in vitro* replication studies.

To remove ribonucleosides from genomic DNA, cells are equipped with topoisomerase 1 (Top1) and RNase H2, responsible for nicking on the 5' side of rN; however, there are instances where ribonucleosides remain embedded in the genome (346-349). This is especially pronounced in patients with Aicardi-Goutieres syndrome, as they lack a functional RNase H2 and are unable to excise ribonucleotides from their genomic DNA (350). Deficiency in RNase H2 results in a massive accumulation of mutations and 2-5 bp deletions, posing a considerable threat to genomic stability (346). Translesion synthesis (TLS) is a cellular pathway that is employed by cells to bypass these and other lesions that block DNA replication. This process uses specialized DNA polymerases, most of which are members of the Y-family, to insert nucleotides opposite and past the damage site (239,351,352). TLS polymerases include the Y-family Pols η, κ, ι, and Rev1, as well as the B-family Pol ζ (351). These polymerases have more spacious active sites than replicative polymerases, largely due to the presence of a little finger domain, allowing them to accommodate bulky lesions and mismatches that distort the DNA double helix structure (239,275). However, they lack a proofreading 3'→5' exonuclease domain; thus, they are often more mutagenic than replicative polymerases, though there are instances where TLS Pols are highly accurate and efficient (155,229,244,351,353-357). This process is crucial to cell survival as it maintains progression of the replication fork and allows bulky and unrepaired lesions to be tolerated by cells.

It has been reported that TLS polymerase(s) and, specifically, Pol ζ may play a major role in protecting yeast cells from replicative stress induced by ribonucleotides in

DNA (347). Pol ζ is able to efficiently extend past up to four ribonucleotides embedded in a DNA strand, which becomes increasingly important in cells lacking RNase H activity (347). However, little is known of the mutagenic and blocking potential of ribonucleotides when encountered by other major TLS polymerases. This research seeks to examine how the TLS polymerases, including human and yeast Pol η, yeast Pol ζ, human Pol ι, and human Pol κ, bypass single ribonucleotides in DNA *in vitro*.

Materials and Methods

Unmodified oligodeoxyribonucleotides (ODNs) and ODNs containing a single ribonucleoside were purchased from Integrated DNA Technologies (Coralville, IA). [γ-^{32}P]ATP was purchased from Perkin-Elmer (Boston, MA). Human DNA Pol κ and *Saccharomyces cerevisiae* DNA Pol ζ (Rev3/Rev7) were purchased from Enzymax (Lexington, KY), and human Pol η and Pol ι were generously provided by Drs. Wei Yang and Roger Woodgate, respectively. *Saccharomyces cerevisiae* Pol η was expressed and purified following previously published procedures (358). All other enzymes unless otherwise specified were purchased from New England BioLabs (NEB, Ipswich, MA), and all other reagents purchased from Sigma-Aldrich (St. Louis, MO).

Preparation of ribonucleoside-containing substrates

Ribonucleoside-containing substrates d(ATGGCGXGCTAT) [X = rA, rU, rC, or rG] were ligated with a 5'-phosphorylated 8 mer, d(GATCCTAG), in the presence of a 30mer ODN template, d(CCGCTCCCTAGGATCATAGCYCGCCATGCT) [Y = dA,

dT, dC, or dG], following previously published procedures (229,359). The resultant 20mer ribonucleoside-containing substrates were purified using 20% denaturing polyacrylamide gel electrophoresis (PAGE), where the gel plates were treated with RNaseZap (Life Technologies, USA).

Steady-state kinetic measurements

Steady-state kinetic assays were carried out following previously published procedures (321). The above-described primer-template complex (10 nM) was incubated with individual polymerases under the aforementioned conditions. The reaction was carried out in the presence of one dNTP at a time at varying concentrations to allow for a maximum of 20% primer extension. After 10 min, the reactions were terminated using an equal volume of formamide gel-loading buffer, which contained 80% formamide, 10 mM EDTA (pH 8.0), 1 mg/mL xylene cyanol, and 1 mg/mL bromophenol blue. Steady-state kinetic parameters V_{max} and K_m were calculated by fitting the data to the Michaelis-Menten equation:

$$V_{obs} = \frac{V_{\max} \times [dNTP]}{K_m + [dNTP]}$$

The k_{cat} values were calculated by dividing the V_{max} by concentration of polymerase used. The fidelity of nucleotide incorporation was then calculated by the following equation:

$$f_{inc} = \frac{(k_{cat} / K_m)_{incorrect}}{(k_{cat} / K_m)_{correct}}$$

Results

Primer Extension past Ribonucleotides

We first assessed the ability of TLS Pols to extend a 13mer primer in the presence of a site-specifically incorporated ribonucleotide (rN) or the complementary unmodified DNA base in a 20mer DNA template (Figures 5.1 & 5.2, Figure D.1). We found that all five TLS polymerases, which include yeast Pol ζ, human Pol κ, human and yeast Pol η, and human Pol ι, could successfully bypass a ribonucleotide misincorporated in a 20mer DNA template in the presence of all four dNTPs, as evidenced by the full-length extension (Figure 5.2). Extension from rA was most efficient for all TLS polymerases, demonstrated by the small amount of unextended primer, followed by rG (Figure 5.2). However, there is a significant amount of stalled replication products in the primer extension reaction mixture for rC- and rU-containing substrates with human Pols η, κ and ι, and yeast Pols ζ and η, indicating a blocking effect of these two pyrimidine ribonucleosides on the TLS polymerases (Figure 5.2).

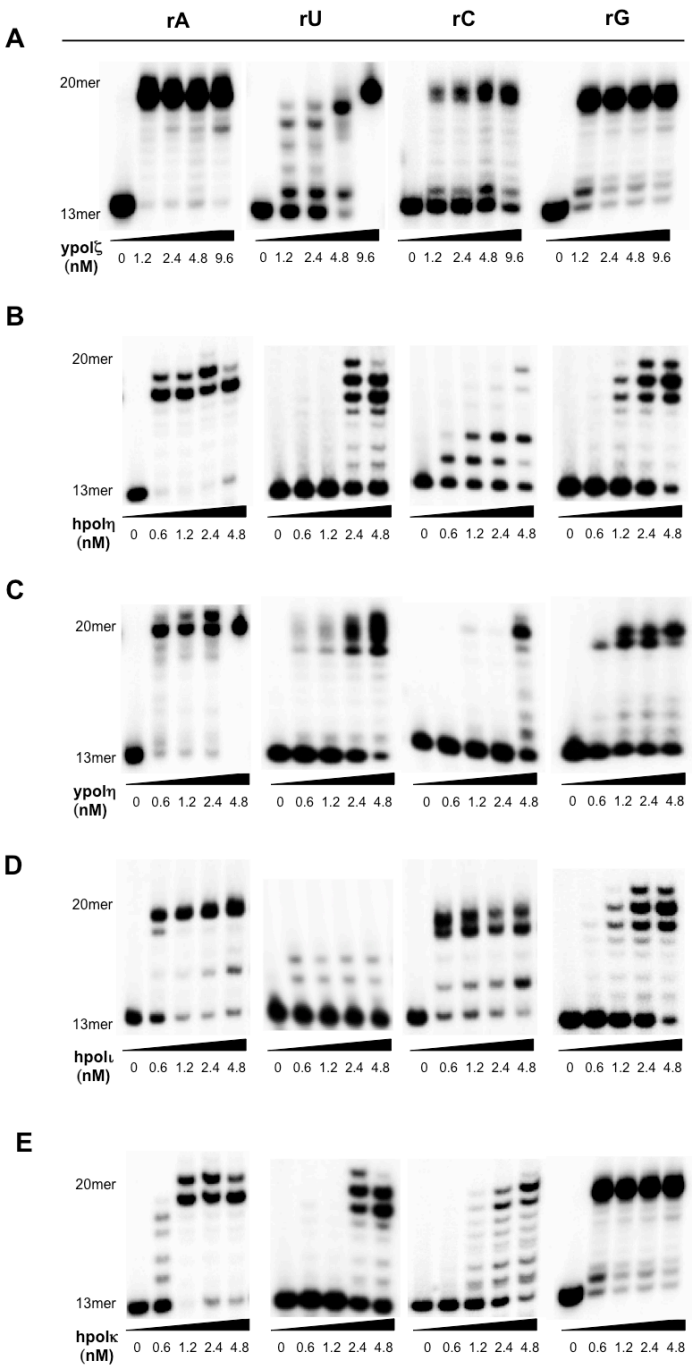

Figure 5.2. Primer extension assays past a single ribonucleotide (rA, rU, rC, or rG) in template DNA, with A) yeast Pol ζ, B) human Pol η, C) yeast Pol η, D) human Pol ι, and E) human Pol κ, with the concentrations of the polymerases being listed in the figure.

We next asked how accurately and efficiently the TLS Pols can insert deoxyribonucleotides opposite a single rN placed in a DNA template. To this end, we determined the steady-state kinetic parameters for nucleotide insertion opposite each rN as well as their respective deoxynucleosides in the presence of one dNTP at a time. We first characterized the yeast Pol ζ-mediated nucleotide incorporation opposite rNs (Table 5.1, Figure 5.3). Our results showed that yeast Pol ζ inserted the correct dTMP opposite rA with ~80% efficiency, and misincorporation of dGMP, dCMP, and dAMP occurred at frequencies of 2.9%, 0.86%, and 0.34%, respectively (Table 5.1, Figure 5.3a). Similarly, it promotes accurate and efficient nucleotide insertion opposite rU, with low frequencies of misinsertion of dCMP (3.2%), dGMP (0.72%), and dTMP (0.96%), and with the dAMP insertion occurring at an efficiency of ~76% relative to the unmodified dT substrate (Table 5.1, Figure 5.3b). On the other hand, nucleotide incorporation opposite rC and rG was somewhat more mutagenic, with frequencies of misinsertion being 9.4% for dCMP opposite rC, and 15% for dAMP opposite rG (Table 5.1, Figure 5.3c-d). However, yeast Pol ζ inserted the correct dCMP opposite rG at ~81% efficiency compared to the control dG substrate, and rC posed the most blocking effect to the polymerase, with a k_{cat}/K_m of 8.7 μM^{-1} min^{-1} for dGMP incorporation relative to 23 μM^{-1} min^{-1} for the corresponding insertion opposite unmodified dC (Table 5.1).

Table 5.1. Steady-state Kinetic Parameters for *S. cerevisiae* Pol ζ-mediated Nucleotide Insertion opposite rA, rU, rC, and rG, and opposite Unmodified dA, dT, dC and dG [a]

dNTP	k_{cat} (min^{-1})	K_m (μM)	k_{cat}/K_m ($\mu M^{-1}min^{-1}$)	f_{inc}
		X = rA-containing substrate		
dTTP	10 ± 1	0.48 ± 0.05	21 ± 2	1
dGTP	11 ± 1	18 ± 0.3	0.61 ± 0.07	2.9×10^{-2}
dCTP	7.5 ± 1	41 ± 0.1	0.18 ± 1	8.6×10^{-3}
dATP	7.1 ± 0.8	62 ± 6	0.072 ± 0.005	3.4×10^{-3}
		X = rC-containing substrate		
dTTP	8.6 ± 0.9	66 ± 7	0.14 ± 0.02	1.6×10^{-2}
dGTP	12 ± 1	1.4 ± 0.1	8.7 ± 0.9	1
dCTP	9.8 ± 1	12 ± 1	0.82 ± 0.09	9.4×10^{-2}
dATP	6.7 ± 0.7	110 ± 10	0.061 ± 0.007	7.0×10^{-3}
		X = rG-containing substrate		
dTTP	7.7 ± 0.8	51 ± 5	0.15 ± 0.1	8.3×10^{-3}
dGTP	9.2 ± 1	7.7 ± 0.8	1.2 ± 0.1	6.7×10^{-2}
dCTP	13 ± 1	0.72 ± 0.07	18 ± 2	1
dATP	11 ± 1	4.1 ± 0.4	2.7 ± 0.3	1.5×10^{-1}
		X = rU-containing substrate		
dTTP	9.2 ± 1	39 ± 4	0.24 ± 0.2	9.6×10^{-3}
dGTP	8.5 ± 0.9	48 ± 5	0.18 ± 0.2	7.2×10^{-3}
dCTP	11 ± 1	14 ± 1	0.79 ± 0.9	3.2×10^{-2}
dATP	14 ± 1	0.56 ± 0.6	25 ± 3	1
		X = dA-containing substrate		
dTTP	12 ± 1	0.46 ± 0.05	26 ± 3	1
dGTP	9.8 ± 1	74 ± 6	0.13 ± 0.01	5.0×10^{-3}
dCTP	7.3 ± 0.8	85 ± 9	0.086 ± 0.009	3.3×10^{-3}
dATP	11 ± 1	44 ± 4	0.25 ± 0.03	9.6×10^{-3}
		X = dT-containing substrate		
dTTP	12 ± 1	46 ± 5	0.26 ± 0.03	7.6×10^{-3}
dGTP	11 ± 1	92 ± 9	0.12 ± 0.01	3.5×10^{-3}
dCTP	7.9 ± 0.8	87 ± 9	0.091 ± 0.01	2.7×10^{-3}
dATP	15 ± 2	0.44 ± 0.05	34 ± 3	1
		X = dC-containing substrate		
dTTP	10 ± 1	81 ± 9	0.12 ± 0.02	5.2×10^{-3}
dGTP	15 ± 2	0.65 ± 0.07	23 ± 2	1
dCTP	13 ± 1	64 ± 3	0.20 ± 0.02	8.7×10^{-3}
dATP	8.6 ± 0.9	85 ± 9	0.10 ± 0.01	5.9×10^{-3}
		X = dG-containing substrate		
dTTP	9.1 ± 1	82 ± 9	0.11 ± 0.01	5.0×10^{-3}
dGTP	10 ± 1	40 ± 3	0.25 ± 0.03	1.1×10^{-2}
dCTP	14 ± 2	0.64 ± 0.07	22 ± 2	1
dATP	6.2 ± 0.7	74 ± 6	0.13 ± 0.01	5.9×10^{-3}

[a] k_{cat} and K_m values were based on three independent measurements

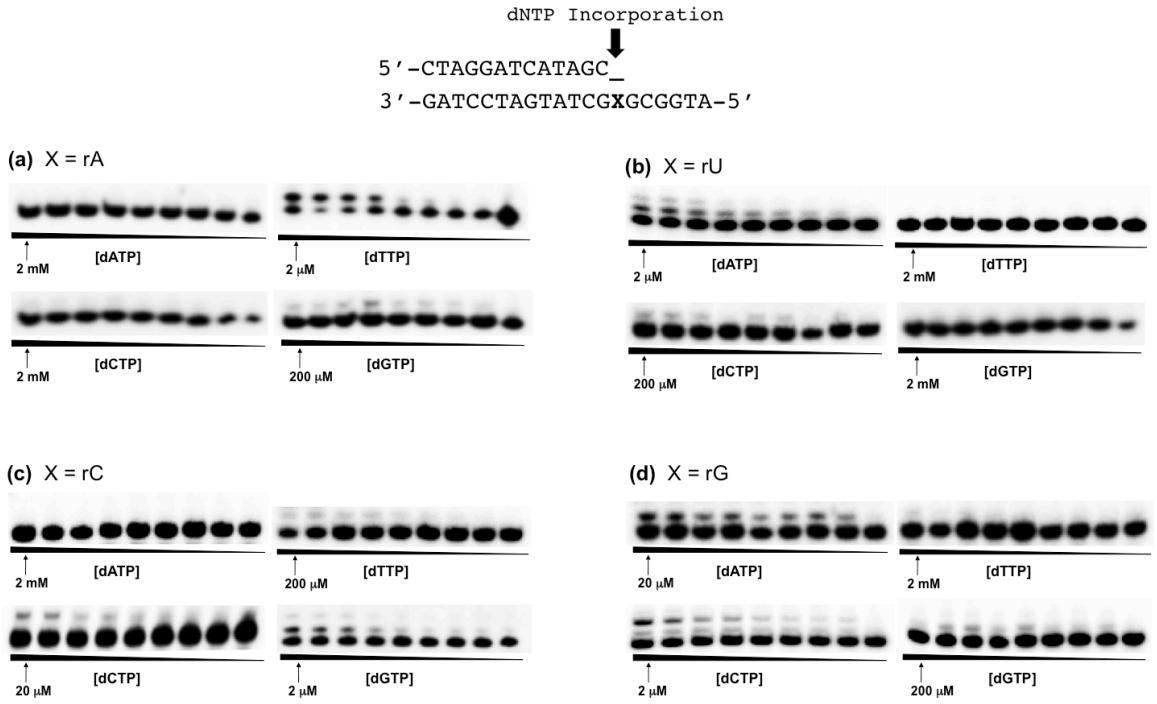

Figure 5.3. Representative gel images for steady-state kinetic assays opposite a) rA, b) rU, c) rC and d) rG using 2.4 nM yeast Pol ζ. Reactions were performed in the presence of individual dNTPs, the highest concentrations of which are indicated in the figures. The concentration ratio between neighboring lanes was 0.50.

Replication with human and yeast Pol η demonstrated much higher mutation frequencies when compared to yeast Pol ζ (Table 5.2-5.3, Figure 5.4). While replication of rA-containing substrate occurred with a moderate amount of misincorporation of dGMP (8.2%), dAMP (1.4%), and dCMP (0.44%), human Pol η inserted the correct dTMP opposite rA with ~65% efficiency compared to the unmodified dA-containing substrate (Table 5.2, Figure 5.4a). Human Pol η also preferentially inserted the correct dCMP opposite rG at an efficiency that is ~50% relative to the dG-harboring substrate, albeit with 8.8%, 4.5%, and 7.6% misincorporation of dTMP, dGMP, and dAMP, respectively, (Table 5.2, Figures 5.4d). Nucleotide insertion opposite rC and rU, however, was more mutagenic and blocking than rA and rG. Opposite rC, human Pol η inserted the incorrect dCMP (40%) and dAMP (15%) with high frequency, which is accompanied with modest frequency (6.4%) of dTMP misincorporation (Table 5.2, Figure 5.4c). Insertion opposite rU was also mutagenic, with 29% misincorporation of dGMP (Table 5.2, Figure 5.4b). In terms of efficiency, human Pol η inserted the correct nucleotide opposite rC and rU at efficiencies that are ~7.3% and ~17% compared to the control dC and dT substrates (Table 5.2). Yeast Pol η displayed similar trends in nucleotide incorporation opposite the ribonucleotides as human Pol η, with rC and rU eliciting the highest mutation frequencies. Opposite rC, there was substantial misincorporation of dCMP (45%) and dAMP (24%), and rU directed the misincorporation of dGMP at a frequency of 39% (Table 5.3, Figure D.2A). Yeast Pol η also misinserted dGMP opposite rA at 13% frequency, and dGMP opposite rG at 18% (Table 5.3, Figure D.2A).

Table 5.2. Steady-state Kinetic Parameters for Human pol η-mediated Nucleotide Insertion opposite rA, rU, rC, and rG, and opposite Unmodified dA, dT, dC and dG

dNTP	k_{cat} (min^{-1})	K_m (μM)	k_{cat}/K_m ($\mu M^{-1}min^{-1}$)	f_{inc}
		X = rC-containing substrates		
dTTP	12 ± 1	32 ± 3	0.38 ± 0.05	6.4×10^{-2}
dGTP	14 ± 1	2.3 ± 0.3	5.9 ± 0.7	1
dCTP	14 ± 1	5.8 ± 0.7	2.4 ± 0.2	4.0×10^{-1}
dATP	15 ± 2	17 ± 2	0.89 ± 0.09	1.5×10^{-1}
		X = rA-containing substrates		
dTTP	16 ± 2	0.50 ± 0.07	32 ± 3	1
dGTP	8.9 ± 1	33 ± 3	2.6 ± 0.3	8.2×10^{-2}
dCTP	19 ± 2	130 ± 15	0.14 ± 0.03	4.4×10^{-3}
dATP	13 ± 1	540 ± 60	0.44 ± 0.05	1.4×10^{-2}
		X = rU-containing substrates		
dTTP	10 ± 1	16 ± 2	0.63 ± 0.07	4.5×10^{-2}
dGTP	13 ± 1	3.2 ± 0.4	4.1 ± 0.5	2.9×10^{-1}
dCTP	8.5 ± 0.9	15 ± 2	0.52 ± 0.06	3.7×10^{-2}
dATP	18 ± 2	1.3 ± 0.2	14 ± 0.2	1
		X = rG-containing substrates		
dTTP	20 ± 2	11 ± 1	1.9 ± 0.2	8.8×10^{-2}
dGTP	24 ± 2	28 ± 3	0.95 ± 0.09	4.5×10^{-2}
dCTP	23 ± 2	1.1 ± 0.1	21 ± 2	1
dATP	9.9 ± 1	6.2 ± 0.7	1.6 ± 0.2	7.6×10^{-2}
		X = dG-containing substrates		
dTTP	9.6 ± 0.9	36 ± 3	0.27 ± 0.02	6.1×10^{-3}
dGTP	11 ± 1	31 ± 35	0.36 ± 0.04	8.2×10^{-3}
dCTP	12 ± 1	0.27 ± 0.03	44 ± 5	1
dATP	4.1 ± 0.4	19 ± 1	0.22 ± 0.02	5.0×10^{-3}
		X = dA-containing substrates		
dTTP	18 ± 1	0.29 ± 0.01	63 ± 7	1
dGTP	11 ± 1	45 ± 4	0.25 ± 0.02	3.9×10^{-3}
dCTP	6.5 ± 0.6	13 ± 1	0.52 ± 0.05	8.3×10^{-3}
dATP	16 ± 2	33 ± 4	0.48 ± 0.05	7.6×10^{-3}
		X = dT-containing substrates		
dTTP	6.4 ± 0.6	16 ± 1	0.41 ± 0.04	4.7×10^{-3}
dGTP	22 ± 2	31 ± 3	0.71 ± 0.08	8.4×10^{-3}
dCTP	3.9 ± 0.2	12 ± 1	0.32 ± 0.03	3.8×10^{-3}
dATP	11 ± 1	0.13 ± 0.01	85 ± 8	1
		X = dC-containing substrates		
dTTP	12 ± 1	67 ± 7	0.18 ± 0.02	2.2×10^{-3}
dGTP	22 ± 3	0.27 ± 0.03	82 ± 9	1
dCTP	15 ± 2	20 ± 3	0.75 ± 0.08	9.1×10^{-3}
dATP	16 ± 2	76 ± 8	0.21 ± 0.02	2.6×10^{-3}

Table 5.3. Steady-state Kinetic Parameters for *S. cerevisiae* Pol η-mediated Nucleotide Insertion opposite rA, rU, rC, and rG, and opposite Unmodified dA, dT, dC and dG [a]

dNTP	k_{cat} (min^{-1})	K_m (μM)	k_{cat}/K_m ($\mu M^{-1}min^{-1}$)	f_{inc}
		X = rC-containing substrates		
dTTP	8.3 ± 0.9	91 ± 9	0.091 ± 0.01	9.9×10^{-3}
dGTP	13 ± 0.2	1.4 ± 0.2	9.2 ± 1	1
dCTP	11 ± 0.1	2.7 ± 0.3	4.1 ± 0.5	4.5×10^{-1}
dATP	12 ± 0.2	5.5 ± 0.6	2.2 ± 0.3	2.4×10^{-1}
		X = rA-containing substrates		
dTTP	21 ± 2	0.70 ± 0.08	30 ± 3	1
dGTP	19 ± 2	4.9 ± 0.6	3.9 ± 0.4	1.3×10^{-1}
dCTP	12 ± 2	160 ± 20	0.075 ± 0.008	2.5×10^{-2}
dATP	14 ± 2	210 ± 20	0.067 ± 0.007	2.2×10^{-2}
		X = rU-containing substrates		
dTTP	15 ± 2	51 ± 5	0.29 ± 0.03	1.5×10^{-2}
dGTP	17 ± 2	0.89 ± 0.09	19 ± 2	3.9×10^{-1}
dCTP	12 ± 2	94 ± 10	0.13 ± 0.02	2.7×10^{-3}
dATP	23 ± 2	0.48 ± 0.05	48 ± 5	1
		X = rG-containing substrates		
dTTP	16 ± 2	29 ± 3	0.55 ± 0.06	1.9×10^{-2}
dGTP	13 ± 2	2.5 ± 0.3	5.1 ± 0.6	1.8×10^{-1}
dCTP	22 ± 2	0.78 ± 0.08	28 ± 3	1
dATP	11 ± 1	66 ± 7	0.17 ± 0.02	6.1×10^{-3}
		X = dG-containing substrates		
dTTP	9.6 ± 0.9	36 ± 3	0.27 ± 0.02	4.8×10^{-3}
dGTP	11 ± 1	24 ± 35	0.46 ± 0.04	8.2×10^{-3}
dCTP	12 ± 1	0.21 ± 0.02	56 ± 5	1
dATP	4.1 ± 0.4	19 ± 1	0.22 ± 0.02	3.9×10^{-3}
		X = dA-containing substrates		
dTTP	15 ± 2	0.41 ± 0.05	37 ± 4	1
dGTP	8.2 ± 0.9	210 ± 20	0.038 ± 0.004	1.1×10^{-3}
dCTP	22 ± 3	400 ± 40	0.089 ± 0.009	2.5×10^{-3}
dATP	9.5 ± 1	310 ± 13	0.033 ± 0.003	9.7×10^{-4}
		X = dT-containing substrate		
dTTP	11 ± 2	190 ± 20	0.057 ± 0.006	6.3×10^{-4}
dGTP	15 ± 2	61 ± 6	0.24 ± 0.03	2.7×10^{-3}
dCTP	23 ± 2	55 ± 6	0.42 ± 0.05	4.7×10^{-3}
dATP	28 ± 3	0.16 ± 0.01	90 ± 20	1
		X = dC-containing substrate		
dTTP	20 ± 2	470 ± 40	0.04 ± 0.005	1.7×10^{-3}
dGTP	24 ± 0.2	1.1 ± 0.1	24 ± 3	1
dCTP	10 ± 1	120 ± 15	0.08 ± 0.009	3.3×10^{-3}
dATP	17 ± 2	160 ± 20	0.11 ± 0.01	4.6×10^{-3}

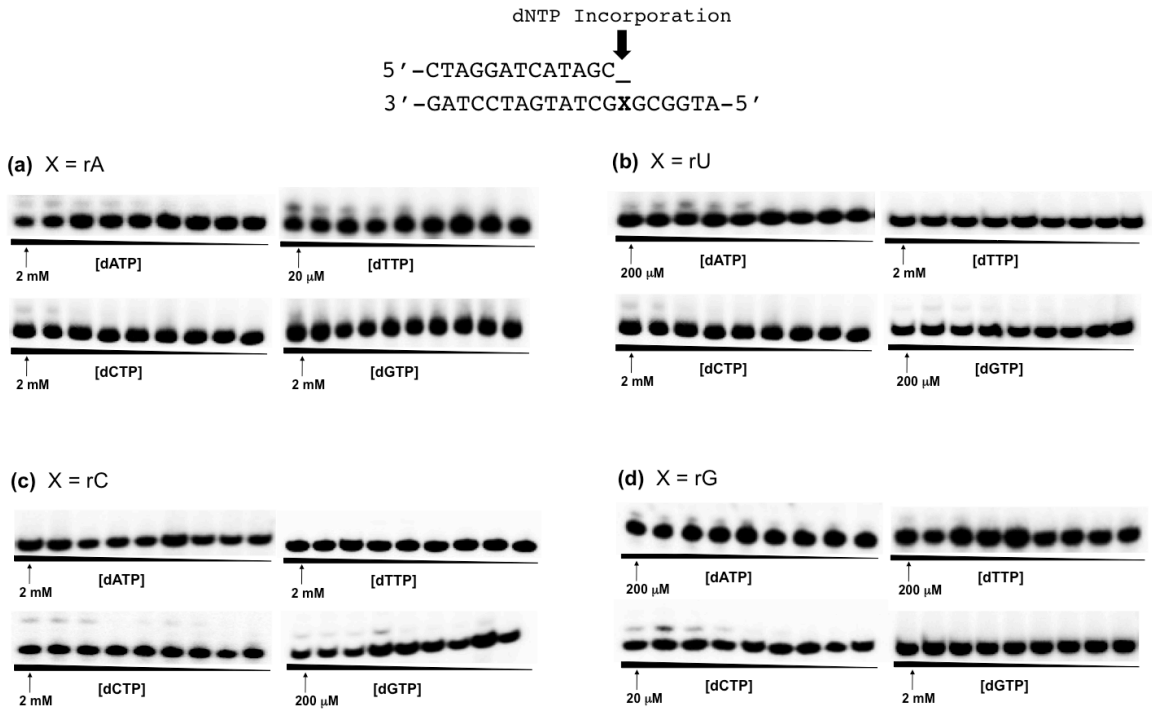

Figure 5.4. Representative gel images for steady-state kinetic assays opposite a) rA, b) rU, c) rC and d) rG using 1.2 nM human Pol η. Reactions were performed in the presence of individual dNTPs, the highest concentrations of which are indicated in the figures. The concentration ratio between neighboring lanes was 0.50.

Human Pol κ-mediated nucleotide insertion opposite rA and rG was modestly accurate and efficient, though the corresponding insertion across rC and rU held more mutagenic potential. Opposite rA, human Pol κ misinserted dAMP (11%) and dCMP (8.9%), with the efficiency for dTMP incorporation at ~77% relative to the corresponding insertion opposite dA (Table 5.4, Figure D.2B). Human Pol κ predominantly inserted the correct dCMP opposite rG with ~82% efficiency compared to the control dG, though it also misincorporated dTMP opposite rG (7.8%) (Table 5.4, Figure D.2B). On the other hand, rC and rU hindered the polymerase *in vitro*, with bypass occurring at efficiencies of ~14% and ~31%, respectively, compared to their corresponding control substrates (Table 5.4). Human Pol κ also displayed misinsertion of dAMP (11%), dTMP (16%), and dCMP (18%) opposite rC, and substantial misincorporation of dGMP (32%) opposite rU (Table 5.4, Figure D.2B).

Human Pol ι inserted nucleotides opposite rA and rG with remarkably low mutation frequencies and relatively high bypass efficiency, whereas rC and rU again hindered the polymerase. Insertion opposite rA occurred with ~62% efficiency compared to the control substrate, and only ~2.5% misincorporation of dGMP was observed (Table 5.5, Figure D.3). Insertion of dCMP opposite rG was ~54% as efficient as opposite the unmodified dG, with only ~5.4% misincorporation of dTMP (Table 5, Figure D.3). Human Pol ι inserted dGMP opposite rC at ~20% efficiency, which is associated with misincorporations of dAMP (19%) and dCMP (15%) (Table 5.5, Figure D.3). Similarly, human Pol ι incorporated dAMP opposite rU at ~9.2% efficiency compared to the

corresponding unmodified dT, with misinsertion of dTMP (29%), dGMP (22%), and dCMP (12%) at relatively high frequencies (Table 5.5, Figure D.3).

Table 5.4. Steady-state Kinetic Parameters for Human Pol κ-mediated Nucleotide Insertion opposite rA, rU, rC, and rG, and opposite Unmodified dA, dT, dC and dG

dNTP	k_{cat} (min^{-1})	K_m (μM)	k_{cat}/K_m ($\mu M^{-1}min^{-1}$)	f_{inc}
		X = rA-containing substrates		
dTTP	23 ± 2	0.36 ± 0.04	64 ± 7	1
dGTP	10 ± 1	21 ± 2	0.47 ± 0.05	7.3×10^{-3}
dCTP	13 ± 2	2.3 ± 0.2	5.7 ± 0.6	8.9×10^{-2}
dATP	15 ± 2	2.1 ± 0.2	7.1 ± 0.8	1.1×10^{-1}
		X = rC-containing substrates		
dTTP	11 ± 1	6.9 ± 0.8	1.6 ± 0.2	1.6×10^{-1}
dGTP	16 ± 2	1.6 ± 0.2	9.9 ± 1	1
dCTP	17 ± 2	9.4 ± 1	1.8 ± 0.2	1.8×10^{-1}
dATP	8.3 ± 0.8	7.5 ± 0.8	1.1 ± 0.1	1.1×10^{-1}
		X = rG-containing substrates		
dTTP	18 ± 2	2.9 ± 0.4	6.2 ± 0.7	7.8×10^{-2}
dGTP	12 ± 1	11 ± 1	1.1 ± 0.1	1.4×10^{-2}
dCTP	24 ± 2	0.31 ± 0.04	79 ± 8	1
dATP	12 ± 1	25 ± 3	0.48 ± 0.3	6.1×10^{-3}
		X = rU-containing substrates		
dTTP	12 ± 1	75 ± 8	0.16 ± 0.02	8.4×10^{-3}
dGTP	17 ± 2	2.8 ± 0.3	6.1 ± 0.7	3.2×10^{-1}
dCTP	14 ± 2	27 ± 3	0.51 ± 0.06	2.7×10^{-2}
dATP	24 ± 2	1.3 ± 0.2	19 ± 2	1
		X = dA-containing substrates		
dTTP	20 ± 2	0.24 ± 0.02	83 ± 8	1
dGTP	15 ± 2	96 ± 20	0.16 ± 0.02	1.9×10^{-3}
dCTP	18 ± 2	27 ± 3	0.66 ± 0.04	8.0×10^{-3}
dATP	12 ± 1	130 ± 13	0.092 ± 0.009	1.1×10^{-3}
		X = dT-containing substrates		
dTTP	13 ± 1	110 ± 15	0.12 ± 0.02	1.9×10^{-3}
dGTP	16 ± 2	48 ± 5	0.33 ± 0.04	5.3×10^{-3}
dCTP	12 ± 2	52 ± 6	0.23 ± 0.02	3.7×10^{-3}
dATP	18 ± 2	0.29 ± 0.03	62 ± 7	1
		X = dC-containing substrates		
dTTP	15 ± 1	45 ± 3	0.33 ± 0.03	4.6×10^{-3}
dGTP	25 ± 3	0.35 ± 0.04	71 ± 6	1
dCTP	11 ± 1	19 ± 2	1.8 ± 0.2	2.5×10^{-2}
dATP	18 ± 2	33 ± 3	0.54 ± 0.05	7.6×10^{-3}
		X = dG-containing substrates		
dTTP	15 ± 1	100 ± 10	0.15 ± 0.02	1.6×10^{-3}
dGTP	12 ± 1	43 ± 4	0.28 ± 0.03	2.9×10^{-4}
dCTP	24 ± 2	0.25 ± 0.03	96 ± 9	1
dATP	13 ± 1	120 ± 10	0.11 ± 0.01	1.1×10^{-3}

Table 5.5. Steady-state Kinetic Parameters for Human Pol ι-mediated Nucleotide Insertion opposite rA, rU, rC, and rG, and opposite Unmodified dA, dT, dC and dG

dNTP	k_{cat} (min^{-1})	K_m (μM)	k_{cat}/K_m ($\mu M^{-1}min^{-1}$)	f_{inc}
		rC-containing substrates		
dTTP	16 ± 1	38 ± 4	0.42 ± 0.05	9.2×10^{-3}
dGTP	21 ± 2	0.46 ± 0.05	46 ± 5	1
dCTP	18 ± 2	2.6 ± 0.3	6.9 ± 0.7	1.5×10^{-1}
dATP	29 ± 3	3.3 ± 0.4	8.7 ± 0.9	1.9×10^{-1}
		rA-containing substrates		
dTTP	26 ± 3	0.14 ± 0.02	180 ± 20	1
dGTP	20 ± 2	4.4 ± 5	4.5 ± 0.5	2.5×10^{-2}
dCTP	17 ± 2	15 ± 2	1.1 ± 0.1	6.3×10^{-3}
dATP	16 ± 1	11 ± 1	1.5 ± 0.2	8.2×10^{-3}
		rU-containing substrates		
dTTP	16 ± 2	6.2 ± 0.7	2.6 ± 0.3	2.9×10^{-1}
dGTP	18 ± 2	9.1 ± 1	2.0 ± 0.3	2.2×10^{-1}
dCTP	9.3 ± 0.9	84 ± 9	0.11 ± 0.01	1.2×10^{-2}
dATP	14 ± 2	1.6 ± 0.2	9.0 ± 1	1
		rG-containing substrates		
dTTP	22 ± 2	2.6 ± 0.3	8.6 ± 0.9	5.4×10^{-2}
dGTP	16 ± 2	13 ± 2	1.2 ± 0.2	7.7×10^{-3}
dCTP	28 ± 3	0.18 ± 0.02	160 ± 20	1
dATP	19 ± 2	26 ± 3	0.74 ± 0.08	4.6×10^{-3}
		dG-containing substrates		
dTTP	21 ± 2	88 ± 9	0.24 ± 0.03	7.7×10^{-4}
dGTP	25 ± 3	93 ± 10	0.27 ± 0.03	8.7×10^{-4}
dCTP	28 ± 3	0.09 ± 0.01	310 ± 30	1
dATP	23 ± 2	58 ± 6	0.39 ± 0.04	1.3×10^{-3}
		dA-containing substrates		
dTTP	32 ± 4	0.11 ± 0.01	290 ± 30	1
dGTP	11 ± 0.5	210 ± 20	0.052 ± 0.003	1.1×10^{-3}
dCTP	40 ± 3	400 ± 30	0.089 ± 0.002	1.8×10^{-3}
dATP	10 ± 1	310 ± 13	0.033 ± 0.001	6.9×10^{-4}
		dT-containing substrates		
dTTP	17 ± 2	15 ± 2	1.1 ± 0.1	1.1×10^{-2}
dGTP	23 ± 2	61 ± 7	0.38 ± 0.04	3.9×10^{-3}
dCTP	18 ± 2	29 ± 3	0.63 ± 0.07	6.4×10^{-3}
dATP	28 ± 3	0.29 ± 0.03	98 ± 9	1
		dC-containing substrates		
dTTP	24 ± 2	130 ± 15	0.18 ± 0.02	7.8×10^{-4}
dGTP	28 ± 3	0.12 ± 0.01	230 ± 25	1
dCTP	33 ± 3	46 ± 5	0.72 ± 0.08	3.1×10^{-3}
dATP	21 ± 2	74 ± 8	0.28 ± 0.03	1.2×10^{-3}

Discussion

Herein, we characterized the replicative bypass of ribonucleotides by TLS polymerases *in vitro*. We found that yeast Pol ζ is able to bypass all four ribonucleotides in DNA, with rG and rC being the most mutagenic with misinsertion occurring at frequencies of 15% and 9.4%, respectively. On the other hand, both human and yeast Pol η displayed mutagenic nucleotide incorporation, especially across rC and rU. Pols ι and κ are capable of inserting correct nucleotides opposite rA and rG with high efficiencies, though the presence of rC and rU in the template hinders the polymerases and leads to highly mutagenic nucleotide insertion.

We found an intriguing correlation in the behavior of rC when encountered by each TLS polymerase. In this vein, rC was ubiquitously the most mutagenic and blocking to the translesion synthesis polymerases among the four ribonucleotides. Based on structures obtained from nuclear magnetic resonance (NMR) and X-ray crystallography, rC was found to perturb the DNA double helical structure most significantly, though all ribonucleotides perturb the DNA helix to some degree (341,360-363). It has also been shown to convert the global conformation of DNA from B-form to the less stable A-form, though more recent reports argue that rC only alters the local conformation of DNA at the ribonucleotide site (360-364). Nevertheless, it is clear that the misincorporation of ribonucleotides in DNA, and especially rC, is a significant threat to the structure and stability of the DNA helix. Based on our results, Pol ζ is the most efficient and displays the least mutagenic nucleotide incorporation opposite a rC embedded in a template DNA strand. This is in keeping with the data demonstrating the

significant role that, in *S. cerevisae*, Pol ζ may play in tolerating damage incurred through the presence of rNs in the genome. However, we demonstrate here that Pol ι is also modestly efficient in replicating a rC, and can insert the correct dGMP with ~20% efficiency compared to a control dC. This is similar to the 37% efficiency exhibited by Pol ζ, albeit with significantly higher mutation rates.

Though it is necessary for rNMPs to be incorporated into the genome by RNA primase during replication initiation of lagging strand, the inadvertent incorporation of rNMPs by DNA polymerases during replication poses a significant threat to the stability of the genome, leaving the DNA strand prone to spontaneous hydrolysis and subsequent cleavage (62,64). Along this line, the size of the rNTP pool is significantly greater than that of the dNTP pool in *S. cerevisiae* and humans, and ribonucleotides are frequently incorporated into the genome by the replicative DNA polymerases α, δ, and ε (61,344,345). Specifically, in the *S. cerevisiae* rNTP pool, rA, rU, rG and rC are present at ~3000 μM, ~1700 μM, ~700 μM, and ~50 μM, respectively (61). Based on our *in vitro* replication experiments, rC and rU pose the greatest threat to genomic stability, especially in the presence of Pols η, ι, and κ, and are present in the smallest amounts in the rNTP pool. This may be a measure for the cell to protect against the deleterious nature of the two ribonucleotides, though further research is needed to determine whether this trend also holds true in mammalian cells. Along this line, we found that yeast Pol ζ, human and yeast Pol η, human Pol κ, and human Pol ι can all replicate a rA efficiently and accurately in the 20mer template DNA strand.

Due to the fragile nature of ribonucleotide misincorporation in DNA, there is a high potential for mutagenesis when replicating these endogenous lesions. To counteract this deleterious effect, cells are equipped with topoisomerase 1 (Top1) and RNase H2, which is responsible for nicking the 5' side of a ribonucleotide in a DNA strand for subsequent excision (348,349,365). However, this process is not entirely efficient, leaving a significant number of ribonucleotides in duplex DNA. Additionally, in cells lacking RNase H activity, there must be protective measures to prevent the deleterious effects that can occur with the massive accumulation of rNMPs (348,349). In this respect, translesion synthesis may constitute an important pathway for tolerating rN in DNA that normally block replicative polymerases. While the role of Pol ζ has been established, we propose that the polymerases η, κ, and ι can also replicate past rA and rG with relatively high efficiencies and low mutation frequencies *in vitro*, though they may be responsible for the adverse cellular consequences seen when replicating past rC and rU, as they hinder the polymerases and direct significant nucleotide misincorporations.

Chapter 6: Mutagenic Replication of Ethylated Thymidine Lesions by Mitochondrial DNA Polymerase γ

Introduction

Mitochondrial DNA (mtDNA) is continuously exposed to a variety of endogenous and exogenous damaging agents; however, mitochondria are equipped with minimal repair pathways to counteract the subsequent formation of DNA lesions (366-368). While mitochondrion has the ability to perform base excision repair, mismatch repair, and, to a lesser extent, double-strand and single-strand break repair, nucleotide excision repair is notably absent, rendering the mtDNA susceptible to accumulation of bulky, helix-distorting lesions (367,369,370). Given that the mtDNA encodes proteins for the mitochondrial electron transport chain, as well as produces the majority of the cell's ATP, the integrity of the mtDNA is crucial for cellular function (371). Recent studies have demonstrated that deletions and mutations in mtDNA could contribute to the etiology of cancer, neurodegeneration, aging, and other human diseases (372-376).

Pol γ is the main polymerase in the mitochondria responsible for replicating mtDNA, and largely carries the burden for replicating the entire 16.6k base pair sequence (377). Pol γ is comprised of both catalytic and exonucleolytic subunits, which are responsible for synthesizing DNA and proofreading mismatched bases that may be incorporated during replication, respectively, as well as an accessory subunit, p55, that facilitates tight binding of Pol γ to the DNA and aids processivity (377-379). However, Pol γ's proofreading is demonstrated to be limited, given its relative inability to recognize

and excise mismatches opposite thymine-thymine dimers (TT dimers), 8-oxo-7,8-dihydro-2′-deoxyguanosine, or the minor-groove γ-hydroxypropano-2′-deoxyguanosine (γ-HOPdG) adduct (209,210,380). A new translesion synthesis polymerase designated PrimPol has recently been discovered to exist in the mitochondria, though its presence is not crucial for mitochondrial function. Thus, it was hypothesized that its main role in mitochondria is to prime leading strand synthesis upon replication stalling (211,215). It is, however, possible that PrimPol may also assist Pol γ in replicating past lesions in mtDNA, though this function requires further exploration. The mitochondrial genome consists primarily of coding DNA, and it has 37 known genes, with 13 encoding proteins that play critical roles in ATP synthesis, calcium signaling, and apoptosis (375,377). Only a very small percentage (~3%) of the mitochondrial DNA is composed of non-coding sequence; therefore, any erroneous replication could prove detrimental to mitochondrial function (381). Along these lines, the mitochondrial genome is subject to a significantly higher mutation rate than the nuclear genome. It is speculated that the elevated mutation rate may be attributed to the easier access of mtDNA to damaging agents as opposed to nuclear DNA given the absence of histones in mitochondria, though the exact mechanisms remain largely unknown (382). Nevertheless, the deleterious consequence from this relatively high mutation rate in mitochondrial genome is lessened due to the presence of numerous mitochondria in any particular cell and multiple copies of DNA per mitochondrion (381,382). Although many aspects of mitochondrial DNA replication remain largely enigmatic, recent developments linking mitochondrial

dysfunction to human diseases and aging have established a fundamental need to understand how lesions in mtDNA may be bypassed by Pol γ.

Multiple sources can lead to ethylation of DNA. A multitude of carcinogenic and mutagenic compounds commonly found in tobacco smoke can be metabolically activated via cytochrome P450 enzymes, notably CYP2E1, that subsequently react with DNA to yield alkylation of all four nucleobases (383). A number of quantification studies of the levels of ethylated lesions in tissue and cellular DNA of habitual smokers versus non-smokers uncovered significantly elevated levels of *N*7-ethylguanine (*N*7-EtG), *N*3-ethyladenine (*N*3-EtA), as well as the three ethylated thymidine lesions, O^2-, O^4-, and *N*3-ethylthymidine (O^2-, O^4-, and *N*3-EtdT, respectively) in smokers (75,384-386). While tobacco smoke is a major contributor to ethylated lesion formation, ethylation of DNA can also result from consumption of alcohol, which occurs through acetaldehyde, an ethanol metabolite (387). Interestingly, alcohol dehydrogenase 2 (ALDH2), the major enzyme responsible for the conversion of ethanol to acetaldehyde, is exclusively located in the mitochondria, which exacerbates the need to understand how ethylated lesions may be bypassed by the mitochondrial replisome (388).

Previous studies have demonstrated that exposure to alkylating agents can lead to loss of mitochondrial function, and that mtDNA is more susceptible to alkylation than nuclear DNA (389). A previous study quantified ethylated adducts in mtDNA upon treatment with *N*-ethyl-*N*-nitrosourea (ENU), a known ethylating agent, and noted a significant amount of stable O^6-ethyl-2′-deoxyguanosine (O^6-EtdG) as well as O^4-EtdT (233). Interestingly, O^6-EtdG was efficiently repaired in mtDNA, indicating that it is an

effective substrate for the O^6-methylguanine DNA methyltransferase (MGMT) (390). In contrast, O^4-EtdT was detected in an amount that is 2.8 times higher than that of O^6-EtdG, and persisted within the mtDNA, indicating the poor repair of O^4-EtdT by the mitochondrial repair pathways (233). Additionally, it has been shown that in nuclear DNA of rats treated with ENU, O^2-EtdT was present at higher levels than O^4-EtdT, suggesting the less efficient repair of the former lesion (391). It is reasonable to assume that O^2-and $N3$-EtdT may also be generated in mitochondrial DNA and be poor substrates for MGMT.

Alkylated thymidine lesions are known to hold significant mutagenic potential (76,231,289,392-395). Recently, Andersen et al. (161) assessed the effects of O^2-, $N3$-, and O^4-EtdT on DNA replication mediated by translesion synthesis DNA polymerases η, ι, κ, and ζ, and exonuclease-deficient Klenow fragment of the *Escherichia coli* Pol I. Primer extension assay results showed that the TLS polymerases could be stalled by these lesions, which is accompanied by the observation of substantial frequencies of mutations, especially the misinsertion of dGMP opposite O^4-EtdT. This finding is corroborated by previous studies demonstrating significant T→C mutations induced by O^4-alkylated thymidine derivatives (76,393,394). It remains unestablished how the ethylated thymidine lesions are recognized by mitochondrial DNA polymerase Pol γ.

In the present study, we assessed the Pol γ-mediated replication of the regioisomeric O^2-, O^4-, and $N3$-EtdT in template DNA, with the use of primer extension, processivity, steady-state kinetic, and exonuclease activity assays. Our results revealed that O^2- and $N3$-EtdT, but not O^4-EtdT, were strongly blocking to Pol γ. We also found

that the three regioisomeric EtdT lesions exhibited distinct pro-mutagenic properties, and Pol γ was incapable of removing effectively the misincorporated nucleotides through its proofreading activity.

Materials and Methods

Materials

Human wild-type polymerase γ proficient or deficient in exonuclease activity (Pol γ^+ and Pol γ^-, respectively) with accessory subunit were expressed and purified following previously published procedures (209,210,396). Briefly, the recombinant catalytic subunit of Pol γ^+ and Pol γ^- with a His_6 tag at the N-terminus were overexpressed in insect *Sf*9 cells. In order to eliminate the 3′→5′ exonuclease activity, the catalytic residues Asp-198 and Glu-200 were mutated to alanines. The p55 accessory subunit with a His_6 tag at C-terminus was expressed in *Escherichia coli* and subsequently purified (396). All other enzymes used in this study were purchased from New England BioLabs (Ipswich, MA). Unmodified oligodeoxyribonucleotides were obtained from Integrated DNA Technologies (Coralville, IA). [γ-^{32}P]ATP was purchased from Perkin-Elmer (Boston, MA), herring sperm DNA was purchased from Promega (Madison, WI), and all other chemicals were obtained from Sigma-Aldrich (St. Louis, MO).

Preparation of Lesion-bearing ODN Substrates

The 12mer lesion-bearing substrates d(ATGGCGXGCTAT) [X = O^2-EtdT, O^4-EtdT, or *N*3-EtdT] were previously synthesized, with identities being confirmed by electrospray ionization-mass spectrometry (ESI-MS) and tandem mass spectrometry

(MS/MS) analyses (161). These substrates were then ligated with a 5'-phosphorylated 13mer, d(GATCCTAGAGCTA), in the presence of a 40mer template ODN, d(CCGCTCCCTATAGCTCTAGGATCATAGCACGCCATGATCG), following published procedures (397). The 25mer lesion-containing ODNs were purified by 20% denaturing polyacrylamide gel electrophoresis (PAGE).

Primer Extension Assay

The 25mer lesion-bearing ODNs or the corresponding unmodified ODN (0.05 μM) were annealed with a 5′-^{32}P-labeled 18mer primer (0.05 μM), d(TAGCTCTAGGATCATAGC), to perform replication experiments. The primer extension reaction was performed under standing-start conditions by incubating 50 nM radiolabeled primer-template complex, exonuclease-deficient Pol γ$^-$ (concentrations indicated in Figure 6.2), a mixture of all four dNTPs (250 μM each), and a Pol γ reaction buffer containing 25 mM HEPES-KOH (pH 7.5), 2 mM 2-mercaptoethanol, 0.1 mM EDTA, and 5 mM $MgCl_2$ at 37°C for 30 min. The reaction was terminated with an equal volume of formamide gel loading buffer containing 95% formamide, 10 mM EDTA, 1 mg/mL xylene cyanol, and 1 mg/mL bromophenol blue. The extension products were boiled at 95°C for 10 min and then resolved on 20% denaturing polyacrylamide gels with 8 M urea, and gel-band intensities were quantified using a Typhoon 9410 Variable Mode Imager (Amersham Biosciences Co.) and ImageQuant 5.2 (Amersham Biosciences Co.).

Steady-state Kinetic Measurements

Steady-state kinetic assays were performed according to previously described procedures (229,398). The radiolabeled primer-template complex (50 nM) was incubated

with exonuclease-deficient Pol γ⁻ (10 nM) in the Pol γ reaction buffer with the presence of individual dNTPs at concentrations indicated in Figure 6.3, where the individual dNTP concentration was optimized to allow for less than 20% incorporation. Single-nucleotide incorporation products were terminated with an equal volume of formamide gel loading buffer, boiled at 95°C for 10 min, resolved on 20% denaturing polyacrylamide gels with 8 M urea, and gel-band intensities again quantified with phosphorimaging analysis. The kinetic parameters were calculated by plotting the observed rate of nucleotide incorporation (V_{obs}) as a function of dNTP concentration using Origin 6.0 (OriginLab) and fitting the data with the Michaelis-Menten equation. The frequency of incorrect nucleotide incorporation (f_{inc}) was determined by dividing k_{cat}/K_m value obtained for the insertion of the incorrect nucleotide over that for the correct nucleotide incorporation. Relative misincorporation frequencies (RMF) represent the f_{inc} values in percentage. The relative incorporation efficiencies (RIE) were calculated by dividing the k_{cat}/K_m for the correct dAMP insertion opposite O^2-, $N3$-, or O^4-EtdT, as well as the incorrect dGMP incorporation opposite O^4-EtdT, by the k_{cat}/K_m for dAMP insertion opposite the control dT substrate. All steady-state kinetic experiments were performed in triplicate, and [dNTP] for each experiment is indicated in Figure 6.3.

Processivity assay

We conducted the processivity assays following previously published procedures (229). Briefly, we preincubated aforementioned 10 nM radiolabeled primer-template complex with 20 nM exonuclease-deficient Pol γ⁻, and Pol γ reaction buffer minus $MgCl_2$. We then initiated the reaction with a mixture of all four dNTPs (250 μM), 5 mM

$MgCl_2$, and excess sonicated herring sperm DNA (1 mg/mL), which served as a trap for polymerase molecules. To assess the trapping efficacy, we preincubated the radiolabeled primer-template complex with 10 nM Pol γ^-, Pol γ reaction buffer minus $MgCl_2$, and herring sperm DNA (1 mg/mL) for 15 min. We then initiated the reaction with 250 μM dNTPs and 5 mM $MgCl_2$. The lack of replication products under such conditions indicated that herring sperm DNA could successfully trap the polymerase molecules in solution and prevent re-binding of polymerase molecules to the primer-template complex (representative gel image shown in Figure 6.5E). The reaction was stopped at 60, 120, and 240 sec time points as indicated in Figure 6.5 using an equal volume of formamide gel loading buffer. Products were boiled at 95°C for 10 min and then resolved by 20% denaturing polyacrylamide gel. Gels were analyzed with a phosphorimager. The 240 sec time point was used to calculate the percentage of active polymerase molecules and the processivity of the Pol γ^- following equations detailed in a previous report (229).

Exonuclease assay

To determine the ability of Pol γ to excise ethylated lesions from template DNA, we radiolabeled a 19mer primer, d(TAGCTCTAGGATCATAGCX), X = dA, dT, dC, or dG) with the 25mer lesion-containing substrates, or control dT substrate. The ^{32}P-labeled primer-template complex (50 nM) was incubated with 10 nM exonuclease-proficient Pol γ^+ in the Pol γ reaction buffer. Reactions were terminated with an equal volume of formamide gel loading buffer at time points indicated in Figure 6.6, then subsequently boiled at 95°C for 10 min. Excision products were resolved on 20% denaturing polyacrylamide gels with 8 M urea and again analyzed with phophorimaging as described

above. The primer bands and all subsequent excision products (<19mer) were quantified and plotted against time. The excision rate (k_{exo}) was calculated by fitting the data to a linear equation in Origin 6.0 software (OriginLab) according to previously published procedures (209). Excision rates were calculated based on data from at least two independent experiments.

Results

Primer Extension past Ethylated Thymidine Lesions

We first determined the ability of Pol γ to bypass each of three regioisomeric ethylated thymidine lesions, O^2-, O^4-, and *N*3-EtdT, using primer extension assays (Figures 6.1 & 6.2). Our results showed that exonuclease-deficient Pol γ (Pol γ$^-$) is able to fully extend past O^4-EtdT, though the lesion presents a minor block to the polymerase as reflected by the presence of stalled replication products at the lesion site (19mer) as well as a significant amount of unextended primer when compared to the control dT substrate. On the other hand, *N*3- and O^2-EtdT significantly hinder the polymerase. There is also a substantial amount of unextended primer (18mer) and comparatively a small percentage of full-length replication products (Figure 6.2). Additionally, Pol γ$^-$ considerably stalls at both the lesion site and its adjacent 5′-nucleoside site, indicating that O^2- and *N*3-EtdT may stall the replication fork in mitochondria.

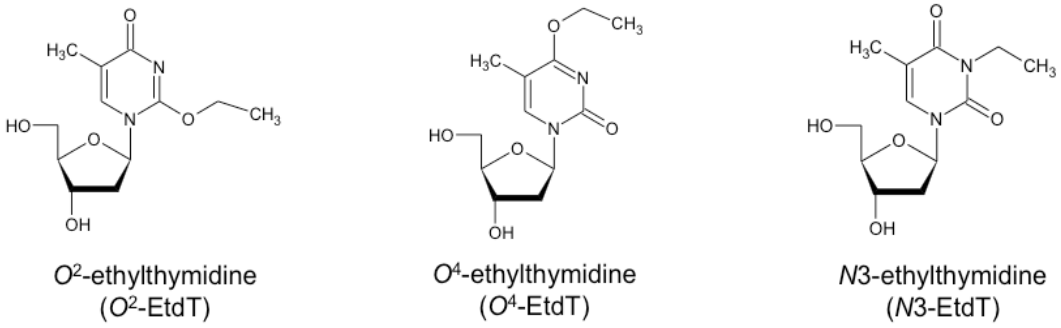

Figure 6.1. Structures of the regioisomeric O^2-, O^4-, and *N*3-EtdT.

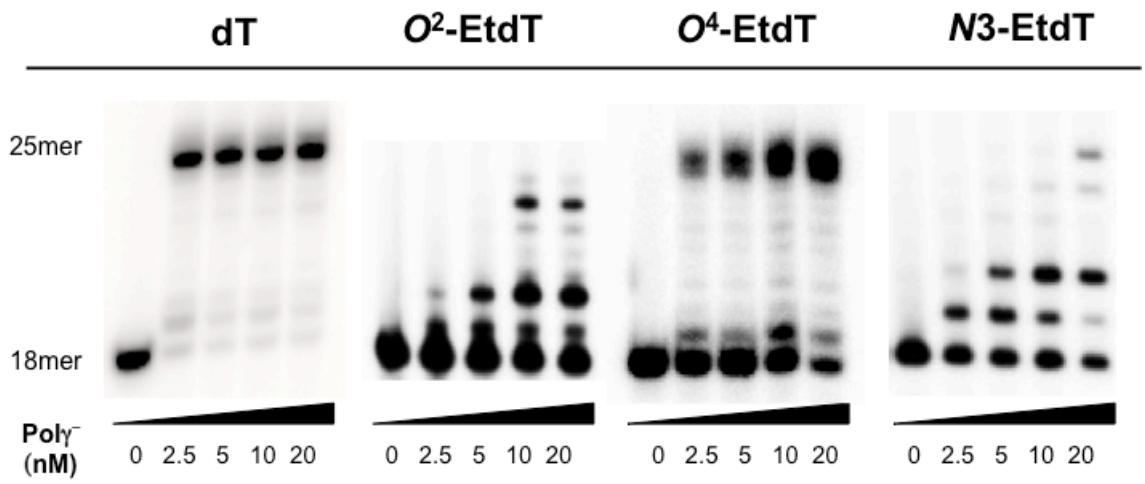

Figure 6.2. Primer extension assay for replication past O^2-, O^4-, and *N*3-EtdT compared with an undamaged dT, with Pol γ concentrations indicated in the figure.

Mutagenic Nucleotide Insertion opposite Ethylated Thymidine Lesions

To determine the incorporation efficiencies and mutagenic potential of the three lesions with exonuclease-deficient Pol γ (Pol γ$^-$), we next measured the steady-state kinetic parameters for nucleotide insertion opposite O^2-, *N*3-, and O^4-EtdT. Our results showed that Pol γ$^-$ preferentially inserts the correct dAMP opposite the O^2-EtdT lesion in template DNA, though at a relative incorporation efficiency (RIE) of 5.3% compared to that of dAMP insertion opposite the control dT substrate (Table 6.1). This is consistent with the blocking effect observed in primer extension assay (Figures 6.2 & 6.4). Moreover, we observed misinsertions of dTMP (30%), dGMP (5.6%), and dCMP (4.3%) opposite O^2-EtdT (Table 6.1, Figures 6.3 & 6.4). For *N*3-EtdT, Pol γ$^-$ again preferentially inserted the correct dAMP with a relatively low RIE of 27%, with a k_{cat}/K_m of 8.1 $\mu M^{-1}min^{-1}$, compared to 30 $\mu M^{-1}min^{-1}$ for the undamaged dT substrate (Table 6.1, Figures 6.3 & 6.4). However, Pol γ$^-$ also exhibited low fidelity in bypassing this lesion with misinsertion of dTMP, dGMP, and dCMP occurring at frequencies of 20%, 10%, and 9.8%, respectively. Insertion opposite the O^4-EtdT lesion was highly mutagenic, where dGMP was preferentially inserted over dAMP, with k_{cat}/K_m values being 21 and 10 $\mu M^{-1}min^{-1}$, respectively (Table 6.1). Interestingly, the efficiency for correct nucleotide insertion opposite O^4-EtdT is relatively low (33%), yet displays much greater ease when inserting dGMP, with RIE at 70%, in line with the primer extension data (Figures 6.3 & 6.4). Taken together, O^2-EtdT and *N*3-EtdT, but not O^4-EtdT, constitute strong blocks to Pol γ$^-$-mediated DNA replication, though all three ethylated thymidine lesions strongly compromise Pol γ's replication fidelity.

Table 6.1. Steady-state kinetic parameters for nucleotide incorporation opposite regioisomeric ethylated thymidine lesions with exonuclease-deficient Pol γ. The data represent the means and standard deviations of three independent experiments.

dNTP	k_{cat} (min^{-1})	K_m (μM)	k_{cat}/K_m ($\mu M^{-1}min^{-1}$)	f_{inc}
		***O*²-EtdT lesion-containing substrate**		
dTTP	6.9 ± 0.5	14 ± 1.4	0.48 ± 0.05	3.0×10^{-1}
dGTP	20 ± 2	230 ± 40	0.089 ± 0.01	5.6×10^{-2}
dCTP	25 ± 3	370 ± 50	0.068 ± 0.01	4.3×10^{-2}
dATP	32 ± 6	20 ± 5	1.6 ± 0.1	1
		***N*3-EtdT lesion-containing substrate**		
dTTP	24 ± 2	15 ± 2	1.6 ± 0.1	2.0×10^{-1}
dGTP	28 ± 1	35 ± 4	0.81 ± 0.1	1.0×10^{-1}
dCTP	23 ± 3	30 ± 4	0.79 ± 0.1	9.8×10^{-2}
dATP	29 ± 1	3.7 ± 0.7	8.1 ± 0.9	1
		***O*⁴-EtdT lesion-containing substrate**		
dTTP	21 ± 3	44 ± 0.8	0.48 ± 0.08	4.8×10^{-2}
dGTP	27 ± 4	1.3 ± 0. 3	21 ± 4	2.1
dCTP	3.7 ± 0.2	8.6 ± 0.2	0.44 ± 0.04	4.4×10^{-2}
dATP	23 ± 0.8	2.4 ± 0.4	10 ± 1	1
		Undamaged dT substrate		
dTTP	4.6 ± 0.3	12 ± 2	0.39 ± 0.06	1.3×10^{-2}
dGTP	5.4 ± 0.6	23 ± 5	0.24 ± 0.03	8.0×10^{-3}
dCTP	12 ± 0.9	120 ± 30	0.11 ± 0.02	3.7×10^{-3}
dATP	25 ± 2	0.83 ± 0.03	30 ± 2	1

[a] f_{inc}, Relative misinsertion efficiency = k_{cat}/K_m (incorrect nucleotide) / k_{cat}/K_m (correct nucleotide)

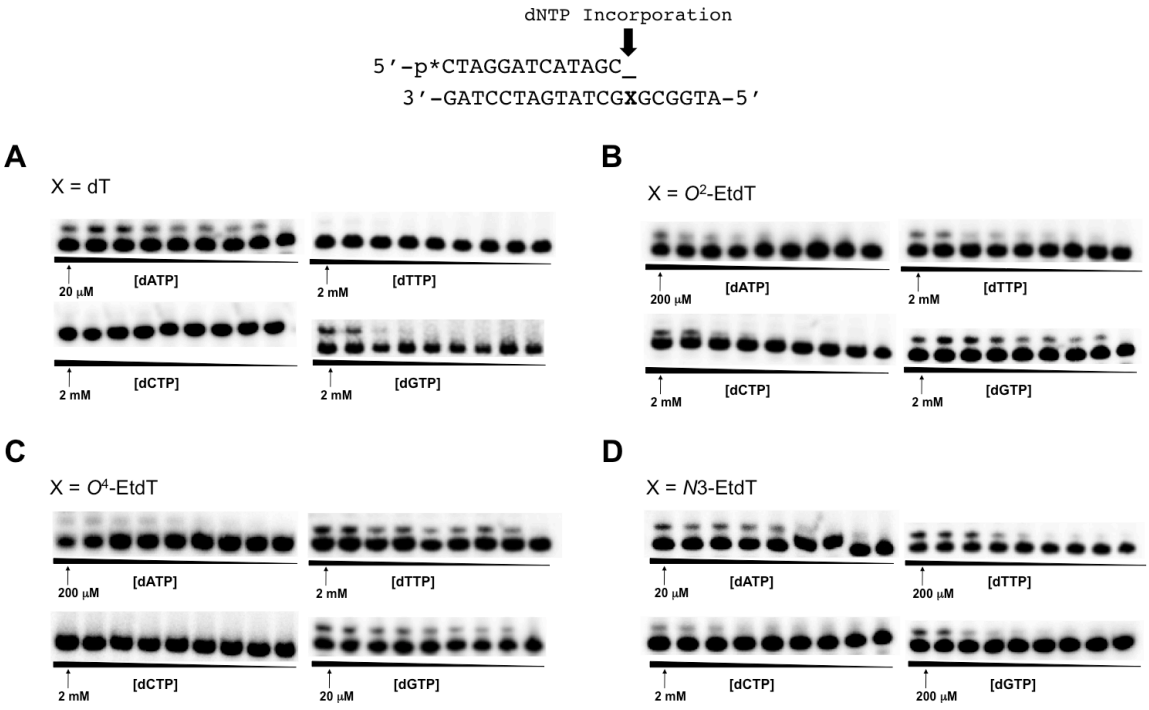

Figure 6.3. Representative gel images for steady-state kinetic assays of Pol γ-mediated nucleotide insertion opposite dT (A), O^2-EtdT (B), O^4-EtdT (C), and *N*3-EtdT (D). Starting nucleotide concentrations are indicated in the figures, with a ratio of 0.5 between neighboring lanes. All experiments were performed in triplicate.

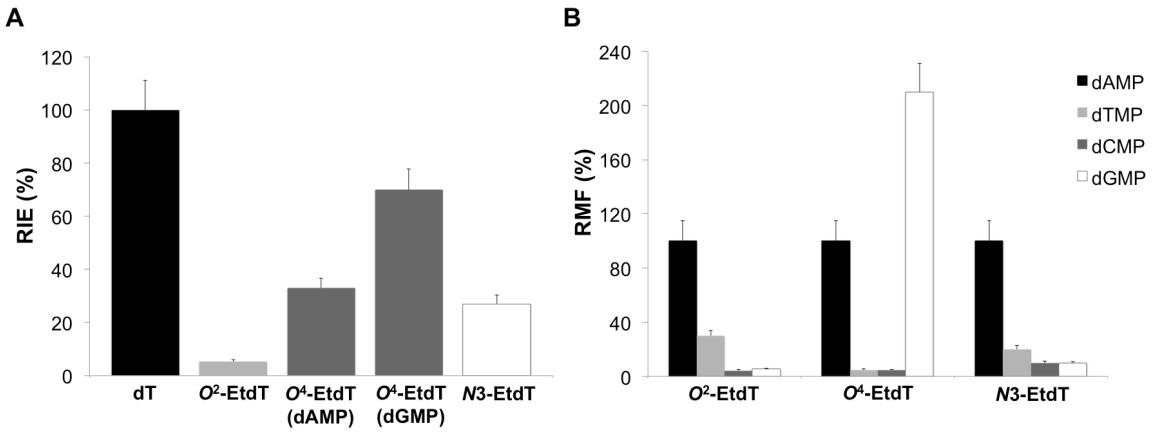

Figure 6.4. A summary of steady-state kinetic assay results: (A) relative incorporation efficiency (RIE) for correct dAMP insertion opposite ethylated lesions (and dGMP incorporation opposite O^4-EtdT) relative to corresponding dAMP incorporation opposite undamaged dT, and (B) relative misincorporation frequency (RMF) opposite O^2-, *N*3-, and O^4-EtdT. Error bars represent the standard deviation from the mean of three independent experiments.

Processivity of Replication past O^2-, O^4-, and N3-EtdT with Human Pol γ

To further assess how the EtdT lesions perturb the efficiency of Pol γ-mediated DNA replication, we performed a processivity assay (detailed in Methods) to monitor the number of nucleotides that Pol γ^- can insert opposite and past the lesion sites before dissociating from the primer-template complex. Our results revealed that Pol γ^- is significantly less processive when replicating past O^2-EtdT and *N*3-EtdT than O^4-EtdT. When O^2-EtdT is present in template DNA, only 31% of polymerase molecules are still adhered to the primer-template complex after incorporating two nucleotides, and only 6% is present after insertion of the 3rd nucleotide (Figure 6.5 A&F). While Pol γ^- is able to insert a total of six nucleotides, this only occurs at the 240 sec time point. Additionally, from the 3rd to 6th nucleotide insertion, extremely low levels (6%-1%) of polymerase molecules remain on the template. Extension past *N*3-EtdT also occurred with low processivity, as only 43% of Pol γ^- molecules remained bound to the DNA after incorporations of two nucleotides (Figure 6.5 B&F). However, subsequent dissociation from the 3rd to the 7th nucleotide at the end of the template was relatively low, indicating that Pol γ^- is most hindered by the insertion opposite the lesion and its adjacent nucleotide. On the other hand, Pol γ^- was significantly more processive in synthesizing past O^4-EtdT, as demonstrated by a relatively similar percentage of active polymerase molecules present after each nucleotide incorporation compared to the control dT substrate (Figure 6.5 D&F).

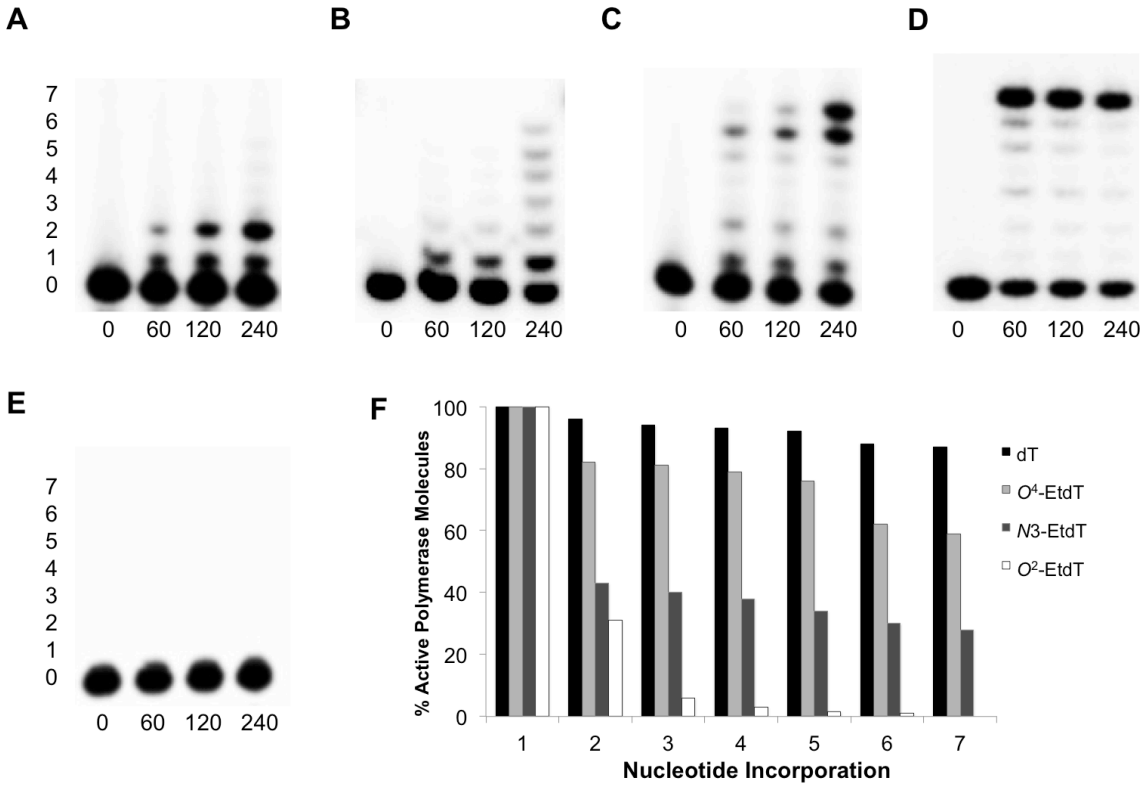

Figure 6.5. Representative gel images for processivity assay past O^2-EtdT (A), *N*3-EtdT (B), O^4-EtdT (C), undamaged dT (D). Displayed in (E) is a control experiment demonstrating the effectiveness of the trap. Shown in (F) is a graph depicting the percentage of active Pol γ^- molecules present at each nucleotide incorporation opposite and past the EtdT lesions and control dT.

The processivity (P_N) of Pol γ$^-$ was then determined from the percentage of polymerase molecules at each nucleotide position when replicating past an undamaged dT- as well as the O^2-, $N3$-, or O^4-EtdT-containing substrates. The average P_N values for nucleotide incorporation opposite and past an undamaged dT, O^2-, $N3$-, and O^4-EtdT lesion were calculated to be 0.93 ± 0.09, 0.21 ± 0.18, 0.44 ± 0.25, and 0.78 ± 0.13, respectively. Accordingly, processivity is low when replicating past the O^2-EtdT and, to a lesser extent, $N3$-EtdT, while synthesis past O^4-EtdT is significantly more processive. These results corroborate with the primer extension and steady-state kinetic data to support a more profound blocking effect of O^2-EtdT and $N3$-EtdT than O^4-EtdT on Pol γ during DNA replication.

Proofreading of O^2-, O^4-, and N3-EtdT

Based on the blocking potential of O^2-EtdT, $N3$-EtdT and, to a lower degree, O^4-EtdT revealed by the primer extension data, as well as the high mutation frequencies observed in steady-state kinetic experiments, we also performed excision assays to determine whether the misincorporated nucleotides opposite the ethylated thymidine lesions may be substrates for Pol γ's exonucleolytic activity. Using exonuclease-proficient Pol γ (Pol γ$^+$), we performed an exonuclease assay (detailed in Methods) and monitored the loss of nucleotide paired with the lesion over time. We subsequently fit the data to a linear equation to calculate the rate of excision of the nucleotide placed opposite the three regioisomeric ethylated thymidine lesions in comparison with the undamaged dT control (Figure 6.6 and Table 6.2). Our results showed that Pol γ$^+$ displays a similar cleavage efficiency of dC when it is mispaired with O^2-EtdT than with the control dT,

with the k_{exo} values being 0.061 s^{-1} and 0.049 s^{-1}, respectively. However, compared to the control dT:dT or dT:dG, the relative excision efficiencies (f_{rel}) of dT and dG from the O^2-EtdT:dT and O^2-EtdT:dG mispairs were reduced to 0.47- and 0.68-fold, respectively. The correct O^2-EtdT:dA pair does not appear to be a favorable substrate for Pol γ's proofreading activity, given a k_{exo} value of 0.0041 s^{-1} relative to a k_{exo} value of 0.011 s^{-1} for the control dT:dA base pair (Table 6.2). Interestingly, misincorporated dC opposite the O^2-EtdT lesion is the only primer terminus for this lesion that appears to be degraded preferentially by Pol γ^+ relative to the control, though, according to steady-state kinetic data, this incorporation opposite the lesion is the least favorable.

Pol γ^+ preferentially cleaves the dA and dC from *N*3-EtdT:dA (f_{rel} = 1.6) and *N*3-EtdT:dC (f_{rel} = 1.2) mispairs when compared with the corresponding mispairs for the control dT substrate (Table 6.2). Interestingly, the rate of excision is the highest when a dC is incorporated opposite *N*3-EtdT during replication; nevertheless, the steady-state kinetic data showed that this misincorporation is the least favorable. According to steady-state kinetic results, the most frequent misinsertion opposite *N*3-EtdT is a dT; however, this mismatch does not appear to be a highly efficient substrate for Pol γ's exonucleolytic activity, given a k_{exo} of 0.025 s^{-1}, and f_{rel} of 0.044 compared to a dT:dT mismatch (Table 6.2). On the other hand, the rates for the excision of dG from the *N*3-EtdT:dG or dT:dG mispair are similar.

Table 6.2. Excision rates of ethylated thymidine lesions by exonuclease-proficient Pol γ. The data represent the means and standard deviations of three independent experiments.

Primer-Template Base Pair	k_{exo} (s^{-1})	f_{rel}[a]
dT:dA	0.011 ± 0.001	1
O^2-EtdT:dA	0.0041 ± 0.0003	0.37
*N*3-EtdT:dA	0.018 ± 0.002	1.6
O^4-EtdT:dA	0.056 ± 0.003	5.1
dT:dT	0.044 ± 0.003	1
O^2-EtdT:dT	0.021 ± 0.002	0.47
*N*3-EtdT:dT	0.025 ± 0.003	0.57
O^4-EtdT:dT	0.057 ± 0.006	1.3
dT:dC	0.049 ± 0.004	1
O^2-EtdT:dC	0.061 ± 0.006	1.2
*N*3-EtdT:dC	0.059 ± 0.005	1.2
O^4-EtdT:dC	0.058 ± 0.005	1.2
dT:dG	0.041 ± 0.004	1
O^2-EtdT:dG	0.028 ± 0.002	0.68
*N*3-EtdT:dG	0.042 ± 0.004	1.0
O^4-EtdT:dG	0.0037 ± 0.0009	0.090

[a] f_{rel}, Relative excision efficiency = k_{exo} of DNA Lesion / k_{exo} of dT

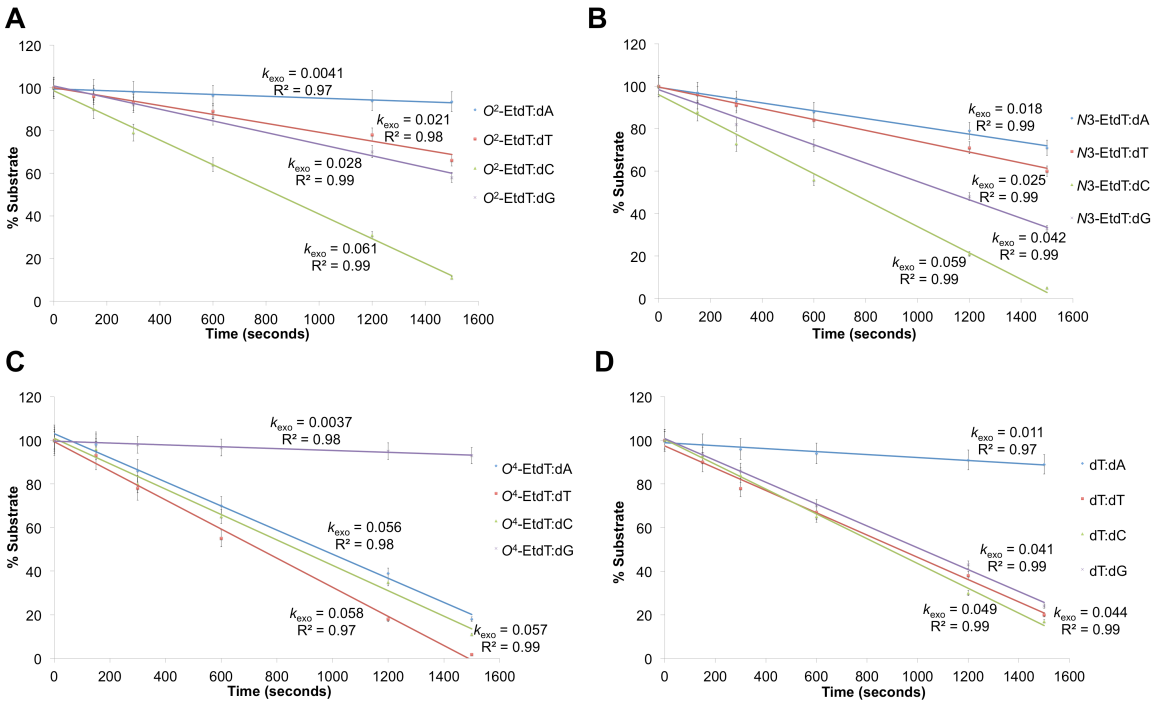

Figure 6.6. Kinetic results for exonuclease-proficient Pol γ-mediated excision of nucleotides placed opposite O^2-EtdT (A), $N3$-EtdT (B), O^4-EtdT (C), and undamaged dT (D), with k_{exo} and R^2 values depicted on the charts. Primers (19mer) with the correct dA, or incorrect dT, dC, or dG being placed opposite the ethylated lesions or undamaged dT were used, and the rate of excision was calculated by fitting the loss of substrate against time to a linear equation.

Strikingly, the removal of the correctly incorporated dA opposite O^4-EtdT (k_{exo} = 0.056 s^{-1}) was 5.1 times more efficient than the corresponding removal from the dT:dA base pair (k_{exo} = 0.011 s^{-1}), suggesting that Pol γ^+ may recognize dA as a misinsertion. By stark contrast, the excision of the misinserted dG opposite O^4-EtdT is more than 10 times less efficient than the corresponding excision from the dT:dG mismatch (Table 2). This is particularly important viewing that Pol γ^- misinserts dGMP opposite O^4-EtdT at an efficiency that is 2.4 times greater than the correct dAMP, as revealed from the steady-state kinetic measurements (*vide supra*). The excision of dT and dC from the O^4-EtdT:dT and O^4-EtdT:dC mispairs were slightly preferred over the excision from the corresponding dT:dT and dT:dC mispairs, with f_{rel} values being of 1.3 and 1.2, respectively (Table 6.2).

Discussion

Mitochondrial DNA is susceptible to alkylation damage, which can be generated following exposure to tobacco smoke and alcohol consumption (387,389). Quantification of ethylated lesions in mtDNA revealed their high persistence, with repair being observed for the ethylation adduct on the O^6-position of guanine, but not the O^4 position of thymine (233). While studies have been conducted to examine how alkylation damage may be repaired in mitochondria, there is a significant gap in our understanding about how the ethylated lesions may be recognized by mitochondrial DNA replication machinery.

In this paper, we characterized the replicative bypass of regioisomeric ethylated thymidine lesions by the mitochondrial Pol γ *in vitro*. We found that replication past O^4-EtdT is relatively efficient, with similar processivity and extension behavior as an undamaged dT. However, this lesion appears to be highly miscoding, generating a significant frequency of T→C mutation. Excision assay with the use of exonuclease-proficient Pol γ also showed that Pol γ does not proofread effectively an O^4-EtdT:dG mismatch. Instead, it preferentially excises a correct O^4-EtdT:dA base pair with extremely high efficiency. Based on these results, O^4-EtdT may be easily bypassed, albeit at the expense of mutagenesis. This result is not highly surprising, given extensive studies demonstrating preferential misinsertion of dGMP opposite alkylation damage at the O^4 position in nuclear DNA (76,393,394). However, this high mutagenic potential could be significantly more detrimental to the mitochondria on the grounds that O^4-EtdT is known to be poorly repaired and persist in mitochondria (233). Thus, O^4-EtdT may contribute significantly to point mutations in mtDNA and loss of mitochondrial function.

Pol γ preferentially inserts the correct dAMP opposite *N*3-EtdT, though this was accompanied with significant misincorporations of dTMP, dGMP, and dCMP. In addition, the proofreading activity of Pol γ does not readily remove the misincorporated dT or dG, indicating that *N*3-EtdT may contribute to T→A and T→C mutations. Pol γ was also moderately hindered by *N*3-EtdT, though, according to processivity data, the lesion and adjacent nucleotide appear to be the most obstructing to replication, with subsequent extension less blocking to the mitochondrial polymerase.

Pol γ may also poorly tolerate the minor-groove O^2-EtdT lesion in mtDNA, conferring a considerable blocking effect and high mutation frequencies. The steady-state kinetic data showed that dTMP is the most prevalent misincorporation opposite O^2-EtdT, followed by dGMP. Pol γ's proofreading activity is also severely limited in removing the misinserted dT or dG opposite the lesion. Therefore, O^2-EtdT could be a significant source of T→A and T→C mutations in mtDNA. In this vein, it is worth noting Pol γ also displayed substantial difficulty in replicating across the minor-groove γ-HOPdG lesion, generating significant mutation products and limited proofreading of mismatched primer termini (209). It is possible that Pol γ is more hindered by minor-groove lesions, which could be responsible for significant amount of mutations in mtDNA. Along this line, future studies on the replication of other minor-groove adducts, such as N^2-(1-carboxyethyl)-2'-deoxyguanosine (N^2-CEdG) (355), are necessary to further substantiate this conclusion.

Taken together, the three regioisomeric EtdT lesions may contribute significantly to point mutations in mtDNA, which may lead to accelerated aging, as well as progression of human diseases, such as cancer and neurodegeneration. Future studies quantifying the levels of the EtdT lesions in mtDNA will further illustrate the biological consequences of these lesions.

Chapter 7: Conclusions and future research

The scope of this dissertation focused on the bypass of endogenously and exogenously generated DNA lesions found in both nuclear and mitochondrial DNA. While a great amount of work was performed to characterize the biological effects of these lesions on DNA replication, it also generated a number of questions that are interesting avenues of future study.

7.1. Bypass of Carboxymethylated Lesions by Pol η

In Chapter 2, I examined how carboxymethylated DNA lesions, which included N^6-CMdA, N^4-CMdC, *N*3-CMdT, and O^4-CMdT, perturbed the efficiency and fidelity of DNA replication mediated by *Saccharomyces cerevisiae* Pol η. My results from steady-state kinetic assay showed that Pol η could readily bypass and extend past N^6-CMdA, and incorporated the correct nucleotides opposite the lesion and its neighboring 5' nucleoside with high efficiency. By contrast, the polymerase could bypass N^4-CMdC inefficiently, with substantial misincorporation of dCMP followed by dAMP, though Pol η could extend past the lesion with high fidelity and efficiency when dGMP was incorporated opposite the lesion. On the other hand, yeast Pol η experienced great difficulty in bypassing O^4-CMdT and *N*3-CMdT and the polymerase inserted preferentially the incorrect dGMP opposite these two DNA lesions; the extension step, nevertheless, occurred with high fidelity and efficiency when the correct dAMP was opposite the lesion, as opposed to the preferentially incorporated incorrect dGMP. The above results

suggest that these lesions may contribute significantly to diazoacetate-induced mutations and those in *p53* gene observed in human gastrointestinal tumors.

My kinetic studies pointed to Pol η bypass of *N3*-CMdT and O^4-CMdT as a potential source of T→C and T→A mutations in cells, which could also contribute to the etiology of gastrointestinal tumors. However, the *in vitro* replication studies are tightly controlled experiments performed in the presence of one nucleotide at a time, and in the absence of other replication factors. Due to the limitations of the *in vitro* replication experiments, it would be interesting to monitor the kinetics of nucleotide insertion and extension in the presence of processivity factors such as PCNA and RPA. These proteins may aid the replicative bypass of these lesions in cells, so it would be interesting to see if the presence of these factors lower the mutagenic potential of these lesions or increase the nucleotide incorporation efficiency. It will also be crucial to monitor the mutagenic and blocking effects of these lesions in human cells that are deficient in Pol η, as well as Pol ι, Pol κ, and Pol ζ, to determine if these polymerases reduce the detrimental effects of these lesions, or also contribute to mutations.

7.2. Bypass of Cyclopurine Lesions by Pol η

Reactive oxygen species (ROS), which can be produced during normal aerobic metabolism, can induce the formation of tandem DNA lesions, including the 5'*S* diastereomers of cdA (*S*-cdA) and cdG (*S*-cdG). Previous studies have shown that *S*-cdA and *S*-cdG accumulate in cells and can block mammalian RNA polymerase II and replicative DNA polymerases. In Chapter 3, I used primer extension and steady-state

kinetic assays to examine the efficiency and fidelity for Pol η to insert nucleotides opposite, and extend primer past, these cyclopurine lesions. I found that *Saccharomyces cerevisiae* and human Pol η inserted 2'-deoxynucleotides opposite *S*-cdA, *S*-cdG, and their adjacent 5' nucleosides at fidelities and efficiencies that were similar to their respective undamaged nucleosides. Moreover, the yeast enzyme exhibited similar processivity in DNA synthesis on templates housing an *S*-cdA or *S*-cdG as those carrying an unmodified dA or dG; the human polymerase, however, dissociated from the primer-template complex after inserting one or two additional nucleotides after the lesion. Pol η's accurate and efficient bypass of *S*-cdA and *S*-cdG indicates that this polymerase is likely responsible for error-free bypass of these lesions, whereas other TLS polymerases may introduce mutations into the genome. Together, my results suggested that Pol η may have an additional function in cells, i.e., to alleviate the cellular burden of endogenously induced DNA lesions, including *S*-cdA and *S*-cdG.

7.3. Bypass of Cyclopurine Lesions *In Vitro* and in Human Cells

In this chapter, I monitored the accuracy and efficiency of *in vitro* bypass using the TLS Pols ι, κ, and ζ, to determine what role, if any, they may play in bypass of the *S*-cdA and *S*-cdG lesions, and compared the results to that of a quantitative bypass assay in cells. Steady-state kinetic assay revealed that Pol η and Pol ι can efficiently insert nucleotides opposite both *S*-cdA and *S*-cdG, but are significantly less efficient in extending past the tandem lesions. On the other hand, Pols ζ and κ were unable to readily insert nucleotides opposite *S*-cdA or *S*-cdG, though Pol ζ could accurately and

efficiently extend past these lesions, and Pol κ promoted efficient extension with a high degree of misincorporations. In human cells, the quantitative TLS assay showed that Pols η, ι, and ζ all played a role in bypassing these lesions. Based on my *in vitro* results corroborated with a TLS assay in human cells, we propose a dual polymerase model for cyclopurine lesion bypass, where Pol η and/or Pol ι performs the insertion step, and Pol ζ carries out the extension step.

This work was crucial in developing a model for the bypass of these oxidatively generated lesions in human cells. As a result, it has brought up several new research questions to address. Our study focused on the bypass of these lesions in nuclear DNA; however, oxidative damage also poses a great threat to the integrity of mitochondrial DNA. *S*-cdA and *S*-cdG are unable to be repaired by BER, and are inefficiently repaired by NER. Given the lack of NER in the mitochondrion, it would be of great interest to quantify these lesions in mitochondrial DNA following cellular exposure to γ-irradiation, as well as in mammalian tissues. It has previously been difficult to accurately monitor these lesions due to equipment and method limitations, but our laboratory has developed and applied a highly sensitive LC-MS/MS coupled with the stable isotope-dilution method for measuring these lesion levels in nuclear DNA. This could also be applied to adduct quantification in the mitochondrion. It is likely that these lesions accumulate at high levels in the mitochondrion due to a lack of repair, so in this respect it would be intriguing to monitor the accuracy and efficiency of bypass mediated by Pol γ, the main replicative polymerase in the mitochondrion. With the recent discovery of PrimPol, it would also be exciting to see if this new polymerase operating in mitochondria can

bypass these lesions, and whether PrimPol-mediated TLS is error-prone or error-free. This work could pave the way towards greater understanding of the development of mitochondrial disorders and disease in the context of these oxidatively generated lesions.

7.4. Bypass of Ribonucleotides Embedded in DNA

The integrity of the human genome depends on the ability of replicative DNA polymerases to exclude ribonucleoside triphosphates (rNTPs) from being incorporated into DNA. The incorporation of ribonucleotides in DNA disrupts the DNA double helix and renders the strand susceptible to breakage, due to the presence of a reactive 2' OH group on the ribose sugar, thereby posing a considerable threat to the genomic stability. By treating ribonucleotides in DNA as lesions, which has been found to be the most common endogenous base lesion in cells, I explored how TLS may protect cells from the deleterious effects of ribonucleotides in the genome. The research in Chapter 5 examined how ribonucleotides may affect DNA replication *in vitro,* by hindering TLS polymerases, including yeast Pol ζ and human Pol η, and inducing mutations. I accomplished this using steady-state kinetic and primer extension assays to assess the efficiency and fidelity of the polymerases in inserting nucleotides opposite ribonucleotides in a DNA template. My results showed that Pol ζ- and Pol ι-mediated insertion is highly efficient and relatively error-free, whereas Pol η and Pol κ are hindered by the presence of a single ribonucleotide, and direct misincorporations. These results indicate that Pol ζ may be responsible for preserving the genomic stability in the presence of ribonucleotides,

whereas bypass by other TLS Pols may contribute to the adverse cellular consequences exemplified by these lesions.

Ribonucleotide incorporation into DNA and the resultant consequences and benefits of this process are exciting new research areas with many avenues left to explore. My work revealed ribonucleotides, most notably rC and rG, as a potential source of mutations and stalled replication forks. It is incredibly important that this work be performed in cells, especially human cells, to see if the mutagenic potential of these "lesions" is an artifact of the *in vitro* replication studies, or if they pose a threat to cellular replication as well. If ribonucleotides embedded in DNA also block the cellular replication machinery, their impact on other cellular processes, including transcription, will be highly exciting topics to study given their identification as the most common endogenous lesions in cells.

It is now known that ribonucleotides are inadvertently incorporated into the yeast genome quite frequently by the replicative Pols δ and ε during replication, in addition to intentional incorporation by Pol α, a primase that initiates replication at origins with the insertion of ribonucleotides. It remains unseen to what extent ribonucleotides are incorporated *in vivo*, which is an important avenue of future research, though it is likely at appreciable levels given the incorporation in yeast. While Pol α is only able to initiate replication with ribonucleotide insertion, PrimPol can prime DNA with deoxyribonucleotides or ribonucleotides. It would be interesting to study whether PrimPol is also a significant source of ribonucleotide incorporation into the genome, or if it prefers to generate DNA:DNA hybrid complexes at origins of replication. If PrimPol

prefers dNTPs as a substrate for its primase activity, it may minimize the impact of ribonucleotides at origins of replication in the genome. Along these lines, other DNA polymerases, including the mitochondrial Pol γ, or the TLS polymerases, may also inadvertently incorporate ribonucleotides into DNA during synthesis, despite the presence of a steric gate at their active sites (which is also present in Pols δ and ε) to prevent such incorporation. If these non-traditional Pols are also sources of ribonucleotide introduction into the genome, it will be important to determine what effects this may have on the cell.

7.5. Bypass of Ethylated Lesions by Mitochondrial Pol γ

Although the predominant amount of studies monitoring lesion bypass has looked at lesions found in the nucleus, mitochondrial DNA is also exposed to numerous endogenous and exogenous damaging agents that generate adduct formation. The mitochondrion has a limited arsenal of repair pathways, which include BER and MMR, but most notably lacks NER. In this respect, lesions that are severely distorting to the DNA double-helix can subsist in mitochondrial DNA, block replication, and induce mutations. The regioisomeric ethylated thymidine lesions O^2-Etdt, $N3$-EtdT, and O^4-EtdT, are induced upon exposure to tobacco smoke, and have been quantified at elevated levels in the leukocyte DNA of smokers compared to non-smokers. In Chapter 6, I investigated how these ethylated thymidine lesions may be replicated by Pol γ, the main polymerase in mitochondrial DNA, using steady-state kinetic, primer extension, and excision assays. My results showed that O^4-EtdT was readily bypassed by Pol γ but

directed a substantial frequency of dGMP misinsertions, corresponding to T→C mutations in cells. Pol γ misinserted dTMP at high frequencies opposite O^2-EtdT and *N*3-EtdT, corresponding to T→A mutations in cells, and was significantly hindered by these lesions *in vitro*. Given the high mutagenic potential, I also performed excision assays in order to determine whether these lesions were a substrate for Pol γ's exonucleolytic proofreading activity. I found that Pol γ was unable to recognize and excise the misincorporated nucleosides opposite O^2-EtdT, *N*3-EtdT, and O^4-EtdT, and most strikingly, I found that Pol γ excises the correct dA opposite O^4-EtdT, but not the predominantly misincorporated dG. In this respect, these ethylated lesions may generate a substantial amount of point mutations in mitochondrial DNA that could contribute to the etiology of mitochondrial and other human diseases.

Future studies on the replication of these lesions in mitochondrial DNA will be highly important in revealing their biological impacts. Currently, only O^4-EtdT has been quantified in mitochondrial DNA, which was shown to be poorly repaired and accumulate in the mitochondrial genome. While O^4-EtdT is highly miscoding in mtDNA, I also report here that replication of O^2-EtdT and *N*3-EtdT with Pol γ is extremely inefficient and inaccurate, and poor substrates for Pol γ's proofreading activity. Given the mutagenic potential of these lesions, it is highly important to quantify these lesion levels in mitochondria following exposure to ethylating agents, such as ENU, and tobacco smoke. If these lesions are quantified at appreciable levels, they may prove to be reliable biomarkers for tobacco smoke exposure, or the etiology of mitochondrial disorders. It will also be interesting to see if PrimPol can bypass these lesions in mtDNA

and mitigate their deleterious effects, or if O^2-EtdT, *N*3-EtdT, and/or O^4-EtdT block this polymerase as well. To this end, steady-state kinetic and primer extension assays could be performed to first understand the mutagenic potential of these lesions *in vitro*, after which, it would be important to understand the role that PrimPol may play in lesion bypass at the cellular level.

Appendix A: Supporting Information for Chapter 2

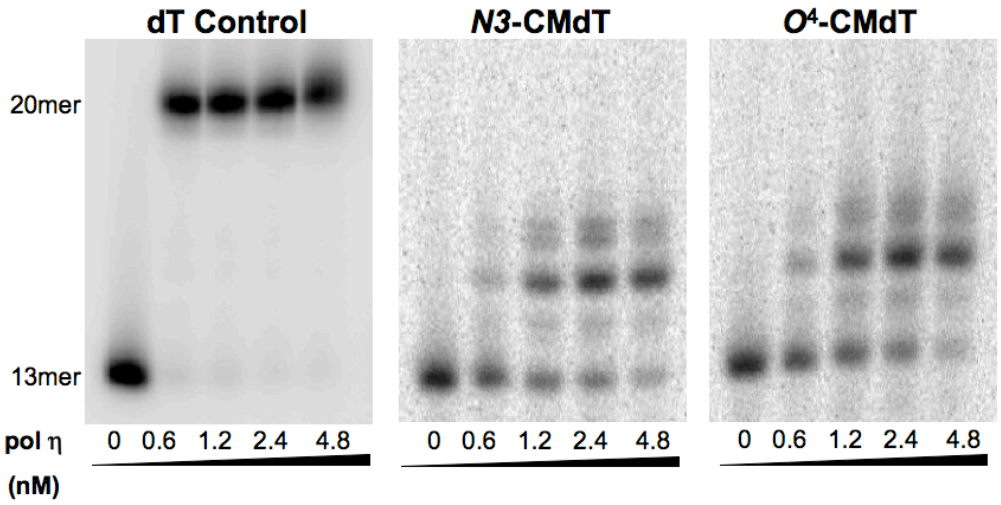

Figure A.1. Primer extension assays opposite the *N*3-CMdT and O^4-CMdT lesions with yeast polymerase η in the presence of all four dNTPs [250 μM each]. The products were resolved with 20% denaturing polyacrylamide gels.

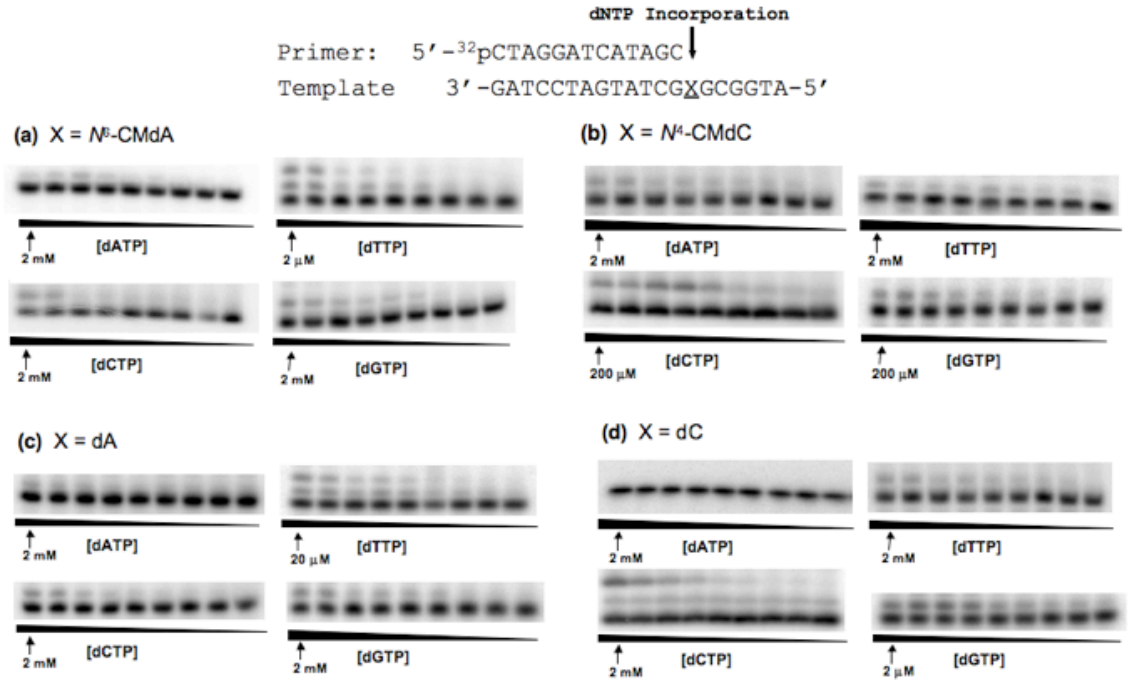

Figure A.2. Representative gel images for steady-state kinetic assays monitoring nucleotide incorporation opposite the N^6-CMdA and N^4-CMdC and the corresponding unmodified dA and dC using 1.2 nM yeast polymerase η. Reactions were carried out in the presence of individual dNTPs with the highest concentrations indicated in the figures. The dNTP concentration ratios between adjacent lanes were 0.50.

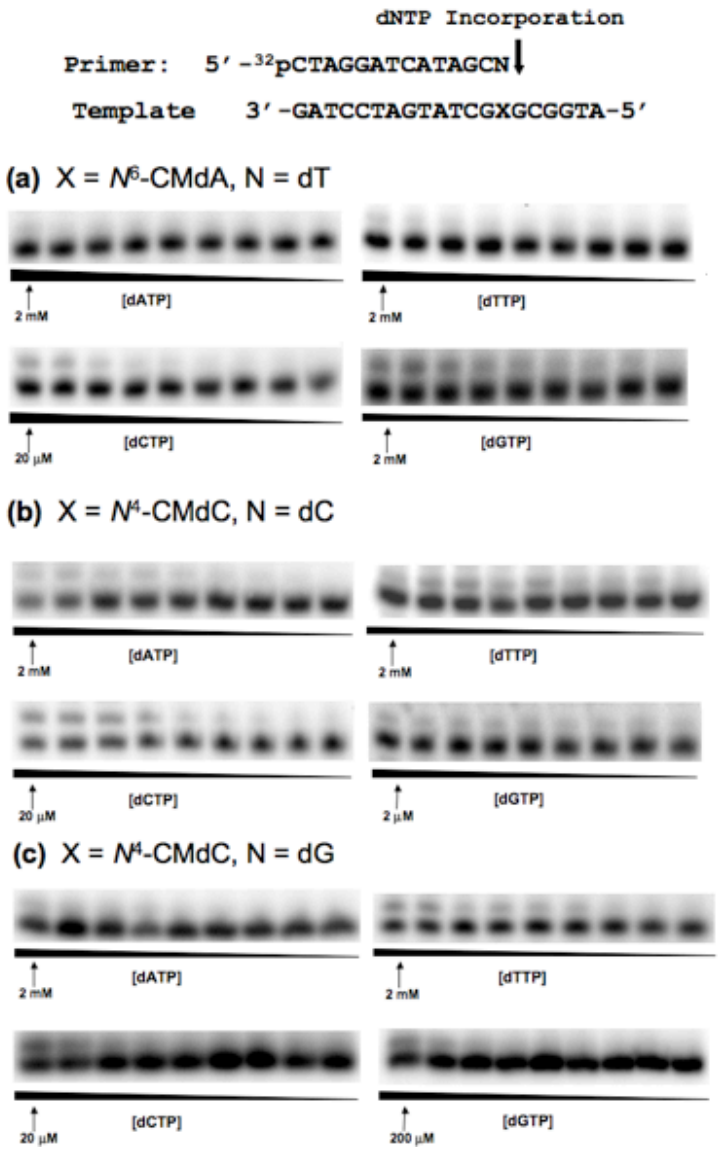

Figure A.3. Representative gel images for steady-state kinetic assays measuring extension past N^6-CMdA and N^4-CMdC lesions with nucleoside opposite the lesions indicated in the figure as 'N'. Reactions were carried out using 1.2 nM yeast polymerase η and in the presence of individual dNTPs with the highest concentrations indicated in the figures. The concentration ratios between neighboring lanes were 0.50.

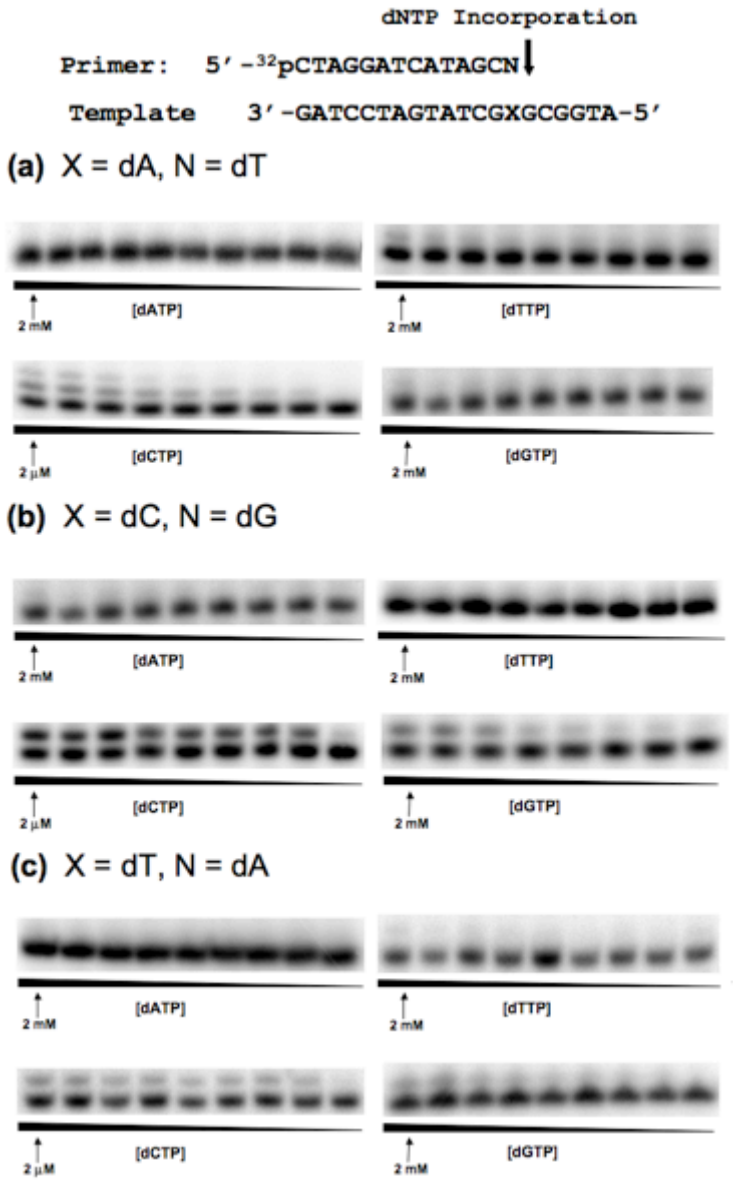

Figure A.4. Representative gel images for steady-state kinetic assays measuring extension past the unmodified controls dA, dC, and dT, with nucleoside opposite the control indicated in the figure as 'N'. Reactions were carried out using 1.2 nM yeast polymerase η and in the presence of individual dNTPs with the highest concentrations indicated in the figures. The concentration ratios between neighboring lanes were 0.50.

Appendix B: Supporting Information for Chapter 3

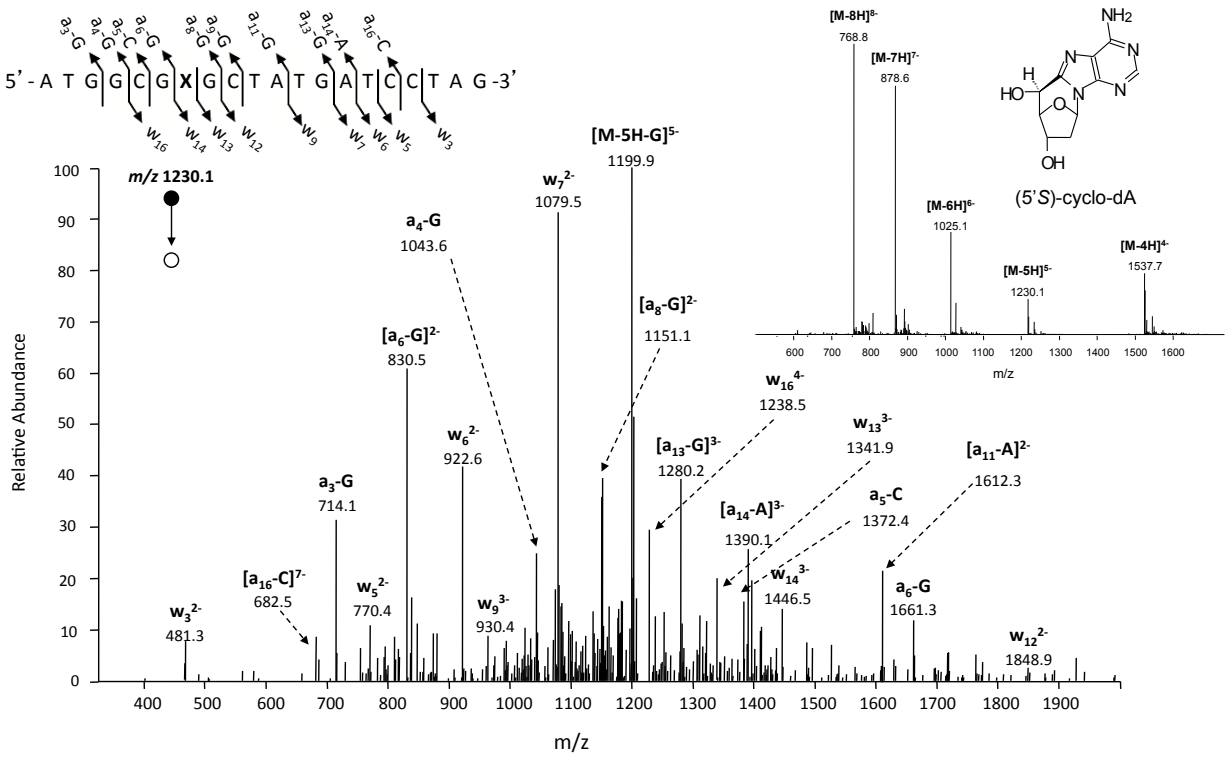

Figure B.1. Product-ion spectrum of the ESI-produced $[M-5H]^{5-}$ ion of d(ATGGCGXGCTATGATCCTAG), where 'X' represents *S*-cdA, depicted as (5'*S*)-cyclo-dA. Illustrated in the inset is the negative-ion ESI-MS.

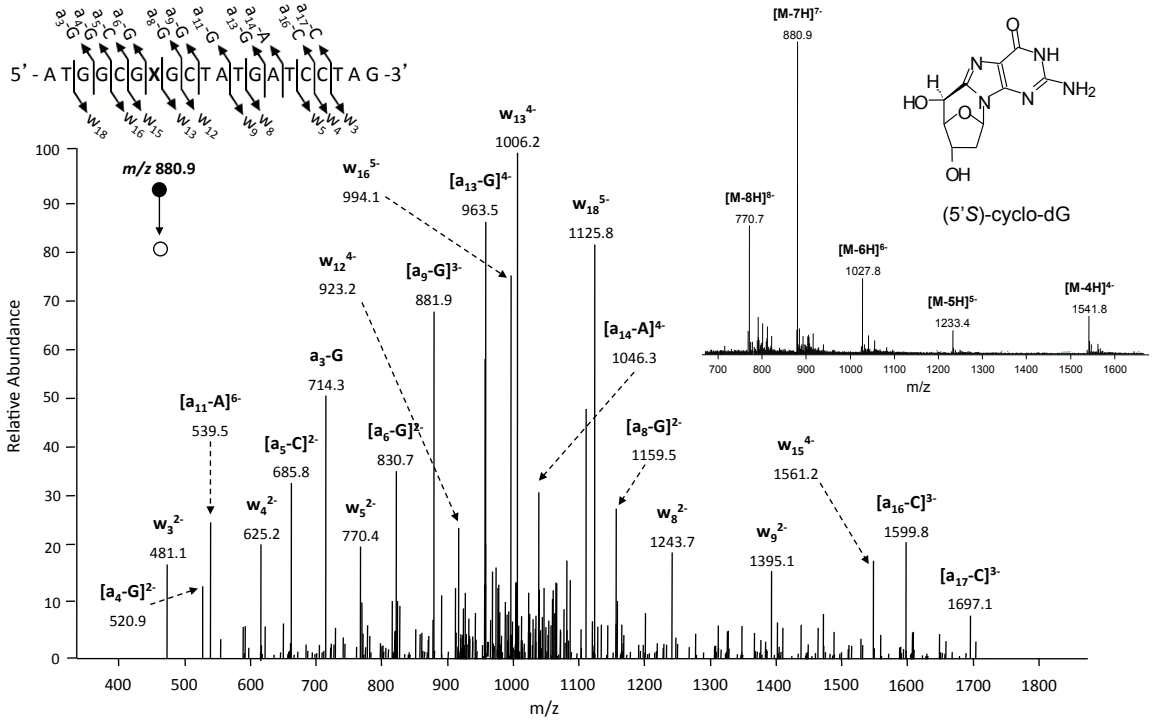

Figure B.2. Product-ion spectrum of the ESI-produced $[M-7H]^{7-}$ ions of d(ATGGCGXGCTATGATCCTAG), where 'X' represents *S*-cdG, depicted as (5'*S*)-cyclo-dG. Illustrated in the inset is the negative-ion ESI-MS.

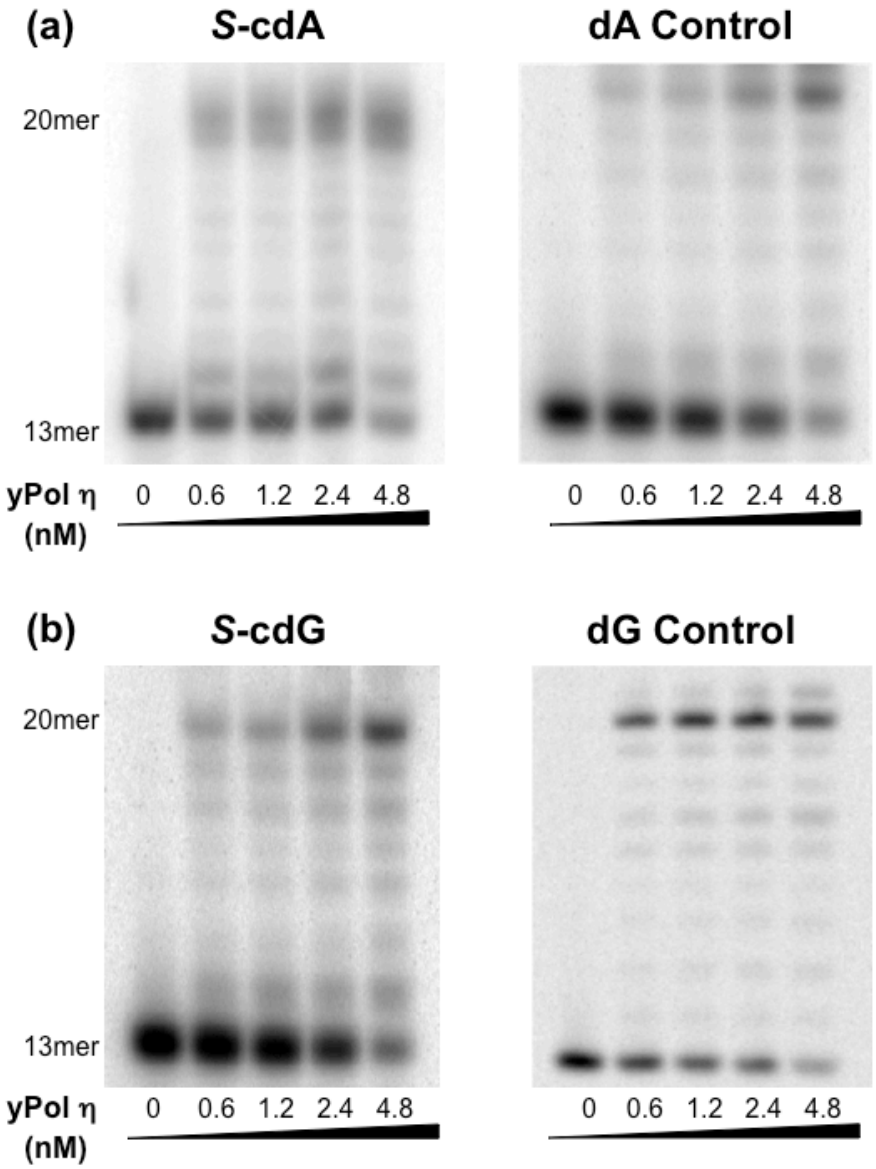

Figure B.3. Primer extension assays for substrates containing *S*-cdA (a), *S*-cdG (b), and the corresponding controls, i.e., dA and dG. Yeast Pol η was employed as the polymerase and the reaction was carried out in the presence of all four dNTPs at 250 μM each. Products were resolved with 20% denaturing polyacrylamide gels.

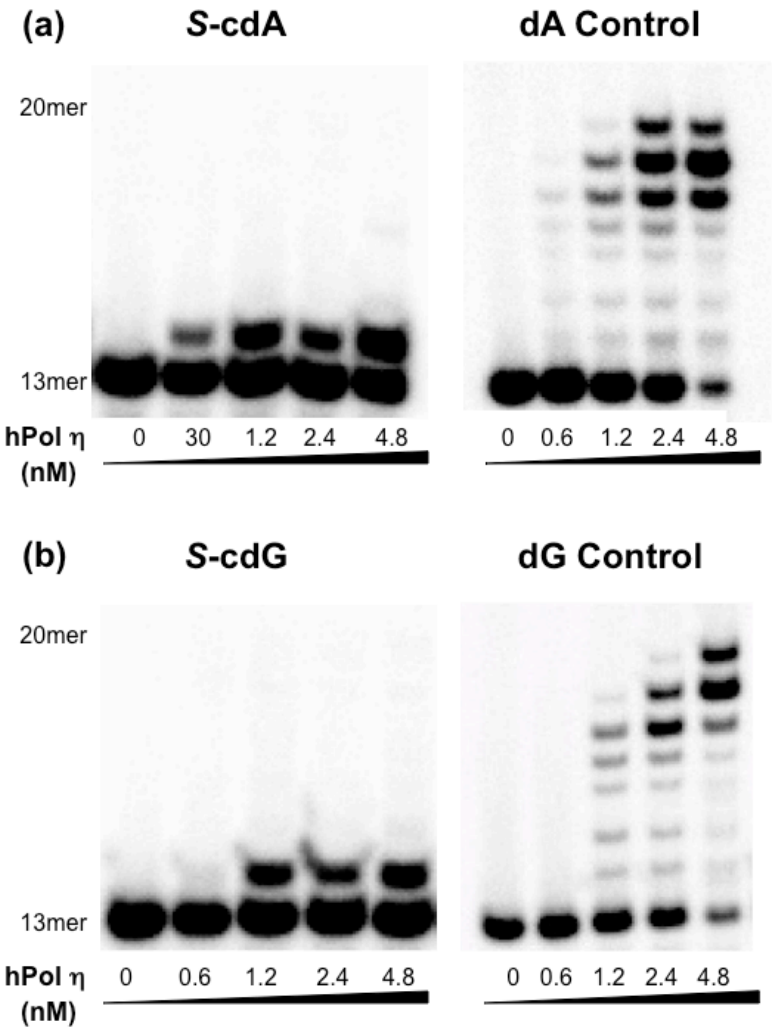

Figure B.4. Primer extension assays for substrates containing *S*-cdA (a), *S*-cdG (b), and the corresponding controls, i.e., dA and dG. Human Pol η was employed as the polymerase and the reaction was carried out in the presence of all four dNTPs at 250 μM each. Products were resolved with 20% denaturing polyacrylamide gels.

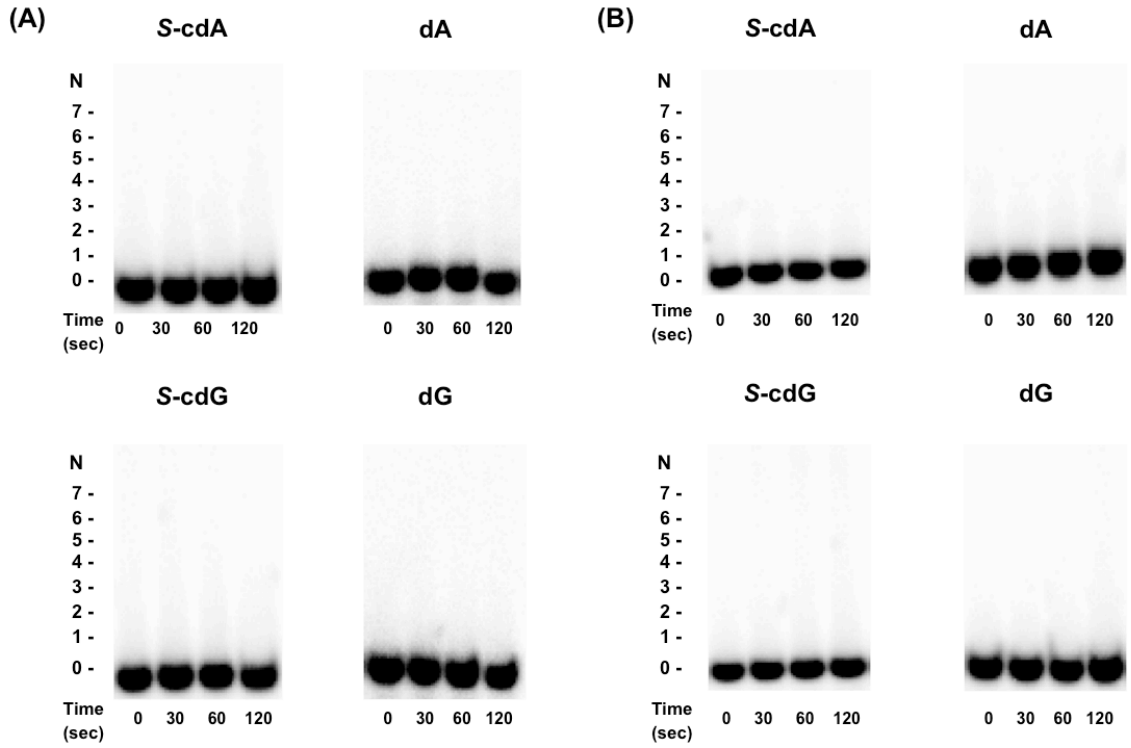

Figure B.5. Control processivity assays with human (A) and yeast (B) Pol η for substrates containing *S*-cdA, *S*-cdG, dA, and dG. The radiolabeled primer-template complex was incubated with yeast or human Pol η and excess herring sperm DNA before addition of dNTPs and $MgCl_2$. The lack of DNA synthesis indicates herring sperm DNA could effectively trap all polymerase molecules. Products were resolved on 20% denaturing polyacrylamide gels.

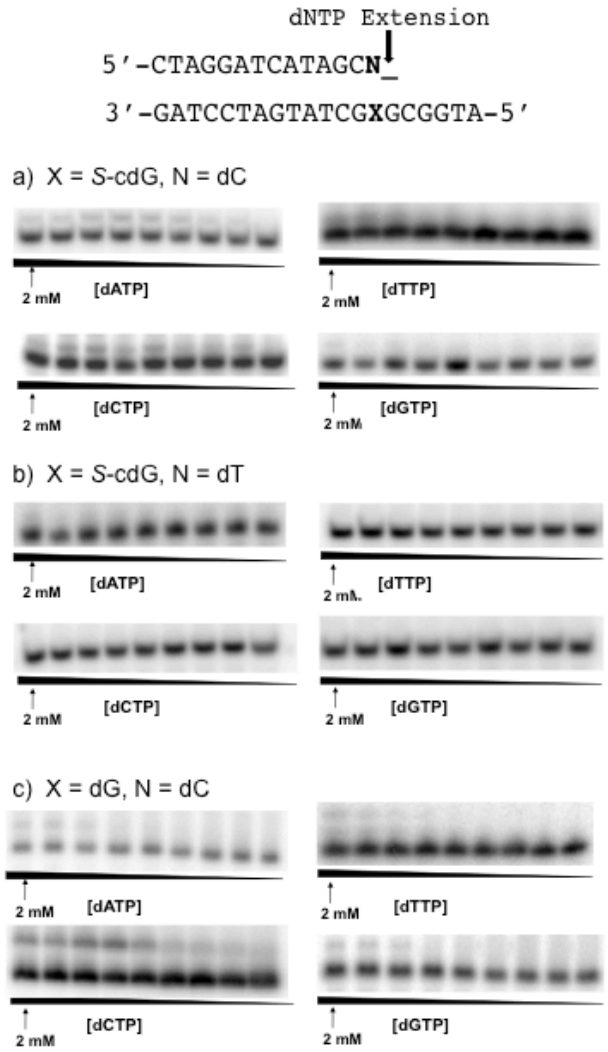

Figure B.6. Representative gel images for steady-state kinetic assays measuring extension past *S*-cdG and dG, with the base opposite the lesions indicated as 'N.' Reactions were carried out using 1.2 nM human Pol η in the presence of individual dNTPs with the highest concentrations indicated in the figures. Concentration ratios between neighboring lanes was 0.50.

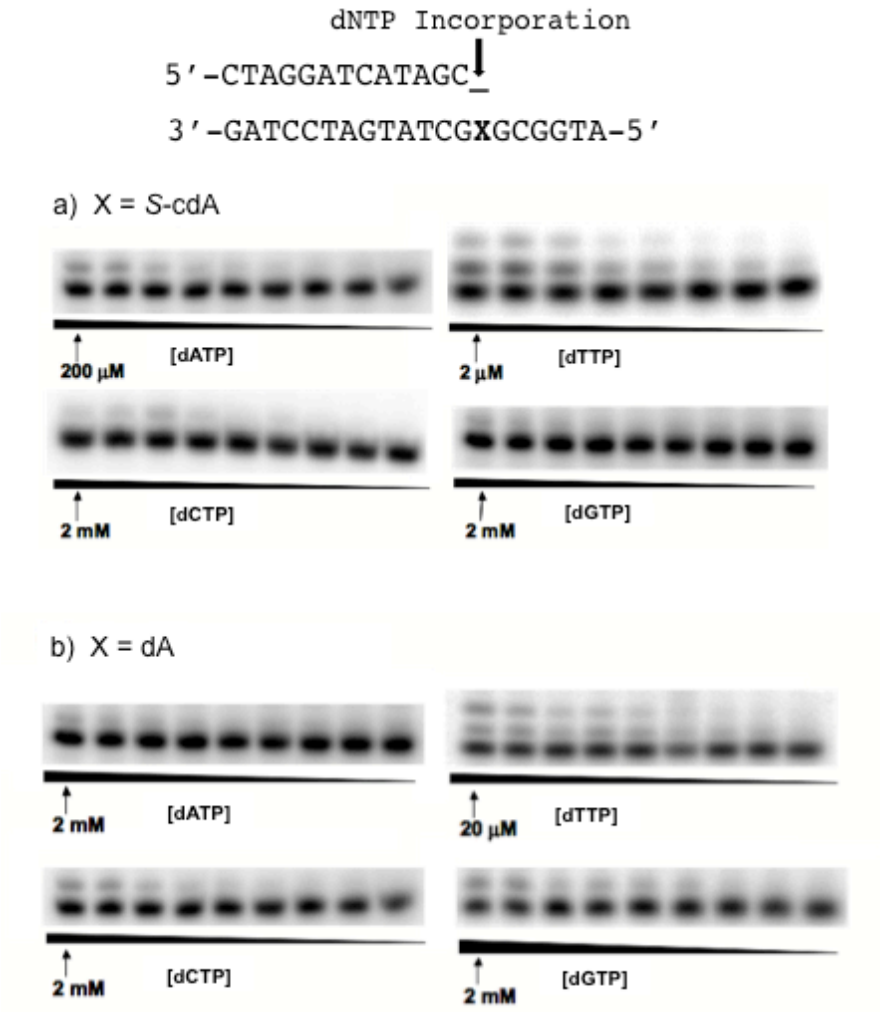

Figure B.7. Representative gel images for steady-state kinetic assays measuring nucleotide incorporation opposite *S*-cdA and unmodified dA. Reactions were carried out using 1.2 nM yeast Pol η in the presence of individual dNTPs with the highest concentrations indicated in the figures. Concentration ratios between neighboring lanes was 0.50.

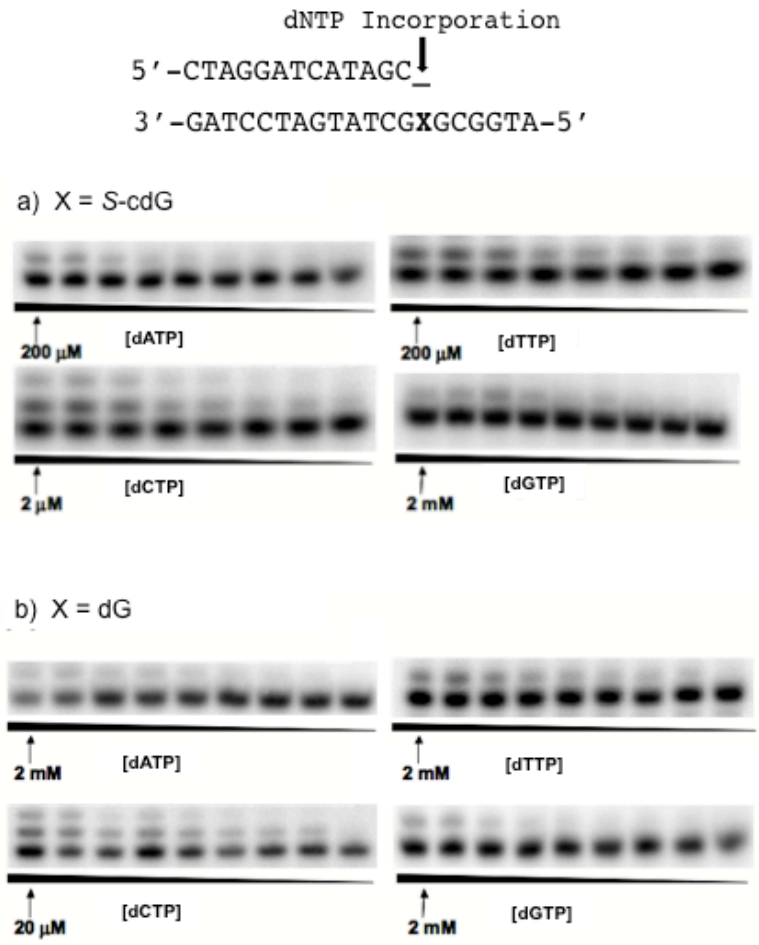

Figure B.8. Representative gel images for steady-state kinetic assays measuring nucleotide incorporation opposite *S*-cdG and unmodified dG. Reactions were carried out using 1.2 nM yeast Pol η in the presence of individual dNTPs with the highest concentrations indicated in the figures. Concentration ratios between neighboring lanes was 0.50.

Appendix C: Supporting Information for Chapter 4

Table C.1. Primers for quantitative RT-PCR analysis.

Gene	Forward primer (5'→3')	Reverse primer (5'→3')
POLH	TGTGCCCTTACCCGCTATGATG	AAGCATTGTGAGAGGAGGAGACC
POLI	GGCGACGACGACGAGGAAG	CTCTGGATGAAGCATTTGGTGTGG
POLK	TGCTGATTTTCCACATCCCTTGAG	CTCCTTTGTTGGTGTTTCCTGTCC
REV3L	GCATTGAGGTTGGCGATAG	CGCCATATACAACCCTAGCC
GAPDH	TTTGTCAAGCTCATTTCCTGGTATG	TCTCTTCCTCTTGTGCTCTTGCTG

Table C.2. Steady-state Kinetic Parameters for Human Pol κ-mediated Nucleotide Insertion opposite *S*-cdA and *S*-cdG, and Unmodified dA and dG[a]

dNTP	k_{cat} (min^{-1})	K_m (μM)	k_{cat}/K_m ($\mu M^{-1}min^{-1}$)	f_{inc}
		***S*-cdA-containing substrate**		
dTTP	6.9 ± 0.7	88 ± 9	0.078 ± 0.008	1
dGTP	4.2 ± 0.5	190 ± 20	0.022 ± 0.002	2.8×10^{-1}
dCTP	5.3 ± 0.6	110 ± 10	0.048 ± 0.005	6.2×10^{-1}
dATP	4.9 ± 0.5	140 ± 15	0.035 ± 0.004	4.5×10^{-1}
		dA Control		
dTTP	20 ± 2	0.24 ± 0.02	83 ± 8	1
dGTP	15 ± 2	96 ± 20	0.16 ± 0.02	1.9×10^{-3}
dCTP	18 ± 2	27 ± 3	0.66 ± 0.04	8.0×10^{-3}
dATP	12 ± 1	130 ± 13	0.092 ± 0.009	1.1×10^{-3}
		***S*-cdG-containing substrate**		
dTTP	5.5 ± 0.6	74 ± 8	0.074 ± 0.008	6.7×10^{-1}
dGTP	8.9 ± 0.9	79 ± 8	0.11 ± 0.01	1.2
dCTP	7.3 ± 0.7	82 ± 8	0.089 ± 0.01	1
dATP	4.4 ± 0.4	180 ± 20	0.024 ± 0.003	2.7×10^{-1}
		dG Control		
dTTP	15 ± 1	100 ± 10	0.15 ± 0.02	1.6×10^{-3}
dGTP	12 ± 1	43 ± 4	0.28 ± 0.03	2.9×10^{-4}
dCTP	24 ± 2	0.25 ± 0.03	96 ± 9	1
dATP	13 ± 1	120 ± 10	0.11 ± 0.01	1.1×10^{-3}

[a] k_{cat} and K_m values were based on three independent measurements

Table C.3. Steady-state Kinetic Parameters for a two-subunit yeast Pol ζ complex (REV3/REV7)-mediated Nucleotide Insertion opposite *S*-cdA and *S*-cdG, and Unmodified dA and dG[a]

dNTP	k_{cat} (min^{-1})	K_m (μM)	k_{cat}/K_m ($\mu M^{-1}min^{-1}$)	f_{inc}
		***S*-cdA-containing substrate**		
dTTP	8.2 ± 0.8	52 ± 6	0.16 ± 0.02	1
dGTP	6.1 ± 0.7	68 ± 7	0.089 ± 0.09	5.6×10^{-1}
dCTP	5.9 ± 0.6	95 ± 10	0.062 ± 0.007	3.9×10^{-1}
dATP	4.8 ± 0.5	97 ± 10	0.049 ± 0.005	3.1×10^{-1}
		dA Control		
dTTP	13 ± 1	0.68 ± 0.07	19 ± 2	1
dGTP	11 ± 1	72 ± 7	0.15 ± 0.02	7.9×10^{-3}
dCTP	8.9 ± 0.9	53 ± 6	0.17 ± 0.02	8.9×10^{-3}
dATP	7.2 ± 0.8	89 ± 9	0.081 ± 0.009	4.3×10^{-3}
		***S*-cdG-containing substrate**		
dTTP	6.3 ± 0.6	95 ± 10	0.066 ± 0.007	5.1×10^{-1}
dGTP	7.3 ± 0.8	54 ± 9	0.14 ± 0.02	1.1
dCTP	7.7 ± 0.7	61 ± 7	0.13 ± 0.02	1
dATP	5.2 ± 0.6	92 ± 10	0.057 ± 0.006	4.4×10^{-1}
		dG Control		
dTTP	9.1 ± 1	82 ± 9	0.11 ± 0.01	5.0×10^{-3}
dGTP	10 ± 1	40 ± 3	0.25 ± 0.03	1.1×10^{-2}
dCTP	14 ± 2	0.64 ± 0.07	22 ± 2	1
dATP	6.2 ± 0.7	74 ± 6	0.13 ± 0.01	5.9×10^{-3}

[a] k_{cat} and K_m values were based on three independent measurements

Table C.4. Steady-state Kinetic Parameters for Human Pol ι-mediated Nucleotide Insertion opposite Downstream 5' Nucleoside (+1 base) to *S*-cdA and *S*-cdG, and Unmodified dA and dG (designated with an X, and N is the nucleoside placed opposite X)[a]

dNTP	k_{cat} (min^{-1})	K_m (μM)	k_{cat}/K_m ($\mu M^{-1}min^{-1}$)	f_{ext}
		X = *S*-cdA-containing substrate, N = dT		
dTTP	19 ± 1	28 ± 3	0.68 ± 0.07	1.3
dGTP	14 ± 1	41 ± 4	0.34 ± 0.04	6.5×10^{-1}
dCTP	12 ± 1	23 ± 2	0.52 ± 0.06	1
dATP	16 ± 1	220 ± 20	0.064 ± 0.005	1.2×10^{-1}
		X = dA, N = dT		
dTTP	21 ± 2	74 ± 8	0.28 ± 0.03	1.2×10^{-3}
dGTP	24 ± 2	130 ± 15	0.18 ± 0.02	7.8×10^{-4}
dCTP	28 ± 3	0.12 ± 0.01	230 ± 25	1
dATP	33 ± 3	46 ± 5	0.72 ± 0.08	3.1×10^{-3}
		X = *S*-cdG-containing substrate, N = dC		
dTTP	11 ± 1	210 ± 20	0.052 ± 0.006	9.8×10^{-2}
dGTP	13 ± 1	91 ± 20	0.14 ± 0.01	2.6×10^{-1}
dCTP	15 ± 2	28 ± 3	0.53 ± 5	1
dATP	21 ± 2	45 ± 5	0.47 ± 0.5	8.8×10^{-1}
		X = dG, N = dC		
dTTP	29 ± 3	68 ± 7	0.43 ± 0.005	1.2×10^{-3}
dGTP	25 ± 3	160 ± 20	0.16 ± 0.02	4.4×10^{-4}
dCTP	34 ± 3	0.13 ± 0.01	360 ± 40	1
dATP	26 ± 3	74 ± 8	0.35 ± 0.04	9.7×10^{-4}

[a] k_{cat} and K_m values were based on three independent measurements

Table C.5. Steady-state Kinetic Parameters for Human Pol κ-mediated Nucleotide Insertion opposite Downstream 5' Nucleoside (+1 base) to *S*-cdA and *S*-cdG, and Unmodified dA and dG (designated with an X, and N is the nucleoside placed opposite X)[a]

dNTP	k_{cat} (min^{-1})	K_m (μM)	k_{cat}/K_m ($\mu M^{-1}min^{-1}$)	f_{inc}
		X = *S*-cdA-containing substrate, N = dT		
dTTP	7.5 ± 0.8	130 ± 10	0.058 ± 0.006	2.0×10^{-2}
dGTP	9.5 ± 1	18 ± 10	0.53 ± 0.05	1.8×10^{-1}
dCTP	10 ± 1	3.4 ± 0.3	2.9 ± 0.3	1
dATP	6.2 ± 0.6	150 ± 20	0.041 ± 0.004	1.4×10^{-2}
		X = dA, N = dT		
dTTP	17 ± 2	71 ± 7	0.24 ± 0.03	2.5×10^{-3}
dGTP	19 ± 2	23 ± 3	0.84 ± 0.09	8.8×10^{-3}
dCTP	21 ± 2	0.22 ± 0.02	95 ± 10	1
dATP	14 ± 1	95 ± 3	0.15 ± 0.02	1.6×10^{-3}
		X = *S*-cdG-containing substrate, N = dC		
dTTP	5.2 ± 0.5	170 ± 20	0.031 ± 0.003	3.6×10^{-2}
dGTP	7.8 ± 0.8	49 ± 5	0.16 ± 0.02	1.9×10^{-1}
dCTP	11 ± 1	13 ± 1	0.85 ± 0.003	1
dATP	5.1 ± 0.6	100 ± 10	0.051 ± 0.005	6.0×10^{-2}
		X = dG, N =dC		
dTTP	18 ± 2	110 ± 10	0.16 ± 0.02	1.8×10^{-3}
dGTP	17 ± 2	22 ± 2	0.77 ± 0.08	8.5×10^{-3}
dCTP	23 ± 2	0.25 ± 0.03	91 ± 9	1
dATP	15 ± 2	160 ± 20	0.094 ± 0.01	1.0×10^{-3}

[a] k_{cat} and K_m values were based on three independent measurements

Table C.6. Steady-state Kinetic Parameters for a two-subunit yeast Pol ζ complex (REV3/REV7)-mediated Nucleotide Insertion opposite Downstream 5' Nucleoside (+1 base) to *S*-cdA and *S*-cdG, and Unmodified dA and dG (designated with an X, and N is the nucleoside placed opposite X)[a]

dNTP	k_{cat} (min^{-1})	K_m (μM)	k_{cat}/K_m ($\mu M^{-1}min^{-1}$)	f_{inc}
		X = *S*-cdA-containing substrate, N = dT		
dTTP	7.5 ± 0.8	41 ± 8	0.18 ± 0.02	1.6×10^{-2}
dGTP	9.3 ± 1	2.4 ± 0.3	3.9 ± 0.4	3.5×10^{-1}
dCTP	10 ± 1	0.91 ± 0.1	11 ± 1	1
dATP	5.9 ± 0.6	82 ± 9	0.072 ± 0.005	6.5×10^{-3}
		X = dA, N = dT		
dTTP	10 ± 1	72 ± 8	0.14 ± 0.02	6.7×10^{-3}
dGTP	12 ± 1	63 ± 7	0.19 ± 0.02	9.0×10^{-3}
dCTP	13 ± 2	0.62 ± 0.07	21 ± 2	1
dATP	8.4 ± 0.9	87 ± 9	0.097 ± 0.01	4.6×10^{-3}
		X = *S*-cdG-containing substrate, X = dC		
dTTP	8.6 ± 0.9	62 ± 7	0.14 ± 0.02	2.1×10^{-2}
dGTP	9.9 ± 1	3.2 ± 3	3.1 ± 0.4	4.6×10^{-1}
dCTP	12 ± 1	1.8 ± 0.2	6.7 ± 0.7	1
dATP	6.7 ± 0.7	99 ± 10	0.068 ± 0.007	1.0×10^{-1}
		X = dG, N = dC		
dTTP	10 ± 1	81 ± 9	0.12 ± 0.02	5.2×10^{-3}
dGTP	13 ± 1	64 ± 3	0.20 ± 0.02	8.7×10^{-3}
dCTP	15 ± 2	0.65 ± 0.07	23 ± 2	1
dATP	8.6 ± 0.9	85 ± 9	0.10 ± 0.01	5.9×10^{-3}

[a] k_{cat} and K_m values were based on three independent measurements

Table C.7. Steady-state Kinetic Parameters for a two-subunit yeast Pol ζ complex (REV3/REV7)-mediated +2 Base Extension past *S*-cdA and *S*-cdG, and Unmodified dA and dG (designated with an X, N is the nucleoside placed opposite X, M is the nucleoside placed opposite dG, the 5' adjacent base)[a]

dNTP	k_{cat} (min^{-1})	K_m (μM)	k_{cat}/K_m ($\mu M^{-1}min^{-1}$)	f_{inc}
		X = *S*-cdA-containing substrate, N = dT, M = dC		
dTTP	12 ± 1	20 ± 2	0.59 ± 0.06	2.4×10^{-2}
dGTP	13 ± 2	0.52 ± 0.05	25 ± 3	1
dCTP	9.0 ± 1	91 ± 10	0.099 ± 0.01	4.0×10^{-3}
dATP	11 ± 1	61 ± 6	0.18 ± 0.03	7.2×10^{-3}
		X = dA, N = dT, M = dC		
dTTP	11 ± 1	41 ± 4	0.27 ± 0.03	9.3×10^{-3}
dGTP	12 ± 1	0.41 ± 0.04	29 ± 3	1
dCTP	7.3 ± 0.8	85 ± 9	0.086 ± 0.009	2.9×10^{-3}
dATP	9.8 ± 1	74 ± 6	0.13 ± 0.01	4.5×10^{-3}
		X = *S*-cdG-containing substrate, N = dC, M = dC		
dTTP	10 ± 1	13 ± 2	0.77 ± 0.08	3.3×10^{-2}
dGTP	11 ± 1	0.48 ± 0.05	23 ± 3	1
dCTP	6.9 ± 0.7	83 ± 9	0.083 ± 0.008	3.6×10^{-3}
dATP	9.2 ± 1	48 ± 5	0.19 ± 0.02	8.3×10^{-3}
		X = dG, N = dC, M = dC		
dTTP	12 ± 1	46 ± 5	0.26 ± 0.03	7.6×10^{-3}
dGTP	15 ± 2	0.44 ± 0.05	34 ± 3	1
dCTP	7.9 ± 0.8	87 ± 9	0.091 ± 0.01	2.7×10^{-3}
dATP	11 ± 1	92 ± 9	0.12 ± 0.01	3.5×10^{-3}

[a] k_{cat} and K_m values were based on three independent measurements

Table C.8. Steady-state Kinetic Parameters for Human Pol κ-mediated +2 Base Extension past *S*-cdA and *S*-cdG, and Unmodified dA and dG (designated with an X, N is the nucleoside placed opposite X, M is the nucleoside placed opposite dG, the 5' adjacent base)[a]

dNTP	k_{cat} (min^{-1})	K_m (μM)	k_{cat}/K_m ($\mu M^{-1}min^{-1}$)	f_{inc}
		X = *S*-cdA-containing substrate, N = dT, M = dC		
dTTP	15 ± 1	39 ± 4	0.38 ± 0.04	1.3×10^{-2}
dGTP	18 ± 2	0.62 ± 0.05	29 ± 4	1
dCTP	9.5 ± 1	110 ± 15	0.086 ± 0.009	3.0×10^{-3}
dATP	17 ± 2	6.8 ± 0.7	2.5 ± 0.03	8.6×10^{-2}
		X = dA, N = dT, M = dC		
dTTP	15 ± 1	45 ± 3	0.33 ± 0.03	4.6×10^{-3}
dGTP	25 ± 3	0.35 ± 0.04	71 ± 6	1
dCTP	11 ± 1	19 ± 2	0.58 ± 0.07	8.2×10^{-3}
dATP	18 ± 2	33 ± 3	0.54 ± 0.05	7.6×10^{-3}
		X = *S*-cdG-containing substrate, N = dC, M = dC		
dTTP	17 ± 2	4.9 ± 0.5	3.5 ± 0.3	1.1×10^{-1}
dGTP	19 ± 2	0.59 ± 0.06	32 ± 2	1
dCTP	5.6 ± 0.6	180 ± 20	0.031 ± 0.003	9.7×10^{-4}
dATP	21 ± 2	33 ± 4	0.64 ± 0.06	2.0×10^{-2}
		X = dG, N = dC, M = dC		
dTTP	19 ± 2	84 ± 9	0.23 ± 0.02	2.6×10^{-3}
dGTP	22 ± 2	0.25 ± 0.03	87 ± 9	1
dCTP	8.3 ± 0.8	140 ± 15	0.059 ± 0.006	6.8×10^{-4}
dATP	12 ± 1	160 ± 20	0.075 ± 0.008	8.6×10^{-4}

[a] k_{cat} and K_m values were based on three independent measurements

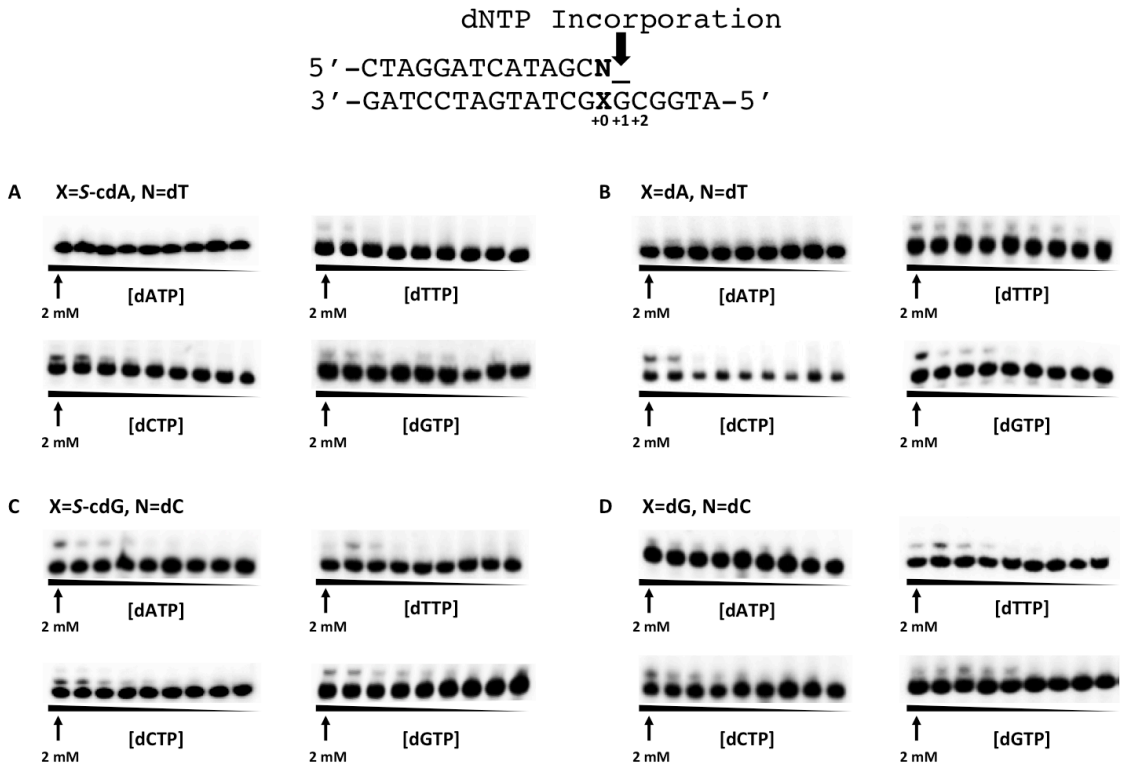

Figure C.1. Representative gel images for steady-state kinetic assays measuring nucleotide incorporation at the +2 base relative to *S*-cdA, *S*-cdG, or corresponding unmodified dA or dG by a two-subunit yeast Pol ζ complex (REV3/REV7).

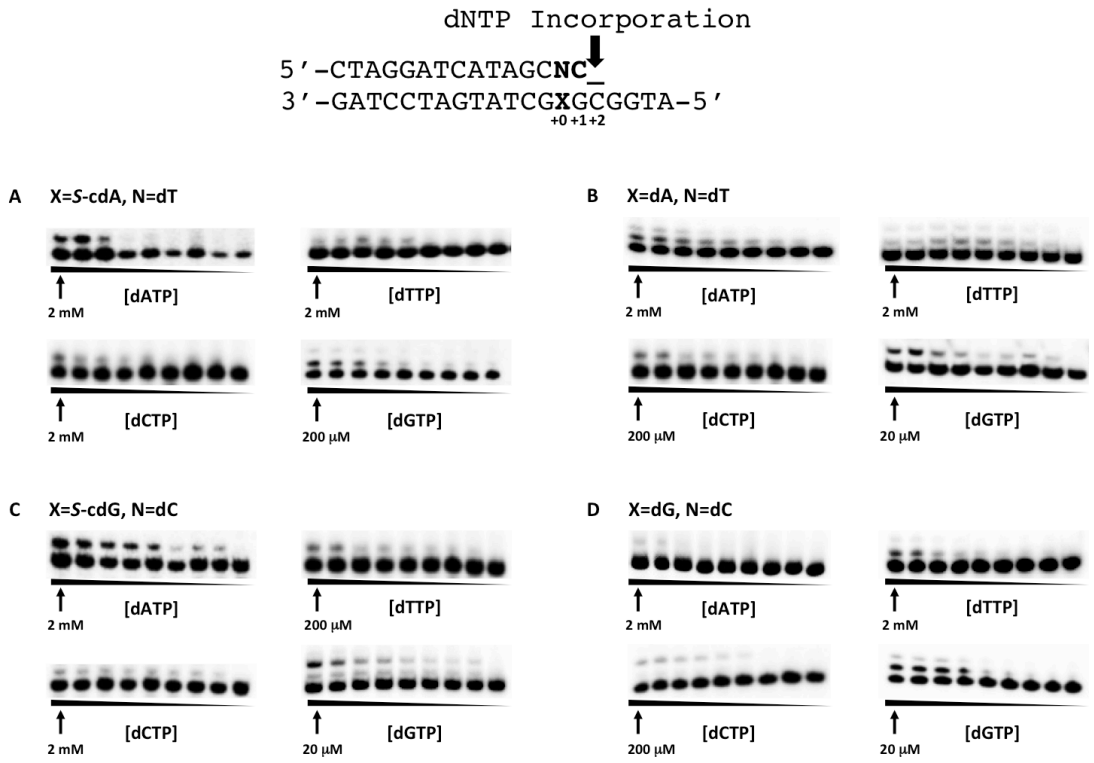

Figure C.2. Representative gel images for steady-state kinetic assays measuring nucleotide incorporation at the +2 base relative to *S*-cdA, *S*-cdG, or corresponding unmodified dA or dG by human Pol κ.

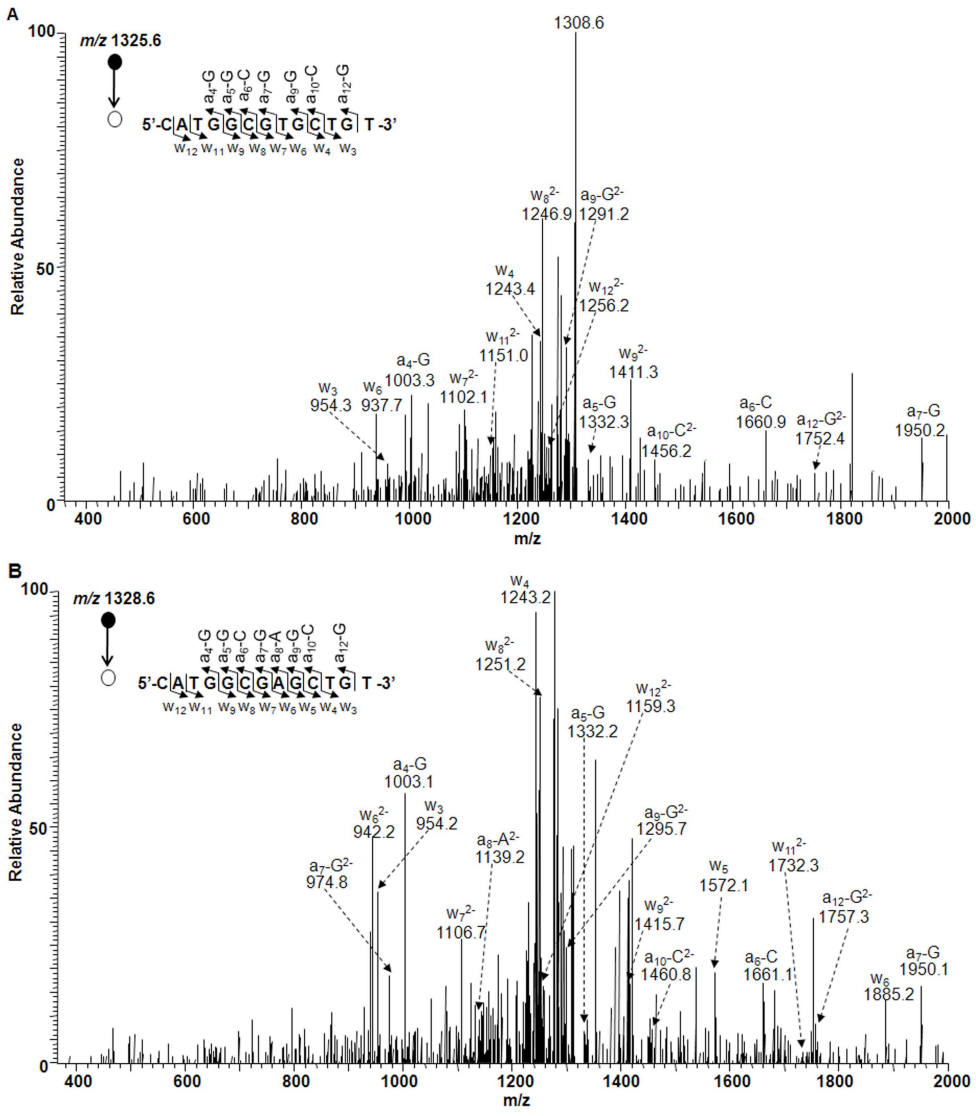

Figure C.3. Representative LC-MS/MS results for monitoring the 13-mer restriction fragments resulting from the *in vivo* replication of *S*-cdA-bearing substrate in human cells. Shown in (A) and (B) are the MS/MS of the $[M–3H]^{3-}$ ions (*m/z* 1325.6 and 1328.6) of the mutant (A→T) and wide-type ODNs, respectively. Shown above the spectrum is a scheme summarizing the observed $[a_n – Base]$ and w_n fragment ions [nomenclature follows that described by McLuckey et al. (1992) *J. Am. Soc. Mass Spectrom.* 3, 60-70].

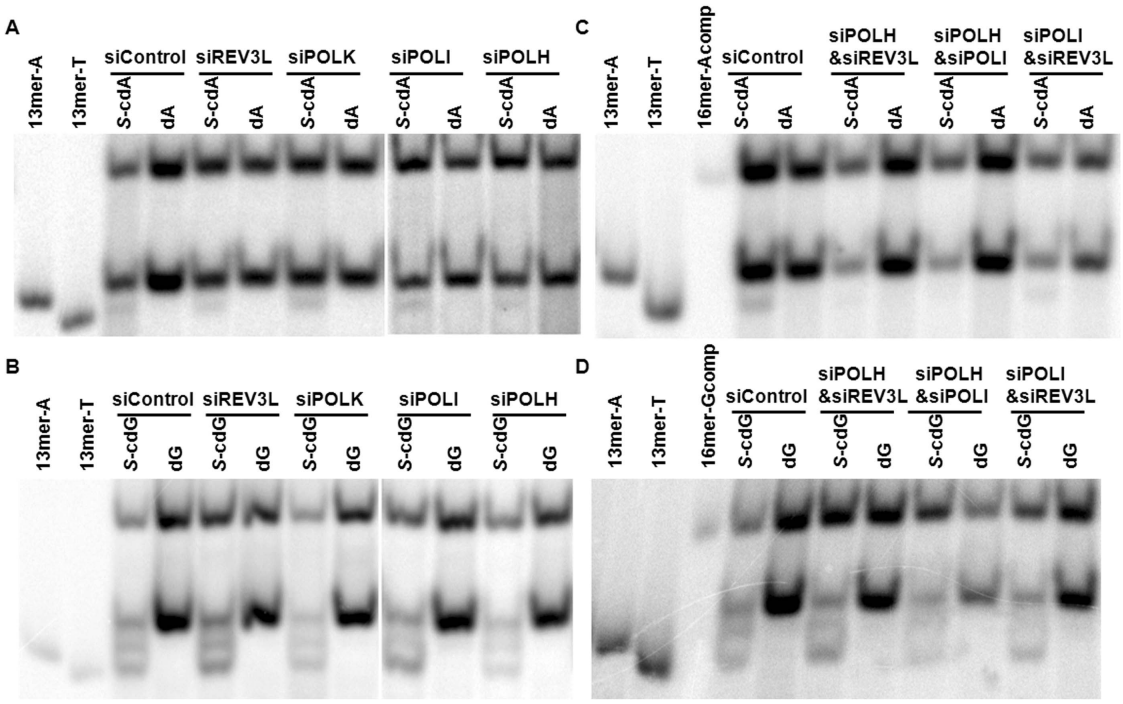

Figure C.4. Representative gel images for assessing the RBE and RMF values of *S*-cdA and *S*-cdG in 293T cells treated with siRNAs of TLS polymerases, including Pol η (POLH), Pol κ (POLK), Pol ι (POLI), and Rev3L (Pol ζ). The restriction fragments arising from the competitor vectors for *S*-cdA and *S*-cdG, i.e., d(CATGGCGAGCAGCTGT) and d(CATGGCGGGCAGCTGT), are designated with '16mer-Acomp' and '16mer-Gcomp', respectively; '13mer-A' and '13mer-T', represent standard ODNs d(CATGGCGAGCTGT) and d(CATGGCGTGCTGT), respectively.

Appendix D: Supporting Information for Chapter 5

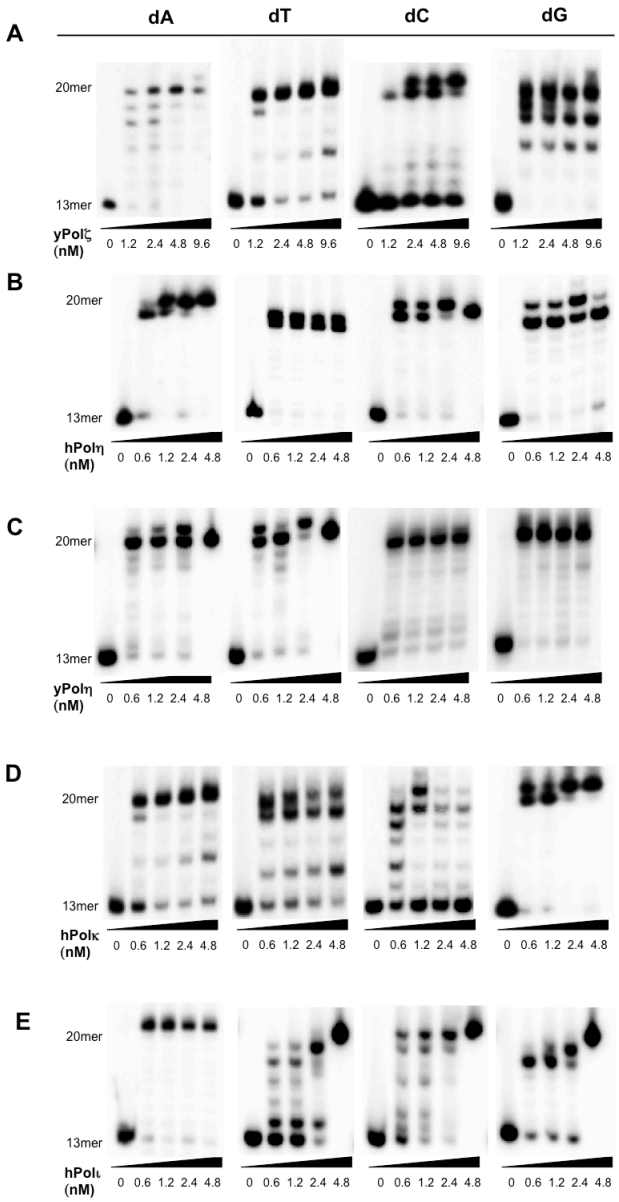

Figure D.1. Primer extension assays past an unmodified dA, dT, dC, or dG in template DNA, with A) yeast Pol ζ, B) human Pol η, C) yeast Pol η, D) human Pol ι, and E) human Pol κ, with the concentrations of the polymerases being listed in the figure.

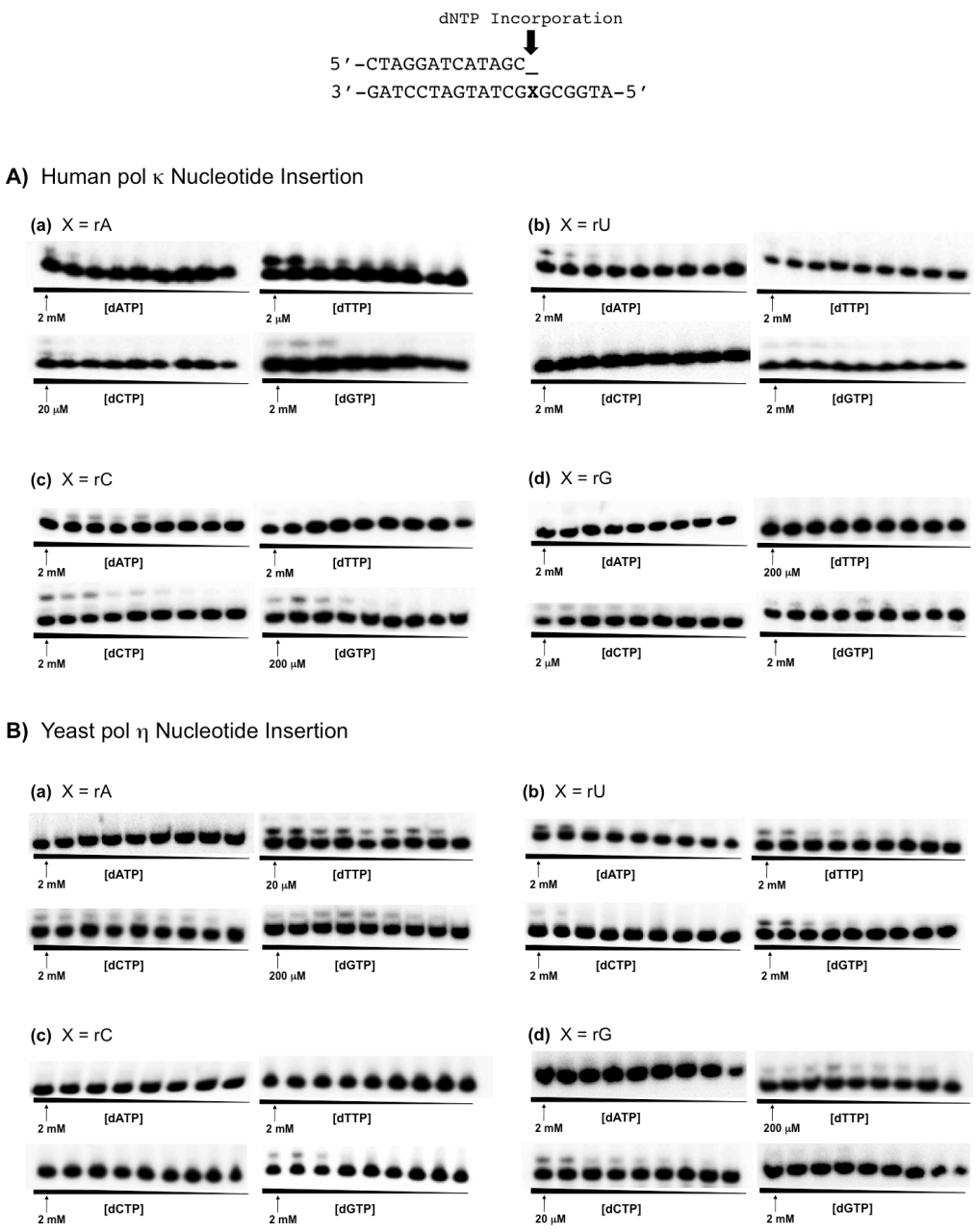

Figure D.2. A) Human Pol κ (1.2nM)-mediated nucleotide insertion opposite a) rA, b) rU, c) rC, and d) rG, and B) representative gel images for steady-state kinetic assays opposite a) rA, b) rU, c) rC, and d) rG using 1.2nM yeast Pol η. Reactions were performed in triplicate in the presence of individual dNTPs, the highest concentrations of which are indicated in the figures. The concentration ratio between neighboring lanes was 0.50.

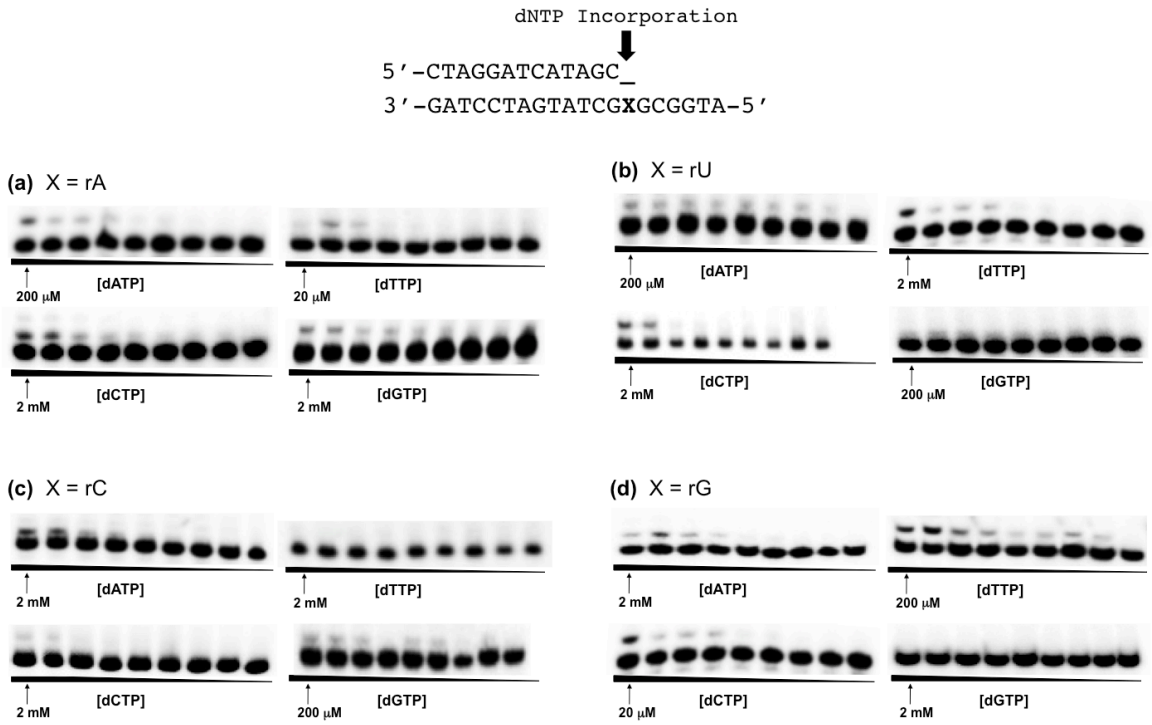

Figure D.3. Representative gel images for steady-state kinetic assays opposite a) rA, b) rU, c) rC and d) rG using 1.2nM human Pol ι. Reactions were performed in the presence of individual dNTPs, the highest concentrations of which are indicated in the figures. The concentration ratio between neighboring lanes was 0.50.

References

1. Lindahl, T. (1993) Instability and decay of the primary structure of DNA. *Nature* **362**, 709-715

2. Chance, B., Sies, H., and Boveris, A. (1979) Hydroperoxide metabolism in mammalian organs. *Physiol. Rev.* **59**, 527-605

3. Friedberg, E. C., McDaniel, L. D., and Schultz, R. A. (2004) The role of endogenous and exogenous DNA damage and mutagenesis. *Curr. Opin. Genet. Dev.* **14**, 5-10

4. Finkel, T., and Holbrook, N. J. (2000) Oxidants, oxidative stress, and the biology of ageing. *Nature* **408**, 239-247

5. Wallace, S. S. (2002) Biological consequences of free radical-damaged DNA bases. *Free Radic. Biol. Med.* **33**, 1-14

6. Cadet, J., Douki, T., Gasparutto, D., and Ravanat, J. L. (2003) Oxidative damage to DNA: formation, measurement and biochemical features. *Mutat. Res.* **531**, 5-23

7. Nohl, H., Kozlov, A. V., Gille, L., and Staniek, K. (2003) Cell respiration and formation of reactive oxygen species: facts and artefacts. *Biochem. Soc. Trans.* **31**, 1308-1311

8. Cadet, J., Delatour, T., Douki, T., Gasparutto, D., Pouget, J. P., Ravanat, J. L., and Sauvaigo, S. (1999) Hydroxyl radicals and DNA base damage. *Mutat. Res.* **424**, 9-21

9. Yamamoto, K., and Kawanishi, S. (1989) Hydroxyl free radical is not the main active species in site-specific DNA damage induced by copper (II) ion and hydrogen peroxide. *J. Biol. Chem.* **264**, 15435-15440

10. Hold, G. L., and El-Omar, E. M. (2008) Genetic aspects of inflammation and cancer. *Biochem. J.* **410**, 225-235

11. Jackson, A. L., and Loeb, L. A. (2001) The contribution of endogenous sources of DNA damage to the multiple mutations in cancer. *Mutat. Res.* **477**, 7-21

12. Cooke, M. S., Evans, M. D., Dizdaroglu, M., and Lunec, J. (2003) Oxidative DNA damage: mechanisms, mutation, and disease. *FASEB J.* **17**, 1195-1214

13. Marnett, L. J. (2000) Oxyradicals and DNA damage. *Carcinogenesis* **21**, 361-370

14. Dizdaroglu, M. (1992) Measurement of radiation-induced damage to DNA at the molecular level. *Int. J. Radiat. Biol.* **61**, 175-183

15. Bellon, S., Ravanat, J. L., Gasparutto, D., and Cadet, J. (2002) Cross-linked thymine-purine base tandem lesions: synthesis, characterization, and measurement in γ-irradiated isolated DNA. *Chem. Res. Toxicol.* **15**, 598-606

16. Epe, B. (2002) Role of endogenous oxidative DNA damage in carcinogenesis: what can we learn from repair-deficient mice? *Biol. Chem.* **383**, 467-475

17. Xiao, W., and Samson, L. (1993) *In vivo* evidence for endogenous DNA alkylation damage as a source of spontaneous mutation in eukaryotic cells. *Proc. Natl. Acad. Sci. U.S.A.* **90**, 2117-2121

18. Holliday, R., and Ho, T. (1998) Gene silencing and endogenous DNA methylation in mammalian cells. *Mutat. Res.* **400**, 361-368

19. Rydberg, B., and Lindahl, T. (1982) Nonenzymatic methylation of DNA by the intracellular methyl group donor *S*-adenosyl-L-methionine is a potentially mutagenic reaction. *EMBO J.* **1**, 211-216

20. Stern, L. L., Mason, J. B., Selhub, J., and Choi, S. W. (2000) Genomic DNA hypomethylation, a characteristic of most cancers, is present in peripheral leukocytes of individuals who are homozygous for the C677T polymorphism in the methylenetetrahydrofolate reductase gene. *Cancer Epidemiol. Biomarkers Prev.* **9**, 849-853

21. Saffhill, R. (1985) *In vitro* miscoding of alkylthymines with DNA and RNA polymerases. *Chem. Biol. Interact.* **53**, 121-130

22. Lindahl, T. (1982) DNA repair enzymes. *Annu. Rev. Biochem.* **51**, 61-87

23. Gentil, A., Renault, G., Madzak, C., Margot, A., Cabral-Neto, J. B., Vasseur, J. J., Rayner, B., Imbach, J. L., and Sarasin, A. (1990) Mutagenic properties of a unique abasic site in mammalian cells. *Biochem. Biophys. Res. Commun.* **173**, 704-710

24. Lawrence, C. W., Borden, A., Banerjee, S. K., and LeClerc, J. E. (1990) Mutation frequency and spectrum resulting from a single abasic site in a single-stranded vector. *Nucleic Acids Res.* **18**, 2153-2157

25. Nakamura, J., and Swenberg, J. A. (1999) Endogenous apurinic/apyrimidinic sites in genomic DNA of mammalian tissues. *Cancer Res.* **59**, 2522-2526

26. Cadet, J., Anselmino, C., Douki, T., and Voituriez, L. (1992) Photochemistry of nucleic acids in cells. *J. Photochem. Photobiol. B* **15**, 277-298

27. You, Y. H., Szabo, P. E., and Pfeifer, G. P. (2000) Cyclobutane pyrimidine dimers form preferentially at the major *p53* mutational hotspot in UVB-induced mouse skin tumors. *Carcinogenesis* **21**, 2113-2117

28. Yoon, J. H., Lee, C. S., O'Connor, T. R., Yasui, A., and Pfeifer, G. P. (2000) The DNA damage spectrum produced by simulated sunlight. *J. Mol. Biol.* **299**, 681-693

29. Clingen, P. H., Arlett, C. F., Roza, L., Mori, T., Nikaido, O., and Green, M. H. (1995) Induction of cyclobutane pyrimidine dimers, pyrimidine(6-4)pyrimidone photoproducts, and Dewar valence isomers by natural sunlight in normal human mononuclear cells. *Cancer research* **55**, 2245-2248

30. Close, D. M., Nelson, W. H., and Bernhard, W. A. (2013) DNA damage by the direct effect of ionizing radiation: products produced by two sequential one-electron oxidations. *J. Phys. Chem. A* **117**, 12608-12615

31. Hutchinson, F. (1985) Chemical changes induced in DNA by ionizing radiation. *Prog. Nucleic Acid Res. Mol. Biol.* **32**, 115-154

32. Ward, J. F. (1988) DNA damage produced by ionizing radiation in mammalian cells: identities, mechanisms of formation, and reparability. *Prog. Nucleic Acid Res. Mol. Biol.* **35**, 95-125

33. Box, H. C., Budzinski, E. E., Dawidzik, J. B., Gobey, J. S., and Freund, H. G. (1997) Free radical-induced tandem base damage in DNA oligomers. *Free Radic. Biol. Med.* **23**, 1021-1030

34. Box, H. C., Budzinski, E. E., Dawidzik, J. B., Wallace, J. C., and Iijima, H. (1998) Tandem lesions and other products in X-irradiated DNA oligomers. *Radiat. Res.* **149**, 433-439

35. Box, H. C., Budzinski, E. E., Dawidzik, J. D., Wallace, J. C., Evans, M. S., and Gobey, J. S. (1996) Radiation-induced formation of a crosslink between base moieties of deoxyguanosine and thymidine in deoxygenated solutions of d(CpGpTpA). *Radiat. Res.* **145**, 641-643

36. Bostrom, C. E., Gerde, P., Hanberg, A., Jernstrom, B., Johansson, C., Kyrklund, T., Rannug, A., Tornqvist, M., Victorin, K., and Westerholm, R. (2002) Cancer risk assessment, indicators, and guidelines for polycyclic aromatic hydrocarbons in the ambient air. *Environ. Health Perspect.* **110 Suppl 3**, 451-488

37. Poirier, M. C., and Beland, F. A. (1992) DNA adduct measurements and tumor incidence during chronic carcinogen exposure in animal models: implications for DNA adduct-based human cancer risk assessment. *Chem. Res. Toxicol.* **5**, 749-755

38. Stowers, S. J., and Anderson, M. W. (1985) Formation and persistence of benzo[*a*]pyrene metabolite-DNA adducts. *Environ. Health Perspect.* **62**, 31-39

39. Veglia, F., Matullo, G., and Vineis, P. (2003) Bulky DNA adducts and risk of cancer: a meta-analysis. *Cancer Epidemiol. Biomarkers Prev.* **12**, 157-160

40. Barbin, A. (1998) Formation of DNA etheno adducts in rodents and humans and their role in carcinogenesis. *Acta Biochim. Pol.* **45**, 145-161

41. Tricker, A. R. (1997) *N*-nitroso compounds and man: sources of exposure, endogenous formation and occurrence in body fluids. *Eur. J. Cancer Prev.* **6**, 226-268

42. Lijinsky, W. (1999) *N*-Nitroso compounds in the diet. *Mutat. Res.* **443**, 129-138

43. Dietrich, M., Block, G., Pogoda, J. M., Buffler, P., Hecht, S., and Preston-Martin, S. (2005) A review: dietary and endogenously formed *N*-nitroso compounds and risk of childhood brain tumors. *Cancer causes & control : CCC* **16**, 619-635

44. Jakszyn, P., Bingham, S., Pera, G., Agudo, A., Luben, R., Welch, A., Boeing, H., Del Giudice, G., Palli, D., Saieva, C., Krogh, V., Sacerdote, C., Tumino, R., Panico, S., Berglund, G., Siman, H., Hallmans, G., Sanchez, M. J., Larranaga, N., Barricarte, A., Chirlaque, M. D., Quiros, J. R., Key, T. J., Allen, N., Lund, E., Carneiro, F., Linseisen, J., Nagel, G., Overvad, K., Tjonneland, A., Olsen, A., Bueno-de-Mesquita, H. B., Ocke, M. O., Peeters, P. H., Numans, M. E., Clavel-Chapelon, F., Trichopoulou, A., Fenger, C., Stenling, R., Ferrari, P., Jenab, M., Norat, T., Riboli, E., and Gonzalez, C. A. (2006) Endogenous versus exogenous exposure to *N*-nitroso compounds and gastric cancer risk in the European Prospective Investigation into Cancer and Nutrition (EPIC-EURGAST) study. *Carcinogenesis* **27**, 1497-1501

45. Busby, W. F., Jr., Shuker, D. E., Charnley, G., Newberne, P. M., Tannenbaum, S. R., and Wogan, G. N. (1985) Carcinogenicity in rats of the nitrosated bile acid conjugates *N*-nitrosoglycocholic acid and *N*-nitrosotaurocholic acid. *Cancer Res.* **45**, 1367-1371

46. Shuker, D. E., and Margison, G. P. (1997) Nitrosated glycine derivatives as a potential source of O^6-methylguanine in DNA. *Cancer Res.* **57**, 366-369

47. Zurlo, J., Curphey, T. J., Hiley, R., and Longnecker, D. S. (1982) Identification of 7-carboxymethylguanine in DNA from pancreatic acinar cells exposed to azaserine. *Cancer Res.* **42**, 1286-1288

48. Harrison, K. L., Jukes, R., Cooper, D. P., and Shuker, D. E. (1999) Detection of concomitant formation of O^6-carboxymethyl- and O^6-methyl-2'-deoxyguanosine in DNA exposed to nitrosated glycine derivatives using a combined immunoaffinity/HPLC method. *Chem. Res. Toxicol.* **12**, 106-111

49. Cupid, B. C., Zeng, Z., Singh, R., and Shuker, D. E. (2004) Detection of O6-carboxymethyl-2'-deoxyguanosine in DNA following reaction of nitric oxide with glycine and in human blood DNA using a quantitative immunoslot blot assay. *Chemical research in toxicology* **17**, 294-300

50. Wang, J., and Wang, Y. (2010) Synthesis and characterization of oligodeoxyribonucleotides containing a site-specifically incorporated N^6-carboxymethyl-2'-deoxyadenosine or N^4-carboxymethyl-2'-deoxycytidine. *Nucleic Acids Res.* **38**, 6774-6784

51. Wang, J., and Wang, Y. (2009) Chemical synthesis of oligodeoxyribonucleotides containing *N*3- and O^4-carboxymethylthymidine and their formation in DNA. *Nucleic Acids Res.* **37**, 336-345

52. Gottschalg, E., Scott, G. B., Burns, P. A., and Shuker, D. E. (2007) Potassium diazoacetate-induced *p53* mutations *in vitro* in relation to formation of O^6-carboxymethyl- and O^6-methyl-2'-deoxyguanosine DNA adducts: relevance for gastrointestinal cancer. *Carcinogenesis* **28**, 356-362

53. Brooks, P. J. (2008) The 8,5'-cyclopurine-2'-deoxynucleosides: candidate neurodegenerative DNA lesions in xeroderma pigmentosum, and unique probes of transcription and nucleotide excision repair. *DNA repair* **7**, 1168-1179

54. Kuraoka, I., Robins, P., Masutani, C., Hanaoka, F., Gasparutto, D., Cadet, J., Wood, R. D., and Lindahl, T. (2001) Oxygen free radical damage to DNA. Translesion synthesis by human DNA polymerase η and resistance to exonuclease action at cyclopurine deoxynucleoside residues. *J. Biol. Chem.* **276**, 49283-49288

55. Kuraoka, I., Bender, C., Romieu, A., Cadet, J., Wood, R. D., and Lindahl, T. (2000) Removal of oxygen free-radical-induced 5',8-purine cyclodeoxynucleosides from DNA by the nucleotide excision-repair pathway in human cells. *Proc. Natl. Acad. Sci. U.S.A.* **97**, 3832-3837

56. Wang, J., Clauson, C. L., Robbins, P. D., Niedernhofer, L. J., and Wang, Y. (2012) The oxidative DNA lesions 8,5'-cyclopurines accumulate with aging in a tissue-specific manner. *Aging cell* **11**, 714-716

57. D'Errico, M., Parlanti, E., Teson, M., Degan, P., Lemma, T., Calcagnile, A., Iavarone, I., Jaruga, P., Ropolo, M., Pedrini, A. M., Orioli, D., Frosina, G., Zambruno, G., Dizdaroglu, M., Stefanini, M., and Dogliotti, E. (2007) The role of CSA in the response to oxidative DNA damage in human cells. *Oncogene* **26**, 4336-4343

58. Jaruga, P., and Dizdaroglu, M. (2008) 8,5'-Cyclopurine-2'-deoxynucleosides in DNA: mechanisms of formation, measurement, repair and biological effects. *DNA repair* **7**, 1413-1425

59. You, C., Dai, X., Yuan, B., Wang, J., Wang, J., Brooks, P. J., Niedernhofer, L. J., and Wang, Y. (2012) A quantitative assay for assessing the effects of DNA lesions on transcription. *Nat. Chem. Biol.* **8**, 817-822

60. Brooks, P. J. (2007) The case for 8,5'-cyclopurine-2'-deoxynucleosides as endogenous DNA lesions that cause neurodegeneration in xeroderma pigmentosum. *Neuroscience* **145**, 1407-1417

61. Nick McElhinny, S. A., Watts, B. E., Kumar, D., Watt, D. L., Lundstrom, E. B., Burgers, P. M., Johansson, E., Chabes, A., and Kunkel, T. A. (2010) Abundant ribonucleotide incorporation into DNA by yeast replicative polymerases. *Proc. Natl. Acad. Sci. U.S.A.* **107**, 4949-4954

62. Nick McElhinny, S. A., Kumar, D., Clark, A. B., Watt, D. L., Watts, B. E., Lundstrom, E. B., Johansson, E., Chabes, A., and Kunkel, T. A. (2010) Genome instability due to ribonucleotide incorporation into DNA. *Nat. Chem. Biol.* **6**, 774-781

63. Traut, T. W. (1994) Physiological concentrations of purines and pyrimidines. *Mol. Cell. Biochem.* **140**, 1-22

64. Reijns, M. A., Rabe, B., Rigby, R. E., Mill, P., Astell, K. R., Lettice, L. A., Boyle, S., Leitch, A., Keighren, M., Kilanowski, F., Devenney, P. S., Sexton, D., Grimes, G., Holt, I. J., Hill, R. E., Taylor, M. S., Lawson, K. A., Dorin, J. R., and Jackson, A. P. (2012) Enzymatic removal of ribonucleotides from DNA is essential for mammalian genome integrity and development. *Cell* **149**, 1008-1022

65. Clausen, A. R., Zhang, S., Burgers, P. M., Lee, M. Y., and Kunkel, T. A. (2013) Ribonucleotide incorporation, proofreading and bypass by human DNA polymerase delta. *DNA repair* **12**, 121-127

66. Williams, J. S., Clausen, A. R., Nick McElhinny, S. A., Watts, B. E., Johansson, E., and Kunkel, T. A. (2012) Proofreading of ribonucleotides inserted into DNA by yeast DNA polymerase ε. *DNA repair* **11**, 649-656

67. Lujan, S. A., Williams, J. S., Clausen, A. R., Clark, A. B., and Kunkel, T. A. (2013) Ribonucleotides are signals for mismatch repair of leading-strand replication errors. *Mol. Cell* **50**, 437-443

68. Ghodgaonkar, M. M., Lazzaro, F., Olivera-Pimentel, M., Artola-Boran, M., Cejka, P., Reijns, M. A., Jackson, A. P., Plevani, P., Muzi-Falconi, M., and Jiricny, J. (2013) Ribonucleotides misincorporated into DNA act as strand-discrimination signals in eukaryotic mismatch repair. *Mol. Cell* **50**, 323-332

69. Hecht, S. S., and Hoffmann, D. (1988) Tobacco-specific nitrosamines, an important group of carcinogens in tobacco and tobacco smoke. *Carcinogenesis* **9**, 875-884

70. Brooks, P. J., and Theruvathu, J. A. (2005) DNA adducts from acetaldehyde: implications for alcohol-related carcinogenesis. *Alcohol* **35**, 187-193

71. Cloutier, J. F., Drouin, R., Weinfeld, M., O'Connor, T. R., and Castonguay, A. (2001) Characterization and mapping of DNA damage induced by reactive metabolites of 4-(methylnitrosamino)-1-(3-pyridyl)-1-butanone (NNK) at nucleotide resolution in human genomic DNA. *J. Mol. Biol.* **313**, 539-557

72. Peterson, L. A. (2010) Formation, repair, and genotoxic properties of bulky DNA adducts formed from tobacco-specific nitrosamines. *J. Nucleic Acids* **2010**, 1-11

73. Lao, Y., Yu, N., Kassie, F., Villalta, P. W., and Hecht, S. S. (2007) Analysis of pyridyloxobutyl DNA adducts in F344 rats chronically treated with (*R*)- and (*S*)-*N*'-nitrosonornicotine. *Chem. Res. Toxicol.* **20**, 246-256

74. Singh, R., Kaur, B., and Farmer, P. B. (2005) Detection of DNA damage derived from a direct acting ethylating agent present in cigarette smoke by use of liquid chromatography-tandem mass spectrometry. *Chem. Res. Toxicol.* **18**, 249-256

75. Chen, H. J., Wang, Y. C., and Lin, W. P. (2012) Analysis of ethylated thymidine adducts in human leukocyte DNA by stable isotope dilution nanoflow liquid chromatography-nanospray ionization tandem mass spectrometry. *Anal. Chem.* **84**, 2521-2527

76. Preston, B. D., Singer, B., and Loeb, L. A. (1986) Mutagenic potential of O^4-methylthymine *in vivo* determined by an enzymatic approach to site-specific mutagenesis. *Proc. Natl. Acad. Sci. U.S.A.* **83**, 8501-8505

77. Singer, B., Spengler, S. J., Fraenkel-Conrat, H., and Kusmierek, J. T. (1986) O^4-Methyl, -ethyl, or -isopropyl substituents on thymidine in poly(dA-dT) all lead to transitions upon replication. *Proc. Natl. Acad. Sci. U.S.A.* **83**, 28-32

78. Op het Veld, C. W., van Hees-Stuivenberg, S., van Zeeland, A. A., and Jansen, J. G. (1997) Effect of nucleotide excision repair on *hprt* gene mutations in rodent cells exposed to DNA ethylating agents. *Mutagenesis* **12**, 417-424

79. Kastan, M. B. (2008) DNA damage responses: mechanisms and roles in human disease: 2007 G.H.A. Clowes Memorial Award Lecture. *Mol. Cancer Res.* **6**, 517-524

80. Ward, I., and Chen, J. (2004) Early events in the DNA damage response. *Curr. Top. Dev. Biol.* **63**, 1-35

81. Huen, M. S., and Chen, J. (2008) The DNA damage response pathways: at the crossroad of protein modifications. *Cell Res.* **18**, 8-16

82. Liu, S., Opiyo, S. O., Manthey, K., Glanzer, J. G., Ashley, A. K., Amerin, C., Troksa, K., Shrivastav, M., Nickoloff, J. A., and Oakley, G. G. (2012) Distinct roles for DNA-PK, ATM and ATR in RPA phosphorylation and checkpoint activation in response to replication stress. *Nucleic Acids Res.* **40**, 10780-10794

83. Matsuoka, S., Ballif, B. A., Smogorzewska, A., McDonald, E. R., 3rd, Hurov, K. E., Luo, J., Bakalarski, C. E., Zhao, Z., Solimini, N., Lerenthal, Y., Shiloh, Y., Gygi, S. P., and Elledge, S. J. (2007) ATM and ATR substrate analysis reveals extensive protein networks responsive to DNA damage. *Science* **316**, 1160-1166

84. Falck, J., Coates, J., and Jackson, S. P. (2005) Conserved modes of recruitment of ATM, ATR and DNA-PKcs to sites of DNA damage. *Nature* **434**, 605-611

85. Zhao, H., and Piwnica-Worms, H. (2001) ATR-mediated checkpoint pathways regulate phosphorylation and activation of human Chk1. *Molecular and cellular biology* **21**, 4129-4139

86. Lavin, M. F., and Kozlov, S. (2007) ATM activation and DNA damage response. *Cell cycle* **6**, 931-942

87. Lindahl, T., Karran, P., and Wood, R. D. (1997) DNA excision repair pathways. *Curr. Opin. Genet. Dev.* **7**, 158-169

88. Seeberg, E., Eide, L., and Bjoras, M. (1995) The base excision repair pathway. *Trends Biochem. Sci.* **20**, 391-397

89. Dianov, G. L., Souza-Pinto, N., Nyaga, S. G., Thybo, T., Stevnsner, T., and Bohr, V. A. (2001) Base excision repair in nuclear and mitochondrial DNA. *Prog. Nucleic Acid Res. Mol. Biol.* **68**, 285-297

90. Fortini, P., Parlanti, E., Sidorkina, O. M., Laval, J., and Dogliotti, E. (1999) The type of DNA glycosylase determines the base excision repair pathway in mammalian cells. *J. Biol. Chem.* **274**, 15230-15236

91. Kim, Y. J., and Wilson, D. M., 3rd. (2012) Overview of base excision repair biochemistry. *Curr. Mol. Pharmacol.* **5**, 3-13

92. Rosenquist, T. A., Zharkov, D. O., and Grollman, A. P. (1997) Cloning and characterization of a mammalian 8-oxoguanine DNA glycosylase. *Proc. Natl. Acad. Sci. U.S.A.* **94**, 7429-7434

93. Lindahl, T., and Wood, R. D. (1999) Quality control by DNA repair. *Science* **286**, 1897-1905

94. Kamileri, I., Karakasilioti, I., and Garinis, G. A. (2012) Nucleotide excision repair: new tricks with old bricks. *Trends Genet.* **28**, 566-573

95. Kuper, J., and Kisker, C. (2012) Damage recognition in nucleotide excision DNA repair. *Curr. Opin. Struct. Biol.* **22**, 88-93

96. de Laat, W. L., Jaspers, N. G., and Hoeijmakers, J. H. (1999) Molecular mechanism of nucleotide excision repair. *Genes Dev.* **13**, 768-785

97. Wood, R. D. (1997) Nucleotide excision repair in mammalian cells. *J. Biol. Chem.* **272**, 23465-23468

98. Hanawalt, P. C., and Spivak, G. (2008) Transcription-coupled DNA repair: two decades of progress and surprises. *Nat. Rev. Mol. Cell Biol.* **9**, 958-970

99. LeDoux, S. P., Wilson, G. L., Beecham, E. J., Stevnsner, T., Wassermann, K., and Bohr, V. A. (1992) Repair of mitochondrial DNA after various types of DNA damage in Chinese hamster ovary cells. *Carcinogenesis* **13**, 1967-1973

100. Kunkel, T. A., and Erie, D. A. (2005) DNA mismatch repair. *Annu. Rev. Biochem.* **74**, 681-710

101. Hwang, B. J., Shi, G., and Lu, A. L. (2014) Mammalian MutY homolog (MYH or MUTYH) protects cells from oxidative DNA damage. *DNA repair* **13**, 10-21

102. Brierley, D. J., and Martin, S. A. (2013) Oxidative stress and the DNA mismatch repair pathway. *Antioxid. Redox Signal.* **18**, 2420-2428

103. Marti, T. M., Kunz, C., and Fleck, O. (2002) DNA mismatch repair and mutation avoidance pathways. *J. Cell. Physiol.* **191**, 28-41

104. Wyrzykowski, J., and Volkert, M. R. (2003) The *Escherichia coli* methyl-directed mismatch repair system repairs base pairs containing oxidative lesions. *J. Bacteriol.* **185**, 1701-1704

105. Mason, P. A., Matheson, E. C., Hall, A. G., and Lightowlers, R. N. (2003) Mismatch repair activity in mammalian mitochondria. *Nucleic Acids Res.* **31**, 1052-1058

106. Ghosal, G., and Chen, J. (2013) DNA damage tolerance: a double-edged sword guarding the genome. *Transl. Cancer Res.* **2**, 107-129

107. Kunkel, T. A. (2004) DNA replication fidelity. *J. Biol. Chem.* **279**, 16895-16898

108. Rajagopalan, M., Lu, C., Woodgate, R., O'Donnell, M., Goodman, M. F., and Echols, H. (1992) Activity of the purified mutagenesis proteins UmuC, UmuD', and RecA in replicative bypass of an abasic DNA lesion by DNA polymerase III. *Proc. Natl. Acad. Sci. U.S.A.* **89**, 10777-10781

109. Lehmann, A. R., Niimi, A., Ogi, T., Brown, S., Sabbioneda, S., Wing, J. F., Kannouche, P. L., and Green, C. M. (2007) Translesion synthesis: Y-family polymerases and the polymerase switch. *DNA repair* **6**, 891-899

110. Walker, G. C. (1995) SOS-regulated proteins in translesion DNA synthesis and mutagenesis. *Trends Biochem. Sci.* **20**, 416-420

111. Sale, J. E., Lehmann, A. R., and Woodgate, R. (2012) Y-family DNA polymerases and their role in tolerance of cellular DNA damage. *Nat. Rev. Mol. Cell Biol.* **13**, 141-152

112. Friedberg, E. C. (2005) Suffering in silence: the tolerance of DNA damage. *Nat. Rev. Mol. Cell Biol.* **6**, 943-953

113. Vandewiele, D., Borden, A., O'Grady, P. I., Woodgate, R., and Lawrence, C. W. (1998) Efficient translesion replication in the absence of *Escherichia coli* Umu proteins and 3'-5' exonuclease proofreading function. *Proc. Natl. Acad. Sci. U.S.A.* **95**, 15519-15524

114. Prakash, S., and Prakash, L. (2002) Translesion DNA synthesis in eukaryotes: a one- or two-polymerase affair. *Genes Dev.* **16**, 1872-1883

115. Bridges, B. A., and Woodgate, R. (1985) The two-step model of bacterial UV mutagenesis. *Mutat. Res.* **150**, 133-139

116. Tang, M., Bruck, I., Eritja, R., Turner, J., Frank, E. G., Woodgate, R., O'Donnell, M., and Goodman, M. F. (1998) Biochemical basis of SOS-induced mutagenesis

in *Escherichia coli*: reconstitution of *in vitro* lesion bypass dependent on the UmuD'$_2$C mutagenic complex and RecA protein. *Proc. Natl. Acad. Sci. U.S.A.* **95**, 9755-9760

117. Schwartz, D. C., and Hochstrasser, M. (2003) A superfamily of protein tags: ubiquitin, SUMO and related modifiers. *Trends Biochem. Sci.* **28**, 321-328

118. Diamant, N., Hendel, A., Vered, I., Carell, T., Reissner, T., de Wind, N., Geacinov, N., and Livneh, Z. (2012) DNA damage bypass operates in the S and G_2 phases of the cell cycle and exhibits differential mutagenicity. *Nucleic Acids Res.* **40**, 170-180

119. Waters, L. S., and Walker, G. C. (2006) The critical mutagenic translesion DNA polymerase Rev1 is highly expressed during G_2/M phase rather than S phase. *Proc. Natl. Acad. Sci. U.S.A.* **103**, 8971-8976

120. Bailly, V., Lamb, J., Sung, P., Prakash, S., and Prakash, L. (1994) Specific complex formation between yeast RAD6 and RAD18 proteins: a potential mechanism for targeting RAD6 ubiquitin-conjugating activity to DNA damage sites. *Genes Dev.* **8**, 811-820

121. Bailly, V., Lauder, S., Prakash, S., and Prakash, L. (1997) Yeast DNA repair proteins Rad6 and Rad18 form a heterodimer that has ubiquitin conjugating, DNA binding, and ATP hydrolytic activities. *J. Biol. Chem.* **272**, 23360-23365

122. Bailly, V., Prakash, S., and Prakash, L. (1997) Domains required for dimerization of yeast Rad6 ubiquitin-conjugating enzyme and Rad18 DNA binding protein. *Mol. Cell. Biol.* **17**, 4536-4543

123. Notenboom, V., Hibbert, R. G., van Rossum-Fikkert, S. E., Olsen, J. V., Mann, M., and Sixma, T. K. (2007) Functional characterization of Rad18 domains for Rad6, ubiquitin, DNA binding and PCNA modification. *Nucleic Acids Res.* **35**, 5819-5830

124. Zheng, N., Wang, P., Jeffrey, P. D., and Pavletich, N. P. (2000) Structure of a c-Cbl-UbcH7 complex: RING domain function in ubiquitin-protein ligases. *Cell* **102**, 533-539

125. Niimi, A., Brown, S., Sabbioneda, S., Kannouche, P. L., Scott, A., Yasui, A., Green, C. M., and Lehmann, A. R. (2008) Regulation of proliferating cell nuclear antigen ubiquitination in mammalian cells. *Proc. Natl. Acad. Sci. U.S.A.* **105**, 16125-16130

126. Kannouche, P. L., and Lehmann, A. R. (2004) Ubiquitination of PCNA and the polymerase switch in human cells. *Cell cycle* **3**, 1011-1013

127. Varga, A., Marcus, A. P., Himoto, M., Iwai, S., and Szuts, D. (2012) Analysis of CPD ultraviolet lesion bypass in chicken DT40 cells: polymerase η and PCNA ubiquitylation play identical roles. *PloS one* **7**, e52472

128. Arakawa, H., Moldovan, G. L., Saribasak, H., Saribasak, N. N., Jentsch, S., and Buerstedde, J. M. (2006) A role for PCNA ubiquitination in immunoglobulin hypermutation. *PLoS Biol.* **4**, e366

129. Hoege, C., Pfander, B., Moldovan, G. L., Pyrowolakis, G., and Jentsch, S. (2002) RAD6-dependent DNA repair is linked to modification of PCNA by ubiquitin and SUMO. *Nature* **419**, 135-141

130. Huang, T. T., Nijman, S. M., Mirchandani, K. D., Galardy, P. J., Cohn, M. A., Haas, W., Gygi, S. P., Ploegh, H. L., Bernards, R., and D'Andrea, A. D. (2006) Regulation of monoubiquitinated PCNA by DUB autocleavage. *Nat. Cell Biol.* **8**, 339-347

131. Kirisako, T., Kamei, K., Murata, S., Kato, M., Fukumoto, H., Kanie, M., Sano, S., Tokunaga, F., Tanaka, K., and Iwai, K. (2006) A ubiquitin ligase complex assembles linear polyubiquitin chains. *EMBO J.* **25**, 4877-4887

132. Komander, D., Reyes-Turcu, F., Licchesi, J. D., Odenwaelder, P., Wilkinson, K. D., and Barford, D. (2009) Molecular discrimination of structurally equivalent Lys 63-linked and linear polyubiquitin chains. *EMBO Rep.* **10**, 466-473

133. Haracska, L., Kondratick, C. M., Unk, I., Prakash, S., and Prakash, L. (2001) Interaction with PCNA is essential for yeast DNA polymerase η function. *Mol. Cell* **8**, 407-415

134. Haracska, L., Acharya, N., Unk, I., Johnson, R. E., Hurwitz, J., Prakash, L., and Prakash, S. (2005) A single domain in human DNA polymerase ι mediates interaction with PCNA: implications for translesion DNA synthesis. *Mol. Cell. Biol.* **25**, 1183-1190

135. Haracska, L., Unk, I., Johnson, R. E., Phillips, B. B., Hurwitz, J., Prakash, L., and Prakash, S. (2002) Stimulation of DNA synthesis activity of human DNA polymerase κ by PCNA. *Mol. Cell. Biol.* **22**, 784-791

136. Makarova, A. V., Stodola, J. L., and Burgers, P. M. (2012) A four-subunit DNA polymerase ζ complex containing Pol δ accessory subunits is essential for PCNA-mediated mutagenesis. *Nucleic Acids Res.* **40**, 11618-11626

137. Vidal, A. E., Kannouche, P., Podust, V. N., Yang, W., Lehmann, A. R., and Woodgate, R. (2004) Proliferating cell nuclear antigen-dependent coordination of

the biological functions of human DNA polymerase ι. *J. Biol. Chem.* **279**, 48360-48368

138. Guo, C., Sonoda, E., Tang, T. S., Parker, J. L., Bielen, A. B., Takeda, S., Ulrich, H. D., and Friedberg, E. C. (2006) REV1 protein interacts with PCNA: significance of the REV1 BRCT domain in vitro and in vivo. *Mol. Cell* **23**, 265-271

139. Pustovalova, Y., Maciejewski, M. W., and Korzhnev, D. M. (2013) NMR mapping of PCNA interaction with translesion synthesis DNA polymerase Rev1 mediated by Rev1-BRCT domain. *J. Mol. Biol.* **425**, 3091-3105

140. Bienko, M., Green, C. M., Crosetto, N., Rudolf, F., Zapart, G., Coull, B., Kannouche, P., Wider, G., Peter, M., Lehmann, A. R., Hofmann, K., and Dikic, I. (2005) Ubiquitin-binding domains in Y-family polymerases regulate translesion synthesis. *Science* **310**, 1821-1824

141. Bienko, M., Green, C. M., Sabbioneda, S., Crosetto, N., Matic, I., Hibbert, R. G., Begovic, T., Niimi, A., Mann, M., Lehmann, A. R., and Dikic, I. (2010) Regulation of translesion synthesis DNA polymerase η by monoubiquitination. *Mol. Cell* **37**, 396-407

142. Pustovalova, Y., Bezsonova, I., and Korzhnev, D. M. (2012) The C-terminal domain of human Rev1 contains independent binding sites for DNA polymerase η and Rev7 subunit of polymerase ζ. *FEBS Lett.* **586**, 3051-3056

143. Guo, C., Fischhaber, P. L., Luk-Paszyc, M. J., Masuda, Y., Zhou, J., Kamiya, K., Kisker, C., and Friedberg, E. C. (2003) Mouse Rev1 protein interacts with multiple DNA polymerases involved in translesion DNA synthesis. *EMBO J.* **22**, 6621-6630

144. Pryor, J. M., and Washington, M. T. (2011) Pre-steady state kinetic studies show that an abasic site is a cognate lesion for the yeast Rev1 protein. *DNA repair* **10**, 1138-1144

145. Ohashi, E., Hanafusa, T., Kamei, K., Song, I., Tomida, J., Hashimoto, H., Vaziri, C., and Ohmori, H. (2009) Identification of a novel REV1-interacting motif necessary for DNA polymerase κ function. *Genes to cells : devoted to molecular & cellular mechanisms* **14**, 101-111

146. Ohashi, E., Murakumo, Y., Kanjo, N., Akagi, J., Masutani, C., Hanaoka, F., and Ohmori, H. (2004) Interaction of hREV1 with three human Y-family DNA polymerases. *Genes to cells : devoted to molecular & cellular mechanisms* **9**, 523-531

147. Centore, R. C., Yazinski, S. A., Tse, A., and Zou, L. (2012) Spartan/C1orf124, a reader of PCNA ubiquitylation and a regulator of UV-induced DNA damage response. *Mol. Cell* **46**, 625-635

148. Juhasz, S., Balogh, D., Hajdu, I., Burkovics, P., Villamil, M. A., Zhuang, Z., and Haracska, L. (2012) Characterization of human Spartan/C1orf124, an ubiquitin-PCNA interacting regulator of DNA damage tolerance. *Nucleic Acids Res.* **40**, 10795-10808

149. Kim, M. S., Machida, Y., Vashisht, A. A., Wohlschlegel, J. A., Pang, Y. P., and Machida, Y. J. (2013) Regulation of error-prone translesion synthesis by Spartan/C1orf124. *Nucleic Acids Res.* **41**, 1661-1668

150. Ghosal, G., Leung, J. W., Nair, B. C., Fong, K. W., and Chen, J. (2012) Proliferating cell nuclear antigen (PCNA)-binding protein C1orf124 is a regulator of translesion synthesis. *J. Biol. Chem.* **287**, 34225-34233

151. Waters, L. S., Minesinger, B. K., Wiltrout, M. E., D'Souza, S., Woodruff, R. V., and Walker, G. C. (2009) Eukaryotic translesion polymerases and their roles and regulation in DNA damage tolerance. *Microbiol. Mol. Biol. Rev.* **73**, 134-154

152. Lange, S. S., Takata, K., and Wood, R. D. (2011) DNA polymerases and cancer. *Nat. Rev. Cancer* **11**, 96-110

153. Tang, M., Shen, X., Frank, E. G., O'Donnell, M., Woodgate, R., and Goodman, M. F. (1999) UmuD'$_2$C is an error-prone DNA polymerase, *Escherichia coli* pol V. *Proc. Natl. Acad. Sci. U.S.A.* **96**, 8919-8924

154. McDonald, J. P., Levine, A. S., and Woodgate, R. (1997) The *Saccharomyces cerevisiae* RAD30 gene, a homologue of *Escherichia coli* dinB and umuC, is DNA damage inducible and functions in a novel error-free postreplication repair mechanism. *Genetics* **147**, 1557-1568

155. Johnson, R. E., Prakash, S., and Prakash, L. (1999) Efficient bypass of a thymine-thymine dimer by yeast DNA polymerase, Pol η. *Science* **283**, 1001-1004

156. Masutani, C., Kusumoto, R., Yamada, A., Dohmae, N., Yokoi, M., Yuasa, M., Araki, M., Iwai, S., Takio, K., and Hanaoka, F. (1999) The *XPV* (xeroderma pigmentosum variant) gene encodes human DNA polymerase η. *Nature* **399**, 700-704

157. Washington, M. T., Johnson, R. E., Prakash, S., and Prakash, L. (2000) Accuracy of thymine-thymine dimer bypass by *Saccharomyces cerevisiae* DNA polymerase η. *Proc. Natl. Acad. Sci. U.S.A.* **97**, 3094-3099

158. Ohkumo, T., Kondo, Y., Yokoi, M., Tsukamoto, T., Yamada, A., Sugimoto, T., Kanao, R., Higashi, Y., Kondoh, H., Tatematsu, M., Masutani, C., and Hanaoka, F. (2006) UV-B radiation induces epithelial tumors in mice lacking DNA polymerase η and mesenchymal tumors in mice deficient for DNA polymerase ι. *Mol. Cell. Biol.* **26**, 7696-7706

159. Biertumpfel, C., Zhao, Y., Kondo, Y., Ramon-Maiques, S., Gregory, M., Lee, J. Y., Masutani, C., Lehmann, A. R., Hanaoka, F., and Yang, W. (2010) Structure and mechanism of human DNA polymerase η. *Nature* **465**, 1044-1048

160. Zhang, Y., Yuan, F., Wu, X., Rechkoblit, O., Taylor, J. S., Geacintov, N. E., and Wang, Z. (2000) Error-prone lesion bypass by human DNA polymerase η. *Nucleic Acids Res.* **28**, 4717-4724

161. Andersen, N., Wang, P., and Wang, Y. (2013) Replication across regioisomeric ethylated thymidine lesions by purified DNA polymerases. *Chem. Res. Toxicol.* **26**, 1730-1738

162. Chen, Y. W., Cleaver, J. E., Hatahet, Z., Honkanen, R. E., Chang, J. Y., Yen, Y., and Chou, K. M. (2008) Human DNA polymerase η activity and translocation is regulated by phosphorylation. *Proc. Natl. Acad. Sci. U.S.A.* **105**, 16578-16583

163. Zeng, X., Winter, D. B., Kasmer, C., Kraemer, K. H., Lehmann, A. R., and Gearhart, P. J. (2001) DNA polymerase η is an A-T mutator in somatic hypermutation of immunoglobulin variable genes. *Nat. Immunol.* **2**, 537-541

164. McDonald, J. P., Frank, E. G., Plosky, B. S., Rogozin, I. B., Masutani, C., Hanaoka, F., Woodgate, R., and Gearhart, P. J. (2003) 129-derived strains of mice are deficient in DNA polymerase ι and have normal immunoglobulin hypermutation. *J. Exp. Med.* **198**, 635-643

165. McDonald, J. P., Rapic-Otrin, V., Epstein, J. A., Broughton, B. C., Wang, X., Lehmann, A. R., Wolgemuth, D. J., and Woodgate, R. (1999) Novel human and mouse homologs of Saccharomyces cerevisiae DNA polymerase η. *Genomics* **60**, 20-30

166. Bebenek, K., Tissier, A., Frank, E. G., McDonald, J. P., Prasad, R., Wilson, S. H., Woodgate, R., and Kunkel, T. A. (2001) 5'-Deoxyribose phosphate lyase activity of human DNA polymerase ι in vitro. *Science* **291**, 2156-2159

167. Nair, D. T., Johnson, R. E., Prakash, S., Prakash, L., and Aggarwal, A. K. (2004) Replication by human DNA polymerase ι occurs by Hoogsteen base-pairing. *Nature* **430**, 377-380

168. Wolfle, W. T., Johnson, R. E., Minko, I. G., Lloyd, R. S., Prakash, S., and Prakash, L. (2005) Human DNA polymerase ι promotes replication through a ring-closed minor-groove adduct that adopts a *syn* conformation in DNA. *Mol. Cell. Biol.* **25**, 8748-8754

169. Zhang, Y., Yuan, F., Wu, X., Taylor, J. S., and Wang, Z. (2001) Response of human DNA polymerase ι to DNA lesions. *Nucleic Acids Res.* **29**, 928-935

170. Tissier, A., McDonald, J. P., Frank, E. G., and Woodgate, R. (2000) Pol ι, a remarkably error-prone human DNA polymerase. *Genes Dev.* **14**, 1642-1650

171. Iguchi, M., Osanai, M., Hayashi, Y., Koentgen, F., and Lee, G. H. (2013) The error-prone DNA polymerase ι provides quantitative resistance to lung tumorigenesis and mutagenesis in mice. *Oncogene*, 1-6

172. Obata, M., Nishimori, H., Ogawa, K., and Lee, G. H. (1996) Identification of the *Par2* (Pulmonary adenoma resistance) locus on mouse chromosome 18, a major genetic determinant for lung carcinogen resistance in BALB/cByJ mice. *Oncogene* **13**, 1599-1604

173. Lee, G. H., Matsushita, H., and Kitagawa, T. (2001) Fine chromosomal localization of the mouse *Par2* gene that confers resistance against urethane-induction of pulmonary adenomas. *Oncogene* **20**, 3979-3985

174. Nair, D. T., Johnson, R. E., Prakash, L., Prakash, S., and Aggarwal, A. K. (2006) Hoogsteen base pair formation promotes synthesis opposite the 1,N^6-ethenodeoxyadenosine lesion by human DNA polymerase ι. *Nat. Struct. Mol. Biol.* **13**, 619-625

175. Choi, J. Y., Zang, H., Angel, K. C., Kozekov, I. D., Goodenough, A. K., Rizzo, C. J., and Guengerich, F. P. (2006) Translesion synthesis across 1,N^2-ethenoguanine by human DNA polymerases. *Chem. Res. Toxicol.* **19**, 879-886

176. Kulaeva, O. I., Koonin, E. V., McDonald, J. P., Randall, S. K., Rabinovich, N., Connaughton, J. F., Levine, A. S., and Woodgate, R. (1996) Identification of a DinB/UmuC homolog in the archeon *Sulfolobus solfataricus*. *Mutat. Res.* **357**, 245-253

177. Ohmori, H., Friedberg, E. C., Fuchs, R. P., Goodman, M. F., Hanaoka, F., Hinkle, D., Kunkel, T. A., Lawrence, C. W., Livneh, Z., Nohmi, T., Prakash, L., Prakash, S., Todo, T., Walker, G. C., Wang, Z., and Woodgate, R. (2001) The Y-family of DNA polymerases. *Mol. Cell* **8**, 7-8

178. Gerlach, V. L., Aravind, L., Gotway, G., Schultz, R. A., Koonin, E. V., and Friedberg, E. C. (1999) Human and mouse homologs of *Escherichia coli* DinB

(DNA polymerase IV), members of the UmuC/DinB superfamily. *Proc. Natl. Acad. Sci. U.S.A.* **96**, 11922-11927

179. Yuan, B., Cao, H., Jiang, Y., Hong, H., and Wang, Y. (2008) Efficient and accurate bypass of N^2-(1-carboxyethyl)-2'-deoxyguanosine by DinB DNA polymerase *in vitro* and *in vivo*. *Proc. Natl. Acad. Sci. U.S.A.* **105**, 8679-8684

180. Jia, L., Geacintov, N. E., and Broyde, S. (2008) The N-clasp of human DNA polymerase κ promotes blockage or error-free bypass of adenine- or guanine-benzo[*a*]pyrenyl lesions. *Nucleic Acids Res.* **36**, 6571-6584

181. Liu, Y., Yang, Y., Tang, T. S., Zhang, H., Wang, Z., Friedberg, E., Yang, W., and Guo, C. (2014) Variants of mouse DNA polymerase κ reveal a mechanism of efficient and accurate translesion synthesis past a benzo[*a*]pyrene dG adduct. *Proc. Natl. Acad. Sci. U.S.A.* **111**, 1789-1794

182. Washington, M. T., Johnson, R. E., Prakash, L., and Prakash, S. (2002) Human *DINB1*-encoded DNA polymerase κ is a promiscuous extender of mispaired primer termini. *Proc. Natl. Acad. Sci. U.S.A.* **99**, 1910-1914

183. Minko, I. G., Harbut, M. B., Kozekov, I. D., Kozekova, A., Jakobs, P. M., Olson, S. B., Moses, R. E., Harris, T. M., Rizzo, C. J., and Lloyd, R. S. (2008) Role for DNA polymerase κ in the processing of N^2-N^2-guanine interstrand cross-links. *J. Biol. Chem.* **283**, 17075-17082

184. Ogi, T., and Lehmann, A. R. (2006) The Y-family DNA polymerase κ (pol κ) functions in mammalian nucleotide-excision repair. *Nat. Cell Biol.* **8**, 640-642

185. Zhang, X., Lv, L., Chen, Q., Yuan, F., Zhang, T., Yang, Y., Zhang, H., Wang, Y., Jia, Y., Qian, L., Chen, B., Zhang, Y., Friedberg, E. C., Tang, T. S., and Guo, C. (2013) Mouse DNA polymerase κ has a functional role in the repair of DNA strand breaks. *DNA repair* **12**, 377-388

186. Okada, T., Sonoda, E., Yamashita, Y. M., Koyoshi, S., Tateishi, S., Yamaizumi, M., Takata, M., Ogawa, O., and Takeda, S. (2002) Involvement of vertebrate pol κ in Rad18-independent postreplication repair of UV damage. *J. Biol. Chem.* **277**, 48690-48695

187. Gibbs, P. E., McGregor, W. G., Maher, V. M., Nisson, P., and Lawrence, C. W. (1998) A human homolog of the *Saccharomyces cerevisiae* REV3 gene, which encodes the catalytic subunit of DNA polymerase ζ. *Proc. Natl. Acad. Sci. U.S.A.* **95**, 6876-6880

188. Murakumo, Y., Roth, T., Ishii, H., Rasio, D., Numata, S., Croce, C. M., and Fishel, R. (2000) A human REV7 homolog that interacts with the polymerase ζ

catalytic subunit hREV3 and the spindle assembly checkpoint protein hMAD2. *J. Biol. Chem.* **275**, 4391-4397

189. Lee, Y. S., Gregory, M. T., and Yang, W. (2014) Human Pol ζ purified with accessory subunits is active in translesion DNA synthesis and complements Pol η in cisplatin bypass. *Proc. Natl. Acad. Sci. U.S.A.* **111**, 2954-2959

190. Lange, S. S., Wittschieben, J. P., and Wood, R. D. (2012) DNA polymerase ζ is required for proliferation of normal mammalian cells. *Nucleic Acids Res.* **40**, 4473-4482

191. Bemark, M., Khamlichi, A. A., Davies, S. L., and Neuberger, M. S. (2000) Disruption of mouse polymerase ζ (Rev3) leads to embryonic lethality and impairs blastocyst development in vitro. *Curr. Biol.* **10**, 1213-1216

192. Esposito, G., Godindagger, I., Klein, U., Yaspo, M. L., Cumano, A., and Rajewsky, K. (2000) Disruption of the Rev3l-encoded catalytic subunit of polymerase ζ in mice results in early embryonic lethality. *Curr. Biol.* **10**, 1221-1224

193. Wittschieben, J., Shivji, M. K., Lalani, E., Jacobs, M. A., Marini, F., Gearhart, P. J., Rosewell, I., Stamp, G., and Wood, R. D. (2000) Disruption of the developmentally regulated Rev3l gene causes embryonic lethality. *Curr. Biol.* **10**, 1217-1220

194. Nelson, J. R., Lawrence, C. W., and Hinkle, D. C. (1996) Deoxycytidyl transferase activity of yeast REV1 protein. *Nature* **382**, 729-731

195. Haracska, L., Prakash, S., and Prakash, L. (2002) Yeast Rev1 protein is a G template-specific DNA polymerase. *J. Biol. Chem.* **277**, 15546-15551

196. Masuda, Y., Takahashi, M., Fukuda, S., Sumii, M., and Kamiya, K. (2002) Mechanisms of dCMP transferase reactions catalyzed by mouse Rev1 protein. *J. Biol. Chem.* **277**, 3040-3046

197. Zhang, Y., Wu, X., Rechkoblit, O., Geacintov, N. E., Taylor, J. S., and Wang, Z. (2002) Response of human REV1 to different DNA damage: preferential dCMP insertion opposite the lesion. *Nucleic Acids Res.* **30**, 1630-1638

198. Washington, M. T., Minko, I. G., Johnson, R. E., Haracska, L., Harris, T. M., Lloyd, R. S., Prakash, S., and Prakash, L. (2004) Efficient and error-free replication past a minor-groove N^2-guanine adduct by the sequential action of yeast Rev1 and DNA polymerase ζ. *Mol. Cell. Biol.* **24**, 6900-6906

199. Nair, D. T., Johnson, R. E., Prakash, L., Prakash, S., and Aggarwal, A. K. (2011) DNA synthesis across an abasic lesion by yeast REV1 DNA polymerase. *J. Mol. Biol.* **406**, 18-28

200. Nair, D. T., Johnson, R. E., Prakash, L., Prakash, S., and Aggarwal, A. K. (2005) Rev1 employs a novel mechanism of DNA synthesis using a protein template. *Science* **309**, 2219-2222

201. Kaguni, L. S. (2004) DNA polymerase γ, the mitochondrial replicase. *Annu. Rev. Biochem.* **73**, 293-320

202. Fridlender, B., Fry, M., Bolden, A., and Weissbach, A. (1972) A new synthetic RNA-dependent DNA polymerase from human tissue culture cells (HeLa-fibroblast-synthetic oligonucleotides-template-purified enzymes). *Proc. Natl. Acad. Sci. U.S.A.* **69**, 452-455

203. Bolden, A., Noy, G. P., and Weissbach, A. (1977) DNA polymerase of mitochondria is a γ-polymerase. *J. Biol. Chem.* **252**, 3351-3356

204. Copeland, W. C., and Longley, M. J. (2003) DNA polymerase γ in mitochondrial DNA replication and repair. *TheScientificWorldJournal* **3**, 34-44

205. Pinz, K. G., and Bogenhagen, D. F. (1998) Efficient repair of abasic sites in DNA by mitochondrial enzymes. *Mol. Cell. Biol.* **18**, 1257-1265

206. Pinz, K. G., and Bogenhagen, D. F. (2000) Characterization of a catalytically slow AP lyase activity in DNA polymerase γ and other family A DNA polymerases. *J. Biol. Chem.* **275**, 12509-12514

207. Lee, Y. S., Kennedy, W. D., and Yin, Y. W. (2009) Structural insight into processive human mitochondrial DNA synthesis and disease-related polymerase mutations. *Cell* **139**, 312-324

208. Hance, N., Ekstrand, M. I., and Trifunovic, A. (2005) Mitochondrial DNA polymerase γ is essential for mammalian embryogenesis. *Hum. Mol. Genet.* **14**, 1775-1783

209. Kasiviswanathan, R., Minko, I. G., Lloyd, R. S., and Copeland, W. C. (2013) Translesion synthesis past acrolein-derived DNA adducts by human mitochondrial DNA polymerase γ. *J. Biol. Chem.* **288**, 14247-14255

210. Kasiviswanathan, R., Gustafson, M. A., Copeland, W. C., and Meyer, J. N. (2012) Human mitochondrial DNA polymerase γ exhibits potential for bypass and mutagenesis at UV-induced cyclobutane thymine dimers. *J. Biol. Chem.* **287**, 9222-9229

211. Garcia-Gomez, S., Reyes, A., Martinez-Jimenez, M. I., Chocron, E. S., Mouron, S., Terrados, G., Powell, C., Salido, E., Mendez, J., Holt, I. J., and Blanco, L. (2013) PrimPol, an archaic primase/polymerase operating in human cells. *Mol. Cell* **52**, 541-553

212. Murakami, Y., Wobbe, C. R., Weissbach, L., Dean, F. B., and Hurwitz, J. (1986) Role of DNA polymerase α and DNA primase in simian virus 40 DNA replication in vitro. *Proc. Natl. Acad. Sci. U.S.A.* **83**, 2869-2873

213. Schneider, A., Smith, R. W., Kautz, A. R., Weisshart, K., Grosse, F., and Nasheuer, H. P. (1998) Primase activity of human DNA polymerase α-primase. Divalent cations stabilize the enzyme activity of the p48 subunit. *J. Biol. Chem.* **273**, 21608-21615

214. Bianchi, J., Rudd, S. G., Jozwiakowski, S. K., Bailey, L. J., Soura, V., Taylor, E., Stevanovic, I., Green, A. J., Stracker, T. H., Lindsay, H. D., and Doherty, A. J. (2013) PrimPol bypasses UV photoproducts during eukaryotic chromosomal DNA replication. *Mol. Cell* **52**, 566-573

215. Mouron, S., Rodriguez-Acebes, S., Martinez-Jimenez, M. I., Garcia-Gomez, S., Chocron, S., Blanco, L., and Mendez, J. (2013) Repriming of DNA synthesis at stalled replication forks by human PrimPol. *Nat. Struct. Mol. Biol.* **20**, 1383-1389

216. Sharma, S., Shah, N. A., Joiner, A. M., Roberts, K. H., and Canman, C. E. (2012) DNA polymerase ζ is a major determinant of resistance to platinum-based chemotherapeutic agents. *Mol. Pharmacol.* **81**, 778-787

217. Zhao, Y., Biertumpfel, C., Gregory, M. T., Hua, Y. J., Hanaoka, F., and Yang, W. (2012) Structural basis of human DNA polymerase η-mediated chemoresistance to cisplatin. *Proc. Natl. Acad. Sci. U.S.A.* **109**, 7269-7274

218. Siddik, Z. H. (2003) Cisplatin: mode of cytotoxic action and molecular basis of resistance. *Oncogene* **22**, 7265-7279

219. Albertella, M. R., Green, C. M., Lehmann, A. R., and O'Connor, M. J. (2005) A role for polymerase η in the cellular tolerance to cisplatin-induced damage. *Cancer Res.* **65**, 9799-9806

220. Alt, A., Lammens, K., Chiocchini, C., Lammens, A., Pieck, J. C., Kuch, D., Hopfner, K. P., and Carell, T. (2007) Bypass of DNA lesions generated during anticancer treatment with cisplatin by DNA polymerase η. *Science* **318**, 967-970

221. Chen, Y. W., Cleaver, J. E., Hanaoka, F., Chang, C. F., and Chou, K. M. (2006) A novel role of DNA polymerase η in modulating cellular sensitivity to chemotherapeutic agents. *Mol. Cancer Res.* **4**, 257-265

222. Doles, J., Oliver, T. G., Cameron, E. R., Hsu, G., Jacks, T., Walker, G. C., and Hemann, M. T. (2010) Suppression of Rev3, the catalytic subunit of Polζ, sensitizes drug-resistant lung tumors to chemotherapy. *Proc. Natl. Acad. Sci. U.S.A.* **107**, 20786-20791

223. Minko, I. G., Harbut, M. B., Kozekov, I. D., Kozekova, A., Jakobs, P. M., Olson, S. B., Moses, R. E., Harris, T. M., Rizzo, C. J., and Lloyd, R. S. (2008) Role for DNA polymerase κ in the processing of N^2-N^2-guanine interstrand cross-links. *J. Biol. Chem.* **283**, 17075-17082

224. Fan, C. H., Liu, W. L., Cao, H., Wen, C., Chen, L., and Jiang, G. (2013) O^6-methylguanine DNA methyltransferase as a promising target for the treatment of temozolomide-resistant gliomas. *Cell Death Dis.* **4**, e876

225. Wang, H., Wu, W., Wang, H. W., Wang, S., Chen, Y., Zhang, X., Yang, J., Zhao, S., Ding, H. F., and Lu, D. (2010) Analysis of specialized DNA polymerases expression in human gliomas: association with prognostic significance. *Neuro. Oncol.* **12**, 679-686

226. Yamanaka, K., Dorjsuren, D., Eoff, R. L., Egli, M., Maloney, D. J., Jadhav, A., Simeonov, A., and Lloyd, R. S. (2012) A comprehensive strategy to discover inhibitors of the translesion synthesis DNA polymerase κ. *PloS one* **7**, e45032

227. O'Driscoll, M., Macpherson, P., Xu, Y. Z., and Karran, P. (1999) The cytotoxicity of DNA carboxymethylation and methylation by the model carboxymethylating agent azaserine in human cells. *Carcinogenesis* **20**, 1855-1862

228. Swanson, A. L., Wang, J., and Wang, Y. (2011) *In vitro* replication studies of carboxymethylated DNA lesions with *Saccharomyces cerevisiae* polymerase η. *Biochemistry* **50**, 7666-7673

229. Swanson, A. L., Wang, J., and Wang, Y. (2012) Accurate and efficient bypass of 8,5'-cyclopurine-2'-deoxynucleosides by human and yeast DNA polymerase η. *Chem. Res. Toxicol.* **25**, 1682-1691

230. You, C., Swanson, A. L., Dai, X., Yuan, B., Wang, J., and Wang, Y. (2013) Translesion synthesis of 8,5'-cyclopurine-2'-deoxynucleosides by DNA polymerases η, ι, and ζ. *J. Biol. Chem.* **288**, 28548-28556

231. Jasti, V. P., Spratt, T. E., and Basu, A. K. (2011) Tobacco-specific nitrosamine-derived O^2-alkylthymidines are potent mutagenic lesions in SOS-induced *Escherichia coli*. *Chem. Res. Toxicol.* **24**, 1833-1835

232. Swenberg, J. A., Dyroff, M. C., Bedell, M. A., Popp, J. A., Huh, N., Kirstein, U., and Rajewsky, M. F. (1984) O^4-ethyldeoxythymidine, but not O^6-

ethyldeoxyguanosine, accumulates in hepatocyte DNA of rats exposed continuously to diethylnitrosamine. *Proc. Natl. Acad. Sci. U.S.A.* **81**, 1692-1695

233. Satoh, M. S., Huh, N., Rajewsky, M. F., and Kuroki, T. (1988) Enzymatic removal of O^6-ethylguanine from mitochondrial DNA in rat tissues exposed to *N*-ethyl-*N*-nitrosourea *in vivo*. *J. Biol. Chem.* **263**, 6854-6856

234. Alexeyev, M., Shokolenko, I., Wilson, G., and LeDoux, S. (2013) The maintenance of mitochondrial DNA integrity- critical analysis and update. *Cold Spring Harb. Perspect. Biol.* **5**, a012641

235. Lindahl, T. (1993) Instability and decay of the primary structure of DNA. *Nature* **362**, 709-715

236. Friedberg, E. C., Walker, G. C., Siede, W., Wood, R. D., Schultz, R. A., and Ellenberger, T. (2006) *DNA Repair and Mutagenesis, 2nd Edition*, ASM Press, Washington, D.C.

237. Hoeijmakers, J. H. (2001) Genome maintenance mechanisms for preventing cancer. *Nature* **411**, 366-374

238. Sancar, A., Lindsey-Boltz, L. A., Unsal-Kacmaz, K., and Linn, S. (2004) Molecular mechanisms of mammalian DNA repair and the DNA damage checkpoints. *Annu. Rev. Biochem.* **73**, 39-85

239. Lehmann, A. R., Niimi, A., Brown, S., Sabbioneda, S., Wing, J. F., Kannouche, P. L., Green, C. M. (2007) Translesion synthesis: Y-family polymerases and the polymerase switch. *DNA Repair* **6**, 891-899

240. Friedberg, E. C. (2003) DNA damage and repair. *Nature* **421**, 436-440

241. Ling, H., Boudsocq, F., Plosky, B. S., Woodgate, R., and Yang, W. (2003) Replication of a cis-syn thymine dimer at atomic resolution. *Nature* **424**, 1083-1087

242. Prakash, S., and Prakash, L. (2002) Translesion DNA Synthesis in eukaryotes: A one- or two-polymerase affair. *Genes Dev.* **16**, 1872-1883

243. Yang, W. W., R. (2007) What a difference a decade makes: insights into translesion DNA synthesis. *Proc. Natl. Acad. Sci. USA* **104**, 15591-15598

244. Jarosz, D. F., Godoy, V. G., Delaney, J. C., Essigmann, J. M., and Walker, G. C. (2006) A single amino acid governs enhanced activity of DinB DNA polymerases on damaged templates. *Nature* **439**, 225-228

245. Yuan, B., Cao, H., Jiang, Y., Hong, H., and Wang, Y. (2008) Efficient and accurate bypass of N^2-(1-carboxyethyl)-2'-deoxyguanosine by DinB DNA polymerase *in vitro* and *in vivo*. *Proc. Natl. Acad. Sci. USA* **105**, 8679-8684

246. Johnson, R. E., Kondratick, C. M., Prakash, S., and Prakash, L. (1999) hRAD30 mutations in the variant form of xeroderma pigmentosum. *Science* **285**, 263-265

247. Cleaver, J. E. (2005) Cancer in xeroderma pigmentosum and related disorders of DNA repair. *Nat. Rev. Cancer* **5**, 564-573

248. Lijinsky, W. (1987) Carcinogenicity and mutagenicity of *N*-nitroso compounds. *Mol. Toxicol.* **1**, 107-119

249. Mirvish, S. S. (1995) Role of *N*-nitroso compounds (NOC) and *N*-nitrosation in etiology of gastric, esophageal, nasopharyngeal and bladder cancer and contribution to cancer of known exposures to NOC. *Cancer Lett.* **93**, 17-48

250. Tricker, A. R. (1997) *N*-nitroso compounds and man: sources of exposure, endogenous formation and occurrence in body fluids. *Eur. J. Cancer Prev.* **6**, 226-268

251. O'Driscoll, M., MacPherson, P., Xu, Y., and Karran, P. (1999) The cytotoxicity of DNA carboxymethylation and methylation by the model carboxymethylating agent azaserine in human cells. *Carcinogenesis* **20**, 1855-1862

252. Harrison, K. L., Fairhurst, N., Challis, B. C., and Shuker, D. E. (1997) Synthesis, characterization, and immunochemical detection of O^6-(carboxymethyl)-2'-deoxyguanosine: a DNA adduct formed by nitrosated glycine derivatives. *Chem. Res. Toxicol.* **10**, 652-659

253. Cannistraro, V. J., and Taylor, J. S. (2004) DNA-thumb interactions and processivity of T7 DNA polymerase in comparison to yeast polymerase η. *J. Biol. Chem.* **279**, 18288-18295

254. Jiang, Y., and Wang, Y. (2009) *In vitro* replication and repair studies of tandem lesions containing neighboring thymidine glycol and 8-oxo-7,8-dihydro-2'-deoxyguanosine. *Chem. Res. Toxicol.* **22**, 574-583

255. Gu, C., and Wang, Y. (2004) LC-MS/MS identification and yeast polymerase eta bypass of a novel gamma-irradiation-induced intrastrand cross-link lesion G[8-5]C. *Biochemistry* **43**, 6745-6750

256. Goodman, M. F., Creighton, S., Bloom, L. B., and Petruska, J. (1993) Biochemical basis of DNA replication fidelity. *Crit. Rev. Biochem. Mol. Biol.* **28**, 83-126

257. Yuan, B., Wang, J., Cao, H., Sun, R., and Wang, Y. (2011) High-throughput analysis of the mutagenic and cytotoxic properties of DNA lesions by next-generation sequencing. *Nucleic Acids Res.*, DOI: 10.1093/nar/gkr1159

258. Fuchs, R. P., Fujii, S., and Wagner, J. (2004) Properties and functions of *Escherichia coli*: Pol IV and Pol V. *Adv. Protein Chem.* **69**, 229-264

259. Lee, C. H., Chandani, S., and Loechler, E. L. (2006) Homology modeling of four Y-family, lesion-bypass DNA polymerases: the case that *E. coli* Pol IV and human Pol κ are orthologs, and *E. coli* Pol V and human Pol η are orthologs. *J. Mol. Graph. Model.* **25**, 87-102

260. Dosanjh, M. K., Essigmann, J. M., Goodman, M. F., and Singer, B. (1990) Comparative efficiency of forming m4T.G versus m^4T.A base pairs at a unique site by use of *Escherichia coli* DNA polymerase I (Klenow fragment) and *Drosophila melanogaster* polymerase α-primase complex. *Biochemistry* **29**, 4698-4703

261. Shrivastav, N., Li, D., and Essigmann, J. M. (2010) Chemical biology of mutagenesis and DNA repair: cellular responses to DNA alkylation. *Carcinogenesis* **31**, 59-70

262. Yuan, B., You, C., Andersen, N., Jiang, Y., Moriya, M., O'Connor, T. R., and Wang, Y. (2011) The roles of DNA polymerases κ and ι in the error-free bypass of N^2-carboxyalkyl-dG lesions in mammalian cells. *J. Biol. Chem.* **286**, 17503-17511

263. Wang, Y. (2008) Bulky DNA lesions induced by reactive oxygen species. *Chem. Res. Toxicol.* **21**, 276-281

264. Tilstra, J. S., Robinson, A. R., Wang, J., Gregg, S. Q., Clauson, C. L., Reay, D. P., Nasto, L. A., St Croix, C. M., Usas, A., Vo, N., Huard, J., Clemens, P. R., Stolz, D. B., Guttridge, D. C., Watkins, S. C., Garinis, G. A., Wang, Y., Niedernhofer, L. J., and Robbins, P. D. (2012) NF-κB inhibition delays DNA damage–induced senescence and aging in mice. *J. Clin. Invest.* **122**, doi:10.1172/JCI45785

265. Wang, J., Yuan, B., Guerrero, C., Bahde, R., Gupta, S., and Wang, Y. (2011) Quantification of oxidative DNA lesions in tissues of Long-Evans Cinnamon rats by capillary high-performance liquid chromatography-tandem mass spectrometry coupled with stable isotope-dilution method. *Anal. Chem.* **83**, 2201-2209

266. Wang, J., Clauson, C. L., Robbins, P. D., Niedernhofer, L. J., and Wang, Y. (2012) The oxidative DNA lesions 8,5'-cyclopurines accumulate with aging in a tissue-specific manner. *Aging Cell*, DOI: 10.1111/j.1474-9726.2012.00828.x

267. Dizdaroglu, M. (1986) Free-radical-induced formation of an 8,5'-cyclo-2'-deoxyguanosine moiety in deoxyribonucleic acid. *Biochem. J.* **238**, 247-254

268. Dizdaroglu, M., Dirksen, M. L., Jiang, H. X., and Robbins, J. H. (1987) Ionizing-radiation-induced damage in the DNA of cultured human cells. Identification of 8,5'-cyclo-2'-deoxyguanosine. *Biochem. J.* **241**, 929-932

269. Huang, H., Das, R. S., Basu, A. K., and Stone, M. P. (2011) Structure of (5'*S*)-8,5'-cyclo-2'-deoxyguanosine in DNA. *J. Am. Chem. Soc.* **133**, 20357-20368

270. Kuraoka, I., Bender, C., Romieu, A., Cadet, J., Wood, R. D., and Lindahl, T. (2000) Removal of oxygen free-radical-induced 5',8-purine cyclodeoxynucleosides from DNA by the nucleotide excision-repair pathway in human cells. *Proc. Natl. Acad. Sci. USA* **97**, 3832-3837

271. Jaruga, P., Xiao, Y., Vartanian, V., Lloyd, R. S., and Dizdaroglu, M. (2010) Evidence for the involvement of DNA repair enzyme NEIL1 in nucleotide excision repair of (5'*R*)- and (5'*S*)-8,5'-cyclo-2'-deoxyadenosines. *Biochemistry* **49**, 1053-1055

272. Kuraoka, I., Robins, P., Masutani, C., Hanaoka, F., Gasparutto, D., Cadet, J., Wood, R. D., and Lindahl, T. (2001) Oxygen free radical damage to DNA. Translesion synthesis by human DNA polymerase η and resistance to exonuclease action at cyclopurine deoxynucleoside residues. *J. Biol. Chem.* **276**, 49283-49288

273. Brooks, P. J., Wise, D. S., Berry, D. A., Kosmoski, J. V., Smerdon, M. J., Somers, R. L., Mackie, H., Spoonde, A. Y., Ackerman, E. J., Coleman, K., Tarone, R. E., and Robbins, J. H. (2000) The oxidative DNA lesion 8,5'-(*S*)-cyclo-2'-deoxyadenosine is repaired by the nucleotide excision repair pathway and blocks gene expression in mammalian cells. *J. Biol. Chem.* **275**, 22355-22362

274. Jaruga, P., and Dizdaroglu, M. (2010) Identification and quantification of (5'*R*)- and (5'*S*)-8,5'-cyclo-2'-deoxyadenosines in human urine as putative biomarkers of oxidatively induced damage to DNA. *Biochem. Biophys. Res. Commun.* **397**, 48-52

275. Lehmann, A. R. (2006) New functions for Y family polymerases. *Mol. Cell* **24**, 493-495

276. Yuan, B., Cao, H., Jiang, Y., Hong, H., and Wang, Y. (2008) Efficient and accurate bypass of N^2-(1-carboxyethyl)-2'-deoxyguanosine by DinB DNA polymerase *in vitro* and *in vivo*. *Proc. Natl. Acad. Sci. USA* **105**, 8679-8684

277. McCulloch, S. D., Kokoska, R. J., Masutani, C., Iwai, S., Hanaoka, F., and Kunkel, T. A. (2004) Preferential cis-syn thymine dimer bypass by DNA polymerase η occurs with biased fidelity. *Nature* **428**, 97-100

278. Washington, M. T., Prakash, L., and Prakash, S. (2003) Mechanism of nucleotide incorporation opposite a thymine-thymine dimer by yeast DNA polymerase eta. *Proc. Natl. Acad. Sci. USA* **100**, 12093-12098

279. Carlson, K. D., and Washington, M. T. (2005) Mechanism of efficient and accurate nucleotide incorporation opposite 7,8-dihydro-8-oxoguanine by *Saccharomyces cerevisiae* DNA polymerase η. *Mol. Cell. Biol.* **25**, 2169-2176

280. Broyde, S., and Patel, D. J. (2010) DNA repair: How to accurately bypass damage. *Nature* **465**, 1023-1024

281. Lee, C. H., Chandani, S., and Loechler, E. L. (2006) Homology modeling of four Y-family, lesion-bypass DNA polymerases: the case that *E. coli* Pol IV and human Pol κ are orthologs, and *E. coli* Pol V and human Pol η are orthologs. *J. Mol. Graph Model.* **25**, 87-102

282. Silverstein, T. D., Johnson, R. E., Jain, R., Prakash, L., Prakash, S., and Aggarwal, A. K. (2010) Structural basis for the suppression of skin cancers by DNA polymerase η. *Nature* **465**, 1039-1043

283. Biertumpfel, C., Zhao, Y., Kondo, Y., Ramon-Maiques, S., Gregory, M., Lee, J. Y., Masutani, C., Lehmann, A. R., Hanaoka, F., and Yang, W. (2010) Structure and mechanism of human DNA polymerase η. *Nature* **465**, 1044-1048

284. Gu, C., and Wang, Y. (2004) LC-MS/MS identification and yeast polymerase η bypass of a novel γ-irradiation-induced intrastrand cross-link lesion G[8-5]C. *Biochemistry* **43**, 6745-6750

285. Romieu, A., Gasparutto, D., and Cadet, J. (1999) Synthesis and characterization of oligonucleotides containing 5',8-cyclopurine 2'-deoxyribonucleosides: (5'*R*)-5',8-cyclo-2'-deoxyadenosine, (5'*S*)-5',8-cyclo-2'-deoxyguanosine, and (5'*R*)-5',8-cyclo-2'-deoxyguanosine. *Chem. Res. Toxicol.* **12**, 412-421

286. Washington, M. T., Johnson, R. E., Prakash, S., and Prakash, L. (1999) Fidelity and processivity of *Saccharomyces cerevisiae* DNA polymerase η. *J. Biol. Chem.* **274**, 36835-36838

287. von Hippel, P. H., Fairfield, F. R., and Dolejsi, M. K. (1994) On the processivity of polymerases. *Ann. N.Y. Acad. Sci.* **726**, 118-131

288. Washington, M. T., Johnson, R. E., Prakash, S., and Prakash, L. (2000) Accuracy of thymine-thymine dimer bypass by *Saccharomyces cerevisiae* DNA polymerase η. *Proc. Natl. Acad. Sci. USA* **97**, 3094-3099

289. Yuan, B., Wang, J., Cao, H., Sun, R., and Wang, Y. (2011) High-throughput analysis of the mutagenic and cytotoxic properties of DNA lesions by next-generation sequencing. *Nucleic Acids Res.* **39**, 5945-5954

290. Jasti, V. P., Das, R. S., Hilton, B. A., Weerasooriya, S., Zou, Y., and Basu, A. K. (2011) (5'S)-8,5'-cyclo-2'-deoxyguanosine is a strong block to replication, a potent pol V-dependent mutagenic lesion, and is inefficiently repaired in Escherichia coli. *Biochemistry* **50**, 3862-3865

291. Maslov, A. Y., and Vijg, J. (2009) Genome instability, cancer and aging. *Biochim Biophys Acta* **1790**, 963-969

292. Friedberg, E. C., Aguilera, A., Gellert, M., Hanawalt, P. C., Hays, J. B., Lehmann, A. R., Lindahl, T., Lowndes, N., Sarasin, A., and Wood, R. D. (2006) DNA repair: from molecular mechanism to human disease. *DNA Repair (Amst)* **5**, 986-996

293. Lange, S. S., Takata, K., and Wood, R. D. DNA polymerases and cancer. *Nat Rev Cancer* **11**, 96-110

294. Sale, J. E., Lehmann, A. R., and Woodgate, R. Y-family DNA polymerases and their role in tolerance of cellular DNA damage. *Nat Rev Mol Cell Biol* **13**, 141-152

295. Livneh, Z., Ziv, O., and Shachar, S. (2010) Multiple two-polymerase mechanisms in mammalian translesion DNA synthesis. *Cell Cycle* **9**, 729-735

296. Guo, C., Fischhaber, P. L., Luk-Paszyc, M. J., Masuda, Y., Zhou, J., Kamiya, K., Kisker, C., and Friedberg, E. C. (2003) Mouse Rev1 protein interacts with multiple DNA polymerases involved in translesion DNA synthesis. *EMBO J* **22**, 6621-6630

297. Murakumo, Y., Ogura, Y., Ishii, H., Numata, S., Ichihara, M., Croce, C. M., Fishel, R., and Takahashi, M. (2001) Interactions in the error-prone postreplication repair proteins hREV1, hREV3, and hREV7. *J Biol Chem* **276**, 35644-35651

298. Masuda, Y., Ohmae, M., Masuda, K., and Kamiya, K. (2003) Structure and enzymatic properties of a stable complex of the human REV1 and REV7 proteins. *J Biol Chem* **278**, 12356-12360

299. Makarova, A. V., Stodola, J. L., and Burgers, P. M. (2012) A four-subunit DNA polymerase zeta complex containing Pol delta accessory subunits is essential for PCNA-mediated mutagenesis. *Nucleic Acids Res* **40**, 11618-11626

300. Johnson, R. E., Prakash, L., and Prakash, S. (2012) Pol31 and Pol32 subunits of yeast DNA polymerase delta are also essential subunits of DNA polymerase zeta. *Proc Natl Acad Sci U S A* **109**, 12455-12460

301. Jaruga, P., and Dizdaroglu, M. (2008) 8,5'-Cyclopurine-2'-deoxynucleosides in DNA: mechanisms of formation, measurement, repair and biological effects. *DNA Repair (Amst)* **7**, 1413-1425

302. Wang, Y. (2008) Bulky DNA lesions induced by reactive oxygen species. *Chem Res Toxicol* **21**, 276-281

303. Shaked, H., Hofseth, L. J., Chumanevich, A., Chumanevich, A. A., Wang, J., Wang, Y., Taniguchi, K., Guma, M., Shenouda, S., Clevers, H., Harris, C. C., and Karin, M. (2012) Chronic epithelial NF-kappaB activation accelerates APC loss and intestinal tumor initiation through iNOS up-regulation. *Proc Natl Acad Sci U S A* **109**, 14007-14012

304. Mitra, D., Luo, X., Morgan, A., Wang, J., Hoang, M. P., Lo, J., Guerrero, C. R., Lennerz, J. K., Mihm, M. C., Wargo, J. A., Robinson, K. C., Devi, S. P., Vanover, J. C., D'Orazio, J. A., McMahon, M., Bosenberg, M. W., Haigis, K. M., Haber, D. A., Wang, Y., and Fisher, D. E. (2012) An ultraviolet-radiation-independent pathway to melanoma carcinogenesis in the red hair/fair skin background. *Nature* **491**, 449-453

305. Cadet, J., Douki, T., Gasparutto, D., and Ravanat, J. L. (2003) Oxidative damage to DNA: formation, measurement and biochemical features. *Mutat Res* **531**, 5-23

306. Wang, J., Yuan, B., Guerrero, C., Bahde, R., Gupta, S., and Wang, Y. (2011) Quantification of oxidative DNA lesions in tissues of Long-Evans Cinnamon rats by capillary high-performance liquid chromatography-tandem mass spectrometry coupled with stable isotope-dilution method. *Anal Chem* **83**, 2201-2209

307. Chatgilialoglu, C., Ferreri, C., and Terzidis, M. A. (2011) Purine 5',8-cyclonucleoside lesions: chemistry and biology. *Chem Soc Rev* **40**, 1368-1382

308. Brooks, P. J. (2008) The 8,5'-cyclopurine-2'-deoxynucleosides: candidate neurodegenerative DNA lesions in xeroderma pigmentosum, and unique probes of transcription and nucleotide excision repair. *DNA Repair (Amst)* **7**, 1168-1179

309. You, C., Dai, X., Yuan, B., Wang, J., Brooks, P. J., Niedernhofer, L. J., and Wang, Y. (2012) A quantitative assay for assessing the effects of DNA lesions on transcription. *Nat Chem Biol* **8**, 817-822

310. Kuraoka, I., Bender, C., Romieu, A., Cadet, J., Wood, R. D., and Lindahl, T. (2000) Removal of oxygen free-radical-induced 5',8-purine cyclodeoxynucleosides from DNA by the nucleotide excision-repair pathway in human cells. *Proc Natl Acad Sci U S A* **97**, 3832-3837

311. Pande, P., Das, R. S., Sheppard, C., Kow, Y. W., and Basu, A. K. (2012) Repair efficiency of (5'S)-8,5'-cyclo-2'-deoxyguanosine and (5'S)-8,5'-cyclo-2'-deoxyadenosine depends on the complementary base. *DNA Repair (Amst)* **11**, 926-931

312. Brooks, P. J., Wise, D. S., Berry, D. A., Kosmoski, J. V., Smerdon, M. J., Somers, R. L., Mackie, H., Spoonde, A. Y., Ackerman, E. J., Coleman, K., Tarone, R. E., and Robbins, J. H. (2000) The oxidative DNA lesion 8,5'-(S)-cyclo-2'-deoxyadenosine is repaired by the nucleotide excision repair pathway and blocks gene expression in mammalian cells. *J Biol Chem* **275**, 22355-22362

313. Marietta, C., Gulam, H., and Brooks, P. J. (2002) A single 8,5'-cyclo-2'-deoxyadenosine lesion in a TATA box prevents binding of the TATA binding protein and strongly reduces transcription in vivo. *DNA Repair (Amst)* **1**, 967-975

314. Abraham, J., and Brooks, P. J. (2011) Divergent effects of oxidatively induced modification to the C8 of 2'-deoxyadenosine on transcription factor binding: 8,5'(S)-cyclo-2'-deoxyadenosine inhibits the binding of multiple sequence specific transcription factors, while 8-oxo-2'-deoxyadenosine increases binding of CREB and NF-kappa B to DNA. *Environ Mol Mutagen* **52**, 287-295

315. Yuan, B., Wang, J., Cao, H., Sun, R., and Wang, Y. (2011) High-throughput analysis of the mutagenic and cytotoxic properties of DNA lesions by next-generation sequencing. *Nucleic Acids Res* **39**, 5945-5954

316. Kuraoka, I., Robins, P., Masutani, C., Hanaoka, F., Gasparutto, D., Cadet, J., Wood, R. D., and Lindahl, T. (2001) Oxygen free radical damage to DNA. Translesion synthesis by human DNA polymerase eta and resistance to exonuclease action at cyclopurine deoxynucleoside residues. *J Biol Chem* **276**, 49283-49288

317. Swanson, A. L., Wang, J., and Wang, Y. (2012) Accurate and efficient bypass of 8,5'-cyclopurine-2'-deoxynucleosides by human and yeast DNA polymerase eta. *Chem Res Toxicol* **25**, 1682-1691

318. Romieu, A., Gasparutto, D., and Cadet, J. (1999) Synthesis and characterization of oligonucleotides containing 5',8-cyclopurine 2'-deoxyribonucleosides: (5'R)-5',8-cyclo-2'-deoxyadenosine, (5'S)-5',8-cyclo-2'-deoxyguanosine, and (5'R)-5',8-cyclo-2'-deoxyguanosine. *Chem Res Toxicol* **12**, 412-421

319. Thakur, M., Wernick, M., Collins, C., Limoli, C. L., Crowley, E., and Cleaver, J. E. (2001) DNA polymerase eta undergoes alternative splicing, protects against UV sensitivity and apoptosis, and suppresses Mre11-dependent recombination. *Genes Chromosomes Cancer* **32**, 222-235

320. de Feraudy, S., Limoli, C. L., Giedzinski, E., Karentz, D., Marti, T. M., Feeney, L., and Cleaver, J. E. (2007) Pol eta is required for DNA replication during nucleotide deprivation by hydroxyurea. *Oncogene* **26**, 5713-5721

321. Goodman, M. F., Creighton, S., Bloom, L. B., and Petruska, J. (1993) Biochemical basis of DNA replication fidelity. *Crit Rev Biochem Mol Biol* **28**, 83-126

322. Baker, D. J., Wuenschell, G., Xia, L., Termini, J., Bates, S. E., Riggs, A. D., and O'Connor, T. R. (2007) Nucleotide excision repair eliminates unique DNA-protein cross-links from mammalian cells. *J Biol Chem* **282**, 22592-22604

323. Yuan, B., You, C., Andersen, N., Jiang, Y., Moriya, M., O'Connor, T. R., and Wang, Y. (2011) The roles of DNA polymerases kappa and iota in the error-free bypass of N2-carboxyalkyl-2'-deoxyguanosine lesions in mammalian cells. *J Biol Chem* **286**, 17503-17511

324. Ziegler, K., Bui, T., Frisque, R. J., Grandinetti, A., and Nerurkar, V. R. (2004) A rapid in vitro polyomavirus DNA replication assay. *J Virol Methods* **122**, 123-127

325. Burns, J. A., Dreij, K., Cartularo, L., and Scicchitano, D. A. (2010) O6-methylguanine induces altered proteins at the level of transcription in human cells. *Nucleic Acids Res* **38**, 8178-8187

326. Sanchez, J. A., Marek, D., and Wangh, L. J. (1992) The efficiency and timing of plasmid DNA replication in Xenopus eggs: correlations to the extent of prior chromatin assembly. *J Cell Sci* **103 (Pt 4)**, 907-918

327. Taylor, E. R., and Morgan, I. M. (2003) A novel technique with enhanced detection and quantitation of HPV-16 E1- and E2-mediated DNA replication. *Virology* **315**, 103-109

328. Ziv, O., Geacintov, N., Nakajima, S., Yasui, A., and Livneh, Z. (2009) DNA polymerase zeta cooperates with polymerases kappa and iota in translesion DNA

synthesis across pyrimidine photodimers in cells from XPV patients. *Proc Natl Acad Sci U S A* **106**, 11552-11557

329. Shachar, S., Ziv, O., Avkin, S., Adar, S., Wittschieben, J., Reissner, T., Chaney, S., Friedberg, E. C., Wang, Z., Carell, T., Geacintov, N., and Livneh, Z. (2009) Two-polymerase mechanisms dictate error-free and error-prone translesion DNA synthesis in mammals. *EMBO J* **28**, 383-393

330. You, C., Dai, X., Yuan, B., and Wang, Y. (2012) Effects of 6-thioguanine and S6-methylthioguanine on transcription in vitro and in human cells. *J Biol Chem* **287**, 40915-40923

331. Delaney, J. C., and Essigmann, J. M. (2004) Mutagenesis, genotoxicity, and repair of 1-methyladenine, 3-alkylcytosines, 1-methylguanine, and 3-methylthymine in alkB Escherichia coli. *Proc Natl Acad Sci U S A* **101**, 14051-14056

332. Delaney, J. C., and Essigmann, J. M. (2006) Assays for determining lesion bypass efficiency and mutagenicity of site-specific DNA lesions in vivo. *Methods Enzymol* **408**, 1-15

333. Gan, G. N., Wittschieben, J. P., Wittschieben, B. O., and Wood, R. D. (2008) DNA polymerase zeta (pol zeta) in higher eukaryotes. *Cell Res* **18**, 174-183

334. Levine, R. L., Yang, I. Y., Hossain, M., Pandya, G. A., Grollman, A. P., and Moriya, M. (2000) Mutagenesis induced by a single 1,N6-ethenodeoxyadenosine adduct in human cells. *Cancer Res* **60**, 4098-4104

335. Yang, I. Y., Johnson, F., Grollman, A. P., and Moriya, M. (2002) Genotoxic mechanism for the major acrolein-derived deoxyguanosine adduct in human cells. *Chem Res Toxicol* **15**, 160-164

336. Newton, C. R., Graham, A., Heptinstall, L. E., Powell, S. J., Summers, C., Kalsheker, N., Smith, J. C., and Markham, A. F. (1989) Analysis of any point mutation in DNA. The amplification refractory mutation system (ARMS). *Nucleic Acids Res* **17**, 2503-2516

337. Yoon, J. H., Prakash, L., and Prakash, S. (2010) Error-free replicative bypass of (6-4) photoproducts by DNA polymerase zeta in mouse and human cells. *Genes Dev* **24**, 123-128

338. Yoon, J. H., Bhatia, G., Prakash, S., and Prakash, L. (2010) Error-free replicative bypass of thymine glycol by the combined action of DNA polymerases kappa and zeta in human cells. *Proc Natl Acad Sci U S A* **107**, 14116-14121

339. Andersen, N., Wang, J., Wang, P., Jiang, Y., and Wang, Y. (2012) In-vitro replication studies on O(2)-methylthymidine and O(4)-methylthymidine. *Chem Res Toxicol* **25**, 2523-2531

340. Joyce, C. M. (1997) Choosing the right sugar: how polymerases select a nucleotide substrate. *Proc. Natl. Acad. Sci. U.S.A.* **94**, 1619-1622

341. Horton, N. C., and Finzel, B. C. (1996) The structure of an RNA/DNA hybrid: a substrate of the ribonuclease activity of HIV-1 reverse transcriptase. *J. Mol. Biol.* **264**, 521-533

342. Rydberg, B., and Game, J. (2002) Excision of misincorporated ribonucleotides in DNA by RNase H (type 2) and FEN-1 in cell-free extracts. *Proc. Natl. Acad. Sci. U.S.A.* **99**, 16654-16659

343. Patel, P. H., and Loeb, L. A. (2000) Multiple amino acid substitutions allow DNA polymerases to synthesize RNA. *J. Biol. Chem.* **275**, 40266-40272

344. Clausen, A. R., Zhang, S., Burgers, P. M., Lee, M. Y., and Kunkel, T. A. (2013) Ribonucleotide incorporation, proofreading and bypass by human DNA polymerase delta. *DNA Repair* **12**, 121-127

345. Watt, D. L., Johansson, E., Burgers, P. M., and Kunkel, T. A. (2011) Replication of ribonucleotide-containing DNA templates by yeast replicative polymerases. *DNA Repair* **10**, 897-902

346. Sparks, J. L., Chon, H., Cerritelli, S. M., Kunkel, T. A., Johansson, E., Crouch, R. J., and Burgers, P. M. (2012) RNase H2-initiated ribonucleotide excision repair. *Mol. Cell* **47**, 980-986

347. Lazzaro, F., Novarina, D., Amara, F., Watt, D. L., Stone, J. E., Costanzo, V., Burgers, P. M., Kunkel, T. A., Plevani, P., and Muzi-Falconi, M. (2012) RNase H and postreplication repair protect cells from ribonucleotides incorporated in DNA. *Mol. Cell* **45**, 99-110

348. Williams, J. S., Smith, D. J., Marjavaara, L., Lujan, S. A., Chabes, A., and Kunkel, T. A. (2013) Topoisomerase 1-mediated removal of ribonucleotides from nascent leading-strand DNA. *Mol. Cell* **49**, 1010-1015

349. Kim, N., Huang, S. N., Williams, J. S., Li, Y. C., Clark, A. B., Cho, J. E., Kunkel, T. A., Pommier, Y., and Jinks-Robertson, S. (2011) Mutagenic processing of ribonucleotides in DNA by yeast topoisomerase I. *Science* **332**, 1561-1564

350. Rabe, B. (2013) Aicardi-Goutieres syndrome: clues from the RNase H2 knock-out mouse. *J. Mol. Med.*

351. Sale, J. E., Lehmann, A. R., and Woodgate, R. (2012) Y-family DNA polymerases and their role in tolerance of cellular DNA damage. *Nat. Rev. Mol. Cell. Biol.* **13**, 141-152

352. Yang, W. W., R. (2007) What a difference a decade makes: insights into translesion DNA synthesis. *Proc. Natl. Acad. Sci. U.S.A.* **104**, 15591-15598

353. Shachar, S., Ziv, O., Avkin, S., Adar, S., Wittschieben, J., Reissner, T., Chaney, S., Friedberg, E. C., Wang, Z., Carell, T., Geacintov, N., and Livneh, Z. (2009) Two-polymerase mechanisms dictate error-free and error-prone translesion DNA synthesis in mammals. *EMBO J.* **28**, 383-393

354. Washington, M. T., Johnson, R. E., Prakash, S., and Prakash, L. (2000) Accuracy of thymine-thymine dimer bypass by Saccharomyces cerevisiae DNA polymerase eta. *Proc. Natl. Acad. Sci. U.S.A.* **97**, 3094-3099

355. Yuan, B., You, C., Andersen, N., Jiang, Y., Moriya, M., O'Connor, T. R., and Wang, Y. (2011) The roles of DNA polymerases κ and ι in the error-free bypass of N^2-carboxyalkyl-2'-deoxyguanosine lesions in mammalian cells. *J. Biol. Chem.* **286**, 17503-17511

356. Carlson, K. D., and Washington, M. T. (2005) Mechanism of efficient and accurate nucleotide incorporation opposite 7,8-dihydro-8-oxoguanine by *Saccharomyces cerevisiae* DNA polymerase eta. *Mol. Cell. Biol.* **25**, 2169-2176

357. Yuan, B., Cao, H., Jiang, Y., Hong, H., and Wang, Y. (2008) Efficient and accurate bypass of N^2-(1-carboxyethyl)-2'-deoxyguanosine by DinB DNA polymerase *in vitro* and *in vivo*. *Proc. Natl. Acad. Sci. U.S.A.* **105**, 8679-8684

358. Gu, C., and Wang, Y. (2004) LC-MS/MS identification and yeast polymerase eta bypass of a novel γ-irradiation-induced intrastrand cross-link lesion G[8-5]C. *Biochemistry* **43**, 6745-6750

359. You, C., Swanson, A. L., Dai, X., Yuan, B., Wang, J., and Wang, Y. (2013) Translesion Synthesis of 8,5'-Cyclopurine-2'-deoxynucleosides by DNA Polymerases eta, iota, and zeta. *J. Biol. Chem.*

360. DeRose, E. F., Perera, L., Murray, M. S., Kunkel, T. A., and London, R. E. (2012) Solution structure of the Dickerson DNA dodecamer containing a single ribonucleotide. *Biochemistry* **51**, 2407-2416

361. Wahl, M. C., and Sundaralingam, M. (2000) B-form to A-form conversion by a 3'-terminal ribose: crystal structure of the chimera d(CCACTAGTG)r(G). *Nucleic Acids Res.* **28**, 4356-4363

362. Egli, M., Usman, N., and Rich, A. (1993) Conformational influence of the ribose 2'-hydroxyl group: crystal structures of DNA-RNA chimeric duplexes. *Biochemistry* **32**, 3221-3237

363. Jaishree, T. N., van der Marel, G. A., van Boom, J. H., and Wang, A. H. (1993) Structural influence of RNA incorporation in DNA: quantitative nuclear magnetic resonance refinement of d(CG)r(CG)d(CG) and d(CG)r(C)d(TAGCG). *Biochemistry* **32**, 4903-4911

364. Ban, C., Ramakrishnan, B., and Sundaralingam, M. (1994) A single 2'-hydroxyl group converts B-DNA to A-DNA. Crystal structure of the DNA-RNA chimeric decamer duplex d(CCGGC)r(G)d(CCGG) with a novel intermolecular G-C base-paired quadruplet. *J. Mol. Biol.* **236**, 275-285

365. Nowotny, M., Gaidamakov, S. A., Crouch, R. J., and Yang, W. (2005) Crystal structures of RNase H bound to an RNA/DNA hybrid: substrate specificity and metal-dependent catalysis. *Cell* **121**, 1005-1016

366. Yakes, F. M., and Van Houten, B. (1997) Mitochondrial DNA damage is more extensive and persists longer than nuclear DNA damage in human cells following oxidative stress. *Proc. Natl. Acad. Sci. U.S.A.* **94**, 514-519

367. Alexeyev, M., Shokolenko, I., Wilson, G., and LeDoux, S. (2013) The maintenance of mitochondrial DNA integrity--critical analysis and update. *Cold Spring Harb. Perspect. Biol.* **5**, a012641

368. Copeland, W. C. (2012) Defects in mitochondrial DNA replication and human disease. *Crit. Rev. Biochem. Mol. Biol.* **47**, 64-74

369. Bohr, V. A., and Anson, R. M. (1999) Mitochondrial DNA repair pathways. *J. Bioenerg. Biomembr.* **31**, 391-398

370. Akbari, M., Visnes, T., Krokan, H. E., and Otterlei, M. (2008) Mitochondrial base excision repair of uracil and AP sites takes place by single-nucleotide insertion and long-patch DNA synthesis. *DNA Repair* **7**, 605-616

371. McKinney, E. A., and Oliveira, M. T. (2013) Replicating animal mitochondrial DNA. *Genet. Mol. Biol.* **36**, 308-315

372. Trifunovic, A., Wredenberg, A., Falkenberg, M., Spelbrink, J. N., Rovio, A. T., Bruder, C. E., Bohlooly, Y. M., Gidlof, S., Oldfors, A., Wibom, R., Tornell, J., Jacobs, H. T., and Larsson, N. G. (2004) Premature ageing in mice expressing defective mitochondrial DNA polymerase. *Nature* **429**, 417-423

373. Kujoth, G. C., Hiona, A., Pugh, T. D., Someya, S., Panzer, K., Wohlgemuth, S. E., Hofer, T., Seo, A. Y., Sullivan, R., Jobling, W. A., Morrow, J. D., Van Remmen, H., Sedivy, J. M., Yamasoba, T., Tanokura, M., Weindruch, R., Leeuwenburgh, C., and Prolla, T. A. (2005) Mitochondrial DNA mutations, oxidative stress, and apoptosis in mammalian aging. *Science* **309**, 481-484

374. Stumpf, J. D., Saneto, R. P., and Copeland, W. C. (2013) Clinical and molecular features of POLG-related mitochondrial disease. *Cold Spring Harb. Perspect. Biol.* **5**, a011395

375. Holt, I. J., and Reyes, A. (2012) Human mitochondrial DNA replication. *Cold Spring Harb. Perspect. Biol.* **4**

376. Yadav, N., and Chandra, D. (2013) Mitochondrial DNA mutations and breast tumorigenesis. *Biochim. Biophys. Acta* **1836**, 336-344

377. Graziewicz, M. A., Longley, M. J., and Copeland, W. C. (2006) DNA polymerase γ in mitochondrial DNA replication and repair. *Chem. Rev.* **106**, 383-405

378. Xu, P., Oum, L., Lee, Y. C., Geacintov, N. E., and Broyde, S. (2009) Visualizing sequence-governed nucleotide selectivities and mutagenic consequences through a replicative cycle: processing of a bulky carcinogen N2-dG lesion in a Y-family DNA polymerase. *Biochemistry* **48**, 4677-4690

379. Lee, Y. S., Lee, S., Demeler, B., Molineux, I. J., Johnson, K. A., and Yin, Y. W. (2010) Each monomer of the dimeric accessory protein for human mitochondrial DNA polymerase has a distinct role in conferring processivity. *J. Biol. Chem.* **285**, 1490-1499

380. Pinz, K. G., Shibutani, S., and Bogenhagen, D. F. (1995) Action of mitochondrial DNA polymerase γ at sites of base loss or oxidative damage. *J. Biol. Chem.* **270**, 9202-9206

381. Taylor, R. W., and Turnbull, D. M. (2005) Mitochondrial DNA mutations in human disease. *Nat. Rev. Genet.* **6**, 389-402

382. Wei, Y. H. (1998) Oxidative stress and mitochondrial DNA mutations in human aging. *Proc. Soc. Exp. Biol. Med.* **217**, 53-63

383. Hecht, S. S. (2008) Progress and challenges in selected areas of tobacco carcinogenesis. *Chem. Res. Toxicol.* **21**, 160-171

384. Prevost, V., and Shuker, D. E. (1996) Cigarette smoking and urinary 3-alkyladenine excretion in man. *Chem. Res. Toxicol.* **9**, 439-444

385. Chao, M. R., Wang, C. J., Chang, L. W., and Hu, C. W. (2006) Quantitative determination of urinary *N*7-ethylguanine in smokers and non-smokers using an isotope dilution liquid chromatography/tandem mass spectrometry with on-line analyte enrichment. *Carcinogenesis* **27**, 146-151

386. Chen, H. J., and Liu, Y. F. (2013) Simultaneous quantitative analysis of *N*3-ethyladenine and *N*7-ethylguanine in human leukocyte deoxyribonucleic acid by stable isotope dilution capillary liquid chromatography-nanospray ionization tandem mass spectrometry. *J. Chromatogr. A* **1271**, 86-94

387. Millonig, G., Wang, Y., Homann, N., Bernhardt, F., Qin, H., Mueller, S., Bartsch, H., and Seitz, H. K. (2011) Ethanol-mediated carcinogenesis in the human esophagus implicates CYP2E1 induction and the generation of carcinogenic DNA-lesions. *Int. J. Cancer* **128**, 533-540

388. Larson, H. N., Zhou, J., Chen, Z., Stamler, J. S., Weiner, H., and Hurley, T. D. (2007) Structural and functional consequences of coenzyme binding to the inactive asian variant of mitochondrial aldehyde dehydrogenase: roles of residues 475 and 487. *J. Biol. Chem.* **282**, 12940-12950

389. Eizirik, D. L., Sandler, S., Ahnstrom, G., and Welsh, M. (1991) Exposure of pancreatic islets to different alkylating agents decreases mitochondrial DNA content but only streptozotocin induces long-lasting functional impairment of B-cells. *Biochem. Pharmacol.* **42**, 2275-2282

390. Rasmussen, A. K., and Rasmussen, L. J. (2005) Targeting of O^6-MeG DNA methyltransferase (MGMT) to mitochondria protects against alkylation-induced cell death. *Mitochondrion* **5**, 411-417

391. Den Engelse, L., Menkveld, G. J., De Brij, R. J., and Tates, A. D. (1986) Formation and stability of alkylated pyrimidines and purines (including imidazole ring-opened 7-alkylguanine) and alkylphosphotriesters in liver DNA of adult rats treated with ethylnitrosourea or dimethylnitrosamine. *Carcinogenesis* **7**, 393-403

392. Grevatt, P. C., Solomon, J. J., and Bhanot, O. S. (1992) *In vitro* mispairing specificity of O^2-ethylthymidine. *Biochemistry* **31**, 4181-4188

393. Andersen, N., Wang, J., Wang, P., Jiang, Y., and Wang, Y. (2012) *In-vitro* replication studies on O^2-methylthymidine and O^4-methylthymidine. *Chem. Res. Toxicol.* **25**, 2523-2531

394. Dosanjh, M. K., Menichini, P., Eritja, R., and Singer, B. (1993) Both O^4-methylthymine and O^4-ethylthymine preferentially form alkyl T.G pairs that do not block *in vitro* replication in a defined sequence. *Carcinogenesis* **14**, 1915-1919

395. Skopek, T. R., Walker, V. E., Cochrane, J. E., Craft, T. R., and Cariello, N. F. (1992) Mutational spectrum at the *Hprt* locus in splenic T cells of B6C3F1 mice exposed to *N*-ethyl-*N*-nitrosourea. *Proc. Natl. Acad. Sci. U.S.A.* **89**, 7866-7870

396. Kasiviswanathan, R., Longley, M. J., Young, M. J., and Copeland, W. C. (2010) Purification and functional characterization of human mitochondrial DNA polymerase γ harboring disease mutations. *Methods* **51**, 379-384

397. Gu, C., and Wang, Y. (2004) LC-MS/MS identification and yeast polymerase η bypass of a novel γ-irradiation-induced intrastrand cross-link lesion G[8-5]C. *Biochemistry* **43**, 6745-6750

398. Swanson, A. L., Wang, J., and Wang, Y. (2011) *In Vitro* Replication Studies of Carboxymethylated DNA Lesions with *Saccharomyces cerevisiae* Polymerase η. *Biochemistry* **50**, 7666-7673